4-21-2014 12:00 AM

Characterization of Fine Powders and Development of Processes for Powder Coatings

Jing Fu, *The University of Western Ontario*

Supervisor: Dr. Jesse Zhu, *The University of Western Ontario*
Joint Supervisor: Dr. Hui Zhang, *The University of Western Ontario*
A thesis submitted in partial fulfillment of the requirements for the Doctor of Philosophy degree in Chemical and Biochemical Engineering

CHARACTERIZATION OF FINE POWDERS AND DEVELOPMENT OF PROCESSES FOR POWDER COATINGS

(Thesis format: Integrated Article)

By

Jing Fu

Graduate Program in Engineering Science
Department of Chemical and Biochemical Engineering

A thesis submitted in partial fulfillment
of the requirements for the degree of
Doctor of Philosophy

The School of Graduate and Postdoctoral Studies
Western University
London, Ontario, Canada

Abstract

Powder coating process is a dry coating technology which utilizes resin based powders (medium particle size between 35 to 60 μm) as coating materials. It is green and economical since the use of harmful solvents can be avoided and most of the overspray materials can be recycled. However, the poor appearance provided by powder coatings has always been a big drawback. Fine powder coating (medium particle size less than 30 μm) was first introduced in around 2001. It was able to provide much smoother coating finishes due to the smaller powder particles. However, fine powder coating has still not been widely used yet because of the unstable fluidization performances. This thesis study comprehensively investigated the fluidization performances and various powder processes of both regular and fine powder coatings. Moreover, it developed numbers of new techniques and methods for powder coating productions and applications.

The flowability of a powder that represented the ability of the powder to be handled used to be assessed by the medium particle size and the amount of small particles in the powder. Yet, experiments conducted in this study disclosed that the conventional methods to characterize the flowability of the fine powders were not accurate, since the flowabllity results scattered with respect to the medium particle size and the amount of small particles. Instead, the parameter, span, which represents the particle size distribution, was found to have a much more accurate correlation with the flowability of the fine powders.

In addition, the material processes of fine powder coatings were investigated. The current processes are designed to aim for the maximum production throughput. Nevertheless, it lacks of the control for the particle size distribution which is crucial for fine powders. The study developed novel designs of grinder and cyclone to reduce the produced powder coatings. The experiments disclosed that the new grinder design could reduce the span of

the produced powder while still maintained a comparable grinding efficiency to a regular grinder. On the other hand, the new cyclone design could also provide significant reduction in the span of the powder. At the same time, it could still retain reasonable collection efficiency.

The study also investigated the electrical property of the fine powder coatings according to the application of the electrostatic spraying. The influence of moisture content of the fine powder coatings was discovered. The experiments indicated that additional moisture on the surfaces of the fine powder particles could significantly reduce the resistivity of the powder so as to enhance the transfer efficiency. However, the regular powder coating had less significant reduction in the resistivity after humidification. As a result, it received less significant improvement on the transfer efficiency. The experiment also disclosed that the improvement on the transfer efficiency of the powder coating was progressive with respect to the increases of the humidification level.

Moreover, a multi-electrode corona spray gun with alternative charging pattern was developed for improving the Faraday Cage resistance. The results obtained from the experiments indicated that the new spray gun could improve the Faraday Cage resistance of the corona spraying with the fine powder sample for various gun voltages. On the other hand, the improvement of the Faraday Cage resistance with regular powder sample was not noticeable until a high gun voltage of -90 kV was reached. The transfer efficiency provided by the new spray gun with fine powder sample was comparable to a conventional spray gun, whereas, the transfer efficiency with regular powder sample was improved.

In the end, the processing techniques for low-cured powder coating and metallic color powder coating were revised. By utilizing the invented dry blending catalyst, pre-curing problems of the low-cured powder coatings could be solved. Moreover, experimental results indicated that the new technique could provide similar curing performances as the conventional low-cure powder sample. More importantly, the new technique could also provide much improved coating quality and much prolonged shelf life of the low-cured powder coating. On the other hand, the bonding problem of the metallic color powder coatings was solved by incorporating the liquid bonder in the blending of powder particles and the metallic pigment. Experiment found that the same concentration of the metallic pigment measured in both pre-sprayed powders and post-sprayed powder could be achieved by using the new technique. It indicated that the liquid bonder could provide good bonding strength between the metallic pigment and powder particles so as to eliminate the separations between the two materials during spraying.

Nowadays, finer powder coatings become more popular to use, since better coating films has to provided for fulfilling higher aesthetic requirements in the applications. The discoveries of the thesis study contributed to the development of the powder coating technology. It provided useful suggestions to the understanding of the fine powder flowability. Furthermore, it also developed several new methods and techniques for improving the current processing of powder coatings.

Keywords: powder flowability, cyclone, fine powder, corona charge spraying, transfer efficiency, Faraday Cage resistance, powder coating, grinding.

CO-AUTHORSHIP

Dr. Jesse Zhu and Dr. Hui Zhang provided full supervision and guidance to this PhD thesis study.

Related publications:

1. **Title:** Improvement on the first pass transfer efficiency of fine polymer coating powders for corona spraying process

   Authors: Jing Fu, Hui Zhang, Jesse Zhu

   All the research works were conducted by Jing Fu under the supervision of Dr. Hui Zhang and Dr. Jesse Zhu. The final version of the manuscript was published on ***Advanced Powder Technology*** in 2013.

ACKNOWLEDGEMENTS

In the beginning, I would like to express my greatest gratitude to Dr. Jesse Zhu, a professor in the Department of Chemical and Biochemical Engineering of Western University and a fellow of Canadian Academy of Engineering. Along my PhD study, Dr. Zhu provided invaluable guidance and enormous encouragement to me. The appreciation was extended to Dr. Hui Zhang, a research professor in the Department of Chemical and Biochemical Engineering of Western University. I had been working with him closely on a daily basis. His detailed instructions and suggestions were vital to the success of this thesis study. I had been deeply infected by his enthusiasm and precision of research.

I am also grateful to Dr. Andy Sun, a professor in the Department of Mechanical and Material of Western University, Dr. Charles Xu, a professor in the Department of Chemical and Biochemical of Western University, and Cedric Briens, a professor in the Department of Chemical and Biochemical of Western University. They provided useful knowledge as well as helpful recommendations to this thesis study from the aspects of their expertises.

In addition, I would like to thank Mr. Bin Xi, the technical manager of Azuratech Fine Powder Coating (MianYang, China) and Ms. JiangPing Yu, the general manager of Azuratech Fine Powder Coating (MianYang, China) for giving me the opportunity to visit their factory site.

Moreover, my appreciations continue to Michael Zhu and Jianzhou Wen for their assistances on fabricating the experimental apparatus for my experiments; to Ms. Ying

Ma for sharing her lab equipments; to Mr. Yong Liu for his assistance on conducting analysis tests on the experimental samples; to Meysaa Hussein and Hanmeng Qi for their assistances on conducting a part of the experiment works of my PhD study; to my colleagues, Danni Bao, Dangchen Xue, Rezwana Yeasmin, Mohammad Bhuiyan, Nicholas Hou, Qingliang Yang, Xi Zhang, Shan Gao, Yijun Dong, Tang Li, Jiangshan Liu and Jingsi Yang for the enjoyments of working with them.

Furthermore, I would like to thank OGS (Ontario Graduate Scholarship) and QEII (Queen Elizabeth II Graduate Scholarship) for providing the financial supports to myself as well as my PhD study.

Particularly, I want to deliver the deepest thankfulness to the most important people in my life: my father Shilin Fu, my mother Xueqin Liu, my daughter Yvonne Fu, my wife Yifan Chu, my mother-in-law Chungui Li and the other family members. Their loves and dedications were the greatest support to me.

TABLE OF CONTENTS

LIST OF FIGURES

LIST OF TABLES

LIST OF ABBREVIATIONS AND SYMBOLS

Abbreviations：

AVA	Avalanche Angle
AOR	Angle of Repose
RBER	Rotational Bed Expansion Ratio
$D_{10, 50, 90}$	particle diameter, where 10, 50 or 90 volume % of the powder smaller than the diameter (μm)
VOC	Volatile Organic Compound
SEM	Scanning Electron Microscope
DSC	Differential Scanning Calorimetry
DBC	Dry blended catalyst
ACM	Air classifying mill

Symbols：

A	Hamaker constant
A_{tc}	Cross-sectional area of the test cell for the resistivity measurements (m^2)
H	The separation distance between two particles (μm)
R	Particle radius (μm)
W	Powder weight (g)
η	Collection efficiency (%)
r	Powder feeding rate (g/s)
E_p	Electrostatic field strength of powder coating (V/m)
R	Resistance of powder coating (ohm)
FPTE	First Pass Transfer Efficiency (%)
ρ_p	Resistivity of powder coating (ohm-m)
μ	Velocity (m/s)
J	Corona current (A/m^2)
l	Measured depth of the test cell for the resistivity measurements (m)

CHAPTER 1: GENERAL INTRODUCTION

1.1 Introduction

1.1.1 Powder

Powders are solid substances in the form of loose particles. Generally, powders can be either obtained by a top-down technique such as pulverizing from their bulk materials or a bottom-up technique such as synthesising from atom to atom [1]. Powders have larger specific surface areas than corresponding bulk materials. Owing to that, they are favorable in many applications for example: chemical reactor, pharmaceutical delivery, coating and so on. Yet, finer powders are more difficult to be handled in process of fluidization, pneumatic transportation and spraying due to the increased powder cohesion. Flowability has been used to determine the ability of the powder to be handled. In 1973, Geldart studied the powder flowability with respect to the powders' sizes and densities. He raised the famous "Geldart's Powder Classification" which divided powder materials into four groups based on their flow characteristics [2]. His theory has been used by researchers as a guideline for the studies of powders.

1.1.2 Powder Coating

Powder coating, which utilizes solid particles as the coating material, is one of the powder applications. Powder coating was first developed in 1960s and the motivation of this innovation, at that time, was to get away from the pollution penalties due to the elimination of the organic solvents [3]. In the applications, other benefits of powder coating were also realized such as the recyclable overspray materials and stronger coating film. As yet, powder coating has gained a remarkable share in the coating industry.

Modern processes for manufacturing powder coatings consist of extrusion, grinding and spraying. Raw materials like resin, curing agent, degassing agent, flow agent, filler and pigment are first hot extruded. During the hot extrusion, the raw materials are mixed into a homogeneous material under high shears. The extruded material is then ground and classified into powders with desired particle sizes. Finally, the powders are sprayed on the coating parts followed by the curing process in a baking oven.

1.2 Challenges and Opportunities of Powder Coating Application

The medium particle sizes of regular powder coatings (can be also called as coarse powder coatings) are in between 30 and 60 μm. After curing, the provided coating film is thick and the coating finish is rough comparing with conventional liquid coatings. Therefore, the applications of powder coatings have always been limited to lower-end products such as coatings on hand tools, office furniture and home appliances that do not have high aesthetic requirements.

The film qualities can be improved by utilizing powders with smaller particle sizes, called fine powder coatings. With the medium particle size reduced below 30 μm, fine powder coatings are able to provide smoother and thinner coating films. Nowadays, fine powder coatings have been used by auto makers for the coatings on the car bodies. General Motor and Daimler-Chrysler are currently using powder primers at their 13 plants across North America [4]. On the other side of the world, BMW has also successfully applied powder clear coats on the car bodies of the 5 series and 7 series at its German plants [5]. In 2005, Zhu and Zhang developed an ultrafine powder coating technology which was able to utilize powders with even smaller size (less than 20μm) to further improve the coating film quality [6].

Every coin has two sides. The fine powder coatings, on the other hand, are more difficult to be produced than the regular powder coatings. Grinding the powder finer generates more of the small particles which will deteriorate the flowability of the powder so as to cause application issues. Currently, powder manufacturers enhance the fine powder flowability by adding flow additives. However, adding the flow additives into fine powder coatings could increase the risk of having coating defects as well.

Moreover, applying fine powder coatings is more challenging than before. Fine powder coatings were experienced to have poor coating efficiency during electrostatic spraying. It was claimed by the researchers that finer particles carried less charges than larger particles and they tended to obtain stronger back ionization [7]. In addition, their flying motions could easier be drifted by air turbulences during spraying [7]. Besides that, fine powder coatings are facing more severe Faraday Cage problem than regular size powder coatings while applying on coating parts with complex geometries. They have to provide sufficient coverage on the recessed surfaces to obtain continuous coating films.

1.3 Research Objectives and Overview

There was a growing demand of the fine powder coatings due to the surpassing coating finishes than the regular powder coatings. Nevertheless, fine powder coatings are still encountering many challenges. The objective of this thesis study was to comprehensively investigate fine powder coatings to resolve problems from powder characterization, powder processing and powder spraying. Furthermore, current problems associated with feature powder coatings were also investigated by the study. Revised processing techniques were developed for improving the material properties as well as resolving the manufacturing problems of the functional powder coatings.

The key to this study was the valuable inputs from the industrial practices of fine powder coatings. Based on the collaborative studies with General Motor, and Azuratech Fine Powder Coating (Mianyang), problems and difficulties of powder coatings, especially fine powder coatings, were recognized. In addition, the current material standards, manufacturing processes and spraying processes in the industrial applications of powder coatings were reviewed.

The experimental works in the study were classified into four sections:

i. Pioneer researchers had done numbers of works on the flowability characterization of powders. However, the existing theories were found not sufficient to be used for fine powder coatings. This study further investigated the flowability of the fine powder coatings with respect to the particle sizes. A better flowability characterization method was discovered for fine powder coatings.

ii. The current manufacturing processes of powder coatings are mainly for maximizing the production throughput. However, the produced fine powder coatings have wide particle size distribution which is not favourable for applications. This section was to revise current manufacturing processes, particularly the grinding and collecting processes, for producing fine powder coatings with narrower particle size distributions. Series of experiments were conducted to validate the revisions.

iii. The third section was the studies on the corona spraying of powder coatings. Previous study suggested that the increased moisture content could improve the coating efficiency of fine powders [8]. To further investigate this finding, the electrical properties of powder coatings with different moisture contents were studied. Furthermore, the

Faraday Cage effect from the corona spraying was investigated and revisions on powder spray gun were made for improving the Faraday Cage resistance.

iv. The final section of the study was to develop processing techniques for functional powder coatings including the low-cure powder coatings and the metallic color powder coatings. The new techniques were to address the problems found in current processes and the experiments for evaluating the new processes were conducted.

1.4 Thesis Structure

This PhD Thesis consists of 11 chapters and follows the "Integrated-Article" format outlined in the *Thesis Regulation Guide* by the School of Graduate Postdoctoral Studies (SGPS) of Western University.

Chapter 1 provides a general introduction of this PhD thesis. It stated the thesis overview and the research objective. It also stated the thesis structure and major contributions from the study.

Chapter 2 covers the literature reviews from series of topics related to this thesis study. It provides background knowledge and theories in powder materials, powder coating and powder coating processes.

Chapter 3 includes the investigation of the fine powder characterization. It explains the differences between various methods for characterizing the flowability of fine powder coatings. It also provides suggestions for the flowability characterization of fine powder coatings.

Chapter 4 describes a revised cyclone design for narrowing the particle size distribution of the fine powder coatings. It reviews the numerical simulations as well as the experimental evaluations of the revised cyclone designs.

Chapter 5 describes another approach to narrow the particle size distributions for produced fine powder coatings by utilizing a revised grinder design. It contains the preliminary work of the revised grinder for its grinding efficiency and the investigation of the particle size distributions of the produced fine powder coatings.

Chapter 6 contains an extended work from a previous study: the influences of moisture on the transfer efficiency of powder coatings. It includes the investigation of the electrical properties of the powder particles prior and after the humidification process. In addition, it also includes the estimation for the potential risk of the flowability deterioration on the humidified powder coatings. Furthermore, it reviews the inspections of the coating qualities of the humidified powder coatings.

Chapter 7 describes a revised spray gun design. It reviews the new spray gun by evaluating Faraday Cage resistance and the transfer efficiency under diverse spraying conditions with both fine and regular powder coatings. It also includes the experiments for the optimization of the electrode adjustments.

Chapter 8 describes a new processing technique for low-cure powder coatings. It includes the evaluations on the low-curing performance of the powder made from the new technique. It also covers the examinations of the low-cure powder coating made from the new technique in three aspects: mechanical property, chemical resistance and coating quality.

Chapter 9 describes a new processing technique for metallic color powder coatings. It includes the evaluations of the bonding performance between the powder particles and the metallic pigment provide by the new technique. It also contains the optimization of the liquid bonder used in the new technique.

Chapter 10 states a general discussion on the results discovered from this study.

Chapter 11 summarizes the experimental results from this study and it provides recommendations for future works.

1.5 Major contributions

Five major contributions of the study can be summarized in below:

- Several revisions on the current manufacturing process of fine powder coatings were made to achieve a narrower particle size distribution. A cyclone with reverse air flow was able to reduce the particle size distribution of the collected powders and the novel design of the intake for the reverse air could retain comparable cyclone efficiency to an ordinary cyclone design. On the other hand, a revised grinder design that utilizing convex impact surface on the grinding elements was able to reduce the over-grindings of the smaller particles so to narrow the particle size distribution.

- The developed corona spray gun with alternative charging pattern on a multi-electrode configuration was able to improve the Faraday Cage resistance during corona charge spraying of both fine and regular powder coatings. The significance of the improvement could be recognized by the sprayer. But then, the transfer efficiency was not deteriorated comparing with a normal corona spray gun.

- The revised technique, which utilized DBC (dry blending catalysts), for processing the low-cure powder coating was able to eliminate the pre-curing problem from the hot extrusion encountering in the past. In addition, the new technique was able to provide outstanding shelf life for the low-cure powder coatings. More importantly, it did not deteriorate the coating quality while accomplishing the low curing feature.

- The revised bonding technique for metallic color powder coating, which utilized liquid bonder, provided strong bond between the powder particles and the metallic pigment. It avoided the separations of the two materials during spraying. As a result, concentration of the metallic pigment in the recycled powders could remain unchanged so that the recycled powders could be successfully reused.

Reference

[1] Guozhong C., 2004, Nanostructures and Nanomaterials: Synthesis, Porosity & Applications., *Imperial College Press*, London, UK.

[2] Geldart D., 1973, Types of gas fluidization, Powder Technology, 7, 285-297.

[3] Hardy R.D., Seitz J.W., 1974, Engineering Savings with Powder Coating, Society of Manufacturing Engineers, FC74-589.

[4] Gribble P., 2003, Development Status of Powder Coatings for OEM Automotive Applications, *Finishing Today*.

[5] Biller K., 2006, OEM Automotive Powder Coatings, *Finishing Today*.

[6] Zhu J., Zhang H., 2005, Ultrafine powder coatings: an innovation. *Powder Coat*, 16, 39-47.

[7] Sharma R., Trigwell S., Biris A.S., Sims R.A., Mazumder M.K., 2003, Effect of Ambient Relative Humidity and Surface Modification on the Charge Decay, *Properties of Polymer Powders in Powder Coating*, 39(1), 87-95.

[8] Fu J., 2010, Study on powder coating particles and development of new powder coating application methods, *Master Thesis*, The University of Western Ontario.

CHAPTER 2: LITERATURE REVIEW

2.1 Powder

A powder can be treated as a two-phase system. The powder with particles in various sizes is a dispersed phase. On the other hand, the gas, usually the air, is a continuous phase. The interaction between the two phases can create an expansion of the powder; a common example is the powder fluidization. The stronger the interaction, the higher the powder can expand. However, the powder particles are always trying to return back to the packed state due to the gravities [1].

2.1.1 Powder Characterizations

Although the powders, for example spice powders, medicine powders and gun powders were used for more than hundreds of years, they had not been comprehensively studied until the 20^{th} century. Nowadays, powders become more and more favorable for applications in material transportation, chemical reaction, drug delivery, powder coating and etc. However, problems due to the powder cohesion such like de-fluidization, agglomeration, and de-agglomeration are discovered as great issues for most of the applications. In order to solve these problems, researchers have started to look into the powders' flowability (or flow property), which is an important measurement of how the powder will perform during handling processes.

The flowability of a powder was usually expressed by charts and indices based on the flow behaviors [2]. In 1973, Geldart [3] proposed a powder classification system that classified powders into four groups (A, B, C and D) based on their sizes and densities. This system was presented by the famous Geldart's chart (as in Figure 2-1), which has been widely used in the fields of powder involved industries. Powders belonging to each group were found to

have common fluidization behaviors. Although this correlation was primarily based on empirical observations, it had been helping most of the researchers to quickly predict the flowability of a powder without conducting a large amount of testing works.

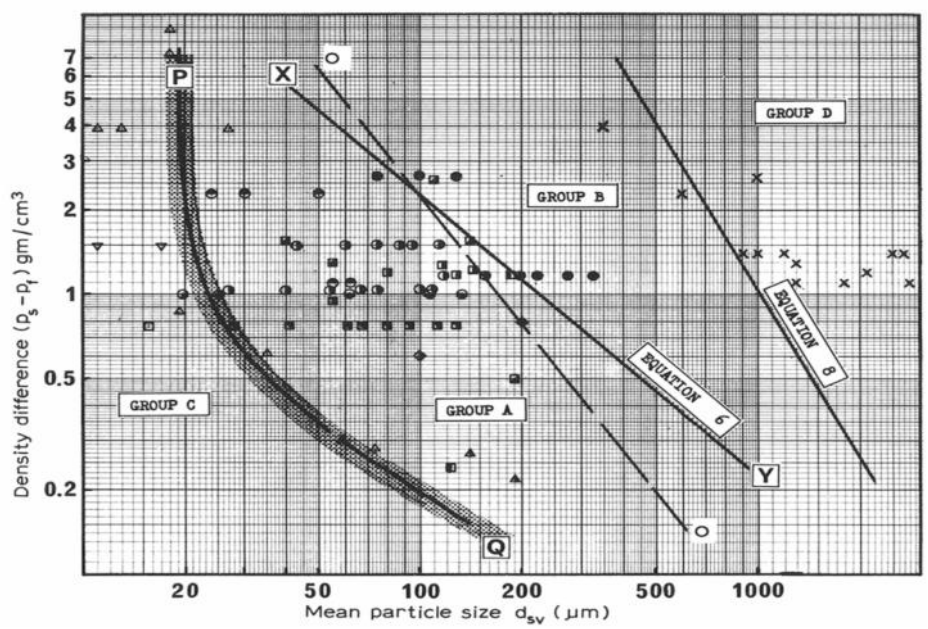

Figure 2-1: Geldart's chart for powder classifications [1]

In addition, Jenike also proposed a classification system that categorized powders into five different groups from "free flowing" to "non-flowing" [4]. This method was based upon the powder's flow function (FF), which analyzed the yield loci from a shear cell. Moreover, Carr suggested ranking the powder flowability by a score combining the results of angle of repose, angle of fall, angle of spatula, uniformity, Carr's cohesion and dispersibility [5]. Similarly, Taylor et al. introduced the idea of composite index to predict powder flow in pharmaceutical applications [6]. Many other analyses for powder flowability had also been developed, but to accurately identify powder flowability was still a difficult task due to the variations between characterization techniques [6-7]. In 2000, Prescott et al. believed that the flow behaviors of a powder should be a multidimensional problem. It should integrate

physical properties of the powders and equipment that used for handling, storing, and/or processing of the materials [8]. Recently, Krantz [9] and Huang [10] confirmed this concept. They resolved the confusion of the flow properties between different powders by using characterization methods in three different powder states: dynamic, dynamic-static and static according to the condition of the powder applications. They also suggested that a universal index or classification should be avoided since it averaged flowabilities of the powders from different stress states that could not fully predict the flow performance across different processes.

2.1.3 Flow Additive for Cohesive Powders

The inter-particle forces, particularly the Van der Waals force, were responsible for the powder cohesion [1, 11]. As particles become smaller and lighter, the gravity forces of the particles are less dominant on the particles' motions. Instead, particles are more subjected to the inter-particle forces. The Van der Waals force F_v between two particles can be expressed in a simplified form [12]:

$$F_v = \frac{AR}{12H^2} \qquad \text{Eq. 2-1}$$

where A is the Hamaker coefficient; R is the particle radius (μm) and H is the separation distance between two particles (μm).

Flow additives which are nano size particles can be used to reduce the powder cohesion so to improve powder flowability [11-12]. They are usually blended with the powder particles by a high shear mixer. As a result, the flow additives or the agglomerations of the flow additives attach to the surfaces of the powder particles acting as spacers [13]. According to Eq. 2-1, the increased separation distance H between the powder particles can reduce the powder cohesion. The flow additives have been commercialized by manufacturers such as

Cabot and Degussa for years. Nevertheless, excessive flow additives in the powders may cause side effects and product defects in some of the applications.

2.2 Powder Coating Technology

Powder coating technology is an application of powders, which was first developed in between late 60's and early 70's [14]. It catered to the strict federal EPA (environmental protection agency) regulations because of the elimination of harmful VOCs (Volatile Organic Compounds). Many industries preferred to use powder coating also because of its ability of recycling the over-sprayed materials.

Powder coating materials can be classified into two categories: thermoplastic and thermosetting. Thermoplastic powder coatings are polymers with high molecular weight, including vinyl, polyester, nylon, polyethylene and so on [15]. As the melting temperature is reached, these materials will transform from solid into liquid so to flow on a surface; as the temperature cools down, they will return to solid so to form coating films. Thermoplastic materials retain their original chemical composition during heating and cooling. When the heating and cooling are re-applied, these materials will start the same transformations again. On the other hand, thermosetting powder coatings do not persist in their original chemical compositions during heating. Instead, they are subjected to cross-linking reactions known as the curing process. Once the cross-linking reactions are complete, the materials will have much higher molecular weight and they cannot be re-melted by the same heating process [16].

The thermosetting powder coatings are the mainstream products in the current market. The cross-linking reaction will not only provide outstanding bonding between the coating and the coating surface, but also better mechanical properties of the coating itself. The thermosetting

powder coatings usually consist of base resin, curing agent, pigment, filler, flowing agent and degassing agent. There are several different thermosetting powder coatings based on their resin types:

Epoxy powder coatings

Epoxy powder coatings have good bonding ability to metal surface, as well as good resistances to corrosion, scratch and impact. They usually provide smooth finish with low risk of having defects such as pinholes and craters due to their low viscosity while melting [17]. However, epoxy powder coatings have poor resistance to UV exposure. Therefore, they are usually limited for indoor applications or as primers for outdoor applications.

Polyester powder coatings

Polyester powder coatings have excellent weatherability. Because they contain polar groups, polyester powder coatings usually obtain better coating performances than others. In addition, they can provide better film quality with higher gloss and less yellowing [16]. Thus, polyester powder coating is favourable for applications on outdoor articles such like air conditioning units and bicycle frames.

Polyester-epoxy powder coatings

Polyester-epoxy powder coatings, also known as hybrid powder coatings, are composed of polyester and epoxy resins. They can benefit from the advantages of both polyester and epoxy resins. The mixing ratio between the two resins can be adjusted to provide desired coating properties according to application criteria.

Acrylic powder coatings

Acrylic powder coatings can provide high gloss finishes with good durability and wetherability. Therefore, they are often used as the top coats, e.g. clear coats. Moreover, acrylic powder coatings are easier to handle in the electrostatic spraying process. However, it has poor compatibility with other types of powder coatings [17].

Polyurethane powder coatings

Polyurethane powder coatings provide excellent smoothness of the coating films due to the low viscosity and long flowing time of the material during curing. They are known to have outstanding bonding to the coating surfaces as well as excellent mechanical properties and chemical resistances. Therefore, they can be utilized as primers.

2.3 Manufacturing Processes for Powder Coatings

A typical processing procedure for producing powder coatings is: ***hot extrusion, grinding, classifying and collecting***. In the following, each of the processes is reviewed in detail.

Hot extrusion

Hot extrusion (or hot melt extrusion) is a classic mixing technique that has been used by the industry for over 70 years [18]. Comparing with other mixing techniques, it is able to mix materials in a much smaller scale due to its high-shear mixing characteristic. The application of hot extrusion process in polymer industry is a long stand. By utilizing this process, polymer materials can be well mixed with additives and other ingredients into a nearly homogenous material with uniform density [19].

Figure 2-2A demonstrates a typical hot extrusion process for powder coatings. In the beginning of the process, dry-mixed raw materials including resin, curing agent, pigment, filler, degassing agent flow agent etc. are first fed into the hot extruder. A hot extruder has

major components including the extruding screw, the heating and the cooling elements. The hot extruder for powder coatings are normally twin-screw extruders with two to three temperature zones. In the first zone, raw materials start to soften at elevated temperature (40-60 ^{o}C) and the twin screws within this zone have large helical treads that push the material forward. The actual mixing begins in the second zone and the temperature is gradually increased to 100-130 ^{o}C. The shapes of the screws in this zone become elliptical with positions shown in Figure 2-2B. In this zone, the softened materials are subjected to high shear mixing during the inter-meshing motion of the screws. It can be an optional third zone for ejecting the mixed material out from the extruder, although the push from the first zone is sufficient in most of the cases. On the other hand, pre-curing of the material can happen during hot extrusion if the temperature inside each zone is not well controlled. Any cured material inside extruder can possibly jam the screws and any ejected pre-cured material will most likely to cause coating defects.

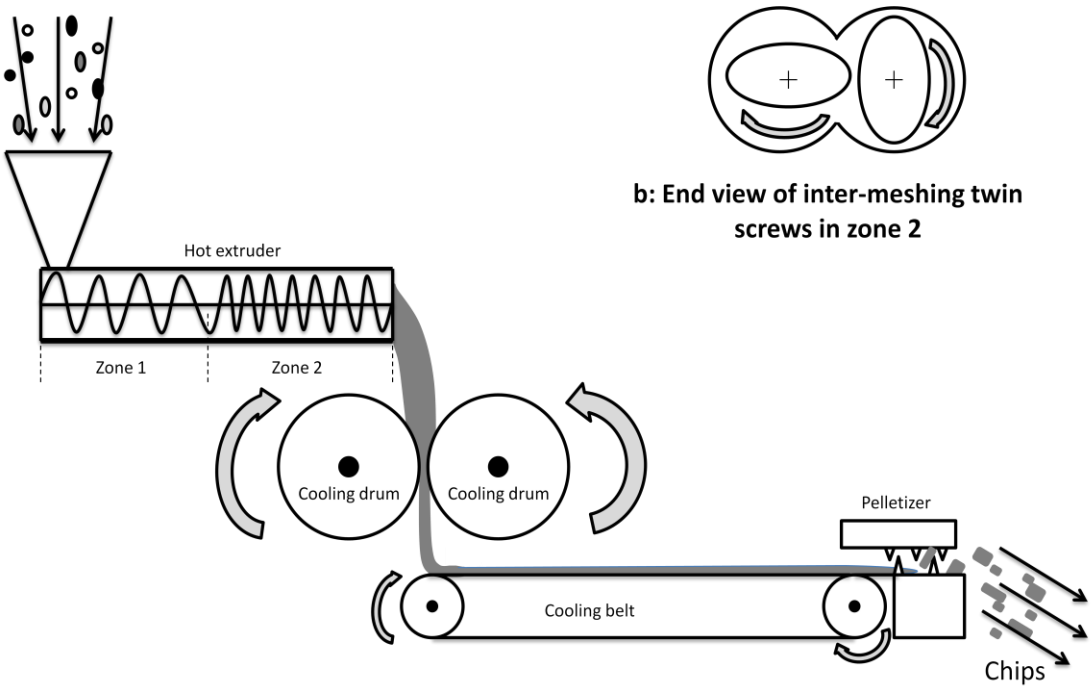

Figure 2-2: A typical hot extrusion process

The mixed material comes from the extruder is in a state of a hot paste. It is then cooled and rolled into a solid thin sheet by two cooling drums followed by a long cooling belt. Finally, the sheet is crushed down by a pelletizer. The end material is called the powder coating chips which is ready for grinding.

Grinding

The grinder for processing powder coatings is a kind of the high speed impact pulveriser. As shown in Figure 2-3, it usually has a rotor with multiple grinding elements placed on the outer edge and a stationary annular wall with vertical grooves. The powder coating chips are fed into the grinding chamber, while the rotor is running at a speed, generally over 110m/s. Due to the impacts, shears and rubbings between the rotating pins and the standing grooves, the chips will be finally broken into powders.

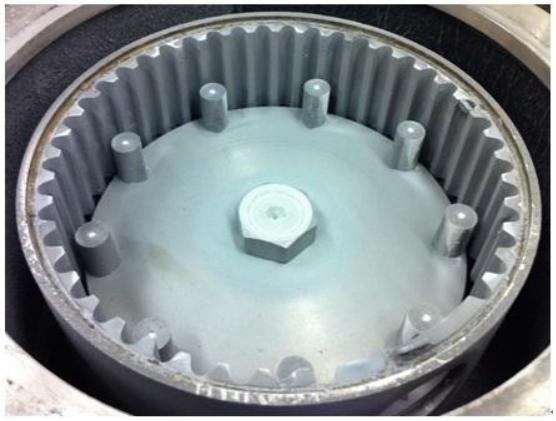

Figure 2-3: A grinder mill for powder coating

Three major theories were developed and used for the correlations between comminution and the comminution energy: (1) Rittinger, in 1867, proposed that the comminution energy was proportional to the increased surface areas. Because the comminution energy had to increase as the particle size became smaller, so as the specific surface area became much larger [20-21]. (2) Kick, in 1885, believed that the comminution energy was used to deform

the material. Once the limit of the deformation was reached, the material started to break up. Therefore, the comminution energy was only proportional to the volume or mass of the material, but not the size [20-21]. (3) Bond, in 1952, stated that material had to break down from cracks. While the external force was acting on the material, internal deformation generated cracks at any weak spot. Afterward, the stresses would concentrate at the crack tip causing further propagations, and finally, the material would split into pieces. He suggested that the comminution energy should be inversely proportional to the square root of the diameter of the material [20-21]. These three theories are complementary to each other. Generally, Kick's theory is suitable for the initial stage of the comminution process, since the deformation of the material is large and the volume of the material increases more remarkable. Bond's theory can then be applied in the second stage, when cracks begin to form. Eventually, Rittinger's theory could be followed due to the largely increased surface area [22].

Classifying

Classifying is the most crucial process for adjusting particle size of a powder coating especially fine powder coatings and it is more effective than ordinary sieving process since the agglomerations caused by the powder cohesion can be broken up by the pneumatic energy. There are various types of classifier including the gravitational classifier or the centrifugal classifier of cross-flow or counter-flow, cascade classifiers, rotor classifiers and circulating air classifiers [23]. The most popular classifier for powder coatings is the centrifugal classifier with counter-flow. Shown in Figure 2-4, particles driven by the air stream enter the classifier and they soon encounter the high-speed classifying rotor that has a number of vanes. Only particles that are small enough can pass through the classifying rotor, whereas the large particles are rejected. Particles that do not pass through the classifier are collected from the bottom of the classifier for further processing.

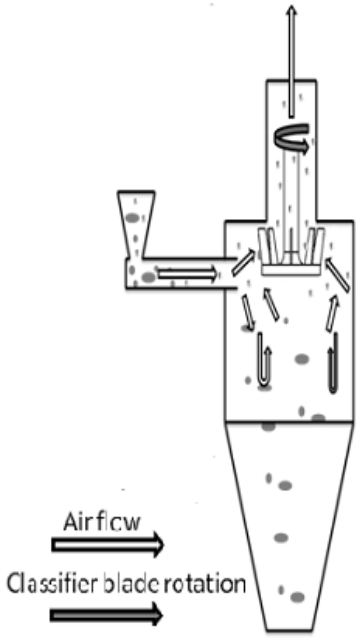

Figure 2-4: A classifier for powder coating

In the space between the classifier vanes, two forces are acting on a particle: the centrifugal force and the drag force indicated by F_c, and F_d in Figure 2-5. The F_c is caused by the spin of the particle around the shaft and the F_d is the drag force generated by the driving air. If these two forces are equal, the particle is in equilibrium. So then the size of the particle is called the cut-size of the classifier. The drag force will be larger, if the particle is smaller than the cut-size; and the centrifugal force will be larger, if the particle is bigger than the cut-size. The cut-size can be varied by enhancing or weakening the centrifugal force on the particle caused by the increasing or decreasing the rotating speed of the vanes accordingly. On the other hand, the cut-size can be carried by changing the air velocity. Increased or decreased air velocity generated larger or smaller drag force on the particle so to increase or reduce the cut-size.

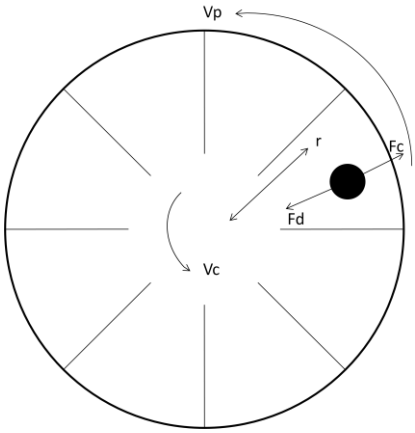

Vp: rotational velocity of the particle; Vc: rotational velocity of the classifier blade;
r: distance from the center of the blade to the particle.

Figure 2-5: Forces acting on particle within a rotating classifier (Top view)

In the real world, the forces acting on the particles are not as simple as the theory. The influences from air velocity gradients, turbulences and eddies are all needed to be considered. For example, eddies generated by the air flowing through the previous vanes can disrupt the particles being classified. As a result, large particle can possibly be driven deeper inside the vanes causing slower circumferential velocity of the particle. Therefore, the centrifugal force will be smaller and the particle will have a higher chance to be carried away by the escaping air flow. On the other hand, small particle can possibly be ejected away due to the transient out-ward drag induced by the turbulences. All these factors are going to affect the cut-size of the classifier. The escaped large particles and ejected small particles will increase the particle size distribution of the classified powder.

Collecting

Collecting is a necessary process because the powder coatings have to be separated from the air after pneumatic transportations. In a mass production of powder coatings, it is always accomplished by a cyclone, which is a classic separator invented in 1800's [24]. Cyclone is popular to use because of its low maintenance and low capital cost. Demonstrated by Figure

2-6, a typical cyclone for powder coating manufacture has a tangential inlet, a cylindrical barrel, a vortex finder, a cone and a solid outlet. Particles enter the cyclone due to the negative pressure at the air outlet. They then flow spirally against the inner wall of the cyclone towards the solids outlet under the combination of centrifugal and gravity forces. But then, the majority of the air that entered with the particles escapes through the vortex finder, while the rest of the air is flowing with the particles along the cyclone creating an "outer vortex" [25-27]; however, the velocity of the air becomes smaller as it moves further down the way. Eventually, the suction at the air outlet will turn the air upward and the air flows spirally towards the vortex finder forming an "inner vortex" in the middle of the cyclone. In the mean time, the inner vortex will carry away some of the air from the outer vortex, known as a horizontal inward drift [25-27].

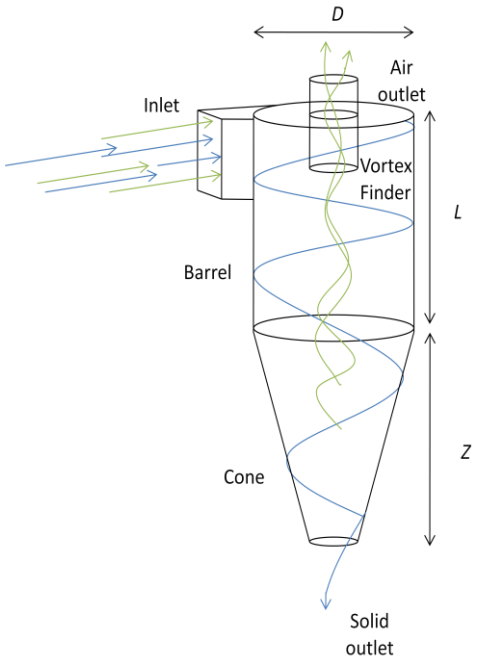

D: diameter of the cyclone barrel; L: length of the cyclone barrel;

Z: length of the cone

Figure 2-6: A typical cyclone for collecting powder coatings

Many studies of cyclones by pioneer researchers were conducted to understand the mechanism of cyclone [24-41]. In 1979, Leith discovered that the spinning gas stream is the key factor to separation particles from the air in a cyclone due to the centrifugal effect [41]. Numerical studies disclosed that particles, on a cross-section of the cyclone, were thrown to the cyclone wall orbiting around the center axis. In addition, the inner air flow moving towards the vortex finder could create inward drag on the particles along the inner cyclone wall [25-27]. Furthermore, previous studies were also focused on the collection efficiency of cyclone [28-40]. They pointed out that the reduced collection efficiency of a cyclone was mainly due to the loss of particles.

Ideally, a cyclone has a theoretical cut-size shown as the solid vertical line in Figure 2-7. If particles smaller than the cut-size, the collection efficiency of the cyclone is 0% since all the particles are removed by the drag from the air flow; and the collection efficiency is 100% for particles that had particle sizes larger than the cut-size because the gravity and centrifugal forces are dominant. However, the real characteristic of a cyclone follows the S-shape curve shown as the dotted line in Figure 2-8 [28]. Stairmand found that smaller particles could agglomerate into larger and heavier clusters [28]. These clusters were no longer dominated by the air drag but retained inside the cyclone just like the larger particles. Furthermore, the smaller particles may also attach to the large particles by inter-particle forces. Therefore, the collection efficiency of the powders that had particle sizes below the cut-size was always higher than 0%. On the other hand, large particles could escape through the inner vortex due to the effects of turbulences, eddies and bounces. The collection efficiency above the cut-size could hardly be 100%.

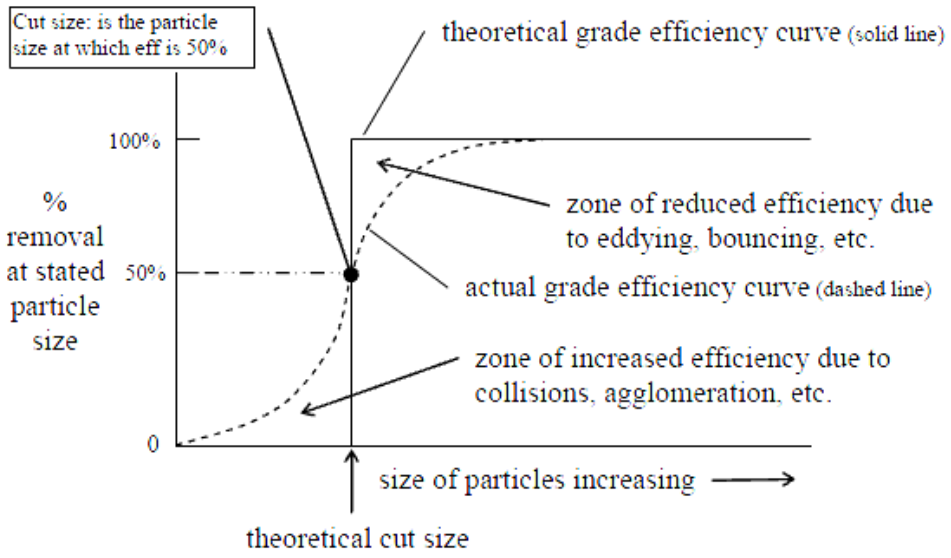

Figure 2-7: Diagram of grade efficiency curve characteristics [27].

For powder coatings, especially fine powder coatings, the escape of the small particles from the cyclone is desired since the small particles can cause powder cohesion. However, the current cyclone designs have no selectivity on the particle size. As stated above, the large particles always escaped with the small particles causing low collection efficiency of the cyclone. A cyclone design which can selectively remove small particles will be beneficial to the powder coating productions.

The air classifying mill

In a powder coating plant, the processes of grinding, classifying and collecting can be integrated into one stage operation. It is achieved by the fully automated machine called the air classifying mill (ACM) shown in Figure 2-8. A continuous ACM operation is much less labour intensive and time consuming comparing with the stage operations for each of the processes.

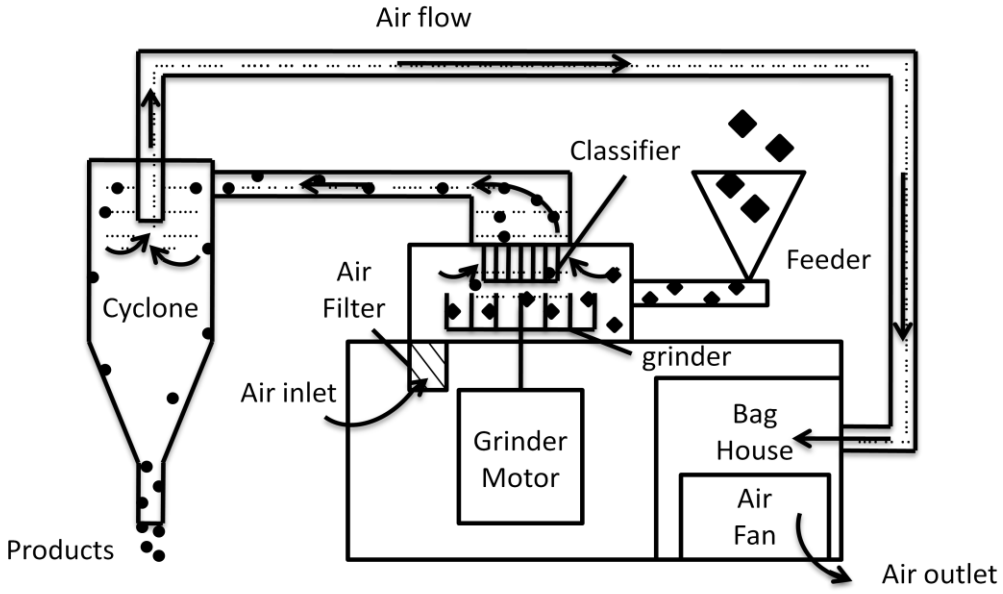

Figure 2-8: A typical air classifying mill (ACM) operation

During an ACM operation, air velocity, grinder speed, feeder speed and classifier speed are usually the four operating parameters [42]. The air velocity influences the collection efficiency of the system. That is because a higher air velocity can increase the centrifugal forces on the particles inside the cyclone. On the other side, the air velocity can influence the classifying efficiency as well. More importantly, the high air flow inside the ACM can help to reduce the temperatures from the moving components. To produce powder coatings with finer particle sizes, classifier speed and/or grinder speed need to be increased. Other than that, lowering the feeder speed and/or the air velocity can also help to reduce the powder sizes. Overall, the performances of an ACM can be fully adjusted by the operating parameters according to the grinding materials and the required particle sizes of the produced powders. Therefore, trials are always conducted prior to the production of a powder coating by the ACM.

2.4 Application of Powder Coatings

The conventional liquid paints usually require large amount of solvent for suspending or dissolving their ingredients. It can be brushed or sprayed onto a surface in thin layers and the materials will eventually dry to form a solid coating film. In contrast, powder coatings are more difficult to apply, since they are all solid particles which do not involve in any liquid. There are two issues that have to be considered during powder coating applications: applying evenly on the coating surface and melting of the particles to form a continuous coating film. Many techniques were invented for powder coating applications and they have been refined for decades. Some typical examples of the powder coating techniques currently used in the industry are reviewed in the following.

Thermal spraying

Thermal spraying process is to soften and melt the powder particles during spraying. Figure 2-9 shows a diagram of a thermal spray gun. Initially, the cold compressed air is heated up by flowing through a heat source. When the powder particles encounter the hot air, they become softened and finally molten. And then, the molten particles impact on the surface to build up a coating film.

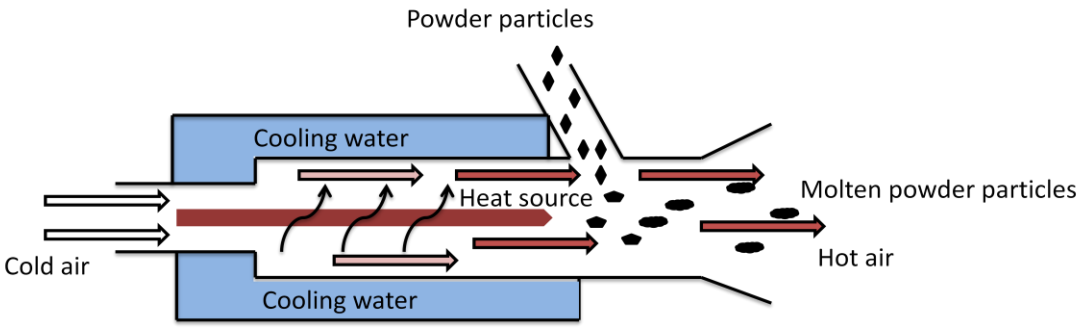

Figure 2-9: A thermal spraying gun

Thermal spraying was the first technique that developed for powder coating application back in late 1940s [43] and it is still being used in the industry nowadays. Thermal spraying can provide coatings with thickness up to few mm. In addition, this application can be used onsite since it does not require additional heating process for curing. However, the heating of the powder is difficult to be well controlled. Therefore, it is more suitable for application of thermal plastic materials. In addition, the resulting coating surface is rough and the bonding between the coating and the surface is low.

Fluidized bed coating

The fluidized bed application for powder coating came out few years later after the development of thermal spraying. It was patented by a German scientist Gemmer in 1955 [44]. Unlike the thermal spraying, the powder particles stay in room temperature during the application. Instead of heating up the particles, the parts are pre-heated in this case. As shown in Figure 2-10, the particles will begin to soften and adhere on the part when the pre-heated part is dipped into the fluidized bed. Eventually, the coating part will be conveyed to an oven for baking so to obtain the final coating.

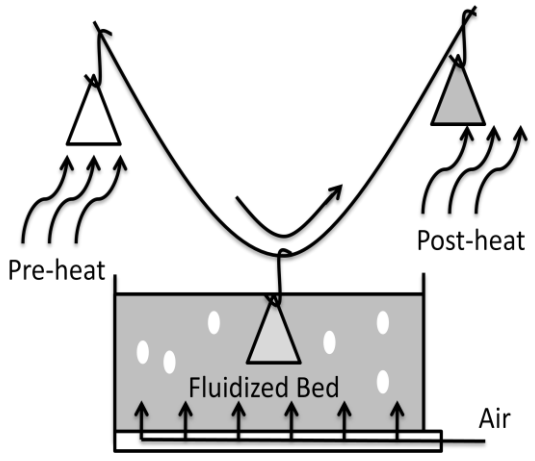

Figure 2-10: A fluidized bed application of powder coating

The fluidized bed application can provide coatings with thickness between 150 to 500 μm [43]. Comparing with thermal spraying, fluidized bed application provides improved coating quality overall because of the reduced film thickness and the better control of the heating. It can be used for both thermoplastic and thermosetting materials. Nowadays, electrostatic charge to the parts can be used to replace the pre-heating process for better attractions of the particles. This application method is mainly used for coatings with purposes of electrical insulation, corrosion resistant and abrasion resistant. It still cannot be used for applying the decorative powder coatings due to the relatively thick film and rough coating finish.

Electrostatic spraying

Electrostatic spraying developed by Pieter was first introduced to the industry in around 1963 [45]. In this application process, powder particles are charged and they are deposited on the surface layer by layer. Since the coating part is grounded, the electrostatic forces can firmly hold the charged particles on the part before baking. Comparing with other application methods, electrostatic spraying can provide coating film with thickness less than 100 μm, leading to significantly improved coating finishes. Nowadays, majority of the decorative powder coatings are applied by electrostatic spraying. There are two types of electrostatic spraying that are commonly used: the corona charge spraying and the Tribo charge spraying.

Corona charge spraying is the most popular way to apply powder coating because of its high coating efficiency. As demonstrated by Figure 2-11, corona charge spraying is applied by a corona spray gun. The spray gun has an external high voltage supply that connects to the tip electrode inside the spraying nozzle. During spraying, negative voltage, normally between -30 kV to -100 kV, is applied to the tip electrode. The high voltage discharged at the electrode tip can ionize the surrounding air, creating free electrons. This phenomenon is

known as the corona discharge. The free electrons will attach to powder particles as the particles are sprayed out from the gun and the particles with the attached free electrons will obtain negative charges. In addition, the corona discharge does not only create free electrons but also a strong electrostatic field between the electrode and the grounded part. As a result, the charged particles are subjected to both aerodynamic forces and electrostatic forces when they are sprayed out from the gun [45]. As they move closer to the part, in a distance within approximate 10mm, the electrostatic forces dominate [46]. Therefore, most of the charge particles in the area will be directed to the surface being coated.

For parts with complex geometries, the electrostatic field does not penetrate into the recessed areas of the coating surface; instead, they will concentrate along the edges and corners due to the Faraday Cage effect. Consequently, the coating tends to build up at the edge and the recessed area can hardly be covered by the powder particles. For that reason, corona charge spraying is not favorable to use if the coating parts that have complex geometries.

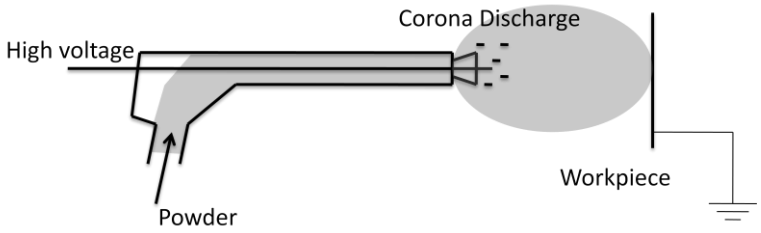

Figure 2-11: A corona charge spraying

Tribo charge spraying has a different charging mechanism from corona charge spraying. As shown in Figure 2-12, there is not external voltage supply to the tribo spray gun. However, there are baffles, with a lower dielectric constant than that of the powder coatings, placed inside the gun barrel. While particles are flowing through these baffles, the intense friction

between the particles and wall surfaces create positive charges due to the differential of the dielectric constants between the two materials. The advantage of the design is that it eliminates the electrostatic field between the gun and the part. Thus, it can avoid Faraday Cage effect so to provide better coating coverage on the recessed areas. Nevertheless, the performance of the tribo charge spraying can be easily influenced by factors such as humidity, surface condition and powder properties. Furthermore, the deposited powder layer has less adhesion to the surface comparing with corona charge spraying since the charging of the particles is less [47-50].

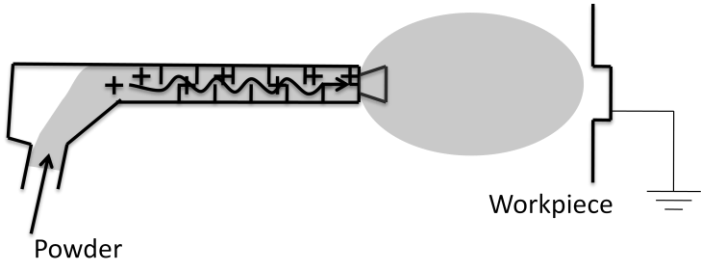

Figure 2-12: A tribo charge spraying

2.5 Fine Powder Coating - the Future of Powder Coating Technology

Powder coating has been well known for its advantages of no VOC emission and the recyclability of over-spray materials. This coating technology has been developed for many years. Recently, it becomes to the fastest growing finishing industry in North America, Europe and Asia [16, 43]. However, powder coating still cannot thoroughly replace the conventional liquid paints. The main restriction is the coating quality. A regular powder coating (also known as coarse powder coating) has its medium particle size between 35 and 60 μm. It usually provides noticeable coating roughness often referred to “orange peel”. In recent years, automotive industry started to develop fine powders with medium particle size less than 30 μm. Since then, powder coatings were not just for coatings on the under-hood

parts but also the surfaces of car bodies which had much higher aesthetic requirements. General Motor and Chrysler now utilize powder coatings for their primer coatings in 13 plants across North America [51]. BMW also applies powder clear coatings on their 5 and 3 series sedans [52]. On the other hand, researchers have been continuing to study fine powder coatings from the aspects of its material properties, flow characteristics and spraying characteristics [9-10, 13, 42, 53-54]. Moreover, Zhu and Zhang patented an ultrafine powder coating technology which was capable of utilizing powder coatings with medium particle sizes less than 20 μm [55].

Fine powder coating is the future of powder coating technology and it can create a large potential for expanding the current market share. However, applications of fine powders have encountered many problems so far. It is realized that the development of the fine powder coating requires efforts not only on material itself but also on the manufacturing processing and application methods. Extensive studies on powder coating processes and other relative topics are demanded to provide more comprehensive solutions for the refinement of fine powder coatings.

Reference

[1] Rietema K., 1984, Powders, what are they?. *Powder Technology*, 37, 5-23.

[2] Schwedes J., 2003, Review on testers for measuring flow properties of bulk solids, *Granul. Matter*, 5, 1-43

[3] Geldart D., 1973, Types of gas fluidization, *Powder Technology*, 7, 285-292.

[4] Jenike AW., 1961, Gravity flow of bulk solids, Bulletin 108, Engineering Experiment station, University of Utah.

[5] Carr R.L., 1965, Evaluating flow properties of solids, *Chemical Engineering*, 18, 163-168

[6] Taylor M.K., Ginsburg J., Hickey A., Gheyas F., 2000, Composite method to quantify powder flow as a screening method in early tablet or capsule formulation development, *AAPS PharmSci Tech*, 1(18).

[7] Ploof D.A., Carson J.W., 1994, Quality control tester to measure relative flowability of powders, *Bulk Solids Handling*, 14(1), 127-132.

[8] Prescott J.J., Barnum R.A., 2000, On powder flowability, *Pharm. Technol.*, 24, 60-84.

[9] Krantz M., Zhang H., Zhu J., 2009, *Characterization of powder flow: static and dynamic testing*, Powder Technology, 194(3), 239-245.

[10] Hang Q., Zhang H., Zhu J., 2010, Flow properties of fine powders in powder coating, *Particuology*, 8(1), 19-27.

[11] Kendall K., Stainton C., 2001, Adhesion and aggregation of fine particles, *Powder Technol.*, 121, 223-229.

[12] Visser J., 1989, An Invited Review: Van der Waals and Other Cohesive Forces Affecting Powder Fluidization, *Powder Technology*, 58, 1-10.

[13] Fu J., Krant M., Zhang H., Zhu J., Kuo H., Wang Y.M., Lis K., 2011, Investigation of the recyclability of powder coatings, *Powder Technolog*.

[14] Hardy R.D, Seitz J.W., 1974, Energy Savings with Powder Coating, *Society of Manufacturing Engineers*, FC74-589.

[15] Richart D., 2001, Powder Coating Process, in Kirk-Othmer Encyclopedia of Chemical Technology, John Wiley & Sons, published online, 7, 35-68.

[16] Bocchi G.J., 2006, Join with PCI to improve powder coating community, *Products Finishing*, 70(6), 73-74.,

[17] Liberto N.P., 2003, *Users Guide to Powder Coating, 4th Edition*., Society of Manufacturing Engineers.

[18] Charlie, M., 2008, Continuous Mixing of Solid Dosage Forms via Hot-Melt Extrusion, *Pharmaceutical Technology*, 32(10), 76-86.

[19] Particle Sciences, 2011, Hot Melt Extrusion, *Technical Brief*, 3.

[20] Li Q.H., 1993, Outlines of The crush theory, *Metallurgical Industry Press*, 36-49.

[21] Zhao M., Lu Y.P., Pan Y.M., 2001, The crush theory and the development of crash equipments, Mining and Metallurgy, (6), 36-41.

[22] Mu F.S., 2006, Current Status and Development Requirements for Research of Theory of Crushing, Sulphur Phosphorus & Bulk Materials Handling arelated Engineering, 4, 20-23

[23] Shapiro M., Galperin V., 2005, Air classification of solid particles: a review, Chem. Eng. Process, 44, 279-285.

[24] Dirgo J., Leith D., 1985, Cyclone Collection Efficiency: Comparison of Experimental Results with Theoretical Predictions, *Aerosol Science and Technology*, 4(4), 401-415.

[25] Xiang R.B., Lee K.W., 2004, Numerical study of flow field in cyclones of different height, *Chemical Engineering and Processing*, 44, 877-883.

[26] Su Y.X., Zheng A.Q., Zhao B.T., 2011, Numerical simulation of effect of inlet configuration on square cyclone separator performance, *Powder Technology*, 210, 293-303.

[27] Bhasker C., 2010, Flow simulation in industrial cyclone separator, *Advances in Engineering Software*, 41, 220-228.

[28] Stairmand C.J., 1951, The Design and Performance of Cyclone Separators, *Transactions Institution of Chemical Engineers*, 29, 256-373.

[29] Lim K.S., Kim H.S., Lee K.W., 2004, Characteristics of the collection efficiency for a cyclone with different vortex finder shape, *Journal of Aerosol Science*, 35, 743-754.

[30] Akiyama T., Marui T., 1989, Dust Collection Efficiency of a Straight-Through Cyclone-Effects of Duct Length, Guide Vanes and Nozzle Angle for Secondary Rotational Air Flow, *Powder Technology*, 58, 181-185.

[31] Trasl P.R., Licht W., 1984, Effect of Recycle on Cyclone Performance, *Ind. Eng. Chem. Process Des. Dev.*, 23, 479-482.

[32] Lee J.W., Yang H.J., Lee D.Y., 2006, Effect of the cylinder shape of a long-coned cyclone on the stable flow-field establishment, Powder Technology, 165, 30-38.

[33] Hffmann A.C., Santen A.V., Allen R.W.K., 1992, Effects of geometry and solid loading on the performance of gas cyclones, *Powder Technology*, 70, 83-91.

[34] Qian FP., Zhang J.G., Zhang M.Y., 2006, Effects of the prolonged vertical tube on the separation performance of a cyclone, *Journal of Hazardous Materials*, B136, 822-829.

[35] Ray M.B., Luning P.E., Hoffmann A.C., Plomp A., Beumer M.I.L., 1998, Improving the removal efficiency of industrial-scale cyclones for particles smaller than five micrometre, *Industrial Journal of Mineral Processing*, 53, 39-47.

[36] Swamee P.K., Aggarwal N., Bhobhiya K., 2009, Optimum Design of Cyclone Separator, *AIChE Journal*, 55(9), 2279-2283.

[37] Ingham D.B., Ma L., 2002, Predicting the performance of air cyclones, International *Journal of Energy Research*, 26, 633-652.

[38] Ji Z.L., Xiong Z.Y., Wu X.L., Chen H.H., Wu H.X., 2009, Experimental investigations on a cyclone separator performance at an extremely low particle concentration, *Powder Technology*, 191, 254-259..

[39] Rong R., Napier-Mum, T.J., 2003, Development of a Efficient Classifying Cyclone, *International Journal of Coal Preparation and Utilization*, 23(4), 149-165.

[40] Tong Z.B., Yang R.Y., Chu K.W., Yu A.B., Adi S., Chan H.K., 2009, Numerical study of the effects of particle size and polydispersity on the agglomerate dispersion in a cyclonic flow, Chemical Engineering Journal, 164, 432-441.

[41] Leith D., 1979, In *Handbook of Environmental Engineering*, (N.C. Pereira and L.K. Wang, eds.). Humana Press, Clifton, N.J., I, 61.

[42] Krantz M., 2009, Powder Characterization and Powder Application in Automobile Coatings, *Master Thesis at The University of Western Ontario*, Charpter 6.

[43] "A history of powder coatings", 2004, Powder & Coatings Industry Magazine, http://www.pcimag.com/articles/a-history-of-powder-coatings.

[44] Gemmer E., 1955, *Patent 933019*.

[45] Bailey A.G., 1998, The science and technology of electrostatic powder spraying, *Transport and Coating J. Electrostat.*, 45, 85-120.

[46] Cross J.A., 1987, *Electrostatics: Principle, Problems and Applications* (Bristol: Hilger).

[47] Mayr M.B., Barringer S.A., 2006, Corona compared with triboelectric charging for electrostatic powder coating, *J food Sci. (JFS) E: Food Eng. Phys. Prop*, 71, 171-177.

[48] Kleber W., Makin B., 1998, Tribo electric powder coating: a particle approach for industrial use, *Particul. Sci. Technol*, 16, 43-53.

[49] Trigwell S., Biris A.S., Sims R.A., Mazumder M.K., 2008, Effects of powder velocity and contact materials on tribocharging of polymer powders for powder coating applications, *Particul. Sci. Technol*, 26, 145-157.

[50] Kleber W., Makin B., 1998, Tribo electric powder coating: a particle approach for industrial use, *Particul. Sci. Technol*, 16, 43-53.

[51] Gribble P., 2003, Development Status of Powder Coatings for OEM Automotive Applications, *Finishing Today*.

[52] Biller K., 2006, OEM Automotive Powder Coatings, *Finishing Today*.

[53] Zhu J. Zhang H., 2005, Ultrafine powder coatings: an innovation. Powder Coat, 16, 39-47.

[54] Fu J., 2010, Study on powder coating particles and development of new powder coating application methods, Master Thesis, The University of Western Ontario.

[55] Zhu J., Zhang H., 2004, Fluidization additives to fine powders, US Patent 6833185.

SECTION Ⅰ

CHARACTERIZATION OF FINE POWDER FLOWABILITY

This section of the thesis study focused on the flow characteristics of the fine powder coatings. It revealed the drawbacks from the current characterization methods for fine powder coatings and it provided suggestions of improving such methods.

CHAPTER 3: THE INVESTIGATION ON FLOWABILITY CHARACTERIZATION OF FINE POWDER COATINGS

3.1 Introduction

Powder coating is a popular coating process because of its advantages of zero VOCs (volatile organic compounds) emission and recyclable over-sprayed materials [1]. In past decades, powder coating (medium size above 35 μm) has been widely used for applications from furniture painting to automobile under-hood parts [2]. The main drawback of powder coatings is their rough coating finishes identified by the textures of "orange peel" due to the large surface waviness caused by the relatively coarse particle sizes [3]. Recently, powder coatings tend to be utilized on high-end products that have much higher aesthetic requirements. Therefore, better coating qualities are demanded for powder coatings.

Fine powder coatings (medium size less than 30 μm) can be used for improving the quality of the coating films [3]. The smaller powder particles can essentially reduce the film thickness and the surface waviness of the coating. According to Geldart's classification [4-5], fine powder coatings belong to group C powder, which are cohesive powders. The cohesion is caused by the inter-particle forces, mainly the Van der Waals force [6]. A powder particle is under a balance of the gravity force and the inter-particle force. As the particle size decreases, the gravity of the particle becomes less significant and the inter-particle force dominant [7]. Therefore, application of the fine powder coatings is more difficult than regular size powder coatings.

In order to reduce the powder cohesion, flow additives, which are nano size particulates, are usually utilized for fine powder coatings [8]. They can be blended with the powder particles by a high shear mixer. After the blending, the flow additives or the agglomerations of the

flow additives strongly attach to the surfaces of the powder particles acting as “spacers”. Based on the study from Visser, the Van der Waals force which was the main inter-particle force could be expressed in a simplified form [6]:

$$F_v = \frac{AR}{12H^2} \qquad \text{Eq. 2-1}$$

where A is the Hamaker coefficient; R is the particle radius (μm) and H is the separation distance between the particles (μm). According to Eq. 2-1, the increased separation distance H by the “spacers” can reduce the powder cohesion. Nevertheless, excessive flow additives in the powders can cause coating defects such as seeds and gloss reduction.

Nowadays, fine powder coatings started to be applied in many industries [9-10]. During applications, the flowabilities of fine powder coatings, which indicate how well the fine powders can be handled, are experienced to be unstable. Powder manufacturers ensure the flowabilities of the produced fine powder coatings mainly based on the particle size, since the powder cohesion of fine powders was caused by the reduced particle size. However, flowability issues are often encountered during fluidization, pneumatic transportation or spraying even though the particle sizes of the fine powder coatings have been well controlled.

This part of the thesis study was to discover the experienced problem stated above and the flowability characterization of fine powder coatings was investigated. The flowability characteristics of the fine powder coatings with respect to several factors were examined. Suggestions on flowability characterization of fine powder coatings are provided to help better ensure the flowabilities of fine powder coatings for applications.

3.2 Materials and Methods

There were 31 fine powder samples prepared for this study. They were all ground from the polyurethane based powder coating chips supplied by Seibert Powder Coatings, Cleveland, USA. The samples had medium sizes in the range from 18 to 29 μm. Several samples were made in each of the size cuts (the difference between each size cut was 1 μm). Since the preparation procedure was similar to the industrial process, these samples can be used to simulate the fine powder coatings in the real applications.

Fluidizations of the fine powders have to rely on flow additives [6, 12, 14]. However, this study would like to minimize the influences from the flow additives since the flow additives could reduce the differences in flowabilities between the samples. Only 0.3 wt% of flow additive (AEROSIL ® R972 Fumed Silica) was blended into each sample for obtaining a basic fluidization. The 31 samples were divided into two groups, where group 1 samples had medium sizes between 18 and 23 μm and group 2 samples had medium sizes between 23 and 29 μm. In this way, the flowabilities of the relatively larger or smaller samples could be either analyzed individually or combined for comparisons.

3.2.1 Flowability Measurements

The flowabilities of the samples were evaluated by the combination of two methods: rotational bed expansion ratio (RBER) and avalanche angle (AVA).

The RBER was measured by the revolution powder analyzer (Mercury Scientific Inc., Sandy Hook, CT, USA). The test requires 120 ml of powder (tapped volume) in a rotational drum (diameter of 10.9 cm and width of 3.5 cm). An electric motor rotates the drum at various speeds. As rotating speed of the drum gradually increased, more air enters into the powder

and volume of the powder expands. In order to measure how well the powder fluidizes, the volumetric expansion ratio (expanded powder volume divided by the initial powder volume) can be obtained by a computer with the video camera. The speed of the rotational drum for measurements was set at 60 rpm in the case of this study. At a certain rotating speed, the powders would be spun to the wall of the drum due to the centrifugal effect. Generally, a larger RBER implies a better fluidization. Comparing with the conventional fluidized bed method, RBER method seals the powder inside the drum during testing so as to avoid the loss of particles. Moreover, moisture of the powder, which is possible to affect the powder flowability, can be persisted inside the closed drum as well. Finally, real-time video of the expansion progress can be observed from the computer screen ensuring the accuracy of the process.

The AVA was also measured by the revolution powder analyzer. The procedure of the sample preparation is the same as for the RBER. However, the drum rotates at a much lower speed in this test, which is 0.6 rpm. During the measurement, the powder rotates with the drum under friction. At an angle which the inter-particle forces cannot sustain the weight of the powder, the powder collapses. The angle is then obtained by the camera known as the AVA. The AVA is averaged from 200 readings. A smaller AVA implies a better flowability. The AVA method is more stable than the similar angle of repose method because of the more accurate reading and the fully automatic operation.

Between the two methods, the RBER represents the dynamic powder flowability whereas the AVA represents the more static powder flowability [15-16]. The dynamic flowability indicates how well the powder will flow in fluidization and pneumatic transportation. On the other hand, the more static flowability indicates how easy the powder will get agglomerated

or accumulated. Previous studies found that characterizations from aspects on both dynamic and static are necessary to fully obtain the powder flowability [15-16].

3.2.2 Particle Size Measurement

The particle sizes of the samples were measured by a laser diffraction size analyser (Model BT-9300S, Better Size Laser Analyser, China). The main parameters obtained from the measurements were D_{10}, D_{50} and D_{90}, where the D_{50} was reported as the median size of the volume distribution meaning half of the particles were smaller than the D_{50} value. Similar to D_{50}, 10% of the particles were smaller than D_{10} value, while 90% of the particles were smaller than D_{90} value.

D_{10}, D_{50} and D_{90} obtained from the laser diffraction measurement can be used to evaluate the basic particle size distribution of the powder. For example in Figure 3-1, the D_{10}, D_{50} and D_{90} were marked on the particle size distribution curve. If the D_{10} and/or D_{90} were closer to the D_{50}, the curve would be steeper. As the three values became equal, the powder would have all uniform size particles.

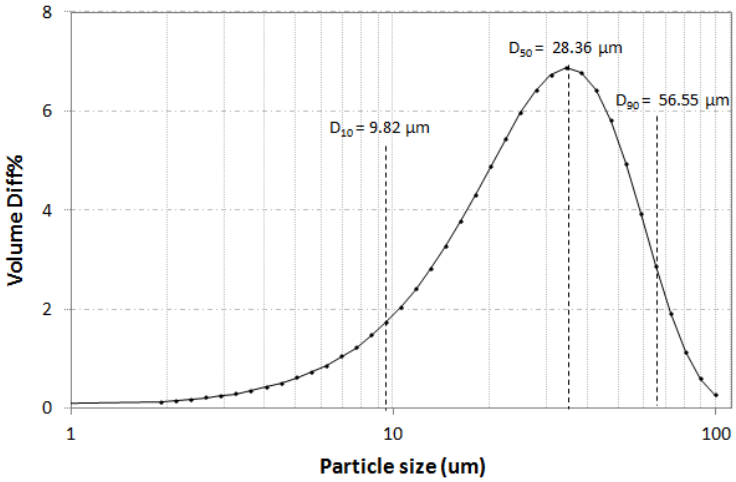

Figure 3-1: An example of particle size distribution (D_{10}: 9.82 µm, D_{50}: 28.36 µm, D_{90}: 56.55 µm)

3.3 Results and Discussion

The particle size was always a crucial parameter to judge the flowability of the powder. Geldart, in 1973, discovered a well known powder classification system based on the densities and sizes of powders [13]. The system classified powders with sizes ranging from 20 to over 1000 μm into Group A, B, C and D which denoted “aeratable”, “bubbly-ready”, “cohesive” and “different”.

For regular size powder coatings, the threshold of the medium sizes, D_{50}, is 30 μm. According to Geldart’s classification, powder coatings with D_{50} larger than 30 μm were the Group A powders and they should not have flowability issues during applications. However, fine powder coatings, which were designed for better coating qualities, had D_{50} smaller than 30 μm and they were classified as the Group C powders. As a result, the flow behaviour of the powders changed from “areatable” to “cohesive”. For fine powder coatings, the flowability became less predictable by the D_{50}. According to the collaborative research with General Motor, the fine powder coating primers that had similar D_{50} exhibited diverse flow behaviours during pneumatic transportation and spraying. It implied that the conventional method of using a threshold of D_{50} was not appropriate for ensuring the flowabilties of fine powder coatings.

In this study, 31 powder samples were made to simulate fine powder coatings with various D_{50}. The flowability characterization of the powder samples were investigated with respect to their D_{50} as shown in Figure 3-2. The trend of the results indicated that the AVA reduced and the RBER increased as the D_{50} of the powder became larger. It implied that the flowability of the powder was improved with the increasing D_{50}. However, the measured flowabilities were found inconsistent with respect to the D_{50}. The AVA and RBER of both group 1 and group 2 samples were scattered for each size cut. The large variations between

the flowabilities of the samples coincide with the findings from the industrial applications that powders with similar D_{50} performed differently. It confirmed that the D_{50} could help to recognize the flowability of a fine powder coating in general, but it could not be used for ensuring the flow performance of a fine powder coating during applications.

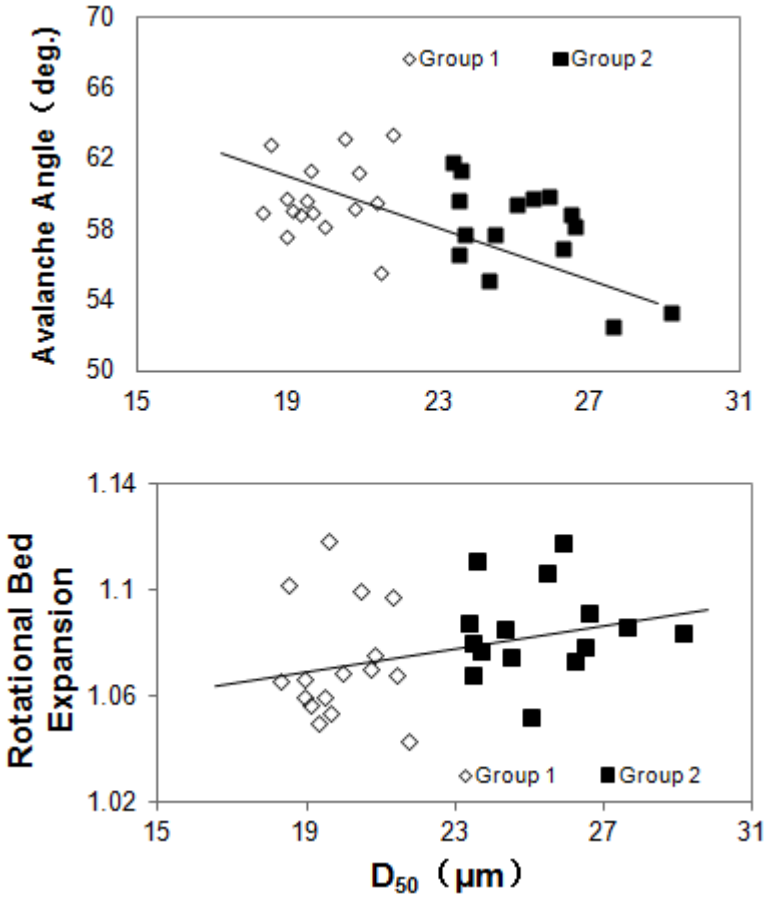

Figure 3-2: Flowabilities of the fine powder samples with respect to D_{50}

A part of the contribution to the scattered flowabilities shown in Figure 3-2 could be the measurement errors. The AVA and RBER methods used in this study are found to be more accurate than other conventional flowability measurements since they are computerized operations. Nevertheless, they are expected to generate larger errors than normal while dealing with more cohesive powders. That is because the powder accumulated on the glass

wall of the measurement drum can hardly be distinguished by the measurement software. In addition, unpredictable powder agglomerations, which behave similar to large particles, could increase the errors from the measurements.

Another factor for the scattered flowabilities was that the flow behaviours of fine powders were more affected by the small particles in the powder instead of the large particles. Previous studies discovered that small particles with diameter less than 10 μm could extend the influence of powder cohesion due to their extensive inter-particle cohesions [6, 17]. This influence was more noticeable for fine powder coatings since the overall particles were smaller than the regular size powder coatings. The D_{50} was not sufficient to indicate the variations on the amount of the small particles in the fine powder coating because it represented the size for half of the particles. Therefore, the measured flowabilities of the fine powder samples with respect to D_{50} were in disorder.

In order to better control the flowabilities, powder manufacturers started to specify the amount of small particles (generally indicated by the D_{10}) of their fine powder coating products in addition the specification of the D_{50} [18, 22-23]. This study realized that this method was not suitable for industrial application as well, since it could only be useable if the powders had similar particle size distributions. However, fine powder coatings produced from mass productions could hardly maintain similar particle size distributions [20]. Because factors such as loading condition, machine condition, labour shifts and others can all contribute to the variations in particle size distributions of the produced fine powder coatings [20]. Therefore, the situation faced in the real application is much more complicated.

A recent study by Krantz compared the flowabilities of fine powders, which were collected from a coating plant, with respect to both D_{10} and D_{50} [19]. He concluded that no clear

distinction was observed between the influences of D_{10} versus D_{50}. It indicated that D_{10} was not able to accommodate the fact of the diverse particle size distributions of the produced fine powder coatings.

Figure 3-3 shows the flowabilities of the powder samples, prepared in this study, with respect to their D_{10}. Although the trend of the results indicated improved flowability as the D_{10} of the sample increased, the AVA and RBER of both group 1 and group 2 were scattered. Therefore, the discovery was similar to Krantz's conclusion and there was no distinction found between the results in Figure 3-3 and Figure 3-2.

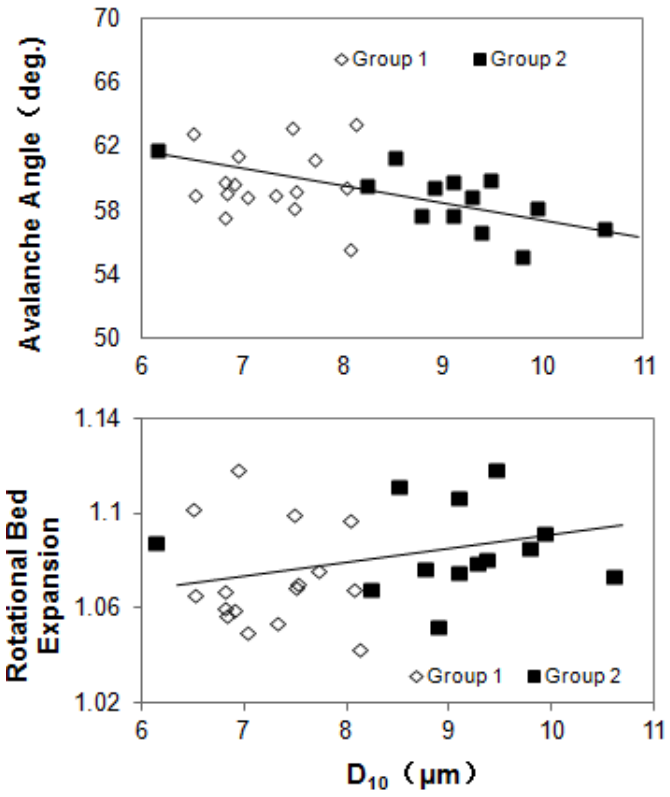

Figure 3-3: Flowabilities of the fine powder samples with respect to D_{10}

It is proposed by this study that the flowability characterization of fine powder coatings should be based on the particle size distribution, because the particle size distribution

comprised significances of both D_{10} and D_{50}. Span is a common parameter to present the particle size distribution of a powder. It can be defined as [21]:

$$Span = \frac{(D_{90} - D_{10})}{D_{50}} \qquad \text{Eq. 3-1}$$

Since the span incorporates parameters of D_{10} and D_{50}, the variations from both D_{10} and D_{50} can be reflected by the span. Figure 3-4 shows the flowability of the fine powder samples with respect to their spans. Nearly linear relations were found for both AVA and RBER for span the less than 1.45. As the span increased beyond 1.45, the results became scattered.

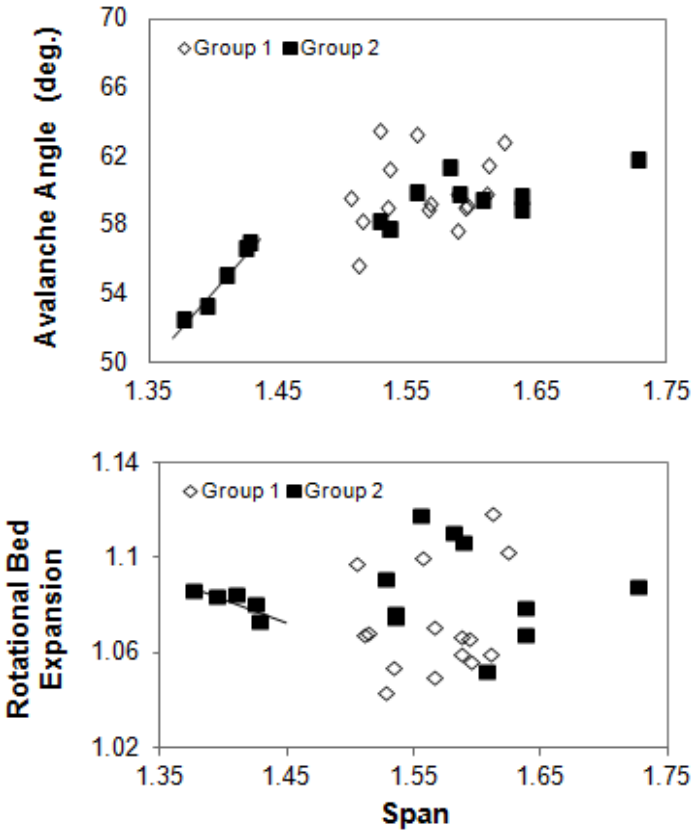

Figure 3-4: Flowabilities of the fine powder samples with respect to the span

Samples with spans larger than 1.45 were mainly the group 1 samples and they had medium particle size between 18 to 23 μm. The group 2 samples with span larger than 1.45 had D_{50} less than 26 μm. These powders were finer than the common fine powder coatings so that they were even more cohesive. As discussed earlier, the AVA and RBER measurement methods were not accurate while dealing with the cohesive powder since the computer software could not distinguish the powder accumulations and powder agglomerations. The scattered results from these powders could be mainly due to the measurement errors.

Figure 3-5 magnified the results for the span within 1.45. As shown by the figure, the flowabilities of the samples did not necessarily follow the variations in the D_{50}, which meant that the D_{50} was not a dominant factor for the fine powder coating samples.

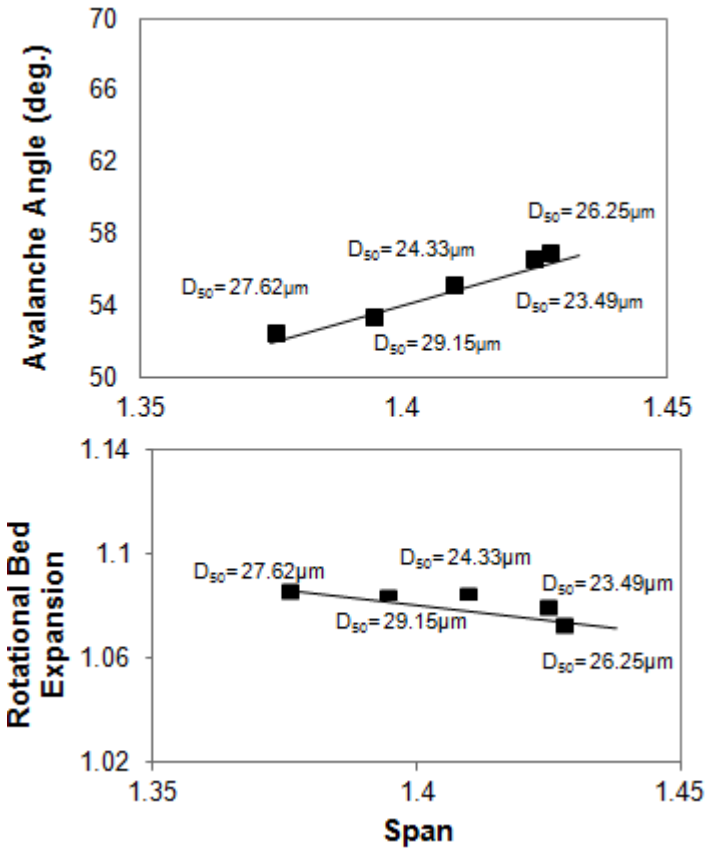

Figure 3-5: Flowability with respect to the span less than 1.45

Overall, the span could better explain the flowabilities of the fine powder samples than others since it incorporated the effects from both D_{10} and D_{50} at the same time. In addition, the flowability characterization with respect to span was able to use with powders that had diverse particle size distributions. Furthermore, the findings from this study should be applicable to other fine powder coatings as well, because most of the powder coatings had similar densities from to 1.3-1.7 g/cm^3. However, the conclusion from the study was based on the results obtained from group 2 samples. Therefore, it was limited for the characterizations of the powders that have D_{50} in the range between 23 to 29 μm. Powders in a wider range of D_{50} might not be able to obtain accurate AVA and RBER measurements with respect to the span due to the limitation of the instrument.

On the other hand, it was discovered that the group 1 samples were difficult to obtain spans less than 1.45. Powders with small D_{50} could hardly achieve narrow size distribution even though additional processes of classifying or sieving were used during the sample preparations.

Finally, results in Figure 3-4 indicated that the threshold of the span of 1.45, yet, it was not limited to other powder coatings. Krantz stated that differences of the types and qualities of the blended flow additives could significantly influence the flowabilities of fine powder coatings [19]. In order to show the distinctions between the samples, the amount of the flow additives blended to the fine powder samples in this study was only 0.3wt%, which was less than usual. Fine powder coatings with optimum amount of flow additives could have much improved flowabilities and the threshold of the span would be expected to be higher than 1.45.

Nowadays, the material standards of fine powder coatings used in the industry only specify the tolerances of D_{10} (or a similar value) and D_{50} individually [22-23]. The results from this study indicated the insufficiency of that. Furthermore, it implied the requirement of the span (or a similar index) should be stated in addition to the current material standards for better ensuring the flowabilities of the produced fine powder coatings.

3.4 Conclusion

This study reviewed the characterization methods for powder flowability that had been commonly used in industrial application. Based on the results, it was found that the flowabilities of the fine powder coatings did not correlate well with D_{50} since the lack of the consideration of small particles. In addition, the D_{10} showed similar results to D_{50} although it is a reflection of, in certain extent, the amount of the cohesive small particles. It is not capable to accommodate the diverse medium sizes and the particle size distributions of the fine powder samples. Nevertheless, the flowabilities of the fine powder coatings had nearly linear correlations with the span of the powders. Therefore, span was found as a better parameter than D_{10} and D_{50} for the flowability characterization of the fine powder samples. However, the conclusion was only suitable for powders with D_{50} between 23 to 29 μm. Furthermore, the variations of the flowabilities did not necessarily follow the changes of D_{50}. For future works, samples loaded with different amount of flow additives should be investigated for a more comprehensive conclusion.

Reference

[1] Bocchi, G.J., 2006, Join with PCI to improve powder coating community, *Products Finishing*, 70(6), 73-74

[2] Richart D., 2001, Powder Coating Process, in: Kirk-Othmer Encyclopedia of Chemical Technology, *John Wiley & Sons, published online*, 7, 35-68.

[3] Bok H.F., Glancy C.W., 1992, Apparatus and Methods for Application of Coatings with Supercritical Fluids and Diluents by Spraying from an orifice. *US Patent 5171613*.

[4] Geldart, D., 1972, The Effect of Particle Size and Size Distribution on the Behavior of Gas Fluidized Beds, *Powder Technology*, 6, 201-209.

[5] Geldart, D., 1973, Types of Gas Fluidization, *Powder Technology*, 7, 285-297.

[6] Visser, J., 1989, An invited review – Van der Waals and other Cohesive Forces Affecting Powder Fluidization, *Powder Technology*, 58, 1-10.

[7] Kendall K., Stainton C., 2001, Adhesion and aggregation of fine particles, *Powder Technol.*, 121, 223-229.

[8] Yang J., Sliva A, Banerjee A.,Dave R., Pfeffer R., 2005, Dry particle coating for improving the flowability of cohesive powder, *Powder Technology*, 158(1-3), 21-33.

[9] Gribble P., 2003, Development Status of Powder Coatings for OEM Automotive Applications, *Finishing Today*.

[10] Biller K., 2006, OEM Automotive Powder Coatings, *Finishing Today*.

[11] Hui Z., Jing F., Matt K., Jesse Z., July 2009, Company report (General Motor).

[12] Kendall K., Stainton C., 2001, Adhesion and aggregation of fine particles, *Powder Technoogy.*, 121, 223-229.

[13] Geldart D., 1973, Types of gas fluidization, *Powder Technology*, 7, 285-292.

[14] Yang J., Sliva A., Banerjee A., Dave R., Pfeffer R., 2005, Dry particles coating for improving the flowability of cohesive powders, *Powder Technology*, 158(1-3), 21-33.

[15] Krantz M., Zhang H., Zhu J., 2009, Characterization of powder flow: static and dynamic testing, *Powder Technology*, 194(3), 239-245.

[16] Hang Q., Zhang H., Zhu J., 2010, Flow properties of fine powders in powder coating, *Particuology*, 8(1), 19-27.

[17] Chen Y., Yang J., Rajesh N.D., Robert P., 2008, Fluidization of Coated Group C Powders, AIChE Journal, 54(1), 104-121.

[18] General Motors Corporation, 2004, *GM Engineering Standard 9984046*: Material Specification Paint, Primer Surface - Powder.

[19] Krantz M, 2008, Powder characterization and powder application in automotive coatings, *Master Thesis*, The University of Western Ontario, 47-75.

[20] Zhang H., Zhu J., Kuo H., Wang Y.M., Lis K.M., 2007, Oshawa Powder Primer Coat Characterization, *General Motor Internal Research Report*.

[21] ISO 13322-2 Particle size analysis – Laser diffraction methods.

[22] C.O.A for GM PRODUCT CODE 9984046G, PUA 1177D WA-224E Primer Surface.

[23] C.O.A for GM PRODUCT CODE 9984046W, PUA 1177D WA-8554 Primer Surface.

SECTION Ⅱ

REVISIONS ON THE MANUFACTURING PROCESSES FOR FINE POWDER COATINGS

Conventional manufacturing processes for powder coatings have been used for decades. Yet, they are not capable of producing quality fine powder coatings. Fine powder coatings are more difficult to make since their particle sizes are smaller. Furthermore, the particle size distributions of the fine powder coatings have to be properly maintained, at the same time, for ensuring the powder flowabilities and coating qualities. This section of the thesis study emphasized the revisions of the manufacturing processes for fine powder coatings.

CHAPTER 4: DEVELOPMENT OF A NOVEL CLASSIFYING CYCLONE FOR REDUCING PARTICLE SIZE DISTRIBUTION OF FINE POWDER COATINGS

4.1 Introduction

Narrow particle size distribution can benefit the powder flowability and the coating quality of a powder coating. However, reducing the particle size distribution of fine powders is a challenging task. There are large amounts of the small particles (< 5 μm) generated from fine grindings. Usually, a classifier has to be utilized for reducing particle size distribution in addition to a conventional sieving process. Multi-classification processes can help further reduce the particle size distribution of fine powders. However, it is not an economical way to operate. This study was to revise an ordinary cyclone into a classifying cyclone which can provide the function of classification while collecting the fine powder coatings.

Cyclone is a classical separator, which was first invented in 1800's [1]. Today, it is still widely used for solid-gas, liquid-gas and solid-liquid separations. Typically, a cyclone has a cylindrical barrel, a vortex finder and a cone as shown in Figure 4-1. The particles flow into the top of the cyclone barrel tangentially with the intake air due to the suction at the air outlet. The particles will then follow a spiral trajectory towards the solids outlet mainly under the combination of the centrifugal forces and the gravities. The majority of the inlet air exits through the vortex finder after entering the cyclone. On the other hand, the remaining air flows with the particles creating the outer vortex against the inner wall of the cyclone [2-4]. However, the air velocity becomes significantly slower as it approaches to the bottom of the cyclone. Eventually, the air flow will turn around towards the vortex finder due to the suction from the air outlet creating an inner vortex in the middle of the cyclone. In the mean

time, the inner vortex will carry away some of the air from the outer vortex along its path, known as a horizontal inward drift. During the process, some of the small particles which are more subjected to the air dynamic forces will be removed from the powder by the air flow.

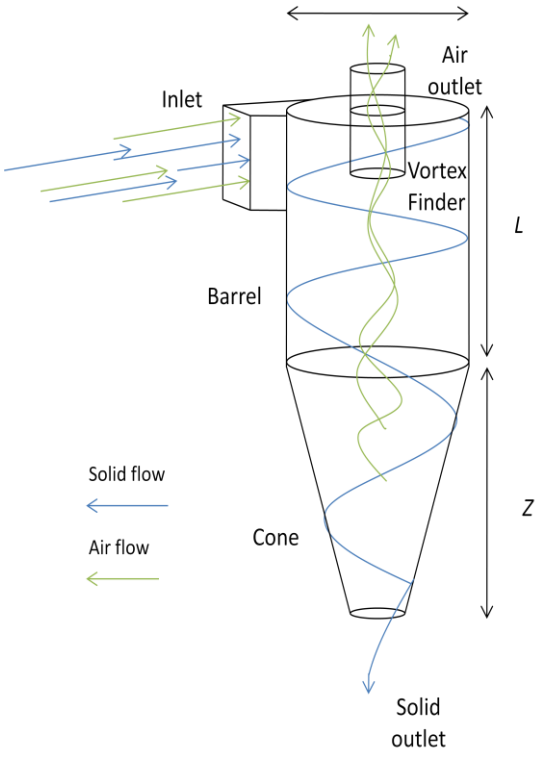

Figure 4-1: The cyclone structure.

The classifying cyclone proposed by this study is somehow contradictious to the original design of a cyclone since ordinary cyclones which more focused on maximizing the collection efficiency instead of removing particles on purpose [1-18]. However, some of the conclusion and findings from previous studies were still valuable to this study. Stated by Leith in 1979 [18], the spinning gas stream was found as the key factor causing the separation of particles from the air in the cyclone due to the centrifugal forces. Numerical studies also indicated that particles were thrown to the cyclone wall orbiting around the cyclone axis on a cross-section of the cyclone; meanwhile, the air stream moved in radial

direction towards the vortex finder for discharge [1-5]. Studies indicated that both the centrifugal forces and the inward air drag are acting on the particles shown in Figure 4-2 [1-4]. If the particle is large and heavy, the combined force points towards the wall, whereas the combination force on a small particle is always towards the cyclone axis. Generally, this phenomenon causes the reduction in collection efficiency. But for a classifying cyclone, it could be utilized for removing the small particles so as to reduce the particle size distribution.

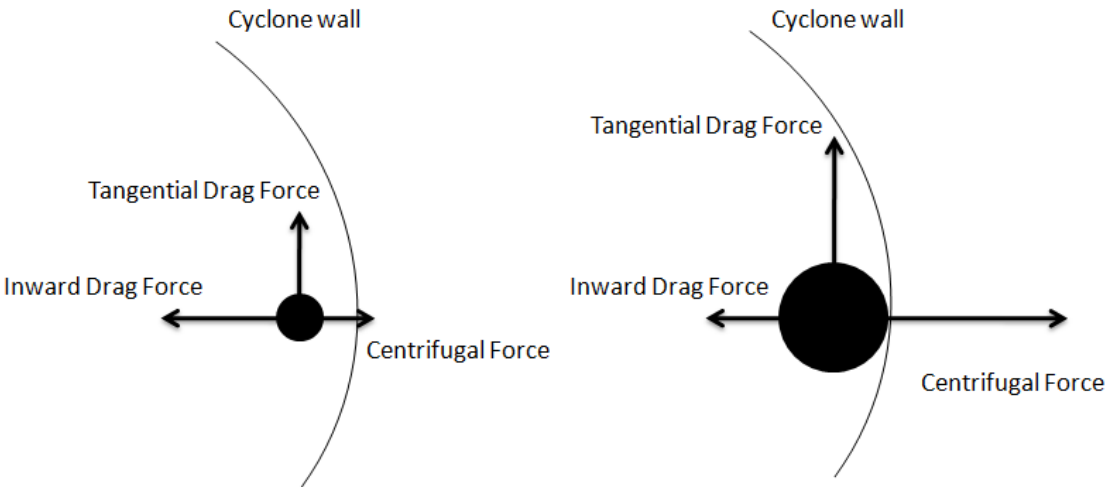

Figure 4-2: Forces acting on small particles (left) and large particles (right) on a cross-section of the cyclone

Moreover, a cyclone has a theoretical cut-size in an ideal situation shown by the solid vertical line in Figure 4-3. The collection efficiency for particles smaller than the cut-size should be 0% and the collection efficiency for particles larger than the cut-size should be 100%. Nevertheless, the real characteristic of a cyclone follows an S-shape shown as the dotted line in Figure 4-3 [5]. Stairmand found that small particles could agglomerate into larger and heavier clusters [5]. These clusters were no longer dominated by the inward drag but retained in the cyclone like the large particles. The small particles may also attach to the

large particles by inter-particle cohesion during pneumatic transportation. Thus, the collection efficiency below the cut-size was higher than 0%. On the other hand, large particles could escape through the inner vortex due to the effects of turbulences, eddies and bouncing. Consequently, the collection efficiency above the cut-size was less than 100%. As an implication to this study, large particles can escape while the small particles are removed.

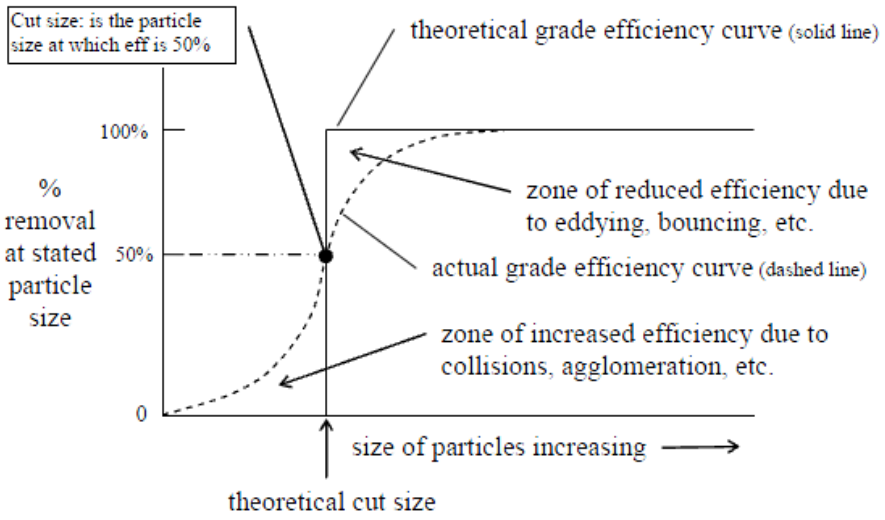

Figure 4-3: Diagram of grade efficiency curve characteristics [5].

4.2 Methods

The design of the classifying cyclone was to utilize a reverse flow which was a secondary air entered the cyclone from a secondary air inlet in the bottom as demonstrated in Figure 4-4. The secondary inlet was a thin gap created below the cyclone cone. Since the gap opening was small, the air flows in the cyclone at a high speed so as to break off the particle agglomerations. At the same time, the enhanced upward air flow was able to remove the small particles. Because the secondary air inlet was open to the atmosphere, the air entered from the bottom of the cyclone could be induced by the negative pressure inside the cyclone. Therefore, this design did not require external power supply.

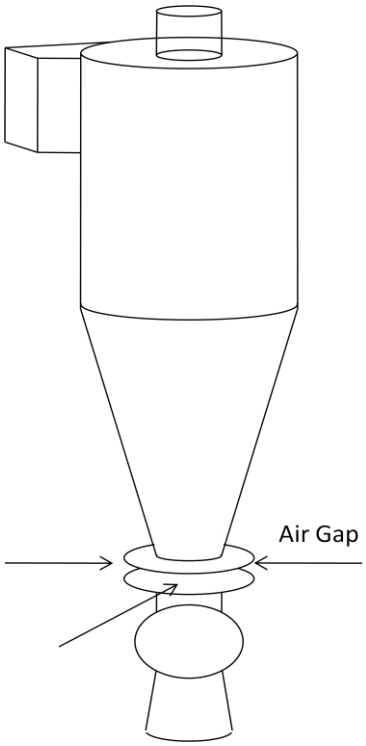

Figure 4-4: Design of the air gap.

By looking up literatures, such design of the classifying cyclone was neither discovered nor studied. However, three inventions, called cyclone classifiers, were found from the patent search as demonstrated in Figure 4-5 [19-21]. Similarly, they utilized additional reverse air flow in the cyclone to remove small particles but with a different inducing method from this study. As stated by the inventors, the reversed flow could reduce particle size distribution of the collected powders; however, it created increased entrainments of the large particles at the same time causing major reduction in collection efficiency. In order to overcome this problem, the inventors added inserts or deflectors in the middle of the cyclone body to reduce the adverse effect from the reverse air flow [19-21]. Nevertheless, the improvements on the collection efficiency were not significant. On the other hand, the designs of these cyclone classifiers were very complicated and they were difficult to be adjusted during applications. More importantly, the powders they run for testing were not fine powders.

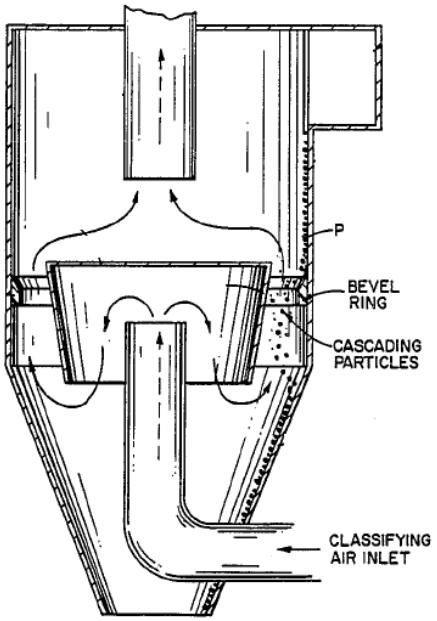

a. design from Darrow [19]

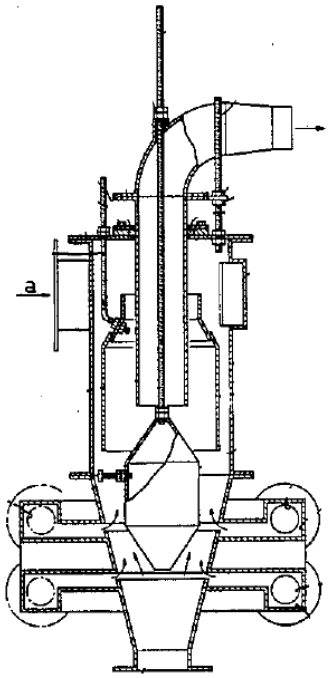

b. design from Ikebuchi et al [20]

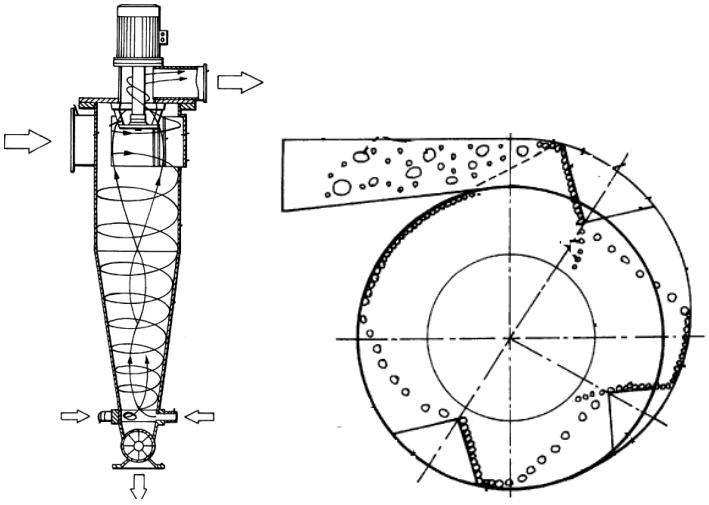

c. design from Schwanborn and Smigerski [21]

Figure 4-5: Previous designs of cyclone classifier

In this study, fine powder coating samples were the target material to be classified. Removing small particles from fine powders was much more challenging since the powder particles aggregate more severely. Comparing with the patented designs, the proposed design by this study was expected to be more capable of removing the small particles due to the

ability to break off the powder agglomerations. In addition, the dimension of the secondary air inlet could be easily adjusted and the rest of the structure of the cyclone remained unchanged.

However, the proposed classifying cyclone could encounter the same problem of large reduction in collection efficiency because it basically used the similar idea of removing particle by a reverse air flow. Therefore, modification of the design on the secondary inlet was made. Figure 4-6 shows the image of the modified secondary inlet which has additional air guiders. The air guiders create a spinning motion of the secondary air so as to speed up the outer vortex in the bottom of the cyclone. This spin motion of the secondary air is in the same direction as the vortex. As disclosed from previous researches, an enhanced outer vortex could help to retain large particles due to centrifugal effect [1-4]. Therefore, high collection efficiency could possibly be retained.

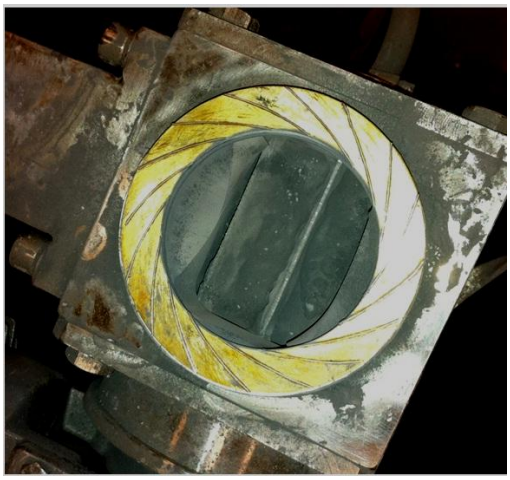

Figure 4-6: Insert to provide the secondary air inlet with air guiders.

4.3 Numerical Study

Numerical simulations were firstly conducted for examining the air flow inside the designed classifying cyclones. An ordinary cyclone manufactured by Donghui Powder Processing

Equipment Co., LTD, China was used for comparisons. It had an involute inlet and its dimensions were shown in Figure 4-7.

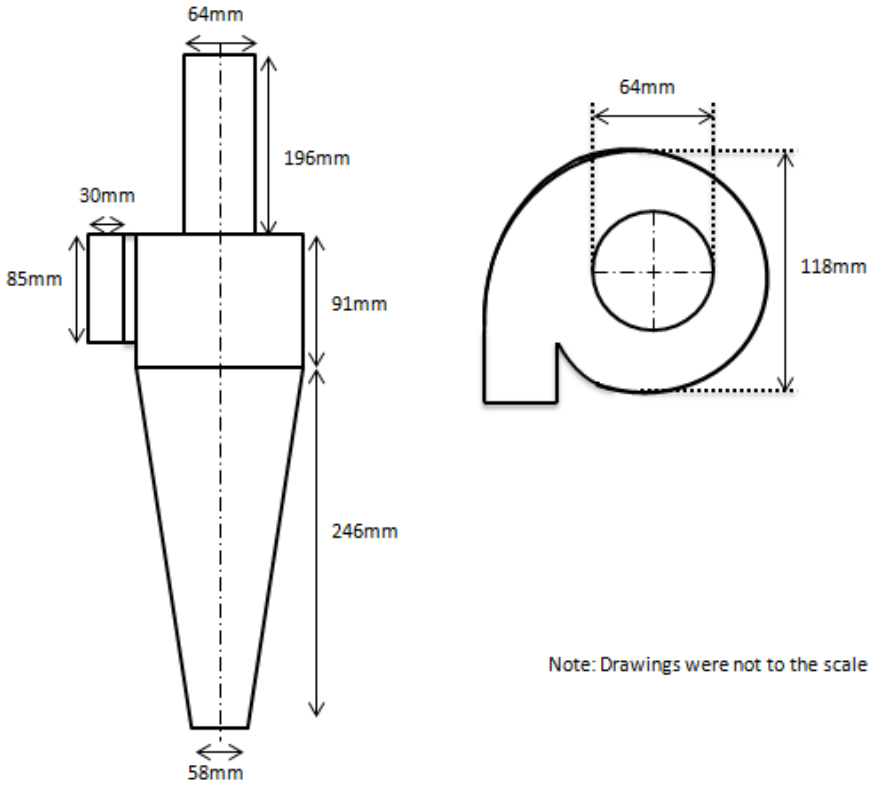

Figure 4-7: Measured ACM dimensions of the original cyclone used in this study

As shown in Figure 4-8, the models of the cyclones were drawn in GAMBIT (version 2.2.30). The bottom of the cyclones was attached by a collecting box to avoid the air escaping from the bottom of the cyclone during particle collecting. It was similar to the purpose of an airlock in a real cyclone system. As shown by the figures, a total of three models were drawn: the ordinary cyclone, the classifying cyclone that had secondary air inlet and the classifying cyclone that had a secondary air inlet with air guiders. For simplification, “Model O”, “Model SA” and “Model SAG” denoting the three cyclone models respectively were used in the following discussions of this chapter. Model SA and

Model SAG shared same dimensions of the vortex finder, cyclone barrel and cyclone cone with Model O. However, Model SA and Model SAG had a 0.7 mm opening in the bottom of the cyclone cone whereas the Model O had the cyclone cone connected to the collecting box directly.

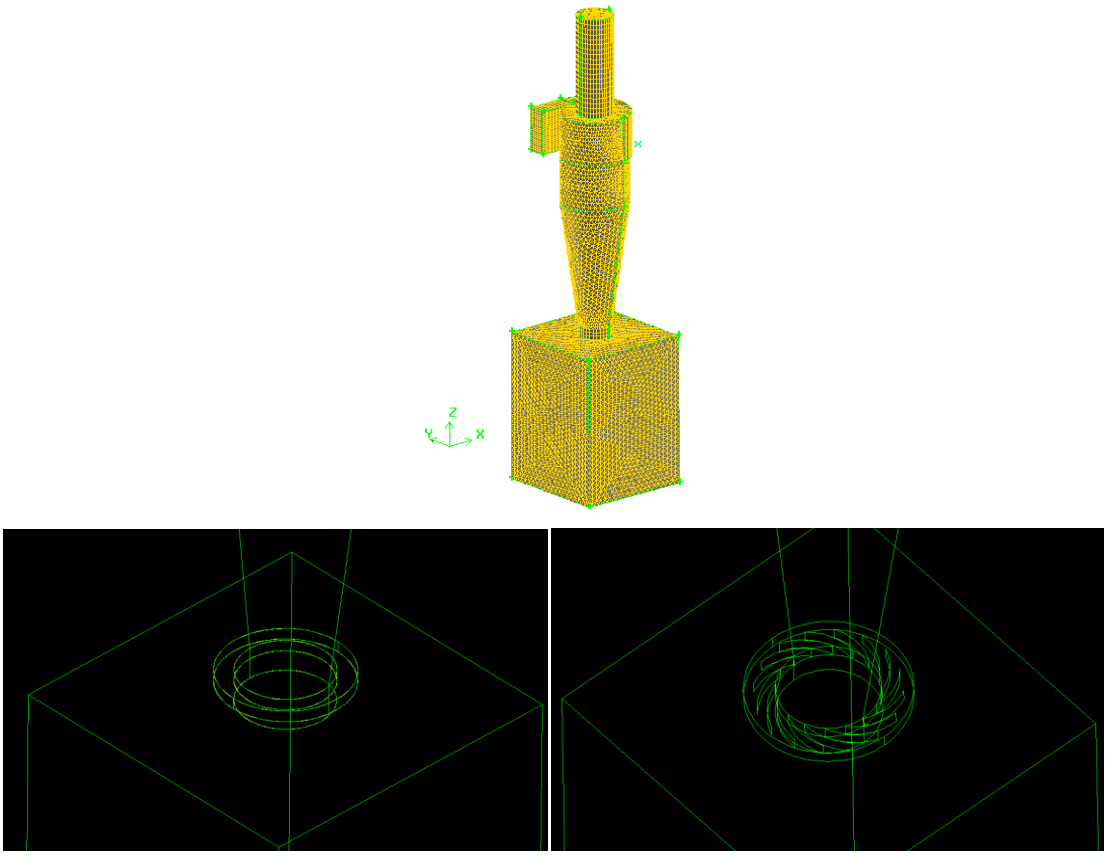

Upper: the mode of the original cyclone, Model O;
Lower left: The drawing of the secondary inlet, Model SA; Lower right: The drawing of the secondary inlet with air guiders, Model SAG

Figure 4-8: Meshed cyclone model by GAMBIT:

The Fluent (version 6.3.26) was used to simulate the air flow inside the three models. The Model O had one air inlet and one air outlet, while Model SA and Model SAG had two air inlets and one air outlet. The inputs for the boundary conditions were measured from the actual cyclone during operation. The parameters for modeling were listed in the Appendix I.

4.3.2 Results and Discussions of the Numerical Simulation

Figure 4-9 demonstrates the velocity vector of the air inside model O, where the arrows represent the directions of the air and the color gradient shows the magnitude of the air velocity. As one can be observed from the figure, the air starts to accelerate when it enters the cyclone and the air velocity reaches its maximum at the vortex finder due to the suction from the air outlet. Majority of the air escapes from the vortex finder while the rest of the air is swirling down towards the bottom of the cyclone. The velocity vectors along the wall indicate the formation of the outer vortex. On the other hand, the velocity vectors pointing upward in the middle of the cyclone indicate the formation of the inner vortex, although it is difficult to be discovered by the static 3D figure. The velocity vectors on a 2D XZ plane demonstrate the air flow more clearly in the middle of the cyclone. The velocity vectors along the wall imply the downward outer vortex. As they are closer to the bottom of the cone, the air decelerates and starts to turn upward shown by the changing colors and directions of the velocity vectors. The upward air stream in the middle of the cyclone accelerates towards the vortex finder; at the same time, it creates inward drag indicated by the vectors in horizontal directions in between the outer and the inner vortexes. The air flow model generated from the simulation is in agreement with the previous numerical studies [1-5].

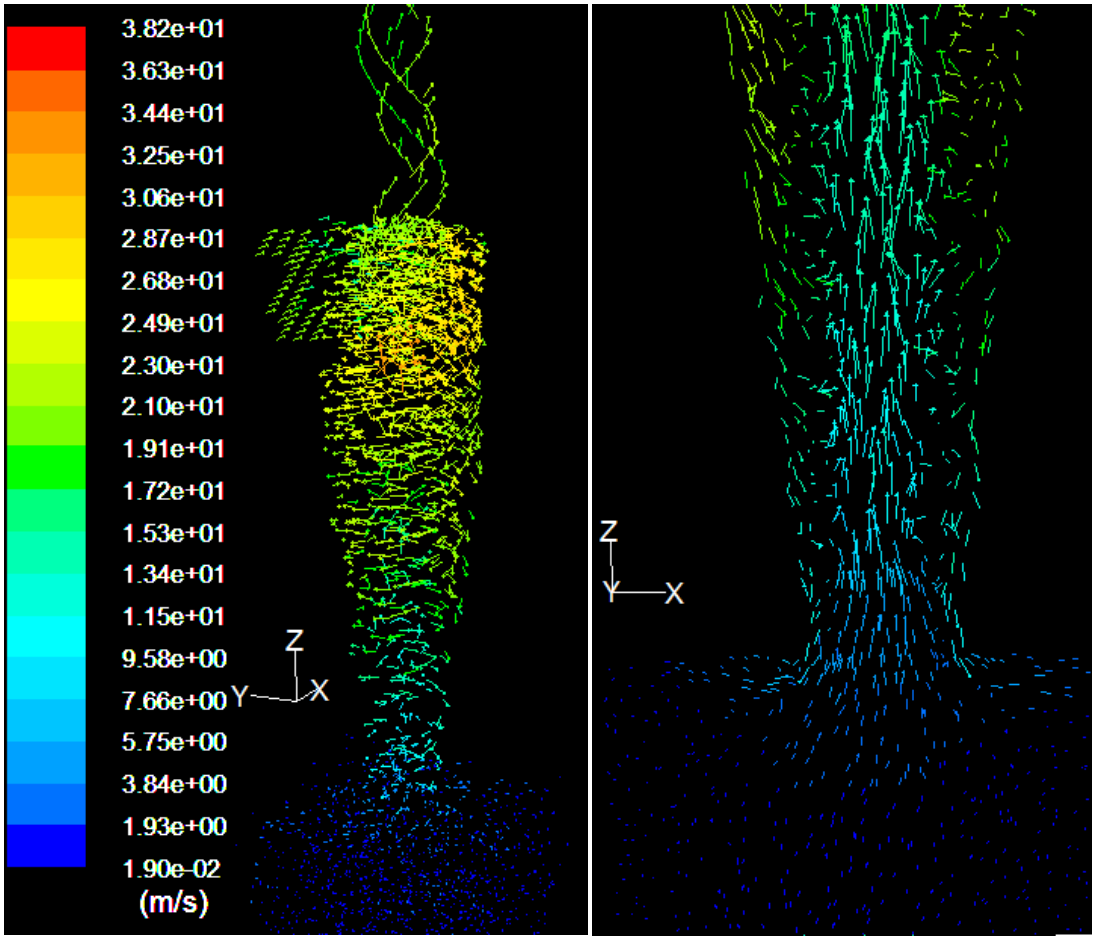

Left: General 3D view of the velocity vectors of the air in the cyclone body;
Right: Close view of the 2D velocity vectors of the air in the bottom of the cyclone cone on XZ plane

Figure 4-9: Velocity vectors of the air in Model O

Figure 4-10 is the axial velocity (the Z-velocity) contour inside the cyclone. The axial velocity is negative close to the cyclone wall indicating downward air flow. The negative air flow reaches the end of the cyclone cone. Therefore, the air flows in the same axial direction as the particles along the wall. On the other hand, the axial velocity around the middle of the cyclone is positive, indicating upward air flow. Shown by the transitions in colors, the upward air flow starts near the bottom of the cone but the initial velocity of the upward air is much slower. Because of that, the particles are less likely to be picked up by the air flow as they gathered at the lower portion of the cyclone cone.

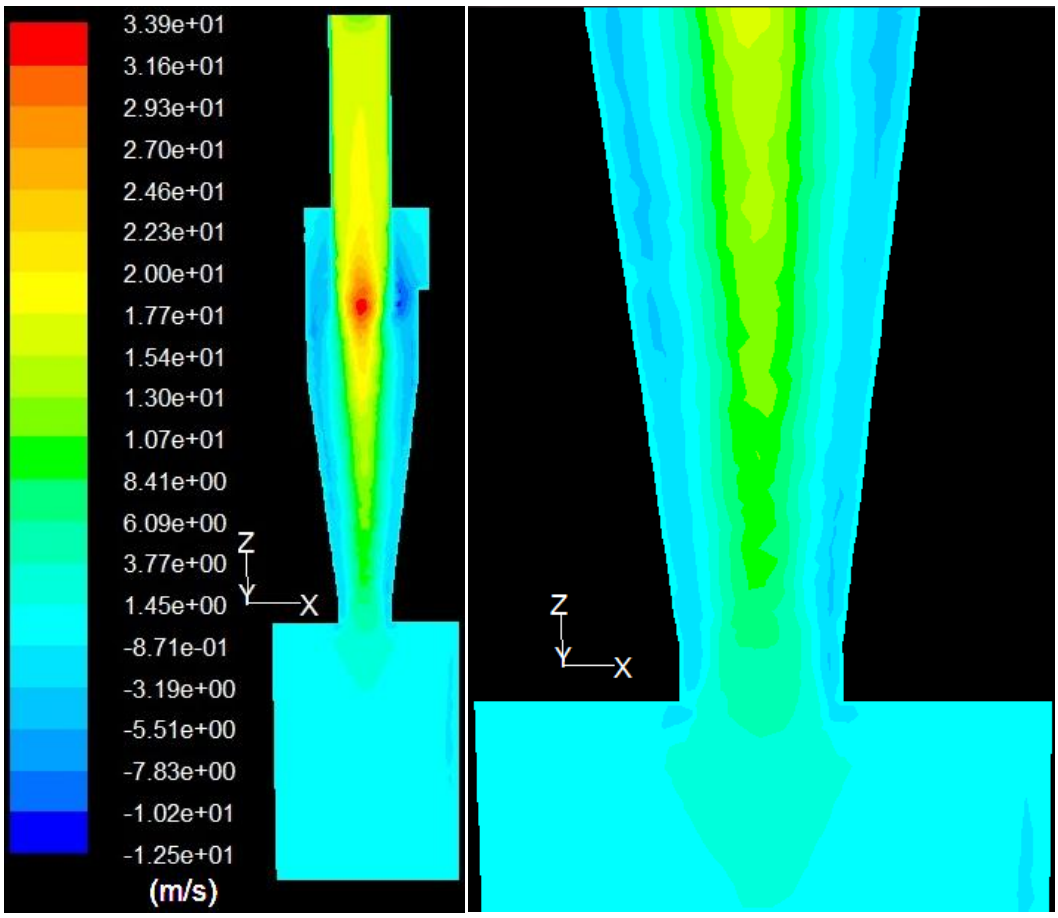

Left: Axial velocity contour on 2D XZ plane; Right: Close view of the axial velocity contour on 2D XZ plane in the bottom of the cyclone

Figure 4-10: The axial velocity contour in Model O on the XZ plane

Figure 4-11 is the plot of the axial air velocity with respect to the cross-sectional radius at the solids outlet of the cyclone. It indicates that the axial air velocity is positive at the center of the cyclone. However, the velocity becomes smaller as radius increased. At approximate 0.02 m away from the center of the cyclone, the air speed is approximately zero. As the radius moves further away from the center, the axial air velocity becomes negative, indicating a change in direction of the axial air flow. At radius of about 0.025 m, the negative axial air velocity reaches a maximum point. Due to the wall effect, the axial air velocity becomes zero as the radius moved closer to the wall. The plot further indicates that

the air flow near the bottom of an ordinary cyclone is always flowing towards the solids outlet.

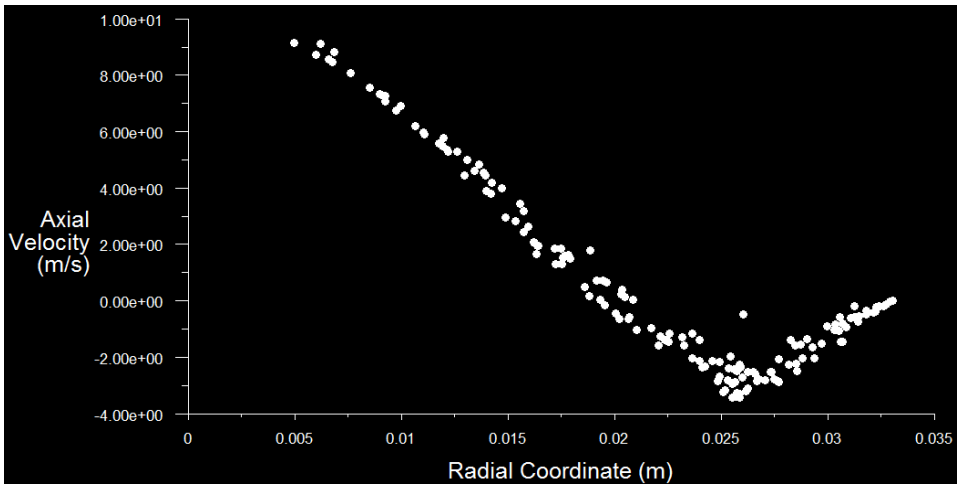

Figure 4-11: The axial velocity at the solids outlet in Model O

Comparing with Model O, Model SA was designed to be a classifying cyclone for achieving narrower particle size distributions of the collected powders. As shown in Figure 4-8, it had a secondary air inlet which was a thin gap at the bottom of the cone. Figure 4-12 demonstrates the simulation of the air flow inside Model SA. The air flow in the cyclone barrel is similar to Model O; however, the air flow in the cyclone cone is distinct from Model O. The simulation indicates that the secondary air flows upward as soon as it enters the cyclone and it has much higher velocity than outer vortex. As a result, it creates strong reverse flow in the lower portion of the cyclone. Based on the observations from the 2D view of the velocity vectors on the XZ plane, the strong reverse flow induced by the secondary air significantly reduces the intensity of the outer vortex in the bottom of the cyclone. Furthermore, it also creates more severe inward drag comparing with Model O.

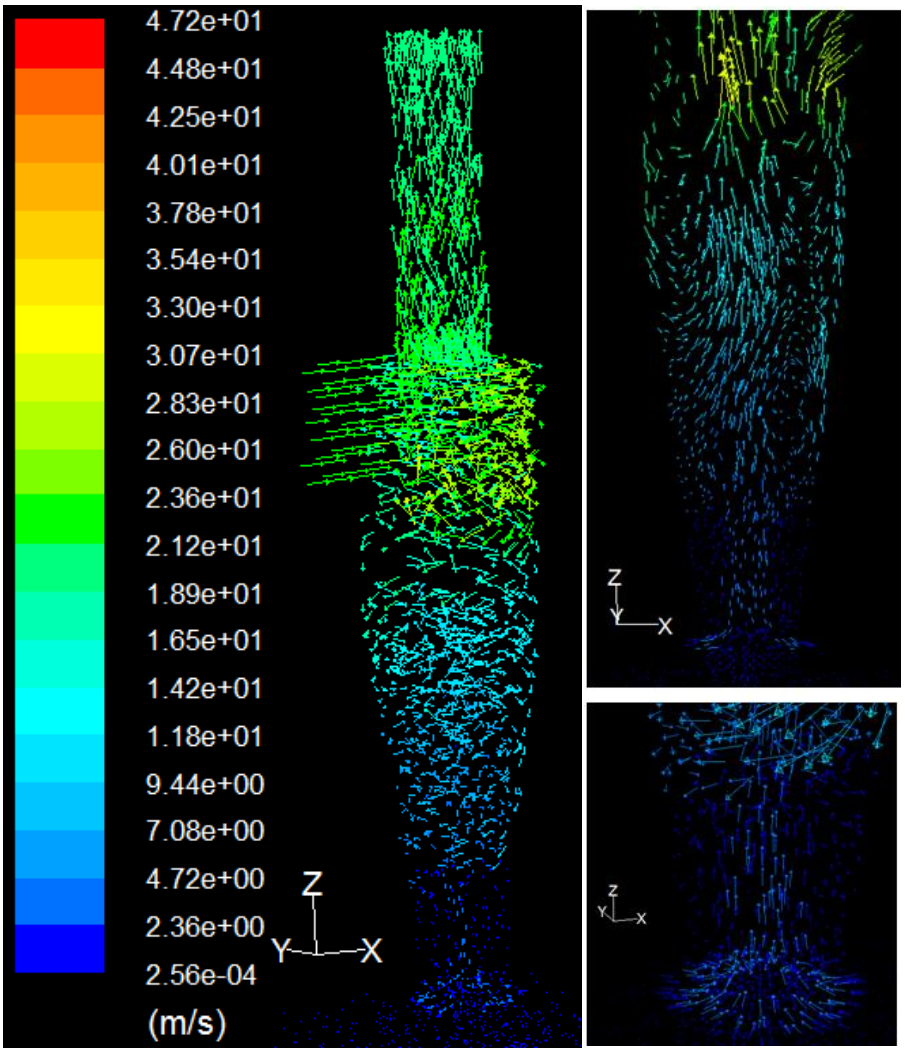

Left: General 3D view of the velocity vectors of the air in the cyclone body;
Right upper: 2D velocity vectors of the air in the bottom of the cyclone cone on XZ plane;
Right lower: 3D view of the velocity vectors of the air at the secondary air inlet

Figure 4-12: Velocity vectors of the air in Model SA

The velocity contour in Model SA on the XZ plane as shown in Figure 4-13 further indicates the much weaker outer vortex in the lower portion of the cyclone and the axial air velocity close to the solids outlet is found positive, indicating an upward air flow. Moreover, the radius of the upward air flow is wider comparing with Model O due to the strong reverse flow and the width of the outer vortex in the cyclone barrel is narrower.

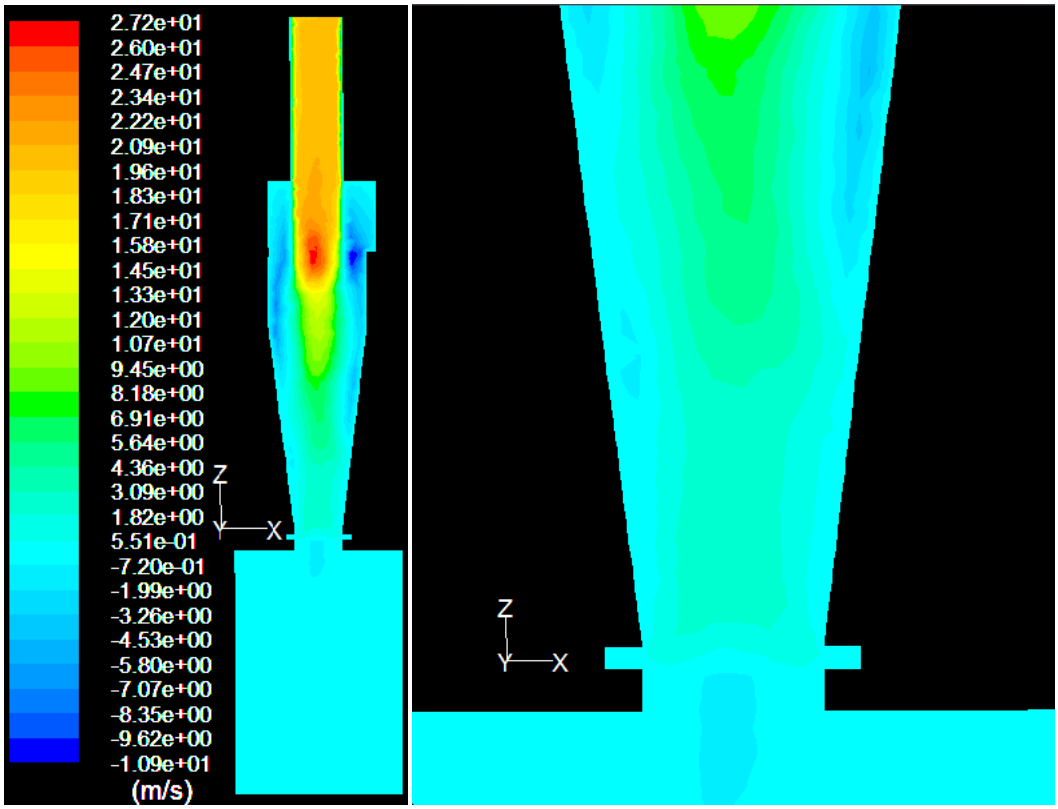

Left: Axial velocity contour on 2D XZ plane; Right: Close view of the axial velocity contour on 2D XZ plane in the bottom of the cyclone

Figure 4-13: The axial velocity contour in Model SA on the XZ plane

Figure 4-14 plots the axial air velocity with respect to the cross-sectional radius at the secondary air inlet. The secondary air starts to flow upward as soon as it enters the cyclone. It accelerates as it moves deeper into the cyclone until a maximum velocity is reached at the radius of about 0.02 m. As it moves further towards the center, the upward air velocity decreases. It is discovered from the velocity profile that there is no negative air velocity across the section, indicating no downward air flow. Therefore, the outer vortex at this location no longer exists More importantly, the maximum upward velocity of the secondary inlet air occurs fairly close to the wall. It implies that particles could encounter the strong upward air flow as they gather at the lower portion of the cyclone cone. The evidences from the simulation of Model SA suggest that this design could cause significant reduction in collection efficiency due to the high potential of excessive loss of particles.

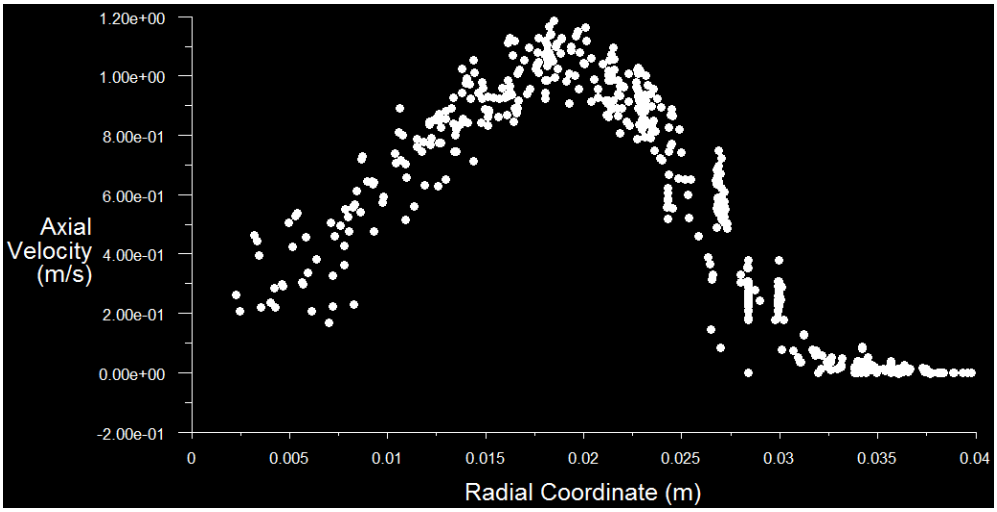

Figure 4-14: The axial velocity at the solids outlet in Model SA

The Model SAG was a modified Model SA. It also utilizes the secondary air inlet to induce the reverse air flow but with an additional air guiders as shown in Figure 4-5 and Figure 4-8. Due to the air guiders, the secondary air enters the cyclone tangentially creating air spinning so as to enhance the outer vortex. A more intensive outer vortex could help further classify particles prior to the powder discharge due to the increased centrifuge effect. On the other hand, the strong upward air flow at the secondary inlet is expected to be avoided.

Figure 4-15 demonstrates the velocity vectors of the air inside the Model SAG. Comparing with the Model SA, the outer vortex in this case is less destructive, especially inside the cone of the cyclone. The velocity vectors at the secondary inlet shows that the air is spinning as it enters the cyclone and the strong upward air flow is not observed. In addition, the reverse flow in lower portion of the cyclone is much less violent comparing with Model SA. Finally, the velocity vectors on the XZ plane indicate that the inner vortex does not cause strong inward drag within the whole cyclone. The air flow characteristics generated by the Model SAG is similar to the Model O.

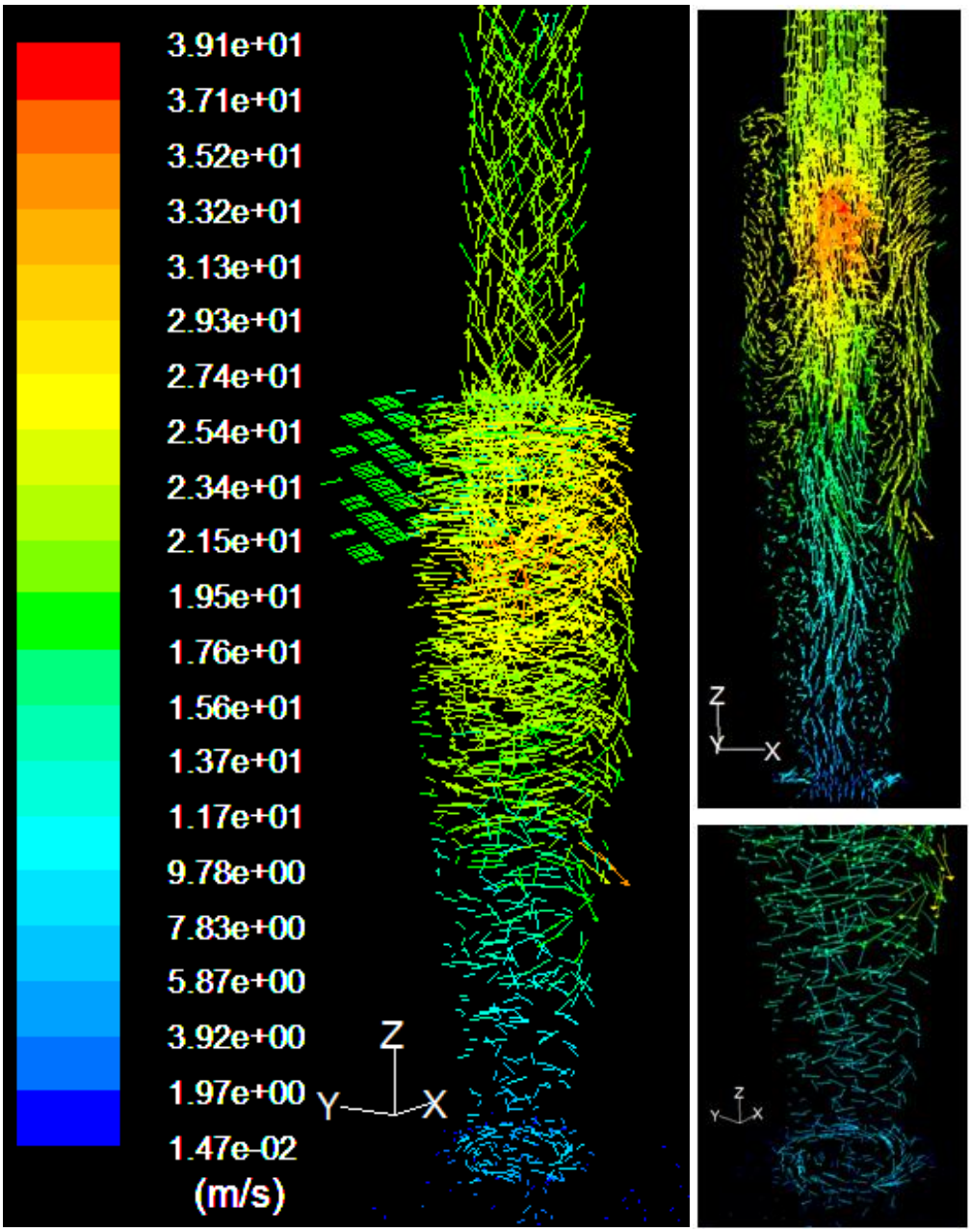

Left: General 3D view of the velocity vectors of the air in the cyclone body;
Right upper: 2D velocity vectors of the air in the bottom of the cyclone cone on XZ plane;
Right lower: 3D view of the velocity vectors of the air at the secondary air inlet

Figure 4-15: Velocity vectors of the air in Model SAG

The axial air velocity contour in Figure 4-16 further explains the velocity profile inside the Model SAG. Comparing with Model SA, the areas in darker blue color, indicating the outer vortex, are wider against the cyclone wall. Furthermore, the velocity contour shows that the

outer vortex is even extended into the collecting box. In contrast, the inner vortex is much narrower and it is further away from the bottom of the cyclone.

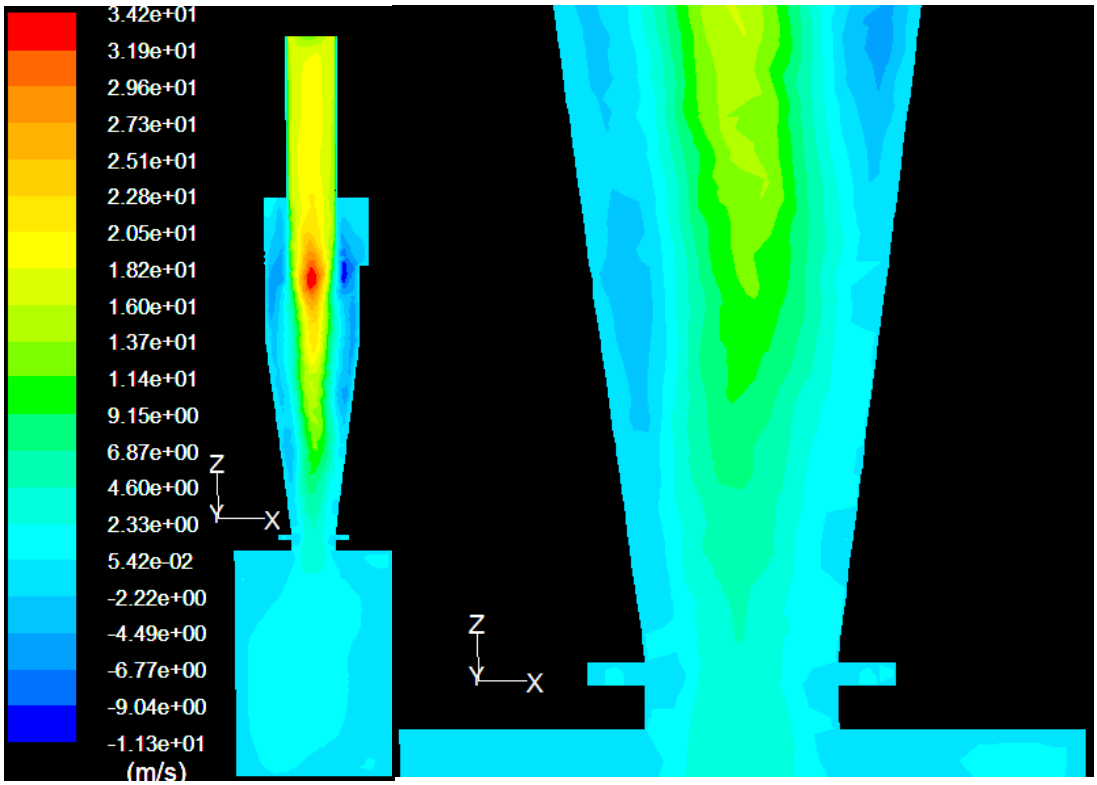

Left: Axial velocity contour on 2D XZ plane; Right: Close view of the axial velocity contour on 2D XZ plane in the bottom of the cyclone

Figure 4-16: The axial velocity contour in Model SAG on the XZ plane

Figure 4-17 plots the axial air velocity with respect to the cross-sectional radius at the secondary air inlet. Results show that the air tends to flow downward once it enters the cyclone from the secondary inlet. The maximum downward air velocity is found at about 0.02 m from the center of the cyclone. As it moves further to the center, the downward air velocity decreases and the air finally turns upward at the radius of 0.015 m. Unlike Model SA, the reverse flow in this case starts near the center of the cyclone and there is no strong upward air flow discovered near the wall. It implies that the particles would less likely to encounter strong upward air flow in the bottom of the cyclone. At the same time, the air

spinning, shown in Figure 4-15, is able to enhance the outer vortex so as to help retain larger particles. Therefore, less loss of particles than Modal SA should be expected.

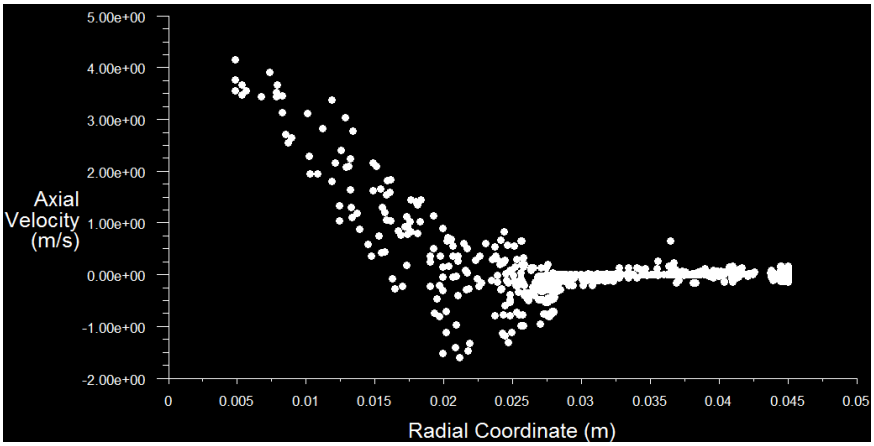

Figure 4-17: The axial velocity at the solids outlet in Model SAG

The results obtained from the numerical simulations disclose that simply adding the secondary air inlet as like Model SA could create strong reverse air flow near the cyclone wall as well as violent inward air drags. The consequence would probably be a drastic reduction in collection efficiency. The design of the air guiders in the secondary inlet has a great potential to solve this problem as shown by the simulated air flow generated by the Model SAG.

4.4 Experimental Study

Experiments were conducted for obtaining the real performances of the classifying cyclones. The classifying cyclones were modified from the cyclone manufactured by Donghui Powder Processing Equipment Co., LTD, China. The cyclones were connected to an air classifying mill (ACM) as shown in Figure 4-18 so that the powders ground from the ACM were collected by the cyclone as samples.

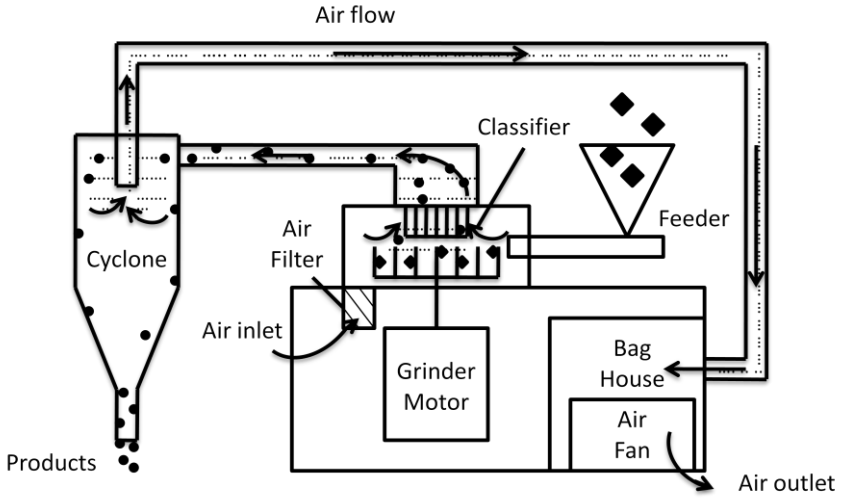

Figure 4-18: The scheme of the experimental process

4.4.1 Materials and Methods

The air classifying mill (ACM) used in the experiments was manufactured by Donghui Powder Processing Equipment Co., LTD, China which was a lab-scale ACM. 6 cyclone configurations as listed in Table 4-1 were prepared for the experiment. The grinding material was the powder coating chips supplied by Seibert Powder Coatings, Cleveland, USA.

Table 4-1: The list of the cyclones tested in the experiment

Cyclones	Sample name	Secondary inlet opening (mm)
Original cyclone	Control	NA
Classification cyclone	SA1	0.27
with secondary air inlet	SA2	0.54
Classification cyclone	SAG1	0.25
with secondary air inlet	SAG2	0.56
and air guider insert	SAG3	1.00

The experimental study analyzes powders with a range of medium particle sizes. During the experiment, the fan speed of the ACM was adjusted, while other parameters such as the grinder speed and the classifier speed were remained unchanged. The fan speeds of 20, 23, 26 and 29 Hz were selected for generating the powders with the target particle sizes.

Furthermore, the cyclone designs were evaluated with two types of classifier installed: the straight-vane classifier and the angled-vane classifier. The straight-vane classifier is used for producing coarser powders with higher production throughput. On the other hand, the angled-vane classifier is used for the production of finer powders. It is because the distinct vane design of the angled-vane classifier could create higher restriction to the particle flow so that the particle sizes of the powder coatings could be reduced more affectively. Obtaining results in both classifiers could further help investigate the performances of the classifying cyclones, while handling with powders in a broad size range. Usually, finer powders are more difficult to be classified due to the increased powder cohesions.

The collecting efficiencies and the size distributions of the powder samples were the two parameters to determine the performance of the classifying cyclone. The particle sizes of the collected samples were measured by a laser particle size analyzer (BT9300S, Better Size Laser Analyzer, China). D_{10}, D_{50} and D_{90} were the three important values obtained from the measurements. These values are the particle sizes which below the corresponding volume percentage. For instance, a D_{10} value is defined as a diameter where 10 vol% of the particles of the powder are less or equal to this diameter. In general, D_{10} and D_{90} are the common parameters to determine the amount of small and large particles in the powder, whereas D_{50} is the medium particle size of the powder. The span which indicates the particle size distribution of the powder is determined by:

$$Span = \frac{D_{90} - D_{1}}{D_{50}} \qquad \text{Eq. 4-1}$$

In order to help understand the particle size and particle size distribution of a powder, an example is presented in Figure 4-19. Increased D_{10} and/or reduced D_{90} while maintaining the

D_{50} can lead to a steeper curve of the particle size distribution. As these two values become identical to D_{50}, the powder will have uniform size particles. The span defines the overall shape of the distribution curve. Narrow particle size distribution is always desirable for powder coatings, especially fine powder coatings, since reduced D_{90} leads to a better coating quality and increased D_{10} leads to improved powder flow properties.

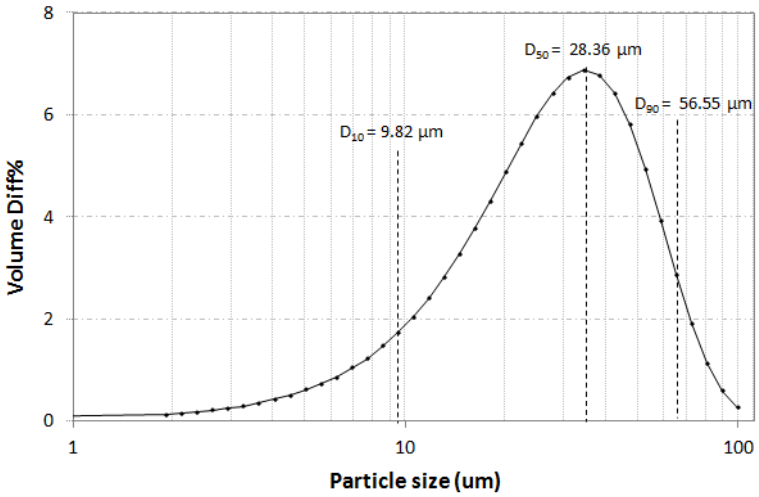

Figure 4-19: An example of particle size distribution

On the other hand, the feeding of the ACM was calibrated and the collection efficiency was calculated by:

$$\eta_{Collecting} = \frac{r_{Feeding} \times t_{Feeding}}{W_{Collecting}} \qquad \text{Eq. 4-2}$$

Where, $\eta_{Collecting}$ was the collection efficiency, $r_{Feeding}$ was the set feeding rate, $t_{Feeding}$ was the measured feeding time and $W_{Collecting}$ was the measured weight of the collected sample. In the experiments, the feeding rate of the ACM remained constant.

4.4.2 Results and Discussion

The experiments began with the straight-vane classifier installed and the experimental results are shown in Figure 4-20. The five classifying cyclones showed better performance than the ordinary cyclone on reducing particle size distribution. Samples collected from SA2 cyclone had largest D_{10} and smallest D_{90} overall. As a result, SA2 cyclone could be able to produce much smaller span of the powders than that provided by the ordinary cyclone indicating a much narrower distribution of the powders. Comparing with SA2 cyclone, SA1 cyclone classified powders less efficiently. The samples collected from SA1 cyclone had smaller D_{10} and larger D_{90} than that collected from SA2 cyclone. Referring to the modeling of the SA cyclone, the strong reverse air flow inside the cyclone is able to remove particles from the solid flow, leading to narrower span of the collected powders. However, reduced D_{90} caused by the SA2 cyclone was a sign of the loss of larger particles. It was in agreement with the discovery from the modeling that the strong reverse air flow could remove excessive particles.

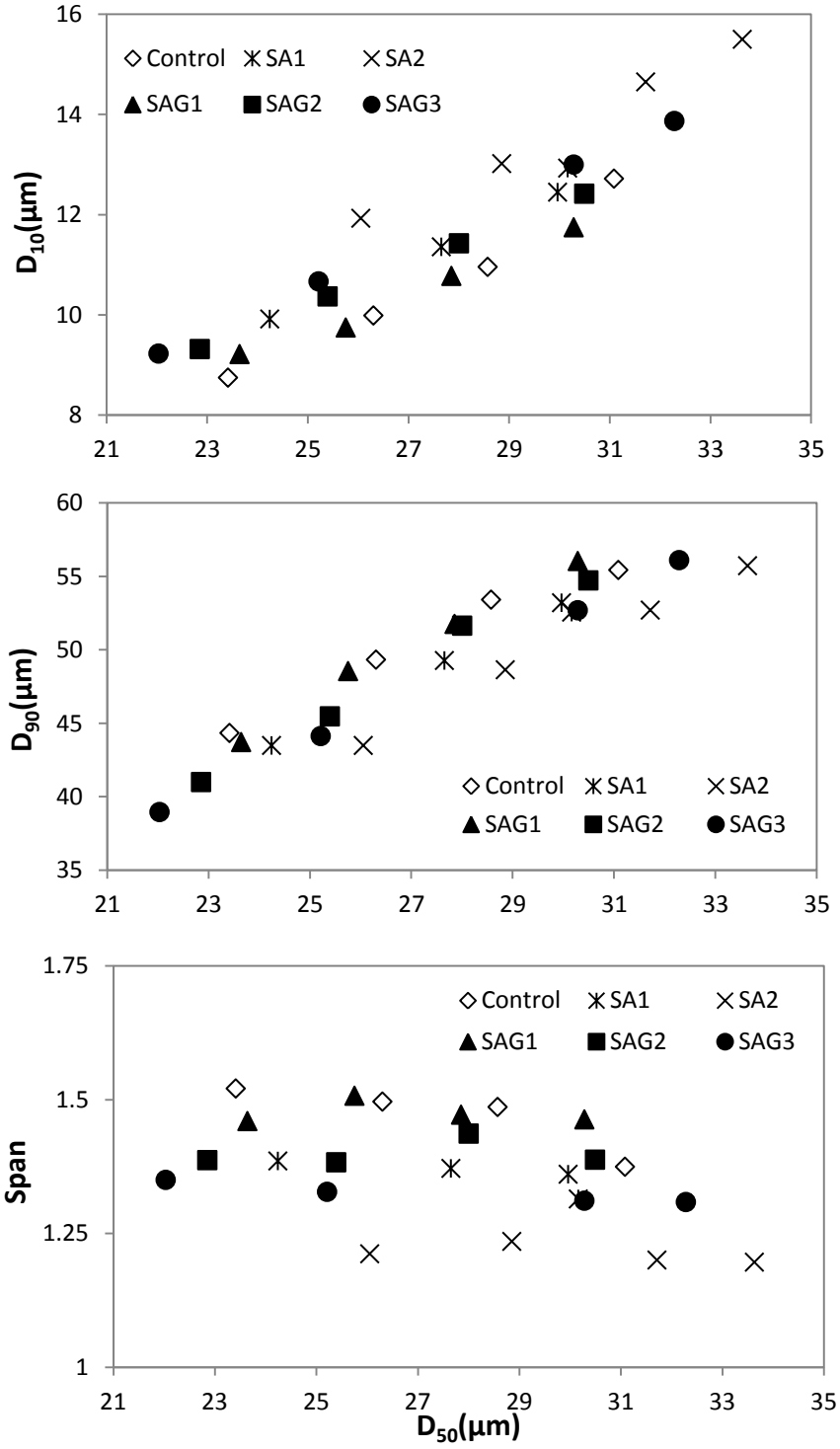

Figure 4-20: Comparisons of D_{10}, D_{90} and the span with respect to D_{50} with the straight-vane classifier installed

On the other hand, SAG cyclones also showed promising results. SAG2 cyclone and SAG3 cyclone performed similarly to the SA1 cyclone whereas SAG1 cyclone performed similar to the ordinary cyclone. It is to note that the reduction of the D_{90} by the SAG cyclone was less significant than the SA cyclone. Similar to the suggestions from modeling results that the use of the air guiders could help to retain the larger particles since the outer vortex in the lower portion of the cyclone cone was enhanced. Results in Figure 4-20 also showed that wider opening of the secondary inlet could lead to a better performance on reducing the particle size distributions of the collected powders. Furthermore, similar results obtained from SA2 cyclone and SAG2 cyclone implied that the SAG cyclone could perform similarly as the SA cyclone. However, SA cyclones were more influenced by the opening size of the secondary inlet.

Collection efficiency was another important performance to evaluate for the classifying cyclones and a desired classifying cyclone was to obtain narrow particle size distributions without compromising collection efficiency. Figure 4-21a showed the determined collecting efficiencies of the cyclones. The first thing to notice was that the SA cyclones had lower collection efficiency than others. As the produced powder become finer, the collection efficiency drop rapidly. It implied that powders with smaller particles were much easier to be removed by the SA cyclones. According to the simulation of SA cyclones, the strong upward air flow near solids outlet could be a major reason for that. This case became worse as the opening size of the secondary inlet of the SA cyclones became wider. The SA2 cyclone could only retain approximately half of the collection efficiency of the original cyclone. The serious deterioration in collection efficiency was similar to the discoveries from the previous the cyclone classifier designs [19-21].

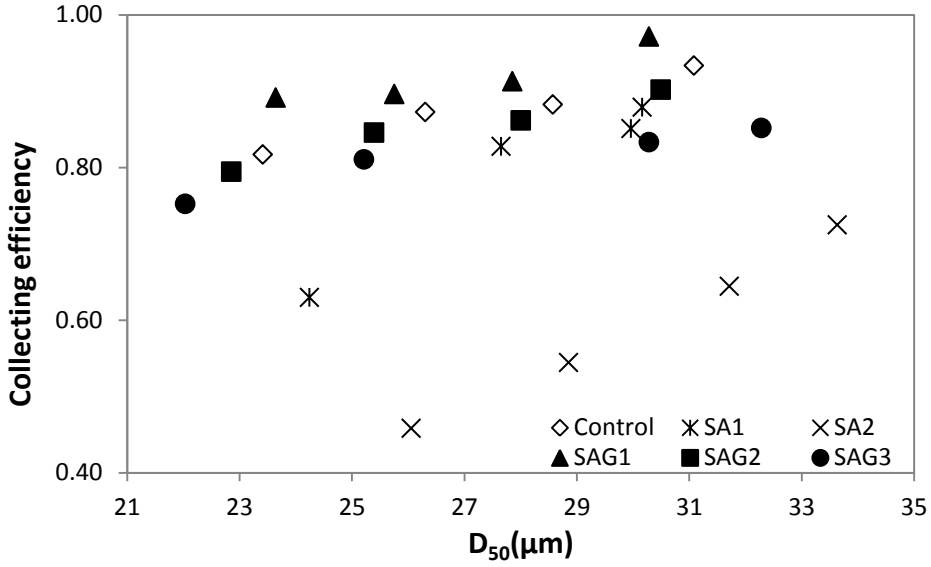

a. The collection efficiency of the cyclones with respect to D_{50}

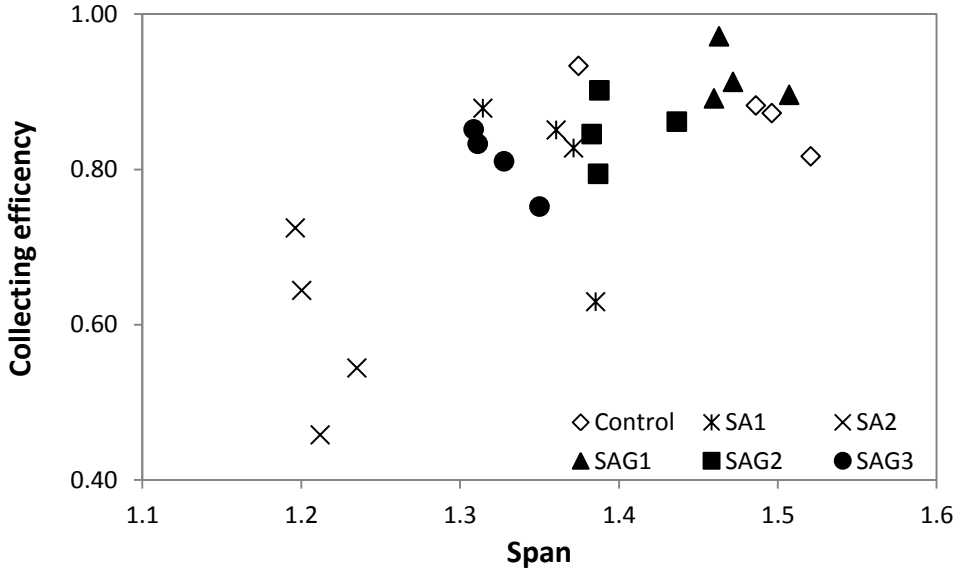

b. The collection efficiency of the cyclones with respect to span

Figure 4-21: The collection efficiency of cyclones with straight-vanes classifier installed

In contrast, all the SAG cyclones provide promising results. Overall, the collecting efficiencies by SAG cyclones are comparable to original cyclone and no rapid descend in the collection efficiency is observed as the sizes of the collected powders become smaller. Shown by the simulations, the characteristics of the outer vortex, inner vortex and the inward

drag inside the SAG cyclone are similar to an ordinary cyclone. Therefore, the collection efficiency of the SAG cyclone follows a very similar trend as the original cyclone. As also shown by the simulations, the SAG cyclone has much less significant upward air flow at the solids outlet because of the added air guiders. In fact, the guided secondary air is able to enhance the outer vortex so as to help retain the particles. It can be the reason why the SAG cyclones can outperform the SA cyclones. It is to note that the SAG1 cyclone even has a slightly better collection efficiency than the original cyclone whereas the span shown in Figure 4-19 indicates that the collected powders from both cyclones have comparable particle size distributions. Similar to SA cyclone, increased the opening of the secondary air inlet of the SAG cyclones causes reduction in the collection efficiency.

Comparison among the classifying cyclones indicated that the collecting efficiencies of the SA cyclones are more sensitive to the opening of the secondary inlet. For the SA cyclone, doubling the opening of the secondary inlet from 0.27 mm to 0.54 mm caused drastically reduction in the collection efficiency. However, increasing the opening of the secondary inlet for four times from 0.25 mm to 1 mm in the SAG cyclone did not significantly reduce the collection efficiency. As an implication to applications, adjustment on the SAG cyclone will be more controllable than the SA cyclone.

On the other hand, Figure 4-21b shows the collection efficiency of the cyclones with respect to the span of the collected powders. According to the objective of the classifying cyclone, the span of the collected powders is desired to be smaller while the cyclone can still obtain high collection efficiency. In other words, the cyclone, which exhibits on the most left-up corner in Figure 4-20b, is preferable. The SAG3 and the SA2 cyclones are both found to be better than the others in this case. Both of them could reduce the spans of collected powders to 1.3 while still maintain the collection efficiency of about 90%. Experienced from the

industrial application, narrowing the span of the powders, especially fine powders, has never been an easy task. Conventional methods including sieving and secondary classifications are pricey and time consuming and they can barely reduce the span of the powder coatings. Thus, the results obtained from the classifying cyclones are very promising considering the significances on the reduction of the span.

The experiment was continued to test the cyclones with the angled-vane classifier installed. The angled-vane classifier is usually used for productions of finer powders since it classifies large particles more effectively than the straight-vane classifier. Figure 4-22 shows the D_{10}, D_{90} and the span with respect to the D_{50} of the collected powder samples. Results show that the collected powders from SA2 cyclone has much larger medium size of the collected powder than others. Furthermore, the SA2 cyclone is able to provide the least span of the collected powders overall. On the other hand, SA1 cyclone and SAG3 cyclone have comparable performances on reducing D_{90} and increasing D_{10} of the powders and the spans of the collected samples from these two cyclones are similar. With the angled-vane classifier installed, the SAG1 cyclone shows better results than the ordinary cyclone. The SAG2 cyclone performs better than the SAG1 cyclone but not as good as the SAG3 cyclone. Comparing with Figure 4-19, Figure 4-21 shows similar trends of the spans of the collected samples with respect to the changes in the medium particle sizes. In addition, it is also found that a wider opening of the secondary inlet could lead to narrower particle size distributions for both SA cyclones and SAG cyclones.

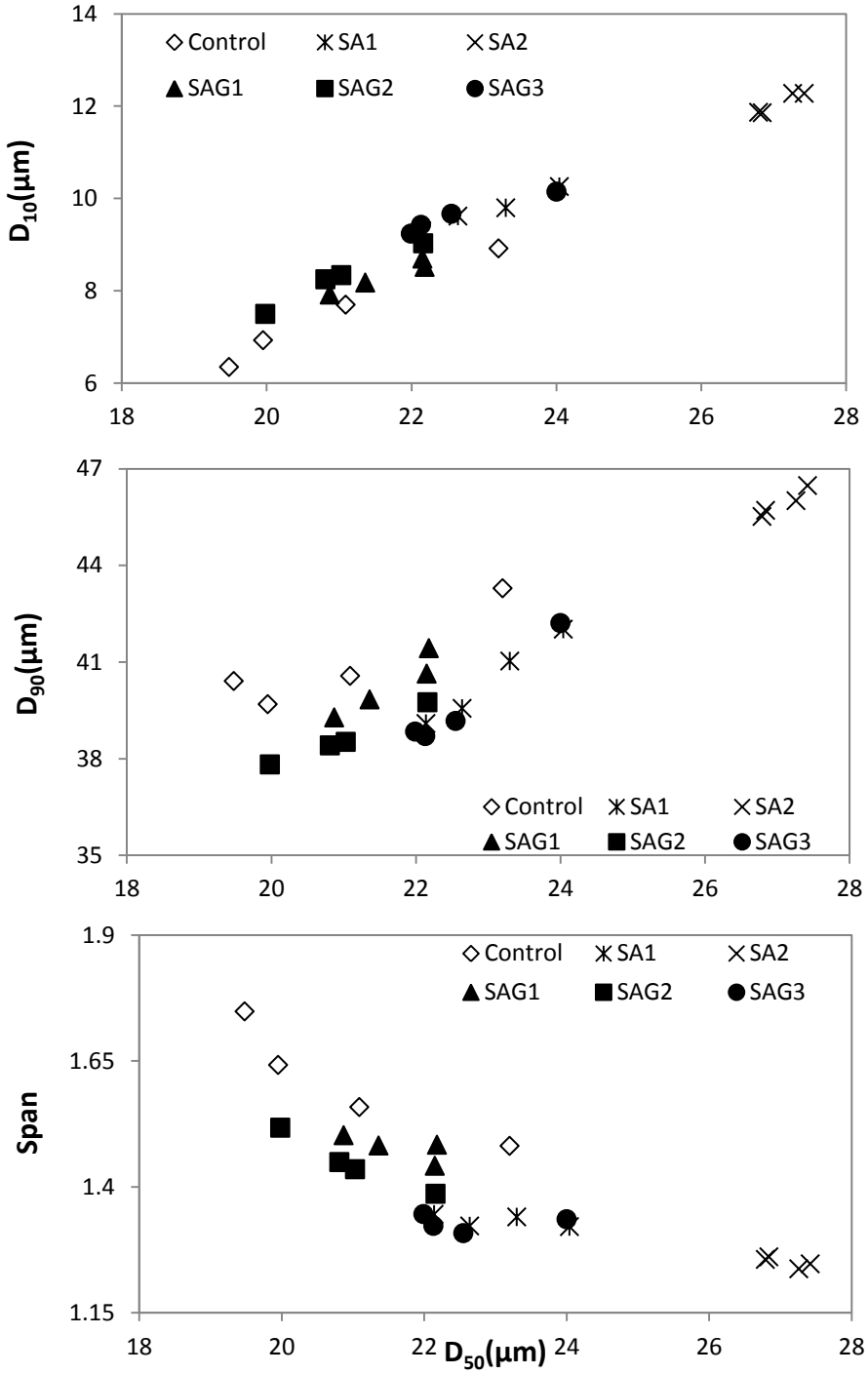

Figure 4-22: Comparisons of D_{10}, D_{90} and the span with respect to D_{50} for angled-vane classifier blade set-up

Results in Figure 4-22 indicates that the classifying cyclones have the capability to deal with fine powder coatings, although the powder coatings become more cohesive. The modeling of the classifying cyclones implies that the high velocity air from the secondary air inlet could break off some of the particle agglomerations, which is in agreement with the increased D_{10} of the collected powders found in Figure-22. However, the reductions in the D_{90} of the collected powders by the classifying cyclones are more significant comparing with the results in Figure 4-20. It indicates that the particle agglomerations in the fine powder coatings could still cause higher loss of the particles than the case with coarser powders.

Figure 4-23a shows the obtained collecting efficiencies of the cyclones. The SA2 cyclone obtains less than half of collection efficiency than the original cyclone whereas the SAG1 cyclone and the SAG2 cyclone are the highest collection efficiency among the classifying cyclones but slightly worse than the original cyclone. The SAG3 cyclone and the SA1 cyclone have similar collection efficiency which is worse than the SAG2 cyclone and the SAG1 cyclone. Overall, the classifying cyclones have more significant impacts on their collecting efficiencies while dealing with finer powder coatings. However, the obtained collection efficiency from the SAG cyclones is still reasonable comparing with the original cyclone. For both SA cyclones and SAG cyclones, larger opening of the secondary air inlet causes more reduction in the collection efficiency. The influence of the opening size of the secondary air inlet is more significant than the case with coarser powders.

Figure 4-23b indicates the collection efficiency of the cyclone with respect to the span of the collected powders. As discussed earlier, the classifying cyclone shown in the left-up corner of the chart is desired since it has the highest collection efficiency with the least span. According to that, the SAG2, the SAG3 and the SA2 are more preferable than others.

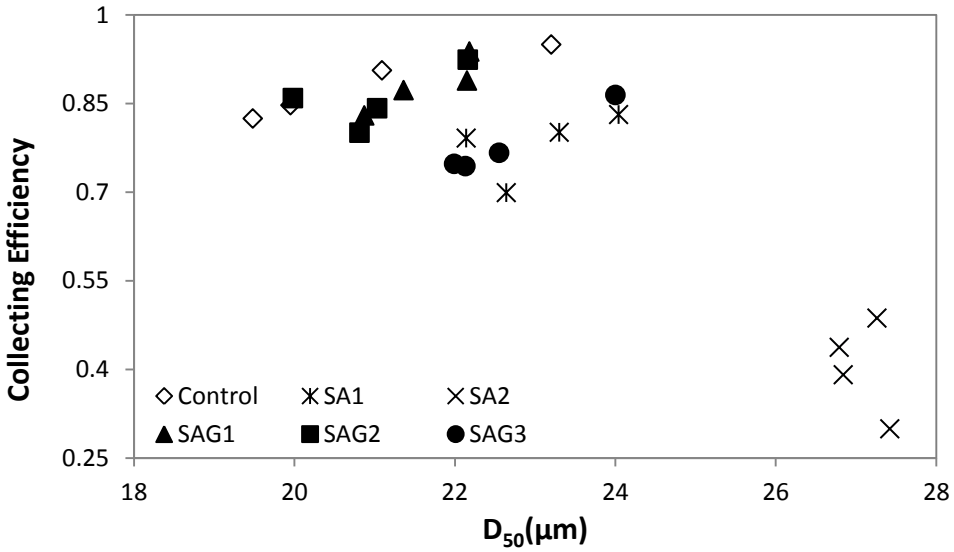

a. The collection efficiency of the cyclones with respect to D_{50}

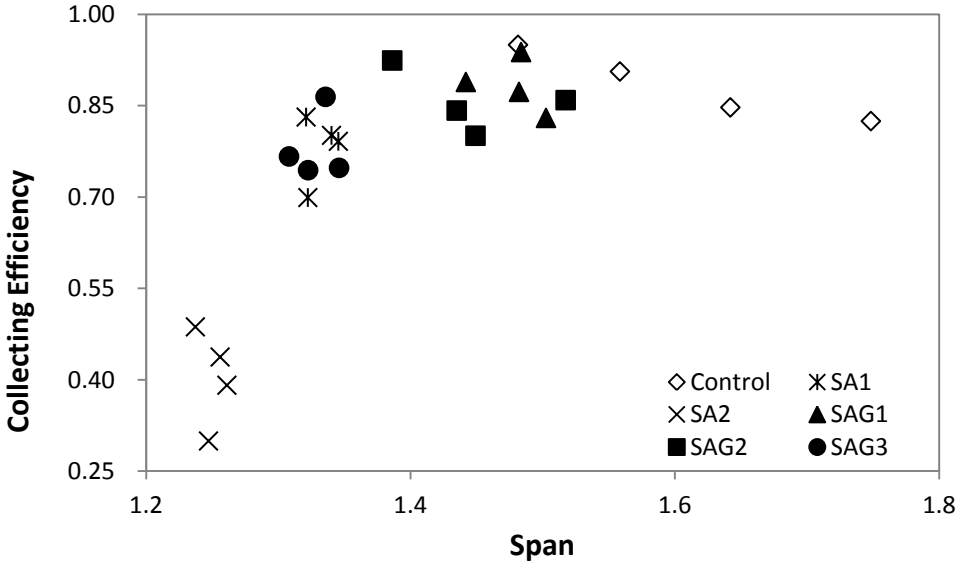

b. The collection efficiency of the cyclones with respect to span

Figure 4-23: The collection efficiency of the cyclones with the angled-vane classifier installed

4.4.3 Observations

Photos in Figure 4-24 were taken inside the cyclone cone near the solids outlet from the SA cyclone. Combinations of coarse and fine particles were found on the cyclone wall after running with the fine powder coatings. The coarse particles could be easily blown away by compressed air; whereas the fine particles were strongly accumulated on the wall surface. It implies that the outer vortex in this area is insufficient to brush off the particles from the wall. Moreover, it indicates that the secondary air is not able to classify the powder particles effectively inside the cyclone.

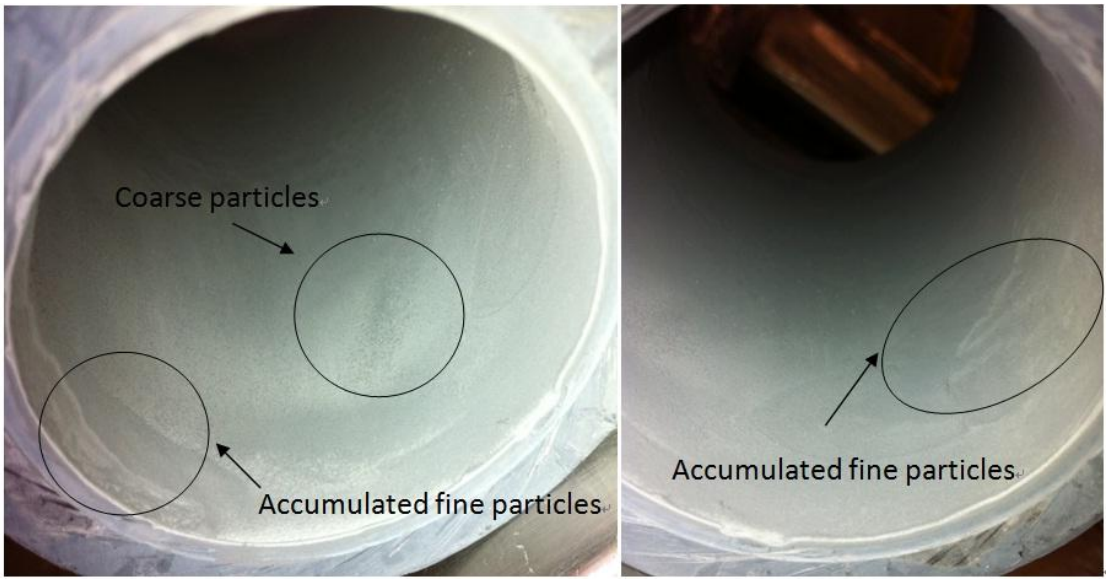

Left: observation right after experiment; Right: After cleaning with compressed air

Figure 4-24: Solids outlet of the SA cyclone

The photos shown in Figure 4-25 were taken near the solids outlet inside the SAG cyclones. Comparing with SA cyclones, it only had a loose lay of coarse particles leftover after running with fine powder coatings. The coarse particles could be easily removed by compressed air and the cyclone wall was clean without strong accumulations of fine particles. The difference between the two cyclones indicates the effect led by the addition of the air guiders. The air

guiders are able to spin the secondary air so as to enhance the outer vortex. The stronger outer vortex inside the SAG is able to create higher momentum of the particles so that the particles could flow faster into the solids outlet. Moreover, the absence of the fine particles indicates that the SAG cyclone could classify powder particles more effectively. The faster spinning of the particles due to the enhanced outer vortex was able to help to separate the smaller particles from the larger particles because of the increased centrifugal effect on the larger particles. The observations from the two cyclones further confirmed the findings from both of the numerical simulations and the experimental results.

Left: observation right after experiment; Right: After cleaning with compressed air

Figure 4-25: Solids outlet of the SAG cyclone

4.5 Conclusions

The development of the classifying cyclone was to provide an additional feature of classification during a collecting process of the powder coatings. Two classifying cyclone

designs, SA cyclone and SAG cyclone, were evaluated in this study. Both of the two designs utilized the reverse air flow, but the SAG cyclone had additional air guiders inside the secondary air inlet. Concluded from the results, the SA cyclone could effectively narrow the particle size distributions of the collected powders; yet, collection efficiency of the SA cyclone was poor due to the excessive losses of particles. With the air guiders, the SAG cyclone could reduce the particle size distribution of the collected powders without sacrificing much of the collection efficiency. On the other hand, the numerical simulation indicated the air guider can spin up the secondary inlet air so as to enhance the outer vortex in the bottom of the cyclone creating stronger centrifugal effect on larger particles. The experimental results also concluded that that the enhanced outer vortex inside the SAG cyclone is able to reduce the losses of the particles and improve the classification efficiency. Finally, the performance of the SAG cyclone is less sensitive to the opening size of the secondary air inlet comparing with SA cyclone. It makes the SAG cyclone easier to adjust during real operations.

Reference

[1] Dirgo J., Leith D., 1985, Cyclone Collection Efficiency: Comparison of Experimental Results with Theoretical Predictions, *Aerosol Science and Technology*, 4(4), 401-415.

[2] Xiang R.B., Lee K.W., 2004, Numerical study of flow field in cyclones of different height, *Chemical Engineering and Processing*, 44, 877-883.

[3] Su Y.X., Zheng A.Q., Zhao B.T., 2011, Numerical simulation of effect of inlet configuration on square cyclone separator performance, *Powder Technology*, 210, 293-303.

[4] Bhasker C., 2010, Flow simulation in industrial cyclone separator, *Advances in Engineering Software*, 41, 220-228.

[5] Tong Z.B., Yang R.Y., Chu K.W., Yu A.B., Adi S., Chan H.K., 2009, Numerical study of the effects of particle size and polydispersity on the agglomerate dispersion in a cyclonic flow, Chemical Engineering Journal, 164, 432-441.

[6] Lim K.S., Kim H.S., Lee K.W., 2004, Characteristics of the collection efficiency for a cyclone with different vortex finder shape, *Journal of Aerosol Science*, 35, 743-754.

[7] Akiyama T., Marui T., 1989, Dust Collection Efficiency of a Straight-Through Cyclone-Effects of Duct Length, Guide Vanes and Nozzle Angle for Secondary Rotational Air Flow, *Powder Technology*, 58, 181-185.

[8] Trasl P.R., Licht W., 1984, Effect of Recycle on Cyclone Performance, *Ind. Eng. Chem. Process Des. Dev.*, 23, 479-482.

[9] Lee J.W., Yang H.J., Lee D.Y., 2006, Effect of the cylinder shape of a long-coned cyclone on the stable flow-field establishment, Powder Technology, 165, 30-38.

[10] Hffmann A.C., Santen A.V., Allen R.W.K., 1992, Effects of geometry and solid loading on the performance of gas cyclones, *Powder Technology*, 70, 83-91.

[11] Qian FP., Zhang J.G., Zhang M.Y., 2006, Effects of the prolonged vertical tube on the separation performance of a cyclone, *Journal of Hazardous Materials*, B136, 822-829.

[12] Ray M.B., Luning P.E., Hoffmann A.C., Plomp A., Beumer M.I.L., 1998, Improving the removal efficiency of industrial-scale cyclones for particles smaller than five micrometre, *Industrial Journal of Mineral Processing*, 53, 39-47.

[13] Swamee P.K., Aggarwal N., Bhobhiya K., 2009, Optimum Design of Cyclone Separator, *AIChE Journal*, 55(9), 2279-2283.

[14] Ingham D.B., Ma L., 2002, Predicting the performance of air cyclones, International *Journal of Energy Research*, 26, 633-652.

[15] Ji Z.L., Xiong Z.Y., Wu X.L., Chen H.H., Wu H.X., 2009, Experimental investigations on a cyclone separator performance at an extremely low particle concentration, *Powder Technology*, 191, 254-259..

[16] Rong R., Napier-Mum, T.J., 2003, Development of a Efficient Classifying Cyclone, *International Journal of Coal Preparation and Utilization*, 23(4), 149-165.

[17] Stairmand C.J., 1951, The Design and Performance of Cyclone Separators, *Transactions Institution of Chemical Engineers*, 29, 256-373.

[18] Leith D., 1979, In *Handbook of Environmental Engineering*, (N.C. Pereira and L.K. Wang, eds.). Humana Press, Clifton, N.J., I, 61.

[19] Darrow D.S., 1988, Classifying Cyclone, *US Patent 4,743,363*.

[20] Ikebuchi I., Nakano M., Fuse K., Ganz A., 1989, Cyclone Classifier, *US Patent 4,872,973*.

[21] Schwamborn K.H., Smigerski H.J., 1999, Cyclone Collector and Cyclone Classifier, *US Patent 5,958,094*.

CHAPTER 5: THE INFLUENCE FROM A REVISED GRINDER DESIGN ON THE PARTICLE SIZE DISTRIBUTIONS OF FINE POWDER COATINGS

5.1 Introduction

Generally, powder can be made from two main strategies: bottom-up, and vice versa, top-down (also known as the small-to-large and the large-to-small approaches). First of all, the bottom-up strategy is usually used for synthesis of nano or sub-micron particles. Typical examples are the productions of salt and nitrate in chemical industry. The methodology of this approach is basically building the material up from the bottom, either molecule-by-molecule or cluster-by-cluster [1]. Some of the modern bottom-up techniques are the gas phase synthesis [2-5], the liquid phase synthesis [6-10] and the phase separation method [6, 11-13]. On the other hand, particles with sizes of sub-microns or up can be obtained by crashing down bulk materials in the top-down strategy [1]. In most of the cases, it is easier and less expensive to operate than the bottom-up method. However, this approach can hardly produce particles in nano size and the particle size distributions of the produced powders are wide [1].

The processing for powder coatings is a top-down approach. Powder coating chips are always ground by an impact mill. Utilizing the top-down approach can retain a high production throughput, yet the particle size distributions of the produced powder coatings are wide, especially during fine grindings. The small particles that contribute to the wide particle size distributions are not desirable for powder fluidization. The cause of these small particles is mainly due to the over-grinding. If over-grinding can be avoided, the amount of the small

particles could be reduced. Air classifying mill that has a classifier to constantly remove small particles is popular for powder coating productions. It helps to reduce the amount of ground particles which re-enter the milling chamber so as to reduce over-grinding.

A revised grinder design was proposed by the study for reducing over-grindings of the powder coatings. An ordinary grinder crashes particles regardless the particle sizes and all size particles are impacted by the rotating grinding elements during crashing. The idea was to modify the design of grinding elements so as to make the crashing exclusive to coarse particles. Demonstrated by Figure 5-1, a grinding element usually had a convex (or flat) impact surface whereas the impact surface of the modified grinding element is concave. During rotation, the modified grinding element could have a pressure built-up in the middle of the impact surface, creating a "cushioning" effect. Fine particles with small inertia would decelerate as they approach to the impact surface. On the other hand, coarse particles with large inertia would not be significantly affected and they would still receive almost full impacts from the grinding elements. In this study, the proposed modification of the grinder design was evaluated by exploratory experiments on a high shear grinder.

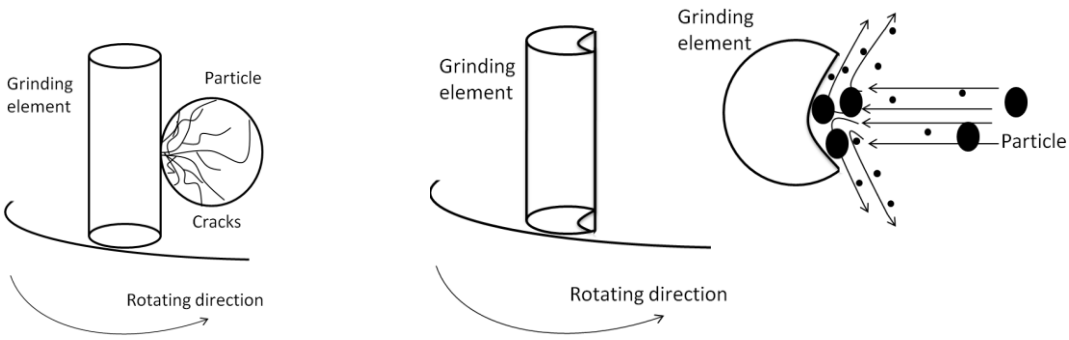

a. Regular grinder pin; b. Modified grinder pin

Figure 5-1: Proposed grinder design for grinding of fine powders

5.2 Materials and Methods

Modifications on the industrial equipment, the air classifying mill (ACM), were not conducted in the first place due to the difficulty in fabrication and the expansive price. Instead, a high shear grinder was manufactured by Strand Manufacturing Co. Inc., USA (Model S102DS) was used for the exploratory experiments. The grinding materials were the powder coating chips supplied by Seibert Powder Coatings, Cleveland, USA. The high shear grinder crashes the powder coating chips into powder by utilizing the rotating grinding blade during the grinding operation, as shown in Figure 5-2. Since the process is sealed inside a closed grinding chamber that had no additional classification involved, the original grinder design can easily create over-ground. On the other hand, it can help observe the influence from the modified grinder design.

 .

Figure 5-2: The blade of the grinder

As shown in Figure 5-3, the original blade had a flat impact surface whereas the modified had a deep notch on the impact surface similar to the concave surface as proposed. The depth

of the notch from the modified blade was 1mm and it was created by the two extensions on the top and bottom surfaces of the blade. In order to reduce the influence from the thickness of the extensions, the leading edges of the extensions were beveled. The grinder speed was kept constant in the experiment, yet the grinding time varied. 5 samples were obtained from grinding times of 10 s, 20 s, 40 s, 50 s and 60 s. The loadings of the powder coating chips for different grinding times were maintained the same.

a. The original blade

b. The modified blade

Figure 5-3: Comparison between original and modified blades

The particle sizes and the particle size distributions of the collected samples were investigated. The particle size was measured by a laser particle size analyzer (BT9300S, Better Size Laser Analyzer). D_{10}, D_{50} and D_{90} were the three important values obtained from the measurements. These values are the particle sizes which below the corresponding volume percentage, for instance, a D_{10} value was defined as a diameter where 10 vol% of the particles of the powder were less or equal to this diameter. In general, D_{10} and D_{90} were the

common parameters to determine the amount of small and large particles in the powders, whereas D_{50} is the medium particle size of the powders. The span which indicates the particle size distribution of the powder could be determined by using D_{10}, D_{50} and D_{90}:

$$Span = \frac{D_{90} - D_{10}}{D_{50}} \qquad \text{Eq. 5-1}$$

Increased D_{10} and/or reduced D_{90} while maintaining the D_{50} can lead to a steeper curve of the particle size distribution. As these two values became identical to D_{50}, the powder will have uniform size particles. The span defines the overall shape of the distribution curve. Narrow particle size distribution is always desirable for powder coatings, especially fine powder coatings, since reduced D_{90} leads to a better coating quality and increased D_{10} is in favour of powder flow properties.

5.3 Results and Discussion

The solid square symbols in Figure 5-4 show that the chips are ground into a powder with medium size of about 33 μm in the first 10 second in the original grinder. As the grinding duration increased to 40 s, the size of the powder is crashed down rapidly to about 15 μm. The particle sizes of ground powders become stable after 40 s. Therefore, the majority of the crashing occurs between the grinding duration of 10 s to 40 s. During this 30 s duration, coarse particles are impacted by the grinder blades and the broken pieces generated from the impacts are involved in the continuous grinding since the process is sealed inside a closed chamber. Therefore, the over-grindings can be observed in this grinding period.

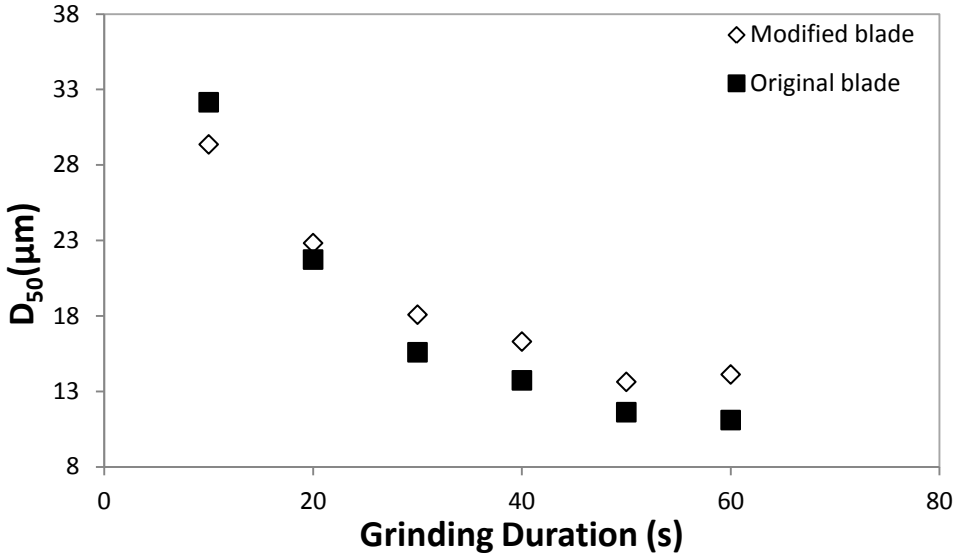

Figure 5-4: The medium particle size with respect to the grinding duration

On the other hand, the modified grinder crashes down the powder coating chips slightly faster than the original grinder in the first 10s. The two extensions of the original grinder blade act as a "dual-blade". While the grinding materials are still in bulk size, they could generate more crashing than the original grinder blade. After 10 s of grinding, the powder had a medium particle size of about 29µm. As the grinding time increased, the powder collected from the modified grinder had less rapid reduction in the medium particle sizes. It indicates that the grinding efficiency of the modified grinder becomes lower than the original grinder from 10 s forward. However, it could be also contributed by the less over-grinding by the modified grinder blade which is desired.

Figure 5-5 shows the particle size measurements of the collected samples. The D_{10} and D_{90} of the produced powders from both grinders decreased drastically as the medium particle size reduces with the increasing grinding time. Comparing with the original grinder, the modified grinder was able to produce powders with larger D_{10} and smaller D_{90} throughout the grinding process. Recalling from the discussions for Figure 5-4, the first 40 s was the

grinding period that the over-grinding could occur the most. The increased D_{10} and reduced D_{90} indicated that the modified grinder blade was able to reduce the over-grinding due to the created "cushioning" effect by the notch on the impact surface.

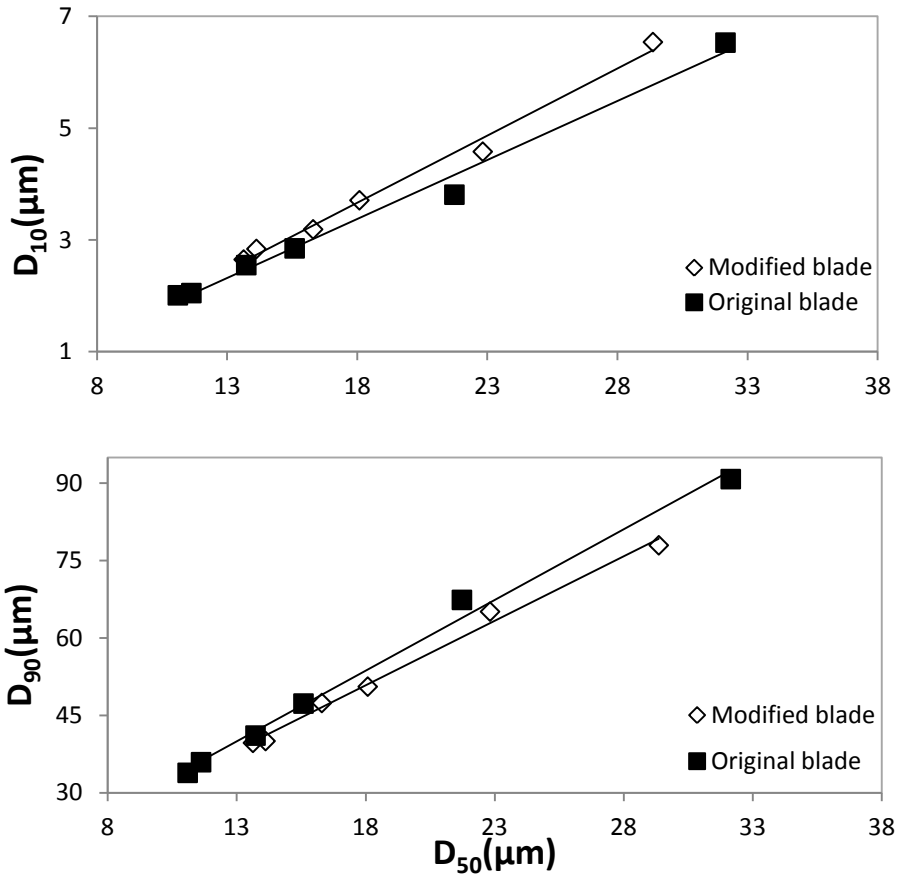

Figure 5-5: D_{10} and D_{90} of the produced fine powders with respect to D_{50}

It is to note that the improvement provided by the modified grinder seems to deteriorate, indicating by the less reduced in D_{90} and the less increased D_{10} shown in Figure 5-5, when the medium particle size decreases. However, this phenomenon could be caused by the reduced powder size. Referring back to Eq. 5-1, the particle size distribution is defined as the difference between D_{90} and D_{10} divided by D_{50}. If the span remains unchanged, the difference between the D_{90} and D_{10} will reduce as the D_{50} becomes smaller. It explains the

reason why the D_{10} and D_{90} of the ground powder from the modified grinder are closer to that from the original grinder, as the D_{50} of the ground powder reduces.

Figure 5-6 further explained that the modified grinder design was able to provide comparable reduction in the span for various D_{50} of the ground powder. Based on the obtained results from Figure 5-6, the reduction of the span provided by the modified blade design was approximately 7.6%.

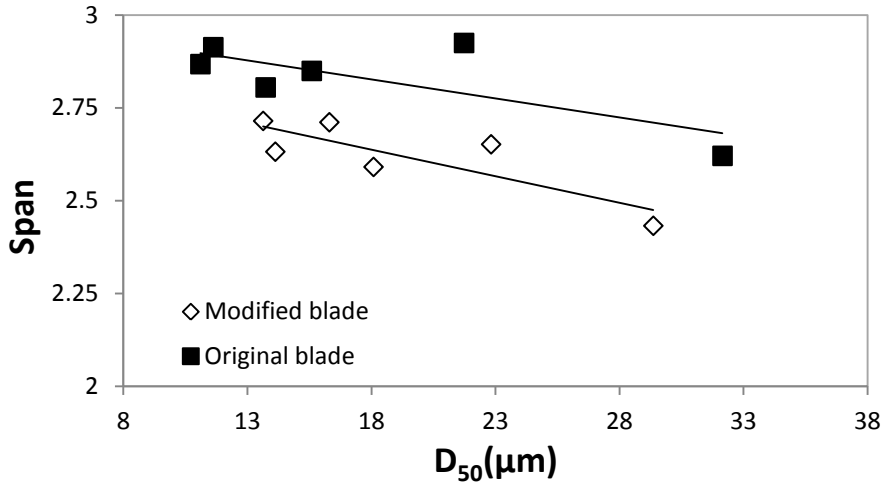

Figure 5-6: The span of the produced fine powders with respect to D_{50}

A smaller span indicates more uniform particle sizes of the powder particles. It is beneficial for fine powder applications since less small particles improve the powder flow behaviour and less coarse particles lead to better coating quality. During mass production, narrowing the span of the produced powder coatings always relies on additional sieving and classification processes which requires expansive equipment and extensive labour work. Yet, the reduction of the span of the powder coatings by these conventional methods has never been effective. In comparison, the improvement on narrowing the span of the ground powder

provided by the modified grinder design, demonstrated by the obtained results, is remarkable.

5.4 Outlook for the industrial-scale grinder

In the industry practices, the air classifying mill (ACM) has been the most popular choice for the productions of powder coatings due to its high throughput and low cost. A typical example of the ACM is shown in Figure 5-7. The grinder of an ACM consists of a stationary shrouding ring with sharp grooves and grinding elements attached to a circular plate. During the grinding operation, the chip materials are first broken into pieces by the impacts with the grinding elements that rotate in high speed. And then, the ground particles will bounce between the shroud ring and the grinding elements for secondary impacts and attritions. After that, the air flows inside the ACM drives the particles towards a rotating classifier. Only particles that small enough can escape through the classifier and others are ejected back into the chamber for further grinding.

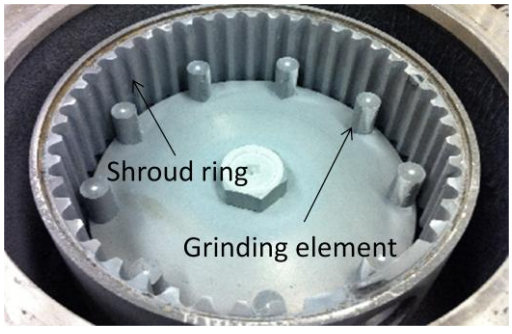

a. The grinding component of the ACM

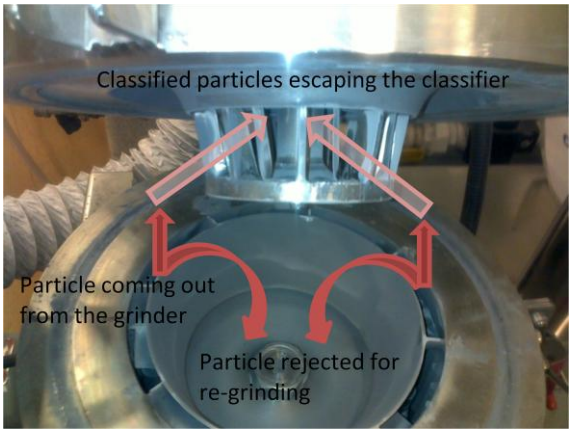

b. The air classifier inside an ACM

Figure 5-7: A typical mechanical mill for powder coating manufacture – The air classifying mill (ACM)

An investigation of the proposed grinder design had not yet been evaluated in an industrial scale ACM due to the lack of resources and the fabrication capability of the laboratory. Nevertheless, the proposed concept has potential to success for improving the fine powder production in an ACM. First of all, the ACM follows similar comminution principle as the regular grinder used in this experiment: the particles are broken down when the kinetic energy (the energy of comminution) exerted by the grinding elements is greater than the breakage energy of the material [15-16]. Numerical studies [17-18] of an ACM disclosed that the impact velocity of the particle is highest at the grinding elements and the impact velocity at the shroud ring is 3 to 6 times lower. In addition, the studies also discovered that the majority of the crashing of particles occurs from the front of the grinding element by both normal and inclined impacts [17-18]. Therefore, modifying the impact surfaces of the grinding elements from convex to concave is the most effective way on reducing the over-grinding of the particles in the grinder. The modification to the grinding elements of an ACM according to the concept proposed by this study is expected to reduce particle size distributions of the produce powder coatings.

Although the proposed modification of the grinding element has not yet been investigated in an industrial scale ACM, preliminary experiments on a lab scale ACM were conducted. The lab scale ACM is manufactured by Donghui Powder Processing Equipment Co., LTD with squared grinding elements installed. The squared grinding elements were special ordered from the manufacturer. There are additional screw threads made to the side faces of the grinding elements so that attachments can be mounted on for obtaining various configurations of the impact surface.

First of all, two side extensions were attached to each of the elements as shown in Figure 5-8. It is similar to the modification on the high shear grinder utilized in the exploratory

experiment. It was expected the created notch on the grinding surface could induce the "cushioning" effect for reducing the over-grinding so as to narrow the span of the ground powders.

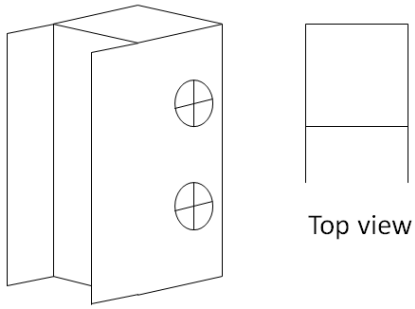

Figure 5-8: The 1st modification of the grinding element of the lab scale ACM

Figure 5-9 shows that the extensions on the grinding elements caused even higher spans of the ground powders. The results indicate that more severe over-grinding probably occurred during the grinding than the case with the unmodified grinding elements. Thus, the modification indicated contradictory results to the exploratory experiment.

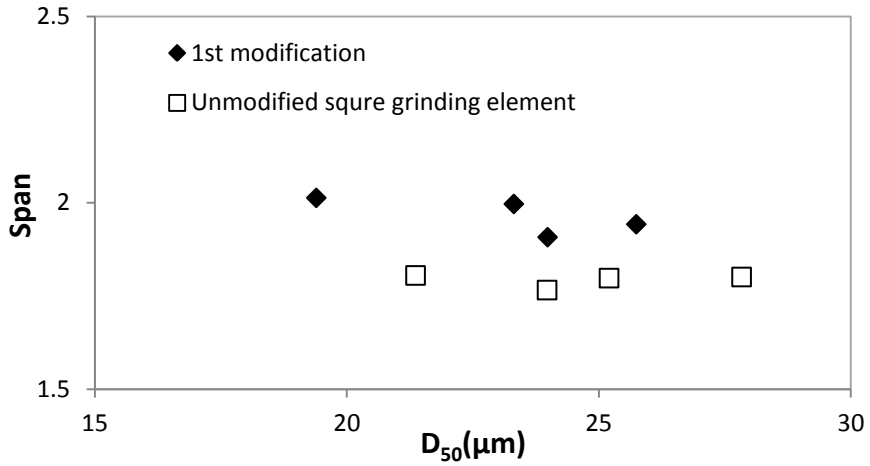

Figure 5-9: The measured spans of the powders ground by the lab scale ACM with the 1st modified grinding elements

The configuration of the grinding element was then changed with only one extension attached to each of the grinding elements, as shown in Figure 5-10. This revision of the modified element design reduces the spans of the ground powders to be the same as that obtained from the unmodified grinding elements, as indicated by Figure 5-11. The differences between results obtained from the two modification designs imply that the double extensions on the grinding elements could function as "dual-blade" which was discussed in the previous section. The two extensions become two impact elements during grinding, generating even more over-grinding than the unmodified elements. On the other hand, the notch opening on the impact surface was wide (8mm). Therefore, the "cushioning" effect created by the notch could be insufficient to reduce the span of the ground powders.

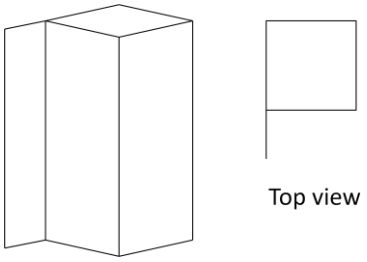

Figure 5-10: The 2nd modification of the grinding element of the lab scale ACM

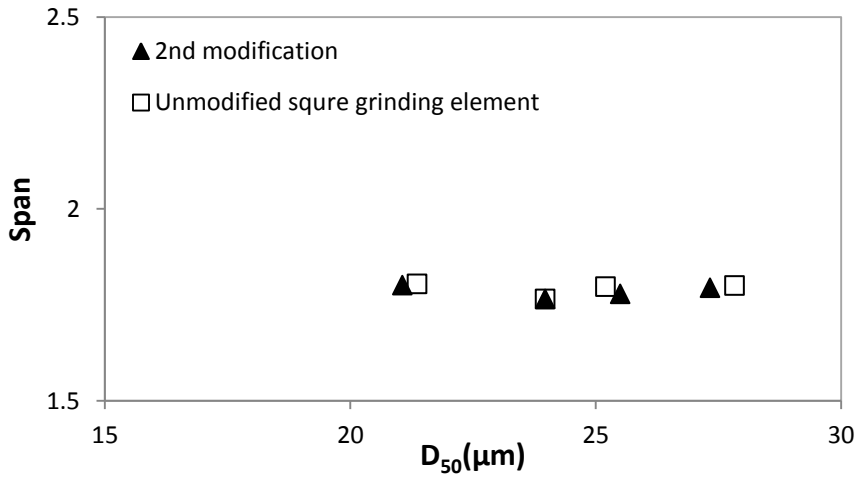

Figure 5-11: The measured spans of the powders ground by the lab scale ACM with the 2nd modified grinding elements

According to the conclusion from the results obtained first two designs, there was a third design of the grinding element as proposed in Figure 5-12. It adds additional plates between the two extensions on the grinding element. In doing so, the opening of the notch is reduced and the "cushioning" effect can be enhanced.

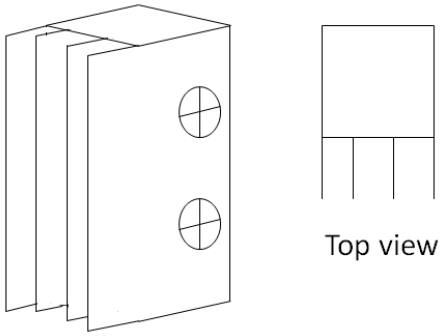

Figure 5-12: The 3rd modification of the grinding element of the lab scale ACM

Fabrication of the new attachments for the grinding elements according to the design in Figure 5-12 is in progress. The testing of grinding elements with this modification design will be a part of the future work to this study.

5.5 Conclusion

Modification on the grinding blade was proposed and evaluated in this study. The concept was to use concave impact surface to reduce over-grinding of the particles during fine powder production. The experiments indicated promising results. The particle size distributions of the produce fine powder coatings were narrowed over a wide particle size range. The comparisons in the span showed a substantial improvement over the original design. On the other hand, the grinding efficiency of the modified grinder was not significantly influenced.

Reference

[1] Cao G.Z., 2004, *Nanostructures and Nanomaterials: Synthesis, Porosity, & Applications*, UK: Imperial College Press.

[2] Wegner K., Walker B., Tsantilis S., Pratsinis S.E., 2002, Design of metal nanoparticle synthesis by vapor flow condensation. *Chemical Engineering Science*, 57, 1753-1762.

[3] Jang H.D., Kin S.K, 2001, Controlled synthesis of titanium dioxide nanoparticles in a modified diffusion flame reactor, *Materials Research Bulletin*, 36, 627-637.

[4] Spicer P.T., Artelt C., Sanders S., Pratsinis S.E, 1998, Flame Synthesis of composite carbon black-fumed silica nanostructured particles, *Journal of Aerosol Science*, 29, 647-659.

[5] Vollath D., 2007, Plasma Synthesis of Nanoparticles, KONA, 27, 39-55.

[6] Keishi G., Hiroaki M., Higashitani, 1997, *Powder Technology Hand Book 2nd Ed.*, Revised and Expanded. New York: Marcel Dekker Inc.

[7] Gaikwad S.P., Dhage S.R., Potdar H.S., Samuel V., Ravi V., 2005, Co-precipitation Method for the Preparation of Nanocrystalline Ferroelectric $SrBi_2Nb_2O_9$ Ceramics, *Journal of Electroceramics*, 14, 83-87.

[8] Koike M., Abe O., 2004, Redox synthesis of magnetite powder under mixing-grinding of metallic iron and hydrated iron oxide, *Solid State Ionics*, 172, 217-220.

[9] Suchanek W.L., Riman R.E., 2006, Hydrothermal Synthesis of Advanced Ceramic Powders, *Advances in Science and Technology*, 45, 184-193.

[10] Somiya S, Roy R., 2000, Hydrothermal synthesis of fine oxide powders, *Bulletin of Material Science*, 23(6), 452-460.

[11] Kakihana M., Okubo T., 1998, Low temperature powder synthesis of $LaAlO_3$ through in situ polymerization route utilizing citric acid and ethylene glycol, *Journal of Alloys and Compounds*, 266, 129-133.

[12] Picciolo J.J., Lee G.F., Goretta K.C., 2001, Synthesis of mullite powders by acrylamide polymerization, *Journal of Material Science Letters*, 20, 1639-1641.

[13] Goncalves O.H., Asua M.J., Hermes P.H., Machado, R.A.F, 2008, Synthesis of PMMA/PS Core-Shell Structured Particles by Seeded Suspension Polymerization, Macromoleculles, 41, 6960-6964.

[14] Mu F.S., 2006, Current Status and Development Requirements for Research of Theory of Comminution, Sulphur Phosphorus & Bulk Materials Handling arelated Engineering, 4, 20-23

[15] Vogel L., Peukert W., 2003, Breakage behaviour of different materials-construction of a mastercurve for the breakage probability, *Powder Technology*, 129, 101-110.

[16] Rumpf H., 1973, Physical aspects of comminution and new formulation of a law of comminution, *Powder Technology*, 7, 145-159.

[17] Petya T., Karl-Ernst W., Wolfgang P., 2011, Grinding in an air classifier mill-Part I: Characterisation of the one-phase flow, *Powder Technology*, 211, 19-27.

[18] Petya T., Karl-Ernst W., Wolfgang P., 2011, Grinding in an air classifier mill-Part II: Characterisation of the two-phase flow, *Powder Technology*, 211, 28-37.

SECTION III

STUDIES ON THE APPLICATION METHOD FOR POWDER COATINGS

Corona charge spraying, a kind of the electrostatic coating method, has been the most common technique for powder coating application. It is capable of providing not only thin but also uniform coating films. However, problems, such as low transfer efficiency and Faraday Cage effect, had been encountered during corona charge spraying of powder coatings, especially fine powder coatings. This section of the thesis study is to develop solutions to improve the corona charge spraying performance.

CHAPTER 6: FURTHER STUDY ON THE INFLUENCE OF HUMIDITY ON IMPROVING FISRT PASS TRANSFER EFFICIENCY OF POWDER COATINGS DURING CORONA CHARGE SPRAYING

6.1 Introduction

A corona charge spraying is a popular method for applying powder coatings due to its flexibility, outstanding reliability and excellent coating efficiency. There are three different charging phenomena for a corona charge spraying with respect to the size of the sprayed material: field charging for particles larger than 0.5 μm [2-3], diffusion charging for particles smaller than 0.2 μm [4-5] and combination of field and diffusion charging for particle in between 0.2 μm and 0.5 μm. Since the powder coating particles are generally in the size between 10 μm and 100 μm, the field charging dominates. In the field charging process, powder particles collide with the ions generated around the corona electrode and the particles catch the ions by the collisions to gain charges.

The corona charge spraying is a typical negative corona point-to-plane discharge process. Based on previous studies [6-7], there are two regions between the corona electrode (the tip of the corona spraying gun) and the plane electrode (the coating target). The first region is the space around the corona electrode known as the ionization region, where free electrons are generated from the ionization process. The powder particles charged by these electrons while flying out from the spray gun are mainly under the aerodynamic force [8]. The second region is called the drift region, which is in between the ionization region and the target that has a weaker electric field. When the powder enters the drift region via the air stream, the

motions of the powder particles are affected not only by the aerodynamic force but also the electrostatic force and gravity [8]. As the powder moves closer to the coating target (about 10mm), the electrostatic force starts to dominate the motions of the particles [6]. The deposited particles finally attach to the grounded target by electrostatic forces.

In recent years, fine powder coatings with median particle sizes smaller than 30μm have attracted increasing attention from the coating industry. Comparing with the coarse powder coating (median particle sizes above 35 μm), it can provide benefits such as better coating quality and thinner coating film. However, such benefits are accompanied by the drawback of the reduction in FPTE (first pass transfer efficiency) during corona charge spraying, which is defined as the mass ratio of powder deposited on the target to the total mass of the powder sprayed [10]. In applications, a higher corona voltage is always used to compensate this problem. The increased voltage can improve the charging intensity so as to direct more particles onto the target. However, the over charged powder can also reach its breakdown field strength much quicker on the coating target. As a result, back ionization, which is the phenomenon of random powder breakdown caused by the over-accumulated charges, can occur much sooner and the improvement in the FPTE is limited [9-10]. In addition, back ionization can also create surface defects such as craters and pinholes. Therefore, boosting the corona voltage cannot essentially solve the low FPTE problem of fine powders.

Studies by Sharma et al. [11] and Messaoudi et al. [12] disclosed that back ionization could be reduced by increased humidity level inside the spray booth. Because the increased humidity could accelerate the charge decay across the deposited powder so to reduce the electrical field strength of the powder on the coating target. It would delay the back ionization so as to improve the FPTE. However, the humidity level inside the spray booth is usually kept below 60%RH in commercial applications. High humidity levels would cause a

decrease in the retention of the electrostatic charges because of the ion cluster formations [12-13]. Berger stated that clustering was attributed to the salvations of the negative or positive ions by water; in other words, the ions were surrounded by water molecules [14-15]. Therefore, these ion clusters which were heavier and bigger due to the increased amount of the moisture in the spray booth reduce the charge mobility in the space, deteriorating the charging performance [16]. It was also discovered by Meng that the additional moisture inside the spray booth could reduce the corona current measured on the target implying that the improvement on the FPTE was limited [17]. Moreover, humidifying an industrial spray booth will require much more energy than normal which is not economical.

The previous study conducted by the author suggested a distinct method of utilizing moisture to improve the FPTE in the corona charge spraying [18]. The method was to humidify the fluidization air so that the powder could gain moisture in the fluidization process prior to the spraying. In this way, humidity level in the spray booth could remain unchanged for avoiding any charging deterioration. Furthermore, it was much easier and more economical to be implemented. This part of the thesis was an extended study to the previous work for investigating the electrical properties of the humidified powders according to the spraying test results. In addition, the results of the flowability tests were reassessed according to the new findings. Finally, the influences from the humidified powders on the coating qualities were examined for obtaining a comprehensive conclusion for this new method.

6.2 Materials and Methods

Three powder materials were used in this study named as powder A, C_1 and C_2 as listed in Table 6-1. These powders were commercial coating powders provided by the manufacturers.

Powder A was polyester-epoxy (hybrid) powder whereas powder C_1 and C_2 were polyurethane powders. Powder A and C_1 were fine powder coatings with median particle size around 25 μm. The regular size powder coating, powder C_2, was the same material as powder C_1 but with a larger particle size. Powder C_2 was prepared for the comparisons with the fine powder coating samples. The compressed air used for spraying and fluidization had controlled humidity level of 12-14%RH. The spray booth was always air conditioned with ambient temperature of 23-25 ^{o}C and 35-40%RH.

Table 6-1: Particle sizes of the test powders

Powders	**Particle size distribution**		
	D10 (μm)	D50 (μm)	D90 (μm)
A	12.6	24.7	45.5
C_1	11.2	24.0	47.0
C_2	13.1	37.8	75.6

Powder coating materials are usually strong dielectrics that have low conductivities. Once they are charged during the spraying, the adhered ions are difficult to be removed. The complete dissipation of the charge on the powder coating will take up to hours even on a metal subtract such as the surface of the coating part. As demonstrated in Figure 6-1, the negatively charged particles on the metal substrate induce an equivalent charge inside the substrate yet with positive polarity, called mirror charge. The attraction between the particle charge and the according mirror charge hold the deposited particle on the substrate and the two charges generates an electrostatic field.

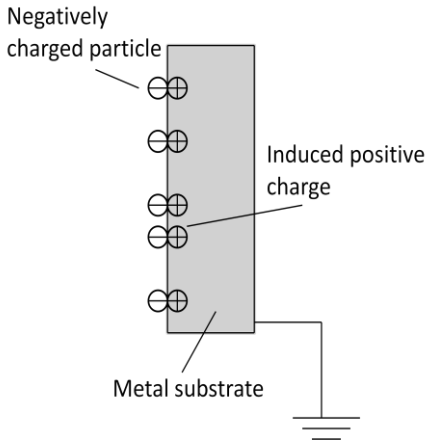

Figure 6-1: A demonstration of charged particles on a metal substrate

The strength of the electrostatic field between the particle charge and the mirror charge, E_p (V/m), can be calculated by [9]:

$$E_p = \rho_p J \qquad \text{Eq. 6-1}$$

where ρ_p (ohm-m) is the resistivity of the powder material and J is the corona current density (A/m^2). E_p of powder coatings usually reaches or surpasses the breakdown field strength easily during corona charge spraying. It has been know as the "self-limiting" property of powder coatings.

If the breakdown field strength is reached, the accumulated charge by the deposited particles creates corona effect, similar to the electrode of the spray gun, so that the air between the deposited particles can be ionized. As shown in Figure 6-2, the negative electrons run towards the metal substrate due to the positive mirror charge since opposite charges attracts; on the other hand, the positive ions escape through the deposited powder particles. Due to the vigorous flow of ions and electrons, the deposited particles can be broken down from the surface of the substrate, more severely, sparks could be generated. This phenomenon is

known as back ionization. Back ionization can significantly restrict the FPTE of powder coatings. Therefore, it is not desired during powder coating spraying.

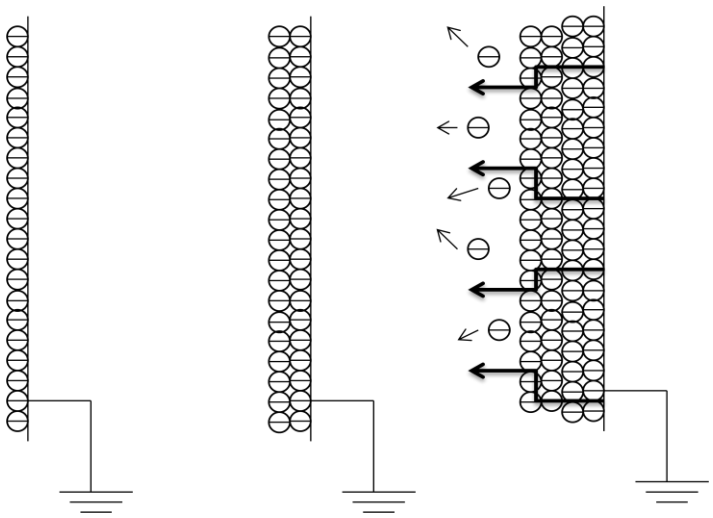

Figure 6-2: Development of back ionization

According to Eq. 6-1, a decreased resistivity could lead to a reduction of the electric field strength of the particles allowing more charged particles to deposit on the coating target before reaching the limit of the breakdown field strength. Therefore, the resistivity of the humidified powder was an important electrical property to investigate. The resistivity of the powder was measured according to ASTM standard D257. Keithley 610C electrometer was used to measure the resistance of the powders in a 7cm X 7cm square testing cell with measured depth. The resistivity was calculated by:

$$\rho = R\frac{A}{l} \qquad \text{Eq.6-3}$$

where ρ is the resistivity (ohm-m), R is the measured resistance (ohm), A is the cross-sectional area of the test cell (m^2) and l is the measured depth (m).

In the experiment, the powders were humidified in a fluidized bed by a humid air with 90%RH. As demonstrated in Figure 6-3, the humidifier was used to increase the humidity level of the fluidizing air to about 90%RH. The moisture content of the powders was expected to be increased during fluidization before spraying. The processed powders taken from the fluidized bed were then fed into the venture pump by a vibrating feeder (FMC Syntron vibrating feeder) with feeding rate of 6 g/min. The gun voltage was set as -35 kV with spraying duration of 1 minutes. The coating target was a circular copper plate with 30cm diameter and the spraying distance was 20 cm.

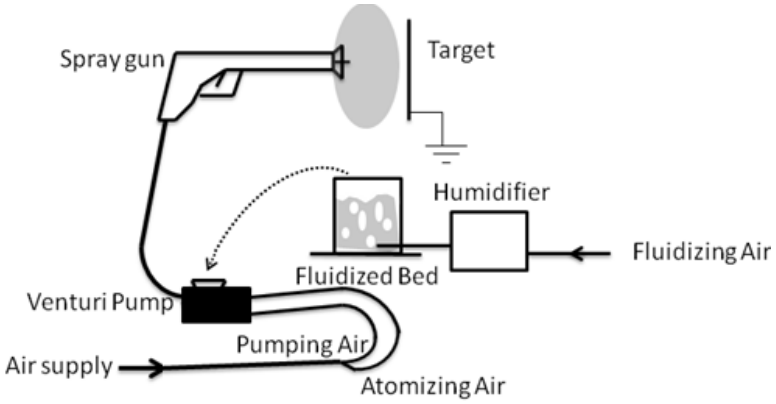

Figure 6-3: Schematic diagram of the apparatus setup for powder humidification

Both of the moisture content and resistivity changes of the humidified samples collected from different fluidization durations were measured. In order to increase the accuracy of the readings, the Mettler Toledo scale (model XS205) with readability of 0.01 mg was used. In addition, the testing cell for the resistivity measurements was shielded within a Faraday Cage to reduce the electrical noises from surroundings.

The corona charge sprayings were conducted to evaluate the FPTE of the humidified powders. The FPTE was calculated as the weight of the powder sprayed on the substrate ($W_{substrate}$) divided by the total weight of the powder sprayed (W_{total}):

$$FPTE = \frac{W_{substrate}}{W_{total}} \qquad \text{Eq. 6-4}$$

Observations on powder flowability and coating quality

On the other hand, the powder flowability that represents the ability of free-flowing in normal handling processes such as fluidization, pneumatic transportation and spraying is crucial in industrial application. Poor flowability will cause application issues and coating defects. Thus, the flowability of the humidified fine powders was examined. The powder samples were placed in a highly humidified environment (99%RH) to simulate the stagnate condition in a humidified fluidized bed. The humidification condition was more severe in the test than the expected real situation since the air humidity level was much higher. However, it could disclose how the powders would behave in an extreme case of the humidification.

The flowability was evaluated by two characterization methods: the avalanche angle (AVA) and the rotational bed expansion ratio (RBER). The AVA was measured by a rotational powder analyzer (Revolution Powder Analyzer, Mercury Scientific Inc., Sandy Hook, CT, USA). The test requires 120 ml of powder (tapped volume) in a drum container (diameter of 10.9 cm and width of 3.5 cm) with transparent side walls made of glass. The drum is powered by an electric motor and it runs at the speed of 0.6 rpm. In the measurements, the powder rotates with the drum under friction. And then, the powder collapses at an angle, which happens when the inter-particle forces cannot sustain the mass of the powder. The angle is the AVA. The powder motion is recorded by the computer controlled camera and the final result is averaged from 200 readings. Previous study found that the AVA is

proportional to the angle of repose representing the same aspect of powder flowability [18]. However, the measurement of AVA is more stable and accurate since more readings are taken and the data-acquisition is fully automatic.

The RBER was also measured by the rotational powder analyzer. The same procedure was followed to load the drum. Unlike the AVA, the drum runs much faster in this test. When the drum speeds up, the air enters the powder and the volume of the powder expands. In order to measure how well the powder fluidized, the volumetric expansion ratio (expanded powder volume divided by the initial powder volume) is obtained. The measurement is taken at the drum speed of 70 rpm which is the maximum speed for most of the powder coating materials. A higher rotational speed can throw the powder to the wall of the drum due to the centrifugal effect. Comparing with the conventional bed expansion, the RBER is obtained from the sealed container. It reduces the error of the readings and it can also ensure that there is no loss of particles during the whole measurement. The RBER can represent similar aspect of the flowability as the conventional bed expansion [19].

Between the two characterizations, the RBER is a more dynamic powder flowability which indicates how well the powder flows during fluidization or pneumatic transportation. On the other hand, the AVA is a more static powder flowability that indicates how easy the powder will get agglomerated or accumulated. These characterization tests are necessary to fully predict the powder flowability [19-20]. A smaller AVA and a larger RBER implies better flowability of the powder.

6.3 Results and Discussion

6.3.1 Effect of Humidity on the Electrical Properties of the Powders

The fine powder A, C_1 and the regular size powder C_2 were used in the experiment. The powder samples were humidified inside a fluidized bed with humid air (90%RH). Figure 6-4 indicates the changes in the moisture content of the samples with respect to humidification time. Results indicate that all of the three powders gain moisture rapidly in the first few minutes. However, the moisture contents started to slow down at about 20 minutes and became more stable in the rest of the test. It implied that particles picked up moisture quickly in the beginning due to the adsorptions of the moisture. As the moisture got saturated on the particle surfaces, slow absorption of the moisture by the particles happened. Powder C_1 and C_2 which are the same material with different particle sizes show very similar trend of the moisture gain overall, although the fine powder gained moisture a bit quicker than the regular size powder in the beginning. On the other hand, powder A obtained much less moisture during the test than the others.

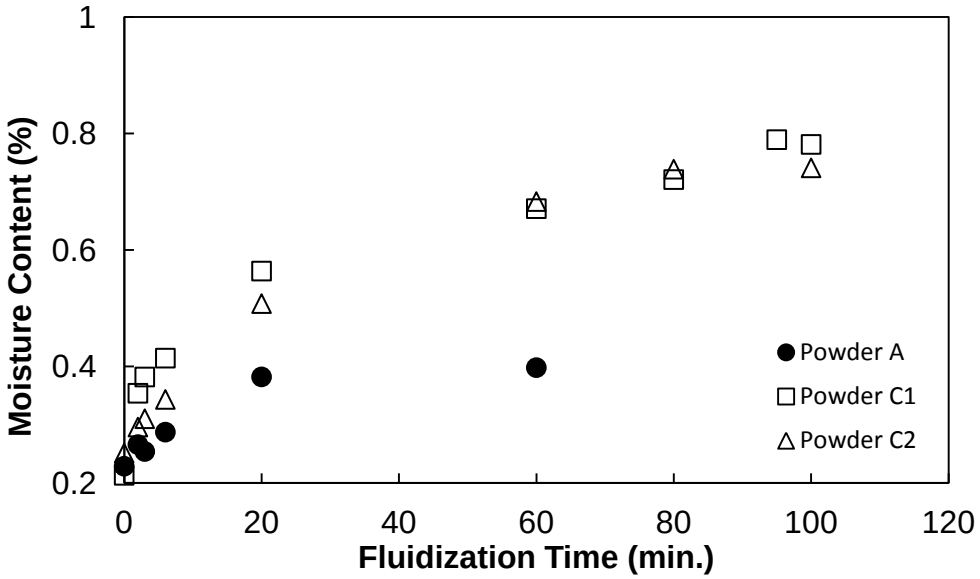

Figure 6-4: The changes in moisture content of the humidified powders

Based on the plots in Figure 6-4, the fluidization by the humidified air was found to cause a maximum moisture gain of about 0.8% for powder C_1 and C_2 whereas about 0.4% for powder A. The differences in the responses to the humidification between powder A and C_1 could be attributed to the differences of the materials. In addition, surface properties could be another possible reason. It could also depend on the surface hydrophobicity of the particles. Rajesh et al. [21] discussed that particles with more hydrophilic surfaces tended to absorb/adsorb more moisture. It was also discovered by Rajesh et al. that the surface resistivity of the particles with different surface roughness could vary in different relative humidity levels [21].

The resistivity of the extracted examples during the fluidization test is shown in Figure 6-5. It is found that the resistivity of the powders decreases drastically in the first few minutes. After 10 minutes of fluidization, the resistivity of all the samples becomes stable. According to the results in Figure 6-4, it is realized that the moisture gained by the adsorption of the moisture on the particle surfaces has most significant influence on reducing the resistivity of the powders. Among the three samples, fine powder A and C_1 have the most significant reduction in the resistivity. Comparing with powder C_1, the regular size powder C_2 has much less changes in its resistivity even with a similar moisture gain as powder C_1. The reason for that could be the larger particle size. When deposited on a surface, the larger particles in the regular size powder create more inter-particle space, or to say, less particle contacts than the case with fine powders. Therefore, the effect from the moisture on the regular size powder seems less significant. On the other hand, fine powder that has much larger surface areas is able to attract more moisture than the regular size powder. It can be another contributing factor to the difference found between powder C_1 and C_2.

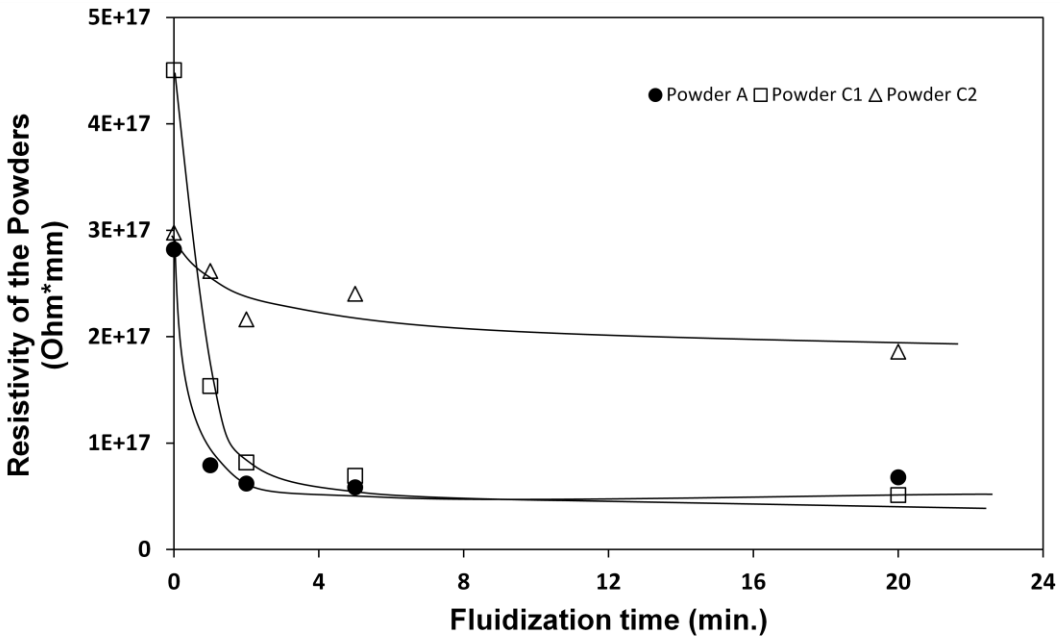

Figure 6-5: Changes in resistivity of the humidified powders

6.3.2 Spraying Test

The results of the spraying tests obtained from the preliminary study are shown in Figure 6-6 [18]. The FPTE of the fine powders is improved by the humidification in the first few minutes. It coincides with the changes in the resistivity and the moisture gain of the powders shown in Figure 6-5 and Figure 6-4. Furthermore, the trend obtained from the experimental results is in agreement with the discussion on Eq. 6-1 that the lower resistivity could weaken the electrical field strength of the accumulated particles on the target, reducing the back ionization and improve the FPTE [11]. The FPTE of the powders becomes stable after about 4 minutes since the resistivity of the powders is measured to be unchanged during the rest of the fluidization. It implies that the moisture gain beyond the first few minutes do not further improve the FPTE. Referring to the discussion for the results in Figure 6-4, the adsorption dominates in the beginning of the humidification test due to the moisture adsorbed on the particle surfaces. Therefore, moisture on the particle surface is really the main factor for the

improvement of the FPTE. On the other hand, the moisture gained by the absorptions of the particles has no significant influence on improving the FPTE.

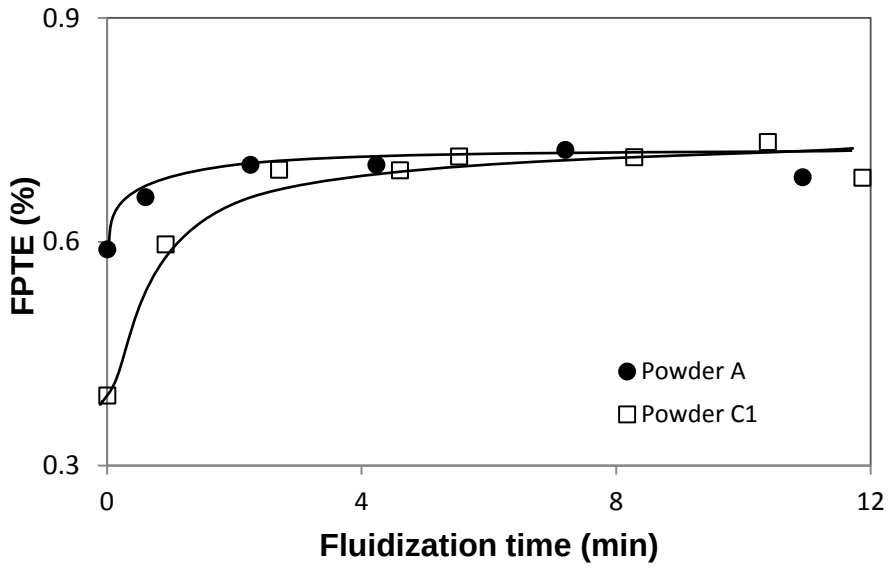

Figure 6-6: FPTE of powder A and powder C_1

The plots in Figure 6-6 indicate that powder C_1 has lower FPTE than powder A in the beginning of the test which is also in agreement with the results in Figure 6-4 that the resistivity of powder A is lower than powder C_1. The results from the two tests also coincide as the fluidization time increased. Both of the resistivity and the FPTE of the two powders become closer and more stable. It further confirms that the improvement of the FPTE was caused by the reduced resistivity of the humidified powders.

This study also investigated the improvement of FPTE of the fine powder coating under various humidity levels of the fluidization air. The variation of the humidity level of the fluidization air was accomplished by a system shown in Figure 6-7. The humid air came out from the humidifier was mixed with dry air to obtain a desired humidity level before entering the fluidized bed. The improvement of the transfer efficiency was obtained by:

$$\text{Improvement} = \frac{(\text{FPTE}_{Fluidized} - FPTE_{Original})}{FPTE_{Original}} \qquad \text{Eq. 6-5}$$

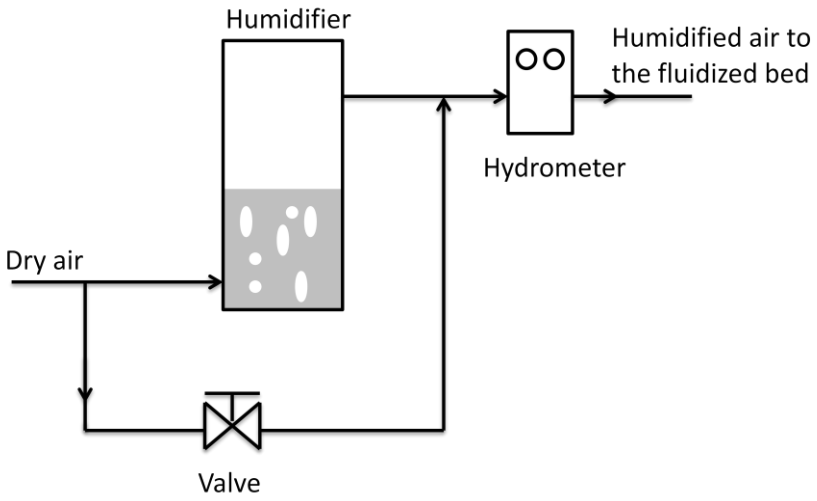

Figure 6-7: The control system for adjusting the humidity level of the fluidized air

Figure 6-8 indicates that the improvement of the FPTE can be strongly influenced by the humidity level of the fluidized air. The results disclose that increasing the humidity level of the fluidized air from 30%RH to 50%RH provided an improvement of the FPTE from about 6% to about 8%. As the humidity level of the fluidized air further increased to 70%RH, the improvement of the FPTE became 9%. Finally, the humidity level of 90%RH of the fluidized air provided the highest improvement of the FPTE which was about 10%. Therefore, the improvement of the FPTE increased progressively with the humidity level of the fluidized air. This finding is encouraging because a lower humidity level than 90%RH of the fluidized air can still provide quite significant improvement of the FPTE. As an implication for applications, extreme humidification of the powders is not necessary and a

lower humidity level of the fluidized air is easier and more economical to achieve in the much larger scale applications.

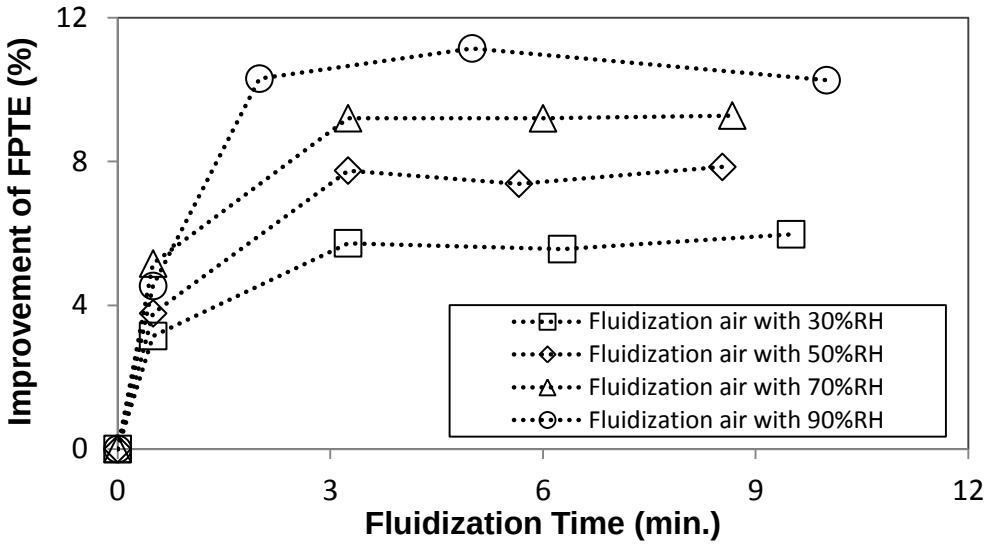

Figure 6-8: The improvements in the FPTE of powder C_1 by various humidity levels of the fluidized air

The results from the spraying test with regular size powder C_2 are plotted in Figure 6-9. Similar to the fine powders, the FPTE of powder C_2 was improved as the fluidization time increased; nevertheless, the improvement was not as significant as powders A and C_1. It can be explained by a less significant reduction in the resistivity of powder C_2 shown in Figure 6-5. Therefore, the regular size powder was not able to obtain a comparable improvement to the fine powder although the gained moisture was almost the same.

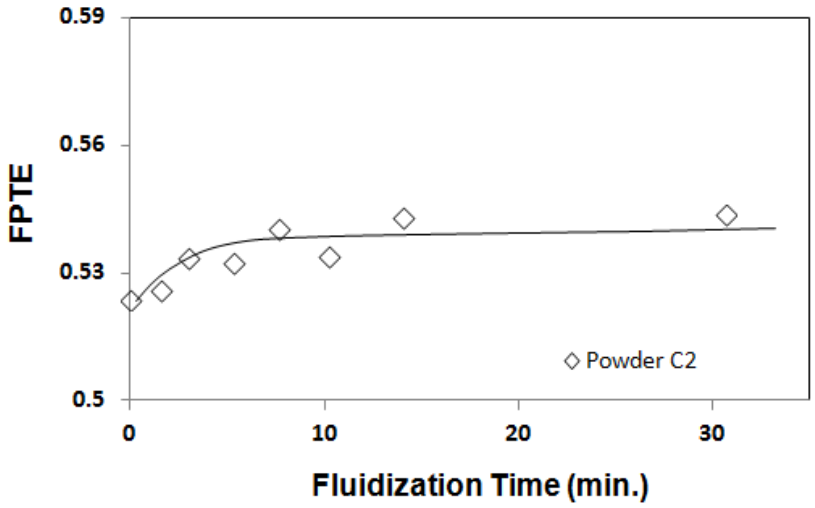

Figure 6-9: FPTE of powder C_2

6.3.4 Effects of the Humidity on Powder Flowability

Powder flowability can be deteriorated by the additional moisture content. The deteriorated flowability will increase the risk of having problems such as powder agglomeration and powder de-fluidization during the applications. This part of the study is to evaluate the flowability of the humidified powders by the fluidization method.

The conducted experiment was to examine the flowability of the powder with different moisture contents. The powder was exposed in a humid environment with 99%RH to achieve high moisture gain. Samples were extracted from different exposure times for observations and the flowability measurements. Powder A and powder C_1 were used in this test.

Shown in Figure 6-10 [18], the moisture gained by the particles of both powders was up to about 1.6% after the humidity exposure. It was two times higher than the humidification by the fluidized bed for powder C_1 and almost four times higher for powder A as presented in Figure 6-4.

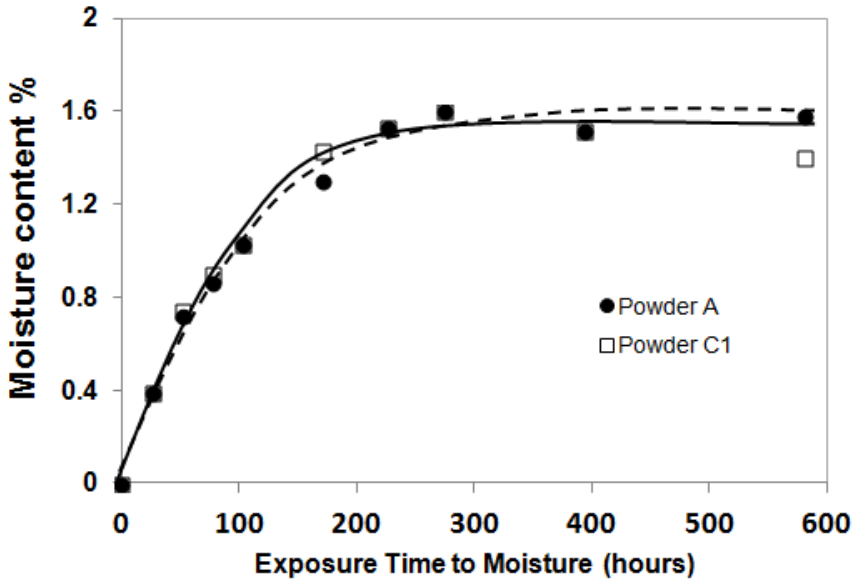

Figure 6-10: The moisture content of the powders after stagnated in an extreme humid environment

Figure 6-11 shows the images taken from the observations of the powder samples during the humidity exposure test. Although powder A was not significantly influenced by the increased humidity, powder C_1 was found to form agglomerations for exposure time over 150 hours. At about 366 hours of exposure, large powder agglomerations could be found in powder C_1.

a. After 192 hours (left: powder C_1; right: powder A)

b. After 366 hours (left: powder C_1; right: powder A)

Figure 6-11: Visual inspection of the powders in different exposure time [18].

Results from the flowability test as listed in Table 6-2 indicate similar discovery to the visual observations. Powder C_1 had much poorer flowability, especially for the dynamic flowability after long time of exposure, whereas powder A had much less deterioration in its flowability. Overall, the results from the flowability tests suggested the maximum exposure time for the powders without causing any flowability problem was about 100 hours. That referred to a maximum moisture gain of about 1.1% according to the plots in Figure 6-10.

Table 6-2: Flowabilities of the powders during humidity exposure

Samples	AVA (°)			RBER		
Exposure time (hr)	0	96	580	0	96	580
Powder A	42.4	42.5	43.5	1.43	1.42	1.41
Powder C_1	44.7	44.6	46.2	1.26	1.22	n/a

The humidified powder by the fluidized bed during the spraying process was less likely to cause flowability problem, since the measured moisture gains from powder C_1 and powder A were only about 0.8% and 0.4% respectively. It was equivalent to the exposure time of about 55 hours for powder C_1 and about 25 hours of powder A in the experiment, which were far below the suggested exposure limit of both powders. Therefore, the flowabilities of the powders should not be affected. As an implication for application, fluidization of powder coatings with humidified air was less concerned than stagnation of the powder coatings in a humidified environment. The study advised that the humidified powders should be fluidized by dry air for a period of time for removing any residual moisture in the fluidized bed before shutting down of operations. Similarly, the powders stagnated from a humid environment should be fluidized by dry air before reuse.

6.3.5 Effect of Humidity on Coating Quality

A humidified fine powder might cause formations of micro-agglomerations that aggregated by small particles, which will lead to increased coating roughness known as “orange peel”. In addition, micro-agglomerations could also cause coating defects. Therefore, further observations of the pre- and post-humidified powder in a micro scale were necessary.

The SEM (Scanning Electron Microscope) images in Figure 6-12 indicate that the particles of both powders were not aggregated after fluidization with humidified air and the micro-agglomerations were not found. The pre- and post-humidified powders were then sprayed on the sample panels and the coating qualities were inspected. By comparing the cured panels between pre- and post- humidified powders, there were no powder balls, seeds or pin hole observed by the necked eyes.

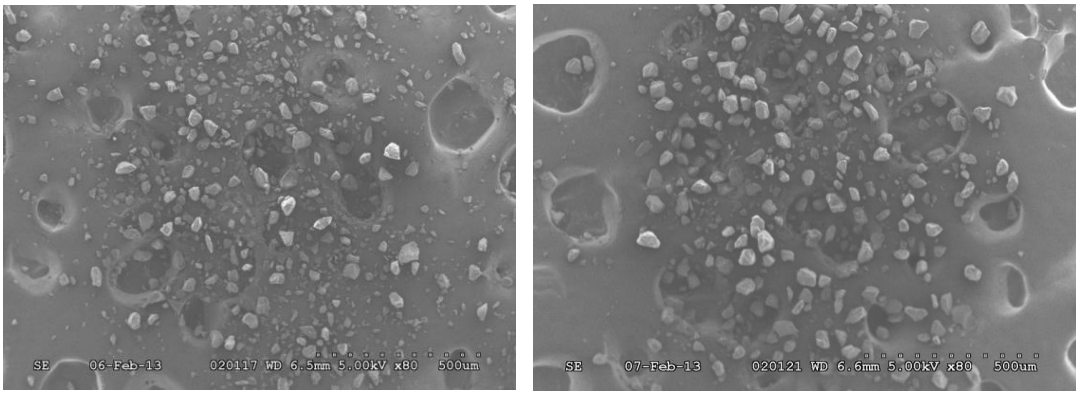

a. Pre-humidified particles b. Post-humidified particles

Powder C_1

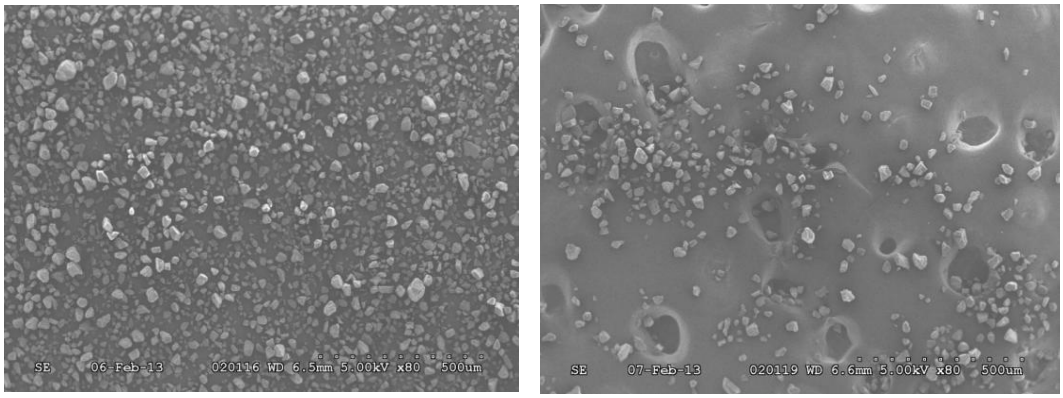

c. Pre-humidified particles d. Post-humidified particles

Powder A

Figure 6-12: SEM images of the powder particles (humidification of 60 minutes)

The sample panel were also inspected under SEM. The coating surfaces from a high magnification are showed in Figure 6-13 (the cutting line of the coating film was included in the image for better focus). As observed, all the coating surfaces had small bits with size under 10 μm which were normally from fillers or additives but there was no sign of micro-agglomerations. The coatings obtained from the post-humidified powders were smooth and there was no surface defect of the coating.

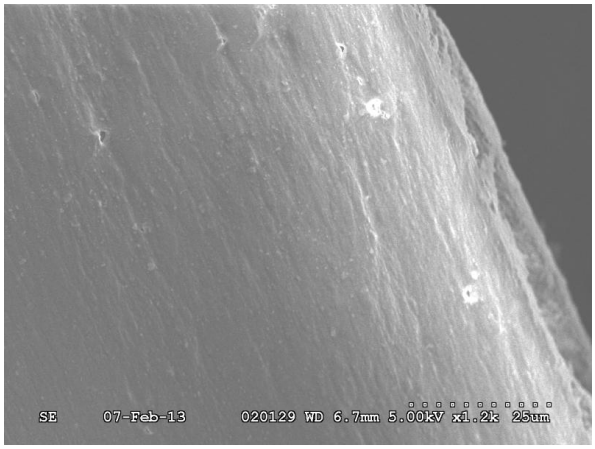

a. coating surface of the pre-humidified

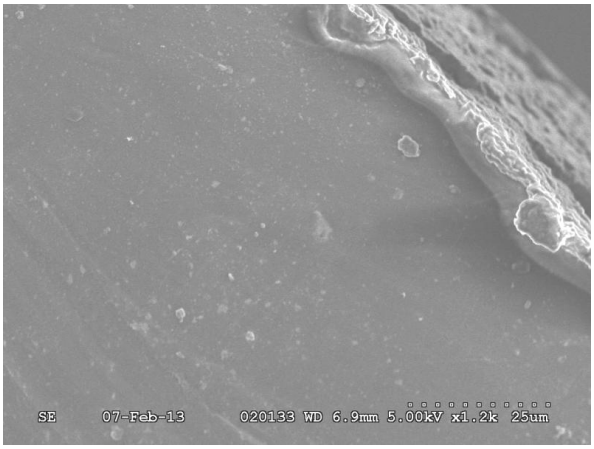

b. coating surface of the post-humidified

Powder C_1

c. coating surface of the pre-humidified

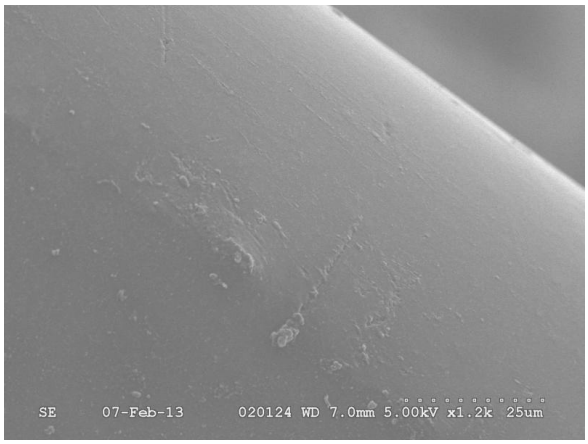

d. coating surface of the post-humidified

Powder A

Figure 6-13: SEM images of the coating surfaces (humidification of 60 minutes)

Based on the results, it can be concluded that the powders humidified by the fluidized bed would not cause micro-agglomerations and the coating quality of the humidified powders would not be affected.

6.4 Conclusion

This study revealed that the moisture content on the particle surfaces had significant influence on the resistivity of the fine powders. Additional moisture on the particle surfaces could reduce the resistivity of a fine powder. Because of that, the back ionization was delayed during corona charge spraying so that the FPTE could be improved. The resistivity of a regular size powder was much less influenced by the moisture on the particles. Therefore, the increased moisture content on the particle surfaces could not significantly improve the FPTE of a regular size powder.

The study also disclosed that the humidification on the powder would not cause serious deterioration in powder flowability if the recommended protocol was followed and the additional moisture on the particles would not cause adverse effects on coating quality.

References

[1] Utech B., A Guide to High Performance Powder Coating. *Society of Manufacturing Engineers*, 2001.

[2] White H.J., Industrial Electrostatic Precipitation (Addison-Wesley Publishing Company, INC.), 1963.

[3] Wu S., Electrostatic charging and deposition of powder coatings, *Polym.-Plast. Tec.;. Eng.*, 7, (1976) 119-220.

[4] Cross J.A., *Electrostatics: Principles*, Problems and Applications, (Bristol: Hiler), 1987.

[5] Mazumder M.K., Sims R.A., Biris A.S., Srirama P.K., Saini D., Yurteri C.U., Trigwell S., De S., and Sharma R., Twenty-first century research needs in electrostatic processes applied to industry and medicine, *Chem. Eng. Sci.*, 61 (2006), 2192-2211.

[6] Chang J.S., Lawless P.A., Yamamoto T., Corona discharge processes, *IEEE Trans. Plasma Sci.*, 19 (1991), 1152-1166.

[7] Meek J.M., Craggs J.D., *Electrical Breakdown of Gases*, (*New York: Wiley*), 1978.

[8] Bailey A.G., The science and technology of electrostatic powder spraying, transport and coating, *J. Electrostat*., 45 (1998), 85-120.

[9] Masuda S., Washes M., Mizuno A., Abuts K., Boxer Charger Proceedings of the 13th IEEE-IAS Annual Meeting (Toronto, Canada), 1B (1978), 16-22.

[10] Sims R.A., Mazumder M.K., Liu Xiaohong, Chok W., Mountain J.R., Wankum D.L., Pettit P., Chasser T., Electrostatic Effects on First Pass Transfer Efficiency in the Application of Powder Coatings, *IEEE Transactions on industry applications*, 37(6) (1997), 1610-1617.

[11] Sharma R., Trigwell S., Biris A.S., Sims R.A., Mazumder M.K., Effect of Ambient Relative Humidity and Surface Modification on the Charge Decay, *Properties of Polymer Powders in Powder Coating*, 39(1) (2003), 87-95.

[12] Messaoudi R., Younsi A., Massines F., Despax B., Mayoux C., Influence of Humidity on Current Waveform and Light Emission of a Low-frequency Discharge Controlled by a Dielectric Barrier 3(4) (1996), 537-543.

[13] Powers H., Dec. Improving First-Pass Transfer Efficiency, *Product Finishing Magazine*, Gardner Publications Inc. 2005.

[14] Berger G., Marode E., Belabed O., Senouci B., Gallimbert I., Osgualdo A., Effect of Water Vapor on the Discharge Regimes and the Deviation from Similarity Law in Compressed SF for Positive Polarity, *J. Phys. D: Appl. Phys.*, 24 (1991). 1551-1556.

[15] Wu S., Electrostatic charging and deposition of powder coatings, *Polym.-Plast. Technol. Eng.*, 7, 1976, 119-220.

[16] Mohnen V.A., Discussion of the Formation of Major Positive and Negative Ions up to the 50 km Level, *Pure and Applied Geophysics*, 84 (1971), 141-153.

[17] Meng X.B., Hui Z., Jesse Z., Edge effects and effects of relative humidty on current and current density distribution during negative point-to-plane corona discharges, *PhD Thesis of UWO*, 2008, 65-80.

[18] Fu.J, Zhang H., Zhu J., 2013, Improvement on the first pass transfer efficiency of fine polymer coating powders for corona spraying process, *Advanced Powder Technology*.

[19] Krantz M., Zhang H., Zhu J., Characterization of powder flow: static and dynamic testing. *Powder Technology*, 194(3) (2009), 239-245.

[20] Hang Q., Zhang H., Zhu J., Flow properties of fine powders in powder coating, *Particuology*, 8(1) (2010), 19-27.

[21] Sharma R., Trigwell S., Biris A.S., Sims R.A., Mazumder M.K., Effect of Ambient Relative Humidity and Surface Modification on the Charge Decay Properties of Polymer Powders in Powder Coating, *IEEE Transactions of Industry Applications*, 39(1) (2003), 87-95.

CHAPTER 7: IMPROVEMENT ON THE FARADAY CAGE RESISTANCE BY REVISED CORONA CHARGE SPRAY GUN

7.1 Introduction

Corona charge spraying is the most popular application method used in powder coating industry. During the process, the single electrode at the tip of the spray gun generates strong ionized electrostatic field to charge powder particles. The charged particles are then deposited and attached on the grounded coating surface [1]. A higher corona voltage of the spray gun usually delivers a better transfer efficiency [2]. However, there is a major drawback of utilizing a high corona voltage. The strength of the generated electrostatic field is invariably concentrated along sharp features and edges of the coating surface and it is reduced within any recessed features or holes [3].Since the charged particles move under the electrostatic forces in the area close to the coating surface (about 10 mm) [4], the recessed areas and tight corners are always received insufficient coverage of sprayed powder coatings. This phenomenon is known as Faraday Cage effect.

Tribo charge spraying can be utilized to overcome the Faraday Cage effect. Different from the corona spray gun, the charging mechanism of a tribo spray gun was to strip off the electrons from the particles during their intensive frictional contacts with the inner gun wall. Therefore, particles are positively charged. Due to the lack of the ionization at the gun tip, no strong electrostatic field is presented so that the Faraday Cage can be eliminated. Nevertheless, the tribo spray gun provides less charging to the particles comparing with the corona spray gun. As a result, the transfer efficiency of a tribo spray gun is usually lower than a corona spray gun. Furthermore, tribo charge spraying is experienced to be less reliable than the corona charge spraying because of its high sensitivities to humidity, particle surface roughness, mechanical and electrical properties, as well as the shape of the particles [5-7].

Methods to overcome the Faraday Cage effect for corona charge spraying is always desired. In industrial applications, the Faraday Cage effect can largely influences the production rate since touch-ups by the extra manual spraying processes are always required. It does not just increase the cost and time but it also causes non-uniform thicknesses of the coatings. Many efforts have been made to reduce the Faraday Cage effect for corona charge spraying. One typical example is the development of the internal charging corona spray gun [8-9]. The internal corona spray gun has the corona electrode enclosed by a grounded cylinder. When coating process starts, the generated electrostatic field converges to the grounded cylinder instead of the coating surface; therefore, the Faraday Cage effect could be reduced. However, large amount of powder particles accumulate on the cylinder surface during spraying. As a result, a reverse discharge, which was caused by severe back ionization due to the over accumulation of the charged particles, could easily occur. It is dangerous since spark from the reverse discharge can ignite the powder coating. On the other hand, the internal charging design reduces the intensity of the ionization since the gun electrode is enclosed inside a limited space and the free electrons always tended to attach to the grounded cylinder surface. Therefore, the charging of the particle is poor. So far, there has been no success with the design of the internal corona spray gun.

This study proposed a new concept to overcome the Faraday Cage effect by a revised corona spray gun. The revised spray gun would have alternative voltage supply instead of the conventional constant voltage supply. In doing so, the induced electrostatic field by the high voltage discharge can be avoided periodically. As a result, more charged particles could be allowed to fly into the recessed areas during spraying. Moreover, the revised spray gun had a multi-electrode configuration which could create repellency of the electrostatic field near the spray gun tip. Particles flew out from the spray gun would encounter an electrostatic field

with much less intensity. In the study, series of experiments were conducted to examine the performances of revised spray gun.

7.2 Materials and Methods

Two powder samples were prepared by grinding from the powder coating chips supplied by Siebert Powder Coatings, Cleveland, USA: one was the fine powder sample with the medium particle size smaller than 25 μm, and the other one was the coarse powder sample with the medium particle size larger than 35 μm. The particle size distributions were shown in Figure 7-1. The fine powder sample was used to simulate the fine powder coatings whereas the coarse powder coating was used to simulate the regular size powder coatings.

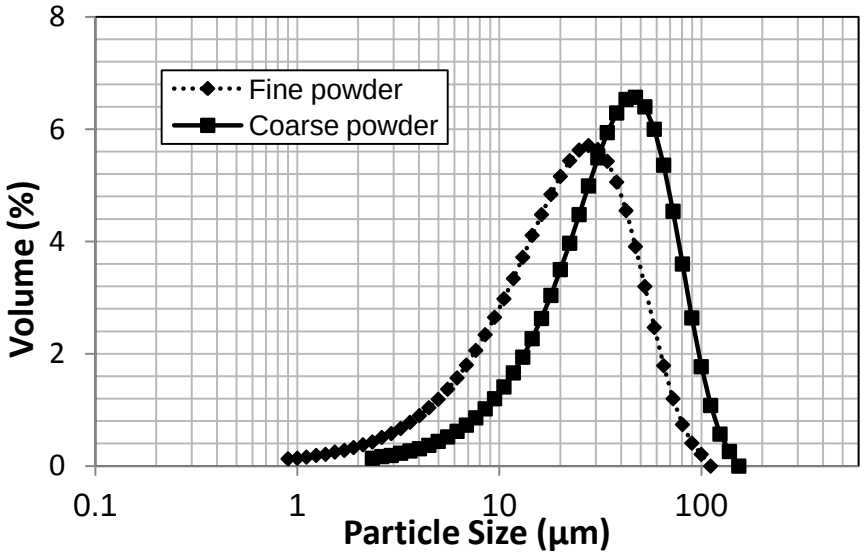

Figure 7-1: The particle size distributions of the powder samples

Generally, an ordinary corona spray gun has one electrode at the gun tip. Constant high voltage is supplied to the electrode for generating the ionization during spraying. Whereas, the new spray gun design proposed by the study had four electrodes and the high voltage was alternatively supplied to each of the two diagonal electrodes. The new spray gun was

modified from a conventional corona spray gun manufactured by Nordson, USA. As shown in Figure 7.2, the original electrode in the middle of the gun tip was disabled; instead, four electrodes were installed on the outer perimeter of the gun, named electrode 1, electrode 2, electrode 3 and electrode 4. The four electrodes were connected to a voltage distributor and the distributor driven by a DC motor distributed the high voltage to each of the two diagonal electrodes at a time. The distribution frequency was adjustable by the voltage input to the DC motor.

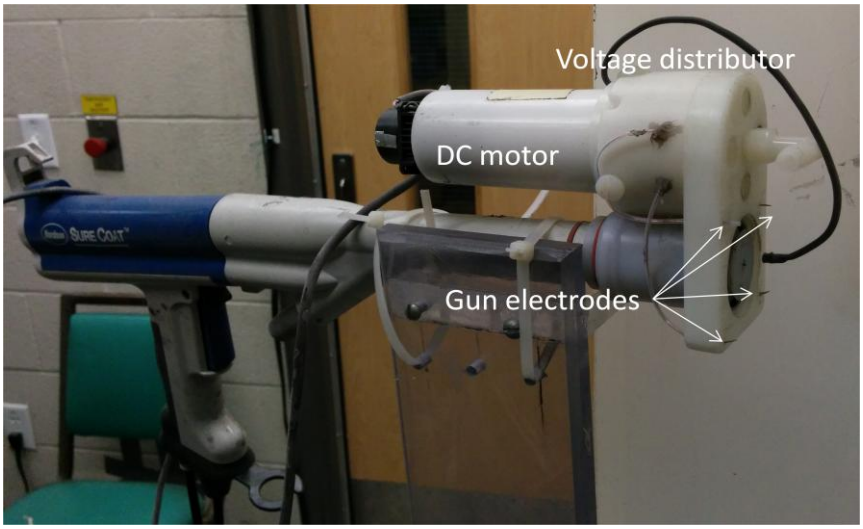

Figure 7-2: The revised corona gun

The charging scheme of the revised corona gun is demonstrated in Figure 7-3. Each pair of the diagonal electrodes has empty periods in between two adjacent charging periods. A self-made IC controller was utilized to control the input voltage to the DC motor of the distributor so as to adjust the charging characteristic. For example, a higher input voltage causes a higher charging frequency. With a higher charging frequency, both of the charging period and the empty period are shorter. It is opposite for the case with a lower input voltage to the voltage distributor.

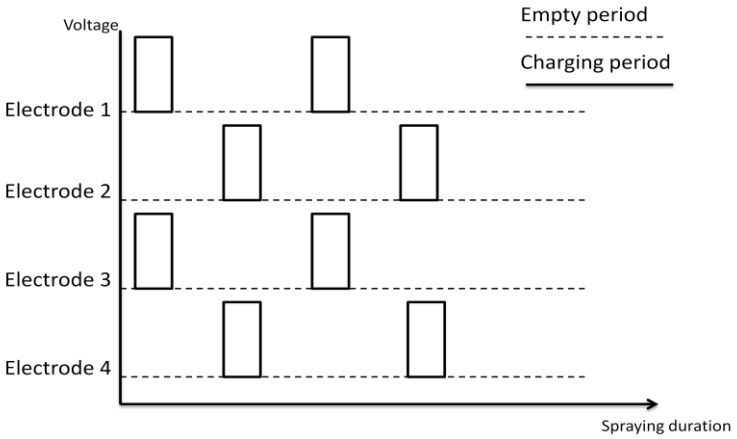

a. Charging cycles of the pins

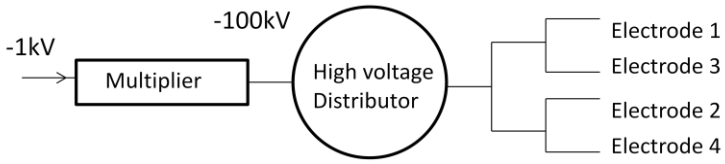

b. Charging scheme of the gun

Figure 7-3: The charging scheme of the revised corona spray gun

In this experiment, the each of the four electrodes were placed 1.75 cm away from the center of the spray gun. In addition, three input voltages to the DC motor of the distributor were used: 4 V, 8 V and 12 V. The corresponding charging frequencies to these three input voltages were measured as 72 Hz, 152 Hz and 230 Hz. In addition, three spray gun voltages were used: -30 kV, -60 kV and -90 kV with three spraying durations of 4 s, 8 s and 12 s. The gun voltage of -30 kV and -90 kV were close to the lower and upper limit in a normal corona spraying. For most of the applications, the gun voltage used is in between. Usually, a lower gun voltage can provide less Faraday Cage effect, nevertheless, it also reduce the charging to the particles.

In order to optimize the spray gun design, the distance between the center of the spray gun and the electrode was adjusted. On the other hand, the Faraday Cage resistance was

measured by a U-shape coating panel, shown in Figure 7-4. As demonstrated by the figure, there were three smaller panels, panel A, B and C, attached to the U-shape coating panel. These small panels were identical in dimensions; however, panel C was placed on recessed surface which had a depth of 2.5 cm, whereas panel A and B were placed on the outer surfaces. The Faraday Cage resistance, FCR, was calculated by:

$$FCR = \frac{2 \times W_{PanelC}}{W_{PanelA} + W_{PanelB}} \qquad \text{Eq. 7-1}$$

where W (g) is the weight of the powders on the panel. If the FCR is one, powder coverage on the panel C is the same as the powder coverage on panel A or B showing that there is no Faraday Cage effect; if FRC is zero, no powder is on panel C, indicating extremely strong Faraday Cage effect.

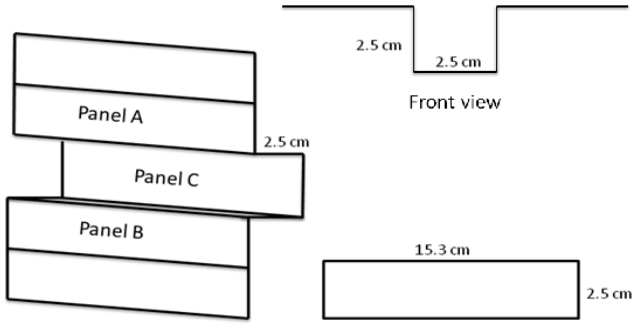

Figure 7-4: The Panel geometry and the panel size for Faraday Cage measurements

In addition, the transfer efficiency of the powder was also obtained. A 30 cm diameter blank printed circular circuit board was used as a target. The first pass transfer efficiency, FPTE was defined as the weight of the powder on the coated surface divided by the weight of powder sprayed:

$$FPTE = \frac{W_{coated}}{W_{Sprayed}} \qquad \text{Eq. 7-2}$$

During spraying, powder loading was accomplished by a screw feeder (SHENCK AccuRate) at a feeding rate of about 0.517 g/s. Distance between the spray gun and the target was 20 cm. The results obtained from an original (un-modified) spray gun were named as control.

7.3 Results and Discussion

7.3.1 Fine Powder Coating

The new spray gun was first tested with the fine powder coating. The results shown in Figure 7-5 indicate that the FCR can be improved by the new spray gun for a lower gun voltage of –30 kV, particularly in a short spraying duration. As the spraying duration increased, the differences between the new spray gun and the original spray gun become less significant. In addition, the largest improvement is found with the slowest alternating frequency of the corona charging. The results also show that the Faraday Cage effect would be more serious as the spraying duration increased.

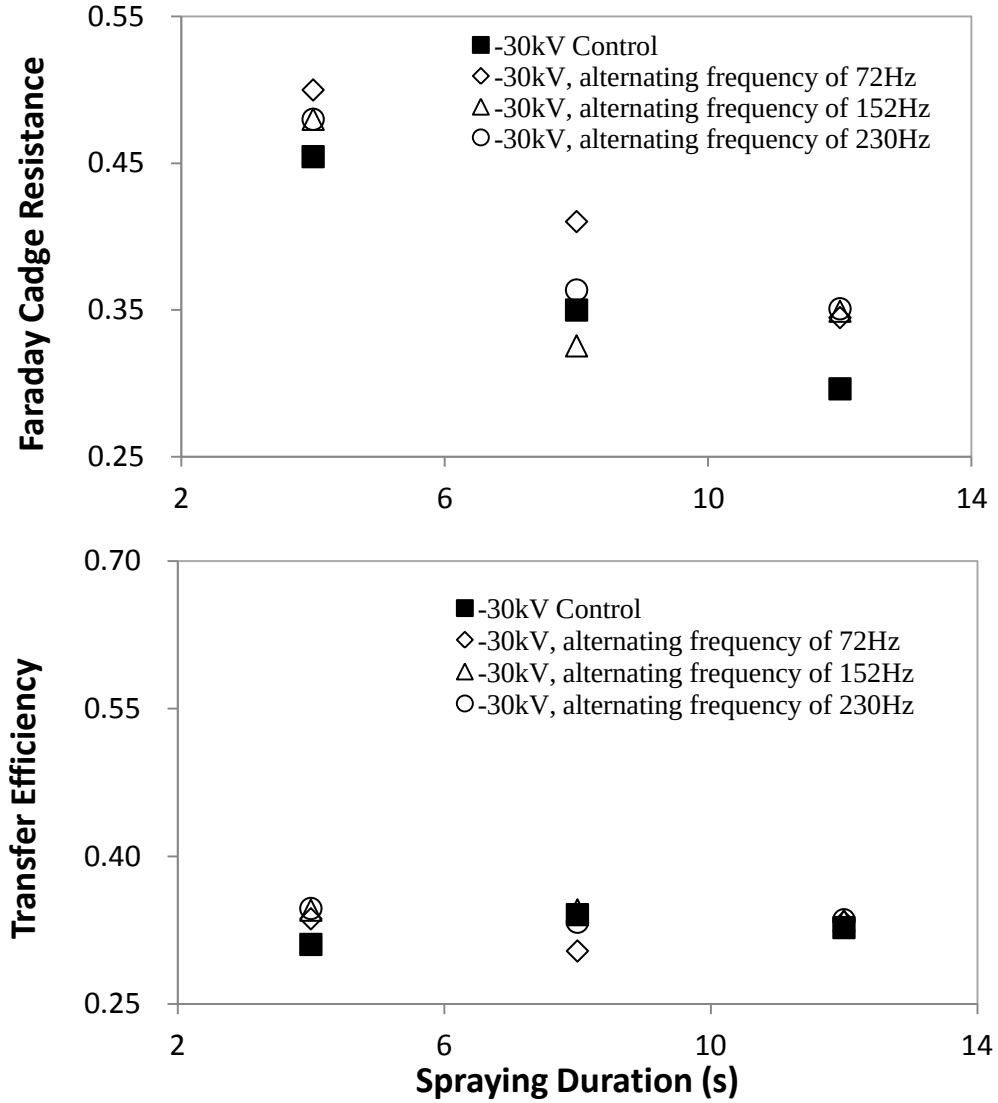

Figure 7-5: The Faraday Cage and transfer efficiency for –30 kV (Fine powder)

On the other hand, the transfer efficiencies obtained from the two spray guns were comparable, although the new gun had a shorter charging time in total due to the empty periods demonstrated in Figure 7-3. It implies that the alternative charging could be desirable due to the reduction in corona quenching. Corona quenching, illustrated in Figure 7-6, is the suppression of corona by particle space charge originally found in application of electrostatic precipitators [10-11]. Indicated by previous studies [11-12], the corona quenching is mainly caused by two reasons: (1) the inhibition of electron avalanches by the

screening effect due to the charged in-flight particles; (2) the deceleration of the ion movement due to the low mobility of the charged particles. Meng [13-18] disclosed that the corona quenching occurred as the spraying duration increased. Furthermore, it could cause remarkable drops (3 to 4 folds) on particle charging. Since the charging period of the electrodes by the new spray gun is much shorter than that, the particle charging can be improved. Therefore, it compensates the influence from the empty periods. As a result of that, there is no significant reduction in the transfer efficiency of the new spray gun.

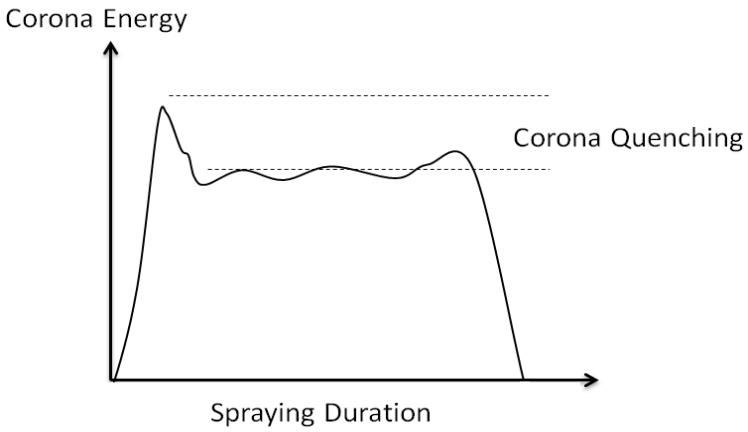

Figure 7-6: An illustration of corona quenching

Figure 7-7 shows the results obtained from a higher gun voltage of –60kV. Once again, the new spray gun indicates promising performances on improving the FCR and the most significant improvement is found at the spraying during of 8s. With a higher gun voltage, the Faraday Cage effect was expected to be more severe. In contrast to Figure 7-5, the differences between the spray guns are larger as the spraying duration increased. As observed from the results, the results obtained from the alternating frequency of 72 Hz outperformed the others. On the other hand, the transfer efficiency obtained from the new gun is less than the original spray gun; however, the reduction is not significant.

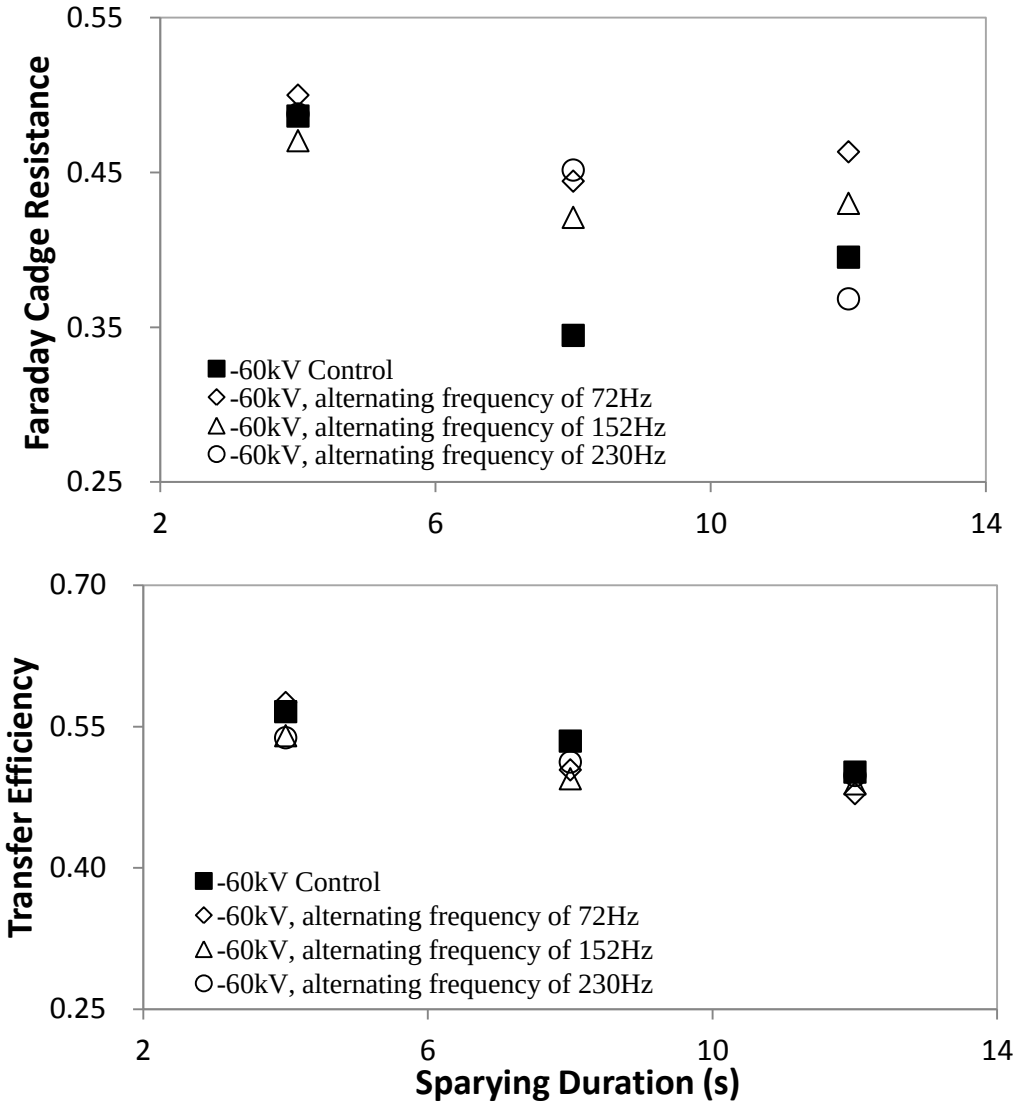

Figure 7-7: The Faraday Cage and transfer efficiency for –60 kV (Fine powder)

Figure 7-8 shows the results obtained from a further increased gun voltage of –90 kV. In this spraying condition, sever back ionizations were visually observed from both of the two guns at spraying duration of 12 s, as well as from the new gun at spraying duration of 8s with alternating frequency of 230 Hz. The back ionizations were expected since the gun voltage was close to the maximum limit for a normal corona charge spraying. Comparing with the results with lower gun voltages, the FCR of the original spray gun in this case is much poorer. For spraying duration of 4 s, the original spray gun had the FCR of only about 0.4.

As the spraying duration increases to 8 s, it is further reduced to around 0.3, indicating a strong Faraday Cage effect. When the spraying duration is increased to 12 s, the Faraday Cage resistance of the original spray gun went back to about 0.5. However, this could be caused by the much lower transfer efficiency on the panel A and B due to the severe back ionization.

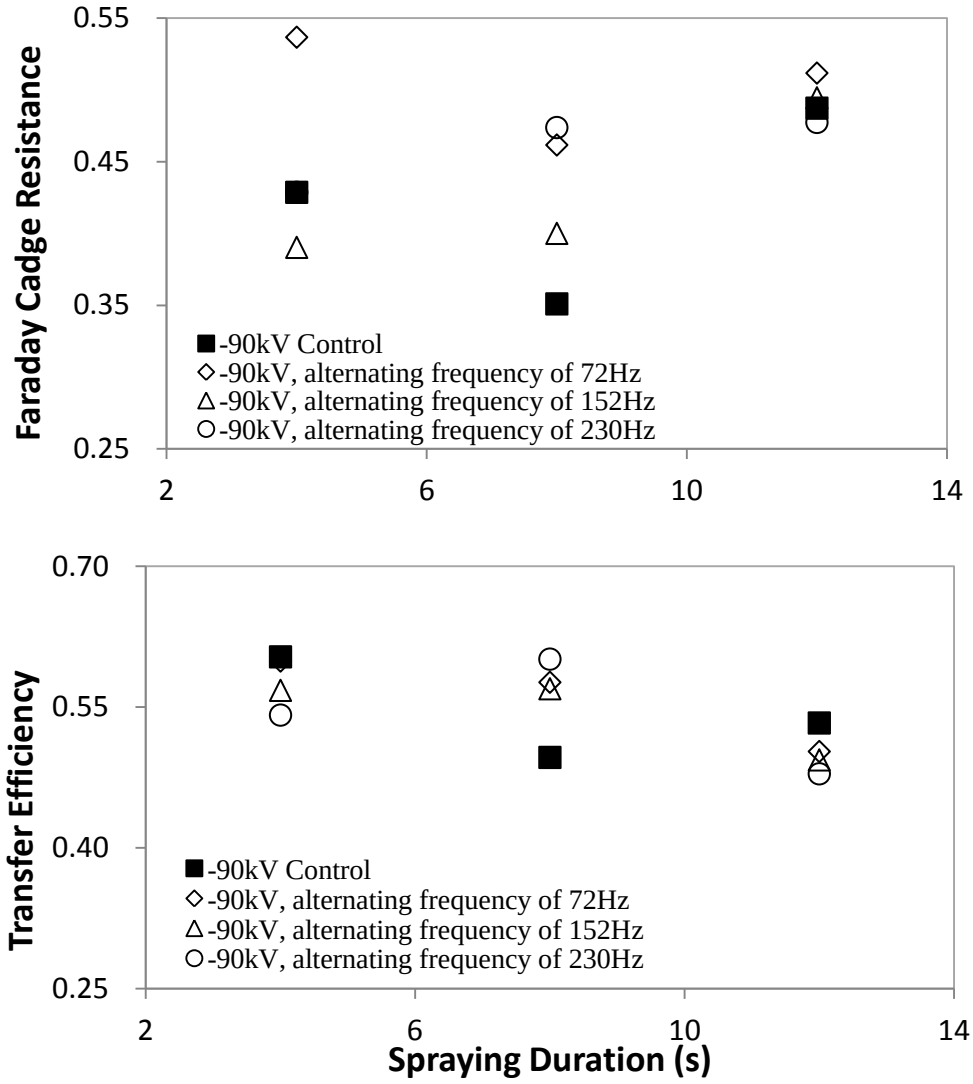

Figure 7-8: The Faraday Cage and transfer efficiency for –90 kV (Fine powder)

On the other hand, Figure 7-8 indicates that the new gun is less influenced by the increased gun voltage. With alternating frequency of 72 Hz, the new spray gun was able to provide similar FCR to the results obtained from lower gun voltages. Furthermore, a slower frequency of the alternating charging is again favorable to use in this case. Meanwhile, the transfer efficiency of the original spray gun decreases as the spraying duration increases and back ionization due to the high voltage caused difficulties in obtaining stable results. The results conclude that the transfer efficiency of the new spray gun is similar to the original spray gun.

Yanagida's [19] disclosed that due to mutual interaction of the two electrodes, the ion cloud emitted from each of the two electrodes tended to mutually repel creating a dead zone towards to the target, as demonstrated in Figure 7-9. By varying the position of the electrodes, the area of the dead zone can be adjusted. As an implication to this study, the design of the new spray gun can be optimized by adjusting the positions of the four electrodes.

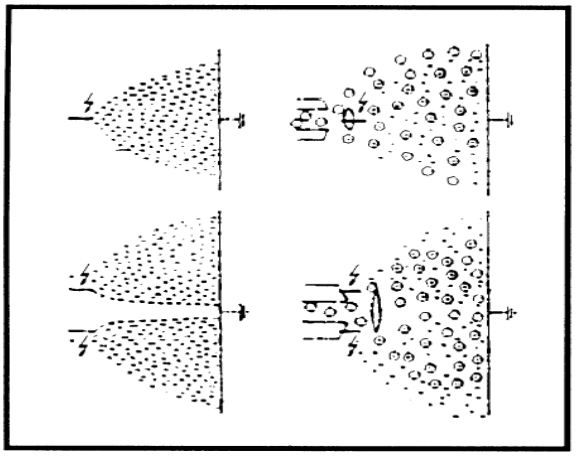

Figure 7-9: The current density pattern with one or two gun electrodes [20]

Results shown in Figure 7-10 indicate an increasing trend of the FCR as the electrodes are moved further away from the center of the gun. The optimum value is at r of 2.25 cm. As r increases further away, the FCR drop rapidly. The transfer efficiency of the spray gun is not influenced by the position of the electrodes.

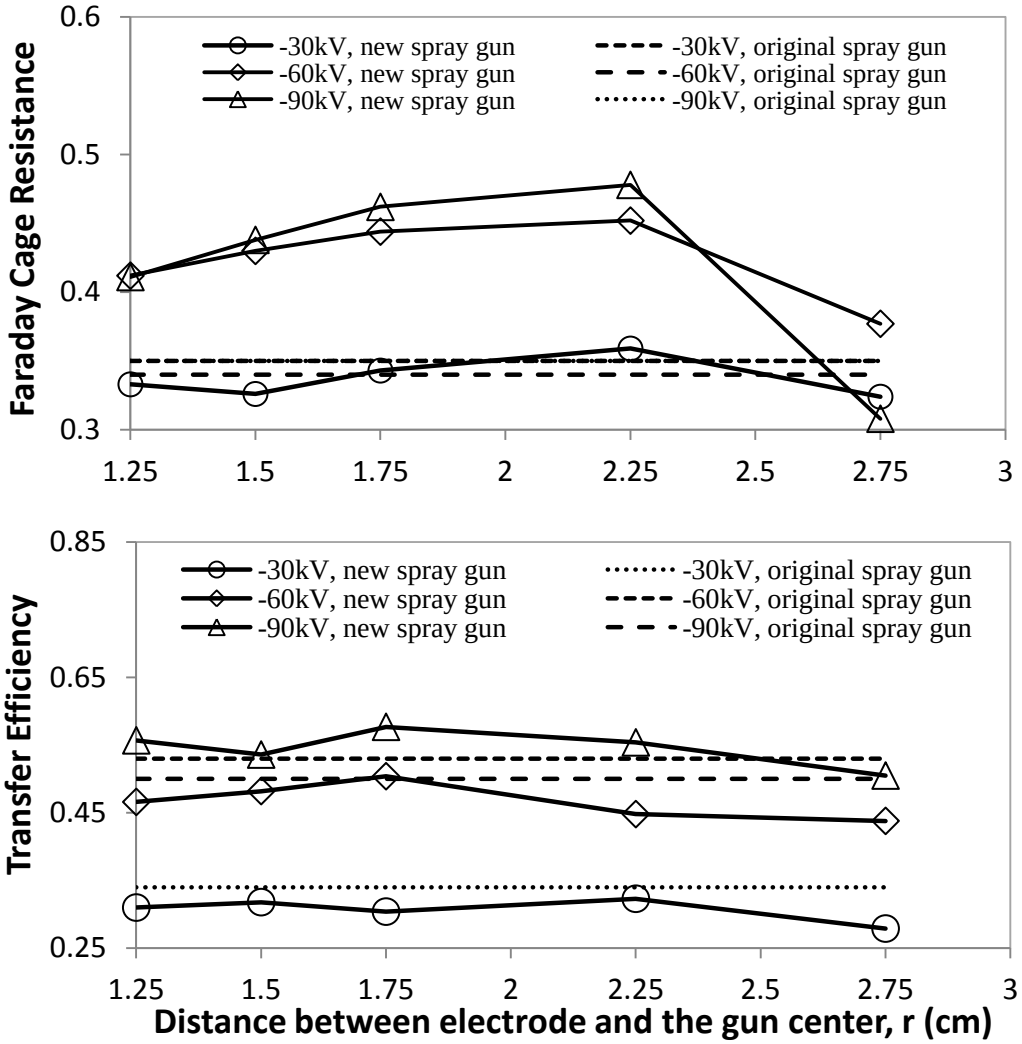

Figure 7-10: The effects of electrode positions of the new spray gun
(Fine powder; alternating frequency of 152 Hz; spraying duration of 8 s)

Overall, the experimental results disclose that the new spray gun design can effective improve the FCR of fine powder coating during corona charge spraying. At the same time, the transfer efficiency is not sacrificed. A visual comparison of the sprayed panel is shown in

Figure 7-11. During the experiment, the difference in powder coverage on the recessed area between the two guns was noticeable by the sprayer.

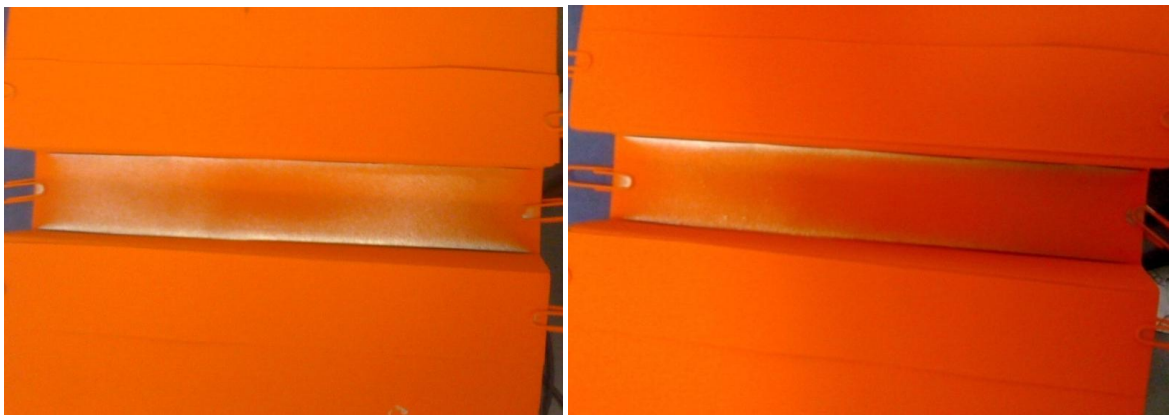

a. the original spray gun b. the new spray gun

Figure 7-11: The comparison between the original and the new spray gun with the gun voltage of –90 kV and the spraying duration of 8 s
(Fine powder coatings; alternating frequency of 72 Hz)

Based on the results, 72 Hz is the most preferable alternative frequency for improving the FRC. However, an even lower frequency was not tested since the DC motor in the gun voltage distributor had already reached the minimum rpm for a stable operation. The distributor design will be revised to accommodate more testing conditions in the future work.

7.3.2 Coarse Powder Coating

Comparing with fine powder coatings, the relatively larger particles in the coarse powders have higher charge-to-mass ratio [2]. In addition, coarse powders usually create less severe corona quenching during corona spray than the fine powders because of the inadequacy in numbers of particles and specific surface area of the particles [15-16].

Figure 7-12 shows the results obtained from the regular powder coatings at gun voltage of –30 kV. Similar to the results from fine powder, the Faraday Cage effect was found more significant as the spraying time became longer. The plot indicates that the original spray gun had a quicker reduction in the FCR than the new spray gun. In addition, the new spray gun with lower alternating frequency was not able to obtain a comparable FCR as the original spray gun at a short spraying duration. On the other hand, the original spray gun achieved higher transfer efficiency due to less severe corona quenching of the coarse powder, as discussed earlier, especially at a lower gun voltage.

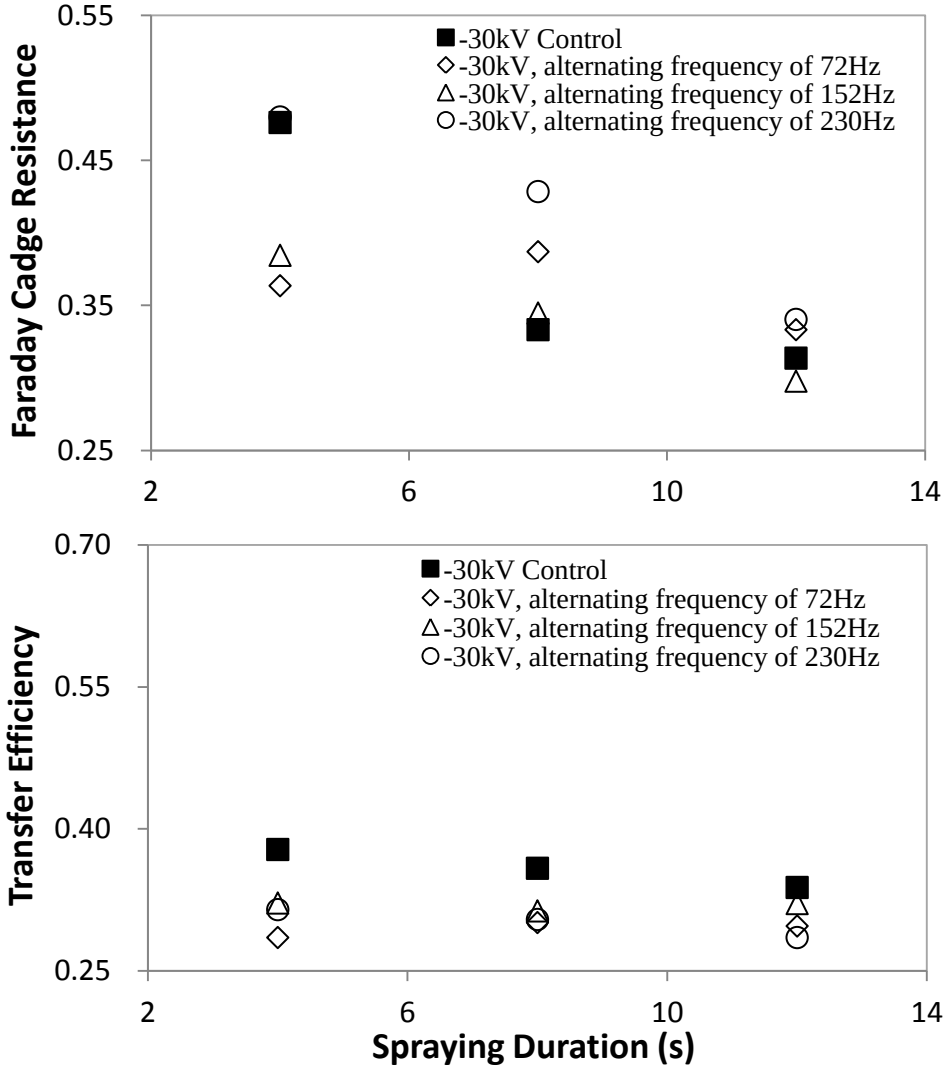

Figure 7-12: The Faraday Cage and transfer efficiency for –30 kV (Coarse powder)

Figure 7-13 indicates that the original spray gun, once again, has better FCR than the new gun at gun voltage of –60 kV. The best results provided by the new spray gun, with alternating frequency of 72 Hz, is still significantly lower than the original spray gun at spraying duration of 3 s and 8 s. The new spray gun only shows its advantage for the spraying duration of 12 s. Corona spraying of the coarse powder could encounter a less significant Faraday Cage effect due to the heavier weight of the particles. While a charged particle is flying from the gun to the coating surface, it is usually subjected to a combination of drag force, gravity force and electrostatic force. The electrostatic force, which is influenced by the Faraday Cage effect, only dominates when the particle is near the coating surface. A lighter particle tends to follow the strong electrostatic field to the edges and corners on the coating surface, whereas the heavier particle tends to retain its original fly path due to its larger momentum. The new spray gun was unable to improve the FCR of the coarse powders, since they were less influenced by the electrostatic field.

On the other hand, the results in Figure 7-13 show that the new spray gun had much better transfer efficiency than the original spray gun. The reduction of secondary charging could be an explanation to that. Discovered by Wu [21], deposited particles may still accept additional charges, which is known as the secondary charging, as a result of the converging and terminating of the current ions on the coating surface. Although the increased accumulated charges on the coating surface might not generate an obvious powder break down, it could still reduce the powder deposition rate during continuous spraying [15-16]. The phenomenon of the secondary charging is usually associated with higher gun voltage. Because of the alternating charging pattern, the new gun is able to reduce the duration of secondary charging so as to improve the transfer efficiency. This advantage was not discovered in the case with a lower gun voltage.

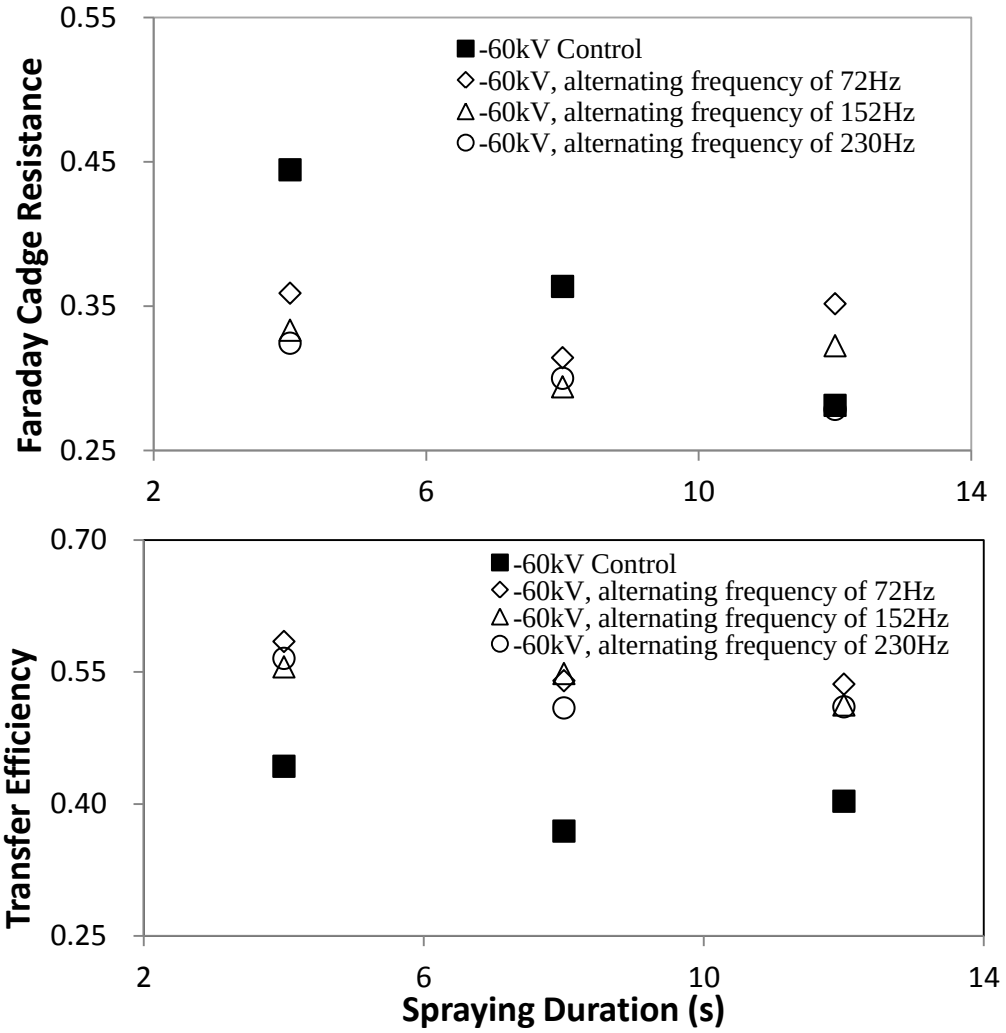

Figure 7-13: The Faraday Cage and transfer efficiency for –60 kV (Coarse powder)

Similar improvement in the transfer efficiency was not found during the corona spray with the fine powder. Studies by Meng [22-23] disclosed that the measured charges obtained from fine powders are significant lower than coarse powders when they are both subjected to the same secondary charging condition at gun voltage of -60 kV. Furthermore, the measured charges of the fine powders deposited on the coating surface found much reduced as the gun voltage increased to -90 kV. Therefore, the fine powder was much less influenced by the secondary charging than the coarse powder.

Figure 7-14 shows the results obtained from gun voltage of -90 kV. With the high gun voltage, the Faraday Cage effect was expected to be much stronger than the previous cases. The original spray gun had a significant drop in the FRC. In contrast, the new spray gun could still obtain almost the same FRC as that with the lower gun voltages. Due to the ability of reducing the secondary charging, the new spray gun obtained a better transfer efficiency than the original spray gun.

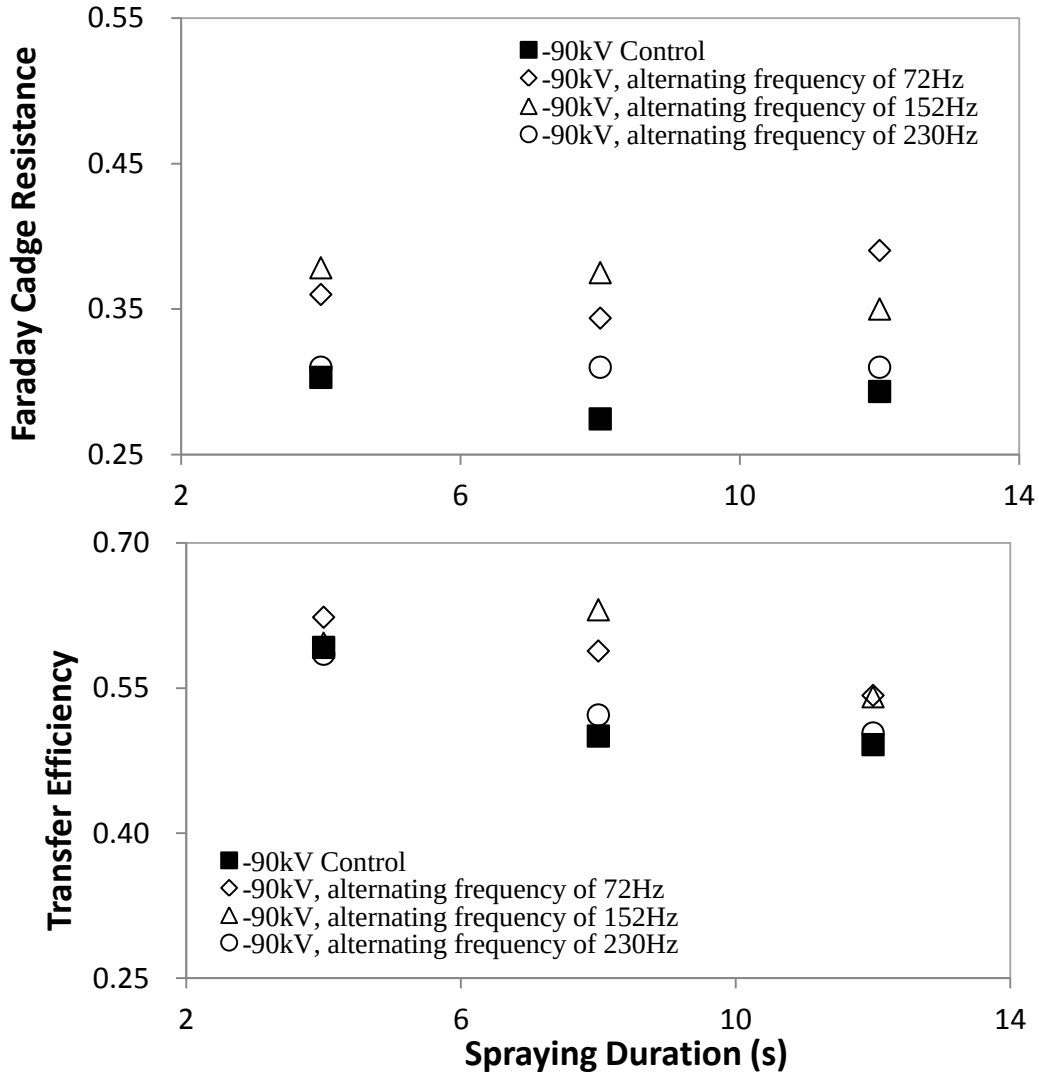

Figure 7-14: The Faraday Cage and transfer efficiency for –90 kV (Coarse powder)

The positions of electrodes were adjusted for discovering the influence on the corona charge spraying of the coarse powder. Figure 7-15 indicates that the new gun had similar FCR to the original spray gun at gun voltage of –60 kV. But then, the new spray gun could obtain higher the FCR for gun voltage of -30kV and -90 kV. However, the increase in the FCR for gun voltage of –30 kV in the plot might not be reflected by a true reduction in the Faraday Cage effect. Instead, it could be caused by the significant reduced transfer efficiency measured on panel A and B due to the deteriorations in the particle charging by the new gun. As the electrodes move further away from the center, the particle charging becomes poorer causing even lower transfer efficiency on the panel A and B. Therefore, the results obtained from the new spray gun at -30 kV showed an increasing trend in the FCR as the radius distance gets larger. In contrast, the new spray gun showed a rather stable FCR as the distance, r, varied at gun voltage of –60 kV and –90 kV. Therefore, the FCR of the new spray gun was found less sensitive to the electrode position while dealing with the coarse powder. On the other hand, the original spray gun had a better transfer efficiency at gun voltage of –30 kV. At higher gun voltages, particularly -60 kV, the new spray gun outperformed the original spray gun, which could be contributed by the reduction in secondary charging as discussed earlier.

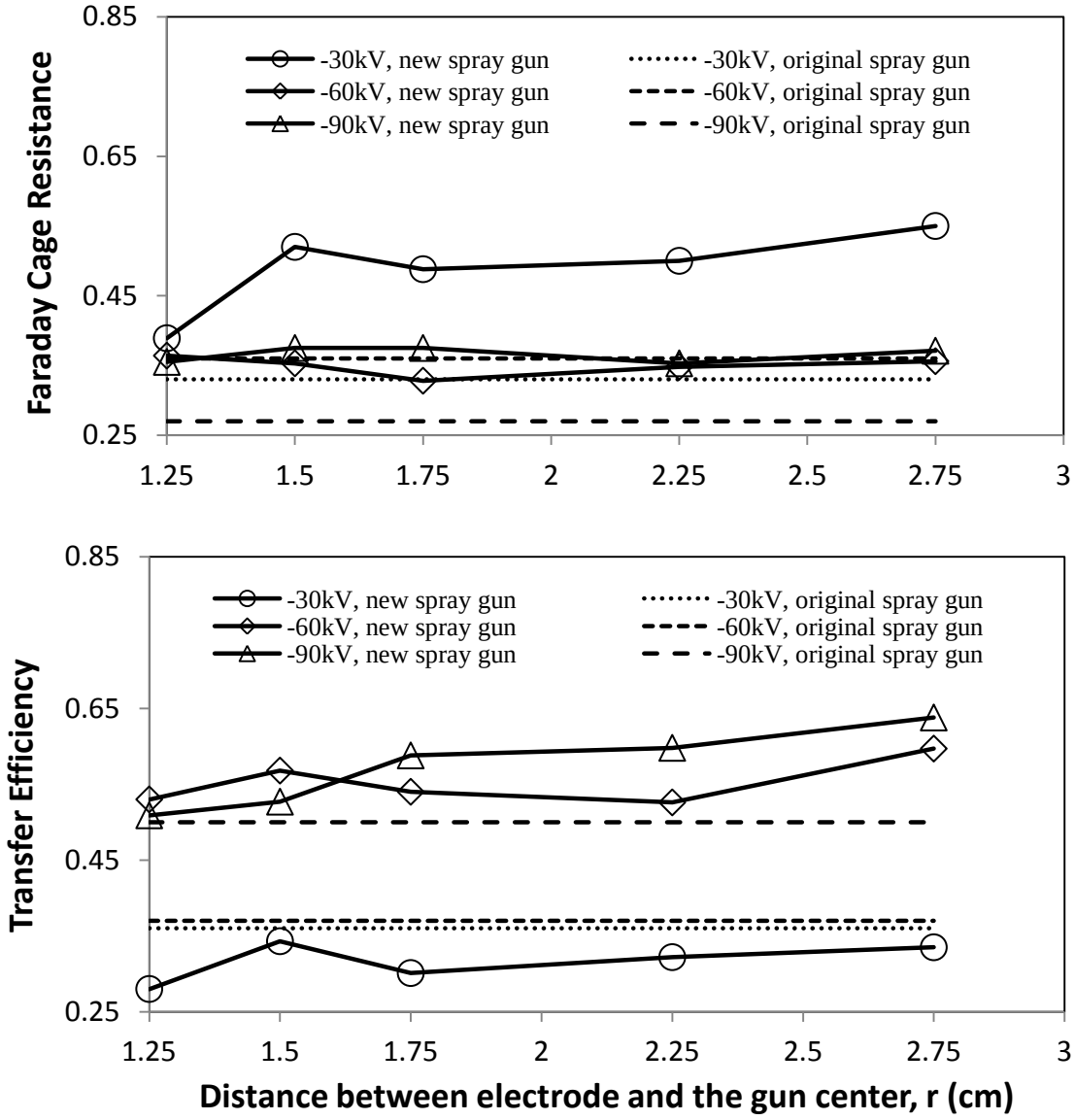

Figure 7-15: The effects of different electrode positions of the new spray gun (Coarse powder; alternating frequency of 72 Hz; spraying duration of 8 s)

7.4 Conclusion

In the study, an ordinary powder spray gun was revised to overcome the Faraday Cage effect during corona charge spraying. Spraying tests indicate the new spray gun design is able to provide noticeable improvement on the Faraday Cage resistance in most of the spraying

conditions for fine powder. In addition, the new spray gun can still obtain comparable transfer efficiency to an ordinary spray gun. More importantly, positions of the electrodes will influence the Faraday Cage resistance provided by the new spray gun. However, the new spray gun design can only provide improved Faraday Cage resistance at higher gun voltage and/or with a longer spraying duration while spraying the coarse powder. Yet, the new spray gun design showed a large potential in improving the transfer efficiency of the coarse powder during corona charge spraying due to the reduced secondary charging.

Experimental results also indicate that a slower alternating frequency on the new spray gun will lead to better resistance to the Faraday Cage effect during corona charge spraying. Nevertheless, an even lower alternating frequency of corona charging than that used in the study has not been tested due to the limitation from the current design of the gun voltage distributor. In the future work, the mechanism of the gun voltage distributor will be revised for accommodate more testing conditions and the design of the new corona spray gun will be further optimized.

References

[1] Creighton J., 2006, Powder Coating Spray Guns, *Product Finishing*, p 62-66.

[2] Sims R.A., Mazumder M.K., Liu Xiaohong, Chok W., Mountain J.R., Wankum D.L., Pettit P., Chasser T., 2001, Electrostatic Effects on First Pass Transfer Efficiency in the Application of Powder Coatings, *IEEE Transactions on industry applications*, 37(6), p 1610-1617

[3] Krant M., 2009, Powder Characterization and Powder Application in Automotive Coatings, *MESc. thesis of UWO*, p 8-27.

[4] Cross J.A., 1987, Electrostatics: Principles, Problems and Applications, (Bristol: Hiler).

[5] Kleber W., Makin B., 1998, Triboelectric powder coating: a practical approach for industrial use, *Particul. Sci. Technol.*, 16, p 43-53.

[6] Mayr M.B., Barringer S.A., 2006, Corona compared with triboelectric charging for electrostatic powder coating, *J. Food Sci. (JFS) E: Food Eng. Phys. Prop.*, 71, p 171-177.

[7] Trigwell S., Biris A.S., Simis R.A., Mazumder M.K., 2008. Effects of powder velocity and contact materials on tribocharging of polymer powders for powder coating applications, *Particul. Sci. Technol.*, 26, p 145-157.

[8] Clements J.S., Bair R.H., 1996, Electrostatic powder coating of insulating surfaces using an alternating polarity internal corona gun, Proceedings of the 31th IEEE-IAS Annual Meeting, 4, p 2017-2025 (San Diego, CA, USA).

[9] Clements J.S., Bair R.H., 1999, Electrostatic powder coating of insulating surfaces using an alternating polarity internal corona gun, *IEEE Transactions on Industry Application*, 35(4), p 743-752.

[10] Isahaya H., 1962, Analysis of corona field intensity distribution by steel ball dropping method in electrostatic precipitators, *Journal of Institute of Electrical Engineers of Japan*, 82, p 219-228.

[11] Awad M.B., Castle G.S.P., 1974, Corona quenching in electrostatic precipitators, *IAS (IEEE Industry Application Society) Annual Meeting Conference Record*, p 945-054.

[12] Awad M.B., Castle G.S.P., 1975, Efficiency of electrostatic precipitators under conditions of corona quenching, *J. Air Pollut Control Assoc.*, 25, p 172-176.

[13] Meng X., Zhu J., Zhang H., 2007, The characteristics of current density distribution during corona charging process of different particulates, *J. Phys. D: Appl. Phys.*, 41(17).

[14] Meng X, Zhang H., Zhu J., 2008, The characteristics of particle charging and deposition during powder coating process with coarse powder, *J. Phys. D: Appl. Phys.*, 41(19).

[15] Meng X, Zhu J, Zhang H., 2009, The characteristics of particles charging and deposition during powder coating processes with ultrafine powder, *J.Phys. D: Appl. Phys.*, 42(6).

[16] Meng X., Zhang H., Zhu J., 2009, Characterization of particle size evolution of the deposited layer during electrostatic powder coating processes, *Powder Technology*, 195(3), p 264-70.

[17] Meng X., Zhang H., Zhu J., 2009, Influences of different powders on the characteristics of particle charging and deposition in powder coating process, *Journal of Electrostatics*, 67(4), p 663-671.

[18] Meng X., Zhang H., Zhu J., 2008, A general empirical formula of current-voltage characteristics for point-to-plane geometry corona discharges, *Journal of Physics D: Applied Physics*, 41(6).

[19] Yanagida K., Kumata M., Yamamoto M., 1996, J. Coat. Technol., 68, p 47-56.

[20] Kleber W., 1993, Electrostatic powder gun design, *Journal of Electrostatics*, 30, p 392-402.

[21] Wu S., 1976, Electrostatic charging and deposition of powder coatings, *Polym.-Plast. Technol. Eng.*, 7, p 119-220.

[22] Meng X, Zhang H, Zhu J, 2008, The characteristics of particle charging and deposition during powder coating processes with coarse powder, *Journal of Physics D: Applied Physics*.

[23] Meng X, Zhang H, Zhu J, 2008, The characteristics of particle charging and deposition during powder coating processes with ultrafine powder, *Journal of Physics D: Applied Physics*.

SECTION Ⅳ

IMPROVEMENTS ON THE PROCESSING TECHNIQUES FOR FUNTIONAL POWDER COATINGS

Powder coatings have been on the market for decades and they are great alternatives to the conventional liquid coatings. For recent years, functional powder coatings become more and more popular to use. However, these powders are usually more difficult to make comparing with the regular powder coatings. This section of the study was to improve the processing techniques for several featured powder coatings.

CHAPTER 8：DEVELOPMENT OF THE DRY BLENDING TECHNIQUE FOR PROCESSING LOW-CURE POWDER COATINGS

8.1 Introduction

The thermosetting powder coating always requires a curing process to obtain its final films. The curing process usually occurs at a temperature from 180 to 200 ˚C for a curing time between 10 and 20 minutes. It has not been an issue for most of the applications, yet there are exceptions. Coating parts that made of plastic, wood or other temperature sensitive materials are almost impossible to be powder coated. On the other hand, heating up large coating parts such as the car bodies and the underground pipes during the powder coating process is not energy efficient. Other than that, the extensive baking and cooling of these large coating parts are time consuming.

The development of low-cure powder coatings is a solution to the problem. This type of powder coating is usually made of a base resin incorporated with curing promoters. The curing promoter is a catalyst to accelerate the reaction between the resin and the curing agent (the crosslinker). Nevertheless, conventional low-cure powder coatings suffer from two major drawbacks: a much narrower temperature window for the extrusion process and constrained transportation/storage temperatures.

During powder coating productions, raw materials including resin, curing agent, pigment, filler and other additives are hot extruded into a homogenous material before grinding. The temperature required by the extrusion is in between 90 and 110 ^{o}C. It is not an issue for regular powder coatings since their curing onset temperatures are usually above 150 ^{o}C.

However, it is always a challenge to low-cure powder coatings because their curing onset temperatures can be as low as 110 ^{o}C. As a result, curing will easily start during the hot extrusion the low-cure powder coatings, known as pre-curing. The pre-curing powder coatings can jam the extruder so as to cause seriously disruption to the powder production.

On the other hand, the low-cure characteristic always causes a shorter shelf life of the low-cure powder coating and air conditioning is often necessary for transportation and storage of low-cure powder coatings. Furthermore, the low-cure characteristic also cuts down the flowing time for the melted particles during the curing process. Consequently, low-cure powder coatings usually provide coatings with strong roughness and lower gloss [1]. Therefore, low-cure powder coatings are mainly used for matt coatings or coatings that require low gloss finishes.

The objective of this study was to overcome the drawbacks of the conventional low-cure powder coatings, as discussed above, by utilizing a new processing technique. DBC (Dry Blended Catalysts) was the most important development for the new technique. As defined by its name, DBC was designed to be dry blended with powder coatings. Comparing with the conventional technique, the use of DBC eliminates the pre-curing problem encountered in the hot extrusion since it is blend with the already extruded and ground powders. Furthermore, DBC will not take into effect until the curing process. Therefore, the shelf life of the low-cure powder coatings can be less influenced. For the same reason, the flowing time of the melted particles is able to be extended so that the coating finish could be improved.

The study explored the fabrication method for DBC. Moreover, the curing performance, the shelf life as well as the coating quality obtained from the low-cure powder coatings that made from the new processing technique were evaluated.

8.2 Materials and Methods

DBC consisted of nano size carriers (particulates) which are coated with curing promoters. Due to the inter-particle cohesion [2-4], DBC is able to attach to the powder coating particles after the blending of the two and the blended DBC will not be removed from powder particles during fluidization, pneumatic transportation and powder spraying [5]. As revealed by previous studies, adding proper amount of nano particulates would not cause surface defects on the coatings [5-6]. Therefore, the DBC should not cause adverse effects on the coating quality.

Material fabrications

Most of the promoters are water soluble; therefore, water can be used to dissolve the promoter for better handling during fabrication of DBC. The fabrication of the DBC started by the mixing the promoter solution (ratio of the promoter to water = 1:2) and the nano silica particulates inside a high shear kneading machine. After that, the mixed material was air dried. It was to note that the water content had to be well controlled for obtaining a paste-like mixture. The paste-like mixture was more desired than the liquid-like mixture for the mixing process since the liquid like mixture could have higher risk of material segregations during drying due to the sedimentation of the nano particulates. The dried mixture was then pulverized by a jet mill so that the agglomerated nano particles could be broken down to their original scales and the product received from the jet mail was the DBC.

Figure 8-1 was the TEM (Transmission Electron Microscope) images of the nano silica and the DBC. The diameters of the DBC particles were found larger than the nano silica. Moreover, the DBC particles had less transparency than the nano silica. These evidences imply that the promoter was successfully carried by the nano silica particulates.

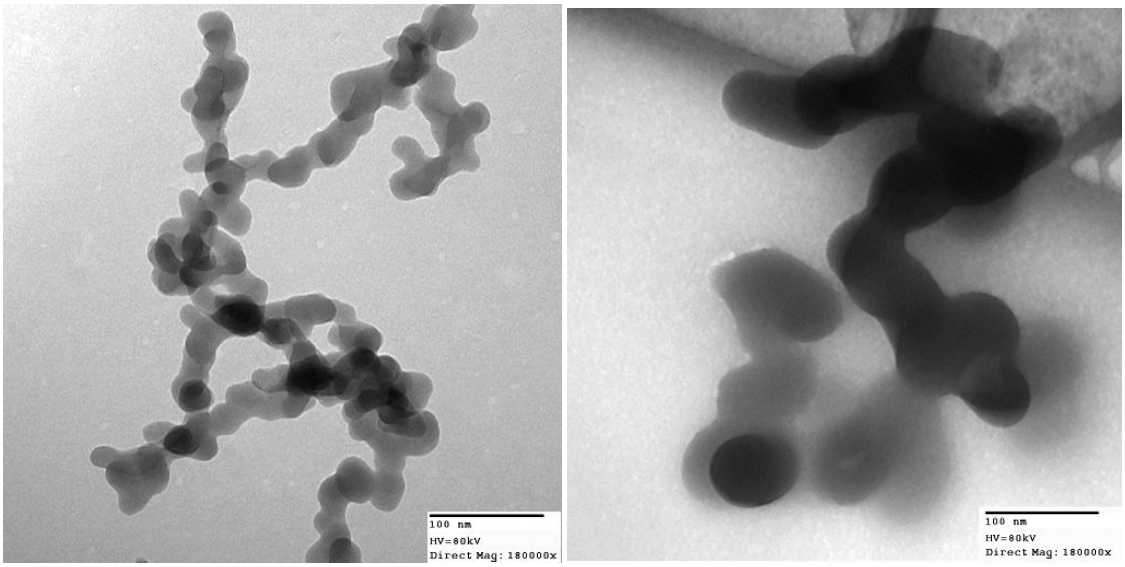

Figure 8-1: Comparison between the original nano silica (left) and the coated nano silica (right) under the TEM

There are various methods to use for dispersing the DBC into the powder coatings. In this study, DBC was dispersed into the powder coatings by utilizing an ultra-sonic sieve since the quantity of the material handled in the experiment was small. The ultra-sonic vibration from the sieve screen could help better disperse the DBA among the powder coating particles. Figure 8-2 shows the SEM (Scanning Electron Microscope) images of the powder particles after coated with DBC. For mass productions, DBC can be blending with powder coating during the milling process.

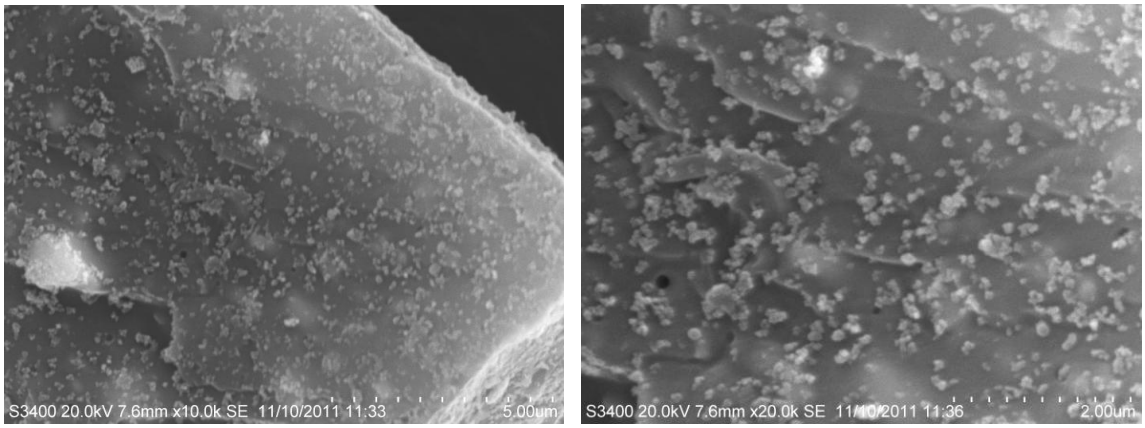

left: SEM image magnification of 10K; right: SEM image magnification of 20K

Figure 8-2: The images of the powder particle with nano additive on the surface taken from the SEM

Influences of the DBC on coating qualities

First of all, the coating quality of the low-cure powder coating made from DBC was explored in the study. Powder coating samples mixed with different DBCs, which were made from various mixture ratios and promoter dosages, were sprayed. The evaluations of the coatings were based on the gloss reduction of the coating film and observed coating defects. The powder coating material was supplied by Prism Powder Coating, Canada (polyester mirror black, Model: PB-0191-H) and it is designed to be cured at 190 ^{o}C for 15 minutes. The high gloss finish provided by this powder coating could help to observe the coating defects caused by the DBC. Fumed silica particulates (AEROSIL ® R972) were used as the promoter carriers and the curing promoter, named as promoter A, was a water soluble onium salt material supplied by Huangsha City Debon Powder Material Co., Ltd., China. Detail information on the chemical contents of the promoter A was not provided due to the confidential reason.

Optimization of the DBC

In the second part of the study, the formulation of DBC was optimized by series of experiments. The selection of the optimum formulation was based on the curing performance

of the powder, the coating quality, the mechanical property and the chemical resistance of the coating.

Evaluation of the DBC low-cure powder coating

Finally, the optimized low-curing powder coating made from DBC, named "DBC sample" was compared with the low-curing powder coating made from conventional extrusion technique, named "extruded sample". Additional tests on the DSC (Differential Scanning Calorimetry) characteristics and shelf life for both powders were conducted.

Test standards

The mechanical property of the coating was examined by the impact test (Elecometer 1615 variable impact tester) according to the ASTM standard D2794 [7] and the chemical resistant property of the coating was examined by the MEK (methyl ethyl ketone) rubbing tests according to the ASTM standard D4752 [8]. In addition, the gloss of the coatings was measured by the glass meter (manufactured by GENEQ inc., Canada) following ASTM standard D523 [9].

On the other hand, the evaluation of the coating quality was not as quantitative as others. The surface defect examinations had to be mainly relied on the observations by the naked eyes. The surface defects were identified by the images shown in Figure 8-3. It is to clarify that the "orange peel" represents the millimeter scale waviness on the coating film, whereas the small roughness is indicated by the sub-micron to micro scale texture on the coating film. The "orange peel" does not affect the gloss of the coating, yet the existence of small roughness can drastically reduce the gloss of the coating.

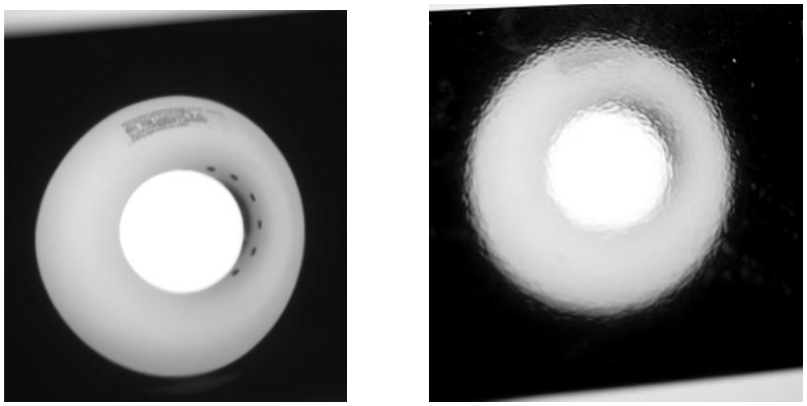

a. Glossy and smooth coating surface b. Coating surface with strong orange peel effect

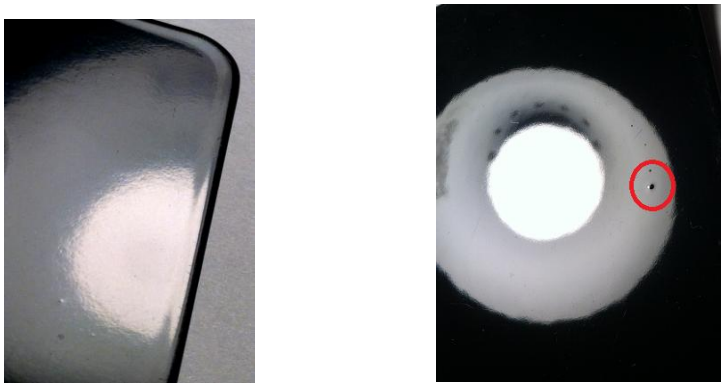

c. Coating surface with small roughness d. Seeds on the coating surface (circled)

Figure 8-3: Image identifications of different coating surfaces

8.3 Results and Discussion

8.3.1 Influences of the DBC on Coating Qualities

Preliminary study was conducted to examine the influences of the DBC on powder coatings. The curing condition for the powder coating samples with added DBC was set at 170^{o}C for 15 minutes and two variables, the mixture ratio (carriers : promoter) and the promoter dosages to powder coating, were used for the experiment. The selected dosages were within suggested limits stated by the supplier.

Table 8-1 lists the reduction in the gloss of the coatings. The reduction of the gloss, ΔG, was calculated by:

$$\Delta G = \frac{G_{DBC} - G_{original}}{G_{original}} \qquad \text{Eq. 8-1}$$

Results disclose that the gloss of the coating is deteriorated when dosage of the promoter A becomes higher. In addition, gloss of the coating is less affected as the mixture ratio increases. With the mixture ratio in 5:1 and 0.075% dosage, the gloss of coating from the low-cure sample is very similar to the original powder coating. Therefore, less dosage of the promoter and higher mixture ratio are both favorable for retaining the gloss of the coating.

Table 8-1: The influences of DBC on the gloss of the coating

DBC with mixture ratio of carriers : promoter A (wt. Ratio)	**The reduction in gloss (%)**		
	0.075% dosage	0.13% dosage	0.22% dosage
3:1	1.5	1.9	6.6
4:1	0.9	2.6	3.4
5:1	-0.3	1.8	2.9

Based on visual inspection, coatings started to have stronger orange peels and small roughness as the mixture ratio of the DBC increased. This situation also occurred with increasing dosage of the promoter. Nevertheless, observations found that the influence from the promoter dosage was more significant since small dosage of the promoter was able to cause severe small roughness on the coating. Therefore, it was similar to the results shown in Table 8-1 that higher mixture ratio with lower dosage was preferred.

However, the higher mixture ratio is not desired for powder coating production. When a higher mixture ratio is used, the promoter is much diluted by the nano carriers. As a result, larger amount of DBC has to be added into the powder coating for obtaining the same promoter dosage. In real production, powder coatings, especially fine powder coatings, could

be loaded with fluidization additives, which are also nano particulates. Therefore, adding excessive amount of DBC would likely to cause seeds on the final coating. Based on the experimental results, the mixture ratio of 4:1 was more reasonable to use and this mixture ratio was selected for the following experiments.

8.3.2 Optimization of the DBC

This part of the study was to optimize the formulation of the DBC. The selection of the optimum formulation was based on the curing performance of the coating. The curing condition was at 170^{o}C for 15 minutes. According to the discussions from section 8.3.1, the promoter A was found to cause small roughness even with the small dosages. In order to maintain the coating quality, a secondary DBC, named DBC', was used together with the DBC. The curing promoter for DBC' was the 2-methyl imidazode material supplied by A.H.A International Co., Ltd., China, named promoter B. The promoter B was claimed to have less influence on the coating quality. The DBC' with the mixture ratio of 4:1 was tested before the optimization experiment. The influences on the gloss of the coating from DBC' were listed in Table 8-2. The selected dosages of the promoter B were within the suggested limits by the supplier.

Table 8-2: The influences of DBC' on the gloss of the coating

DBC with mixture ratio of Nano silica : promoter B (wt. Ratio)	**The reduction in gloss (%)**		
	0.015% dosage	0.02% dosage	0.03% dosage
4:1	-11.5	-12.1	-14.8

The results in Table 8-2 reveal that the gloss of the coating is improved by the addition of the DBC'. As dosage increases, the coating is able to obtain even higher gloss than the original coating. From the visual inspections, the small roughness could still be observed on

the coating as the dosage increased, yet it was much less significant than the case with promoter A. Furthermore, the "orange peel" on the coating was not largely affected by the changing dosage. Overall, DBC' provides less adverse effect on the coating quality than the DBC. Thus, replacing a portion of the DBC with the DBC' is expected to improve the coating quality of the low-cure powder coating. The reason not to replace the DBC completely by the DBC' is that the DBC, on the other hand, had much wider range for dosage. The wider range for dosage was preferable, since it could provide extra operational window during production.

For the optimization of the DBC formulation, powder samples with different promoter dosages were spray. The panel used for spraying was a standard aluminum coating panel with dimension of 8.9 cm by 5.1 cm. The curing performances were mainly determined by the MEK (methyl ethyl ketone) resistance and the mechanical property of the provided coatings. The MEK resistance of the coating was evaluated by the rubbing test according to ASTM standard D4752. In the test, the coating is rubbed by cotton cloth damped with the MEK, which is a solvent that can dissolve un-cured powder coatings. Coatings that are not fully cured can be softened and/or wiped off during the rubbing test. On the other hand, the mechanical property of the coating was evaluated by the impact test according to ASTM standard D2794. A sudden impact on the test panel exerted by the calibrated hammer head could cause the test panel to deform. Coatings that are not fully cured will form cracks on the surface; more seriously, the coating film will even shed off from the panels.

Based on the test results, coatings were rated as good, marginal or poor. Coatings that received good rating could retain its original condition after suffering from both the impact and the rubbing tests. Coatings that received marginal rating would expect to have 1 to 2 hairline cracks after the impact test and the surface would expect to be softened but not

wiped off after the rubbing test. In worst cases scenario, the coatings that rated as poor would be badly damaged after the tests. Poor rated coatings would have major cracks on the surface after the impact test and the coating would be dissolved during the rubbing test.

Table 8-3 lists the results from the curing tests. The control sample with a design curing temperature was not able to cure at of 170 ^{o}C for 15 minutes. Indicated by the results, the curing performance can be improved by the increasing dosages of the promoters. The MEK resistance of the coating receives good results with low promoter dosage, where the mechanical property of the coating can only be satisfied at a much higher promoter dosage. The powder coating is able to obtain a good curing performance with the promoter A dosage of 0.03% and the promoter B dosage of 0.35%. Observations found that there was no surface defect on all the coatings.

Table 8-3: Curing performances of the control sample and the samples with different dosage of promoter A and B for 15 minutes of curing period at 170^{o}C

Sample	Dosage of promoter A	Dosage of promoter B	MEK resistance	Impact resistance
Control	0%	0%	Poor	Poor
1	0.005%	0.005%	Poor	Poor
2	0.005%	0.01%	Marginal	Poor
3	0.01%	0.025%	Marginal	Marginal
4	0.02%	0.025%	Good	Marginal
5	0.025%	0.025%	Good	Marginal
6	0.03%	0.025%	Good	Marginal
7	0.03%	0.035%	Good	Good

Figure 8-4 shows the images taken from the test panels. Based on past experiences, the properties of the coatings are usually not settled until 72 hours. Therefore, two sets of

rubbing test and impact test were conducted on all the coatings: the first set of tests was performed 1 hour after the curing was completed and the second set of tests was performed 72 hours after the curing was completed. The rubbing tests could be hardly seen from the images; however, the transition of the changes in the mechanical property of the coating could be discovered. It is to note that the deformation on the bottom of the panel was made by the 1 hour impact test whereas the deformation on the top of the panel was made by the 72 hour impact test. The results indicate that:

- From control sample to sample 2, large cracks occurred even in the 1 hour impact tests.
- As the dosage increased, samples 3, 4, 5, and 6 could pass the 1 hour test as shown by. It was also discovered that the cracks on the coatings caused by the 72 hour impact test became smaller and less noticeable as the promoter dosage increased.
- The sample 7 performed the best with excellent impact resistance shown with no formation of crack on the coating surface.

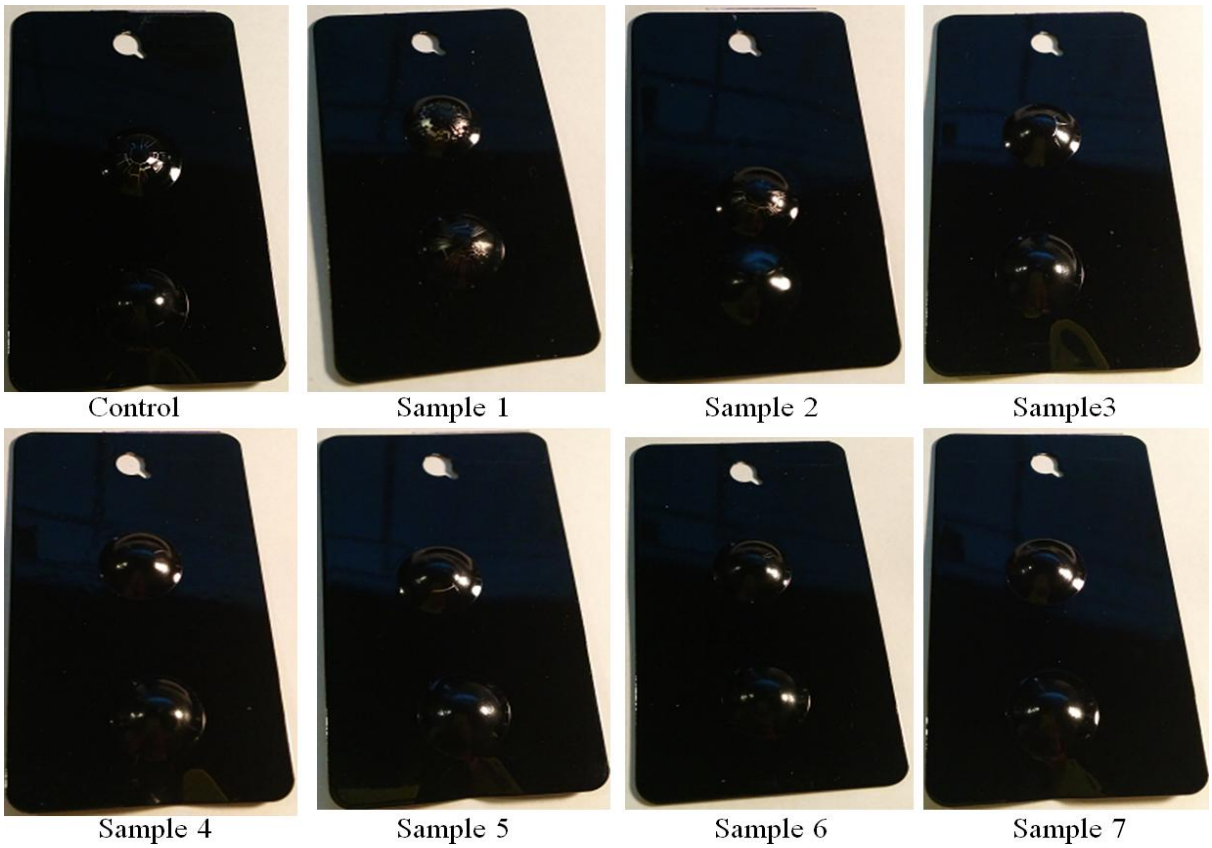

Figure 8-4: The images of the coating by samples with different curing performances

Samples with further increased promoter dosages were also examined. As the dosage became even higher, the coating started to obtain strong orange peel effect. Furthermore, the coating started to fail the impact test again although the chemical resistances of the coatings could still retain good results. It can be explained by the over-cured of the coating. When excessive amount of curing promoter is incorporated in the powder coating, the flowing time of the melted powder particles was much reduced. As a result, there will not be sufficient leveling of the melted particles during curing so that "orange peel" can develop. Moreover, the over-cured coating was found to be more brittle than the normal coatings. The lack of the ductility made the coating become easier to crack under deformations. Therefore, the promoter dosage of sample 7 was selected as the optimum formulation for the tested powder coating for the curing temperature of 170 ^{o}C and the curing time of 15 minutes.

8.3.3 Evaluation of the DBC Low-cure powder coating

In order to fully evaluate the DBC low-cure powder coating, the optimized low-cure powder coating with DBC, named DBC sample, was compared with the original powder coating, named control sample. Furthermore, a low-cure sample made from conventional extrusion technique, name extruded sample, was also prepared for the comparison. According to the suggestion from the promoter supplier, the extruded sample was incorporated with 0.1% of promoter A by an extruder (model SLJ-30D manufactured by Donghui Powder Processing Equipment Co., China). The temperature inside the extruder was set to 95 ^{o}C during the mixing process.

First of all, the curing performances of the DBC, extruded and control samples were compared for a curing time of 15 minutes with various curing temperatures. The results could help to determine the minimum curing temperature for each sample. Powder coatings that achieve lower curing temperature have better advantage for energy savings. Similar evaluation on curing performance as used in Table 8-3 was followed. A fully cured coating has to receive good ratings from both the impact resistance test and MEK resistance test.

Results reviewed by Table 8-4 show that both the DBC and the extruded samples outperformed the control sample. The extruded sample is able to cure at temperature of 165^{o}C, whereas the DBC requires a higher curing temperature of 170^{o}C. In contrast, the control sample could only cure at its designed curing temperature of 190^{o}C. The gloss obtained from the DBC sample was similar to the control sample and it was not affected by the curing temperature. However, the extruded sample suffered a significant reduction in gloss.

Table 8-4: Comparisons of the control sample, the DBC sample and extruded sample with various curing temperatures.

Test (15 min. of curing)	**DBC sample**			**Extruded sample**	**Control sample**		
Curing temperature (^{o}C)	165	170	185	165	165	175	190
Impact test	Marginal	Good	Good	Good	Poor	Poor	Marginal
Rubbing test	Good	Good	Good	Good	Poor	Poor	Pass
Gloss (^{o})	95.6	96.4	96.3	69.2	96.8	97.3	97.1
Surface quality	Smooth	Smooth	Smooth	Orange peely	Smooth	Smooth	Smooth

Although the extruded sample had a slightly lower curing temperature than the DBC sample, the coating quality of the extruded panel was not satisfied. Figure 8-5 shows the comparison between the three samples (the control was cured at 190 ^{o}C, DBC sample was cured at 170 ^{o}C and the extruded sample was cured at 165 ^{o}C). The DBC sample provides a remarkable coating finish which is very close to the original sample. But then, the extruded sample had much stronger "orange peel" on the coating surface. Based on visual inspections, there was no other surface defect found on both low-cure samples.

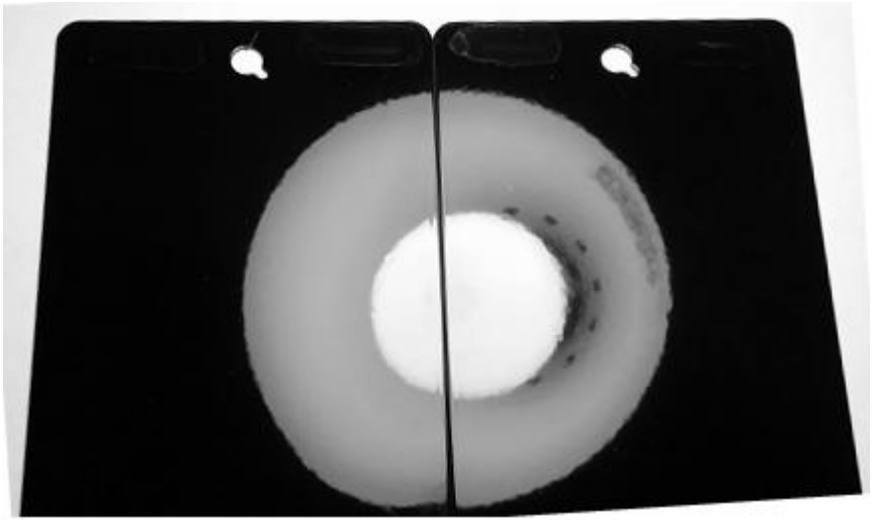

Left: control sample; Right: DBC sample

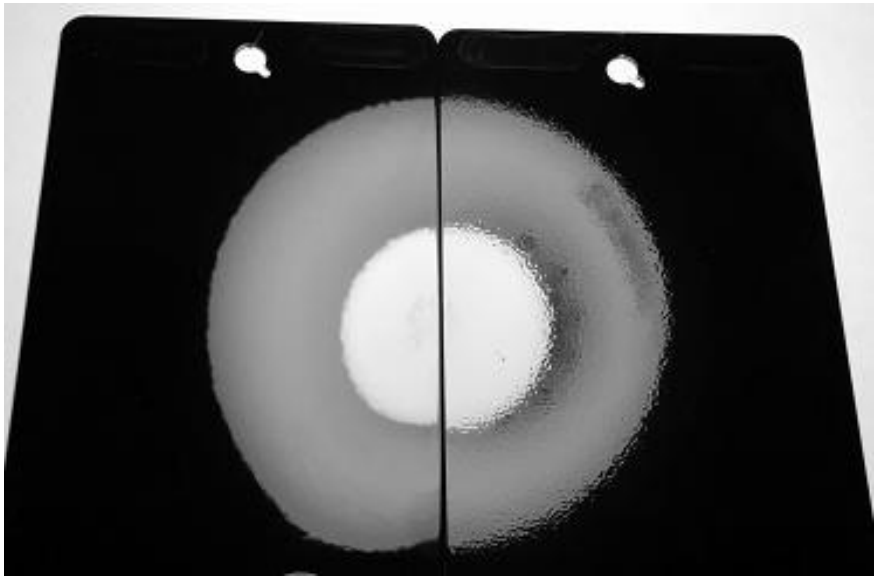

Left: control sample; Right: Extruded sample

Figure 8-5: The comparison of the coating quality between DBC, extruded and control samples

The curing performances of the three samples were then compared at the curing temperature of 190 ^{o}C but with various curing times. It was to determine the minimum curing time of the samples. A shorter curing time is the other feature offered by the low-cure powder coatings. It can lead to energy savings since the curing process is accelerated. On the other hand, it can

also increase the production throughput due to the potential to increase the conveyer speed on the coating line.

The results reviewed in Table 8-5 show that both DBC and extruded samples can be able to cure at a much shorter curing time of 8 minutes, but control sample can only cure at its designed curing time of 15 minutes. The gloss of the DBC sample is similar to the control samples, and it is not affected by the curing time. Similar to the result shown in Table 8-4, the extruded sample has much stronger "orange peel" and much less gloss than the control sample. Therefore, DBC sample provides a much more desirable coating finish than the extruded sample.

Table 8-5: Comparisons of the control sample, the DBC sample and extruded sample with various curing time.

Test (curing temperature of 190 ^{o}C)	**DBC sample (sample 7)**			**Extruded sample**	**Control sample**	
Curing time (min.)	8	10	12	8	8	15
Impact test	Good	Good	Good	Good	Poor	Good
Rubbing test	Good	Good	Good	Good	Poor	Good
Gloss (^{o})	96.1	96.3	96.9	69.3	96.7	97.1
Surface quality	Smooth	Smooth	Smooth	Orange peel	Smooth	Smooth

A dynamic run on the DSC (Differential Scanning Calorimetry) of the three samples were plotted in Figure 8-6. As indicated, the extruded and the DBC samples have curing onset temperatures around 140 ^{o}C which is almost 15 ^{o}C lower than the curing onset temperature of the control sample. Studies on the curing mechanism of powder coatings [10-11]

disclosed that an earlier curing onset temperature implies a lower curing temperature. Other than that, the peak curing temperatures, which represents the temperature for the fast curing reaction, of both the extruded and the DBC samples are lower than the control sample. In other word, the extruded and the DBC samples can cure faster than the control sample at a lower temperature. More importantly, the plot indicates that the melting points of the DBC and the control samples are similar. On the other hand, the melting point of the extruded sample is almost 10 ^{o}C higher than the original sample, which is a reflection of pre-curing (or partial-curing) of the powder sample [12]. Pre-curing is the most common problem of the conventional low-cured powder coatings. It almost cannot be avoided in the current processing method since raised temperature during the hot extrusion process and transportation/storage causes different degrees of pre-curing of the low-cured powder coatings. Therefore, the differences of the melting point among the three samples also demonstrate the advantage of the DBC sample over the extruded sample.

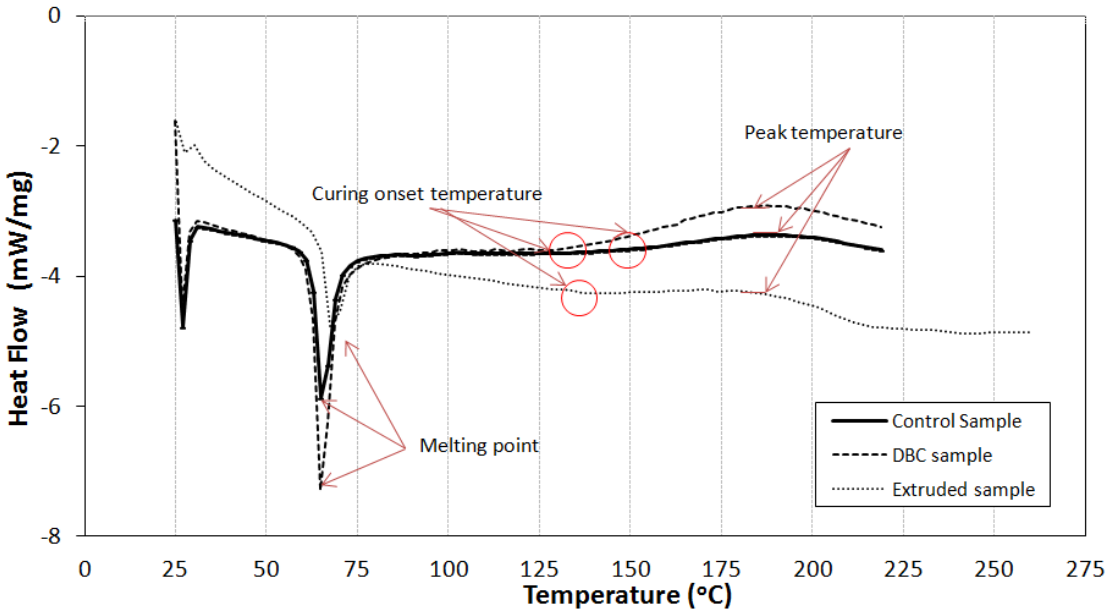

Figure 8-6: Dynamic run on the DSC of the three samples with heating rate of 20 ^{o}C/min.

Overall, the DSC plot is in agreement with the experimental results shown in Table 8-4 and Table 8-5. The curing characteristics indicate that the DSC sample has comparable curing performances to the extruded sample. Since DBC sample retains a much better coating finish, it is more preferable than the extruded sample.

However, the shelf life of the samples had to be examined prior to the final conclusion. Improvement on the shelf life of the low-cure powder is one of the major challenges to accomplish by the study. Storage and transportation of the conventional low-cure powder often require lower temperature than the ambient. Otherwise, powder particles can aggregate so as to cause powder agglomerations.

In order to evaluate the shelf life, the extruded, DBC and control samples, placed in separate test containers, were subjected to baking with a temperature of 40 ^{o}C. It is similar to the situation that the powders are stagnated during storage or transportation in a warm weather. Overtime, the samples were extracted from the containers for visual inspections. Since the stagnated powder coatings are always fluidized before further application, the test container was shook before each extraction of the sample. The time span for the shelf life test was set to 100 hours and the sample with a better shelf life could be indicated by less particle agglomerations.

Figure 8-7 shows the images of the samples taken during the shelf life tests. Control sample had agglomerations among loose powder particles after the first 24 hours in the test. The agglomerations were soft to touch and they could be easily broken down. 72 hours later, the numbers of agglomeration were increased and the size of the agglomeration was bigger. Comparing with the control sample, the extruded sample performed even worse. Agglomerations found after the first 24 hours were much chunkier. Furthermore, these agglomerations were harder to be broken down. Similar observations were found from the

extruded sample in the rest of the test. But then, the DBC sample had much better results. Images show that the DBC samples could almost retain the powder form throughout the entire test. It is to note that the DBC sample even outperform the control sample. It can be contributed by the increased inter-particle distances due to coated DBC on the powder particles. Since the inter-particle distances are increased, agglomerations are less likely to occur. In addition, the studies on fine powder fluidizations discovered that nano particulates attached on the particle surfaces are able to reduce the powder cohesion so as to improve powder flow behaviour [2-4].

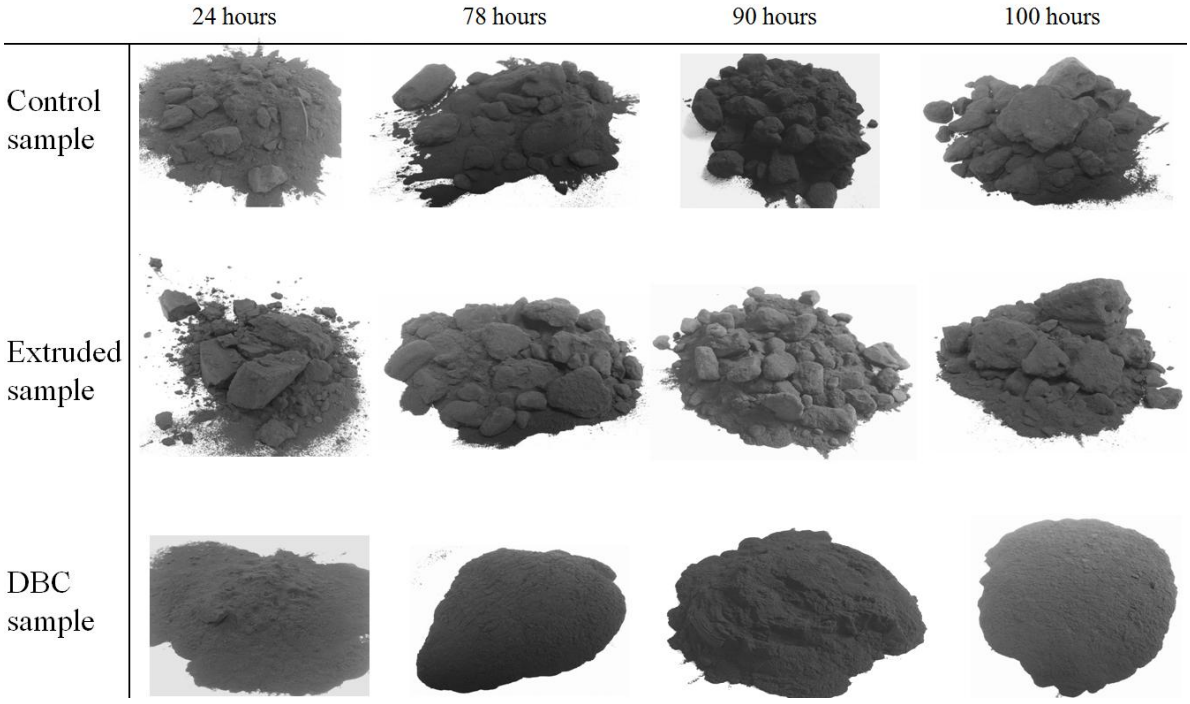

Figure 8-7: Images of the samples extracted during the shelf life tests

8.4 Conclusion

This part of the thesis work examined a novel processing technique for low-cure powder coatings. Experimental results indicated the DBC sample had a comparable curing performance to the conventional low-cure powder coating made from extrusion. Furthermore, the DBC sample obtained a desirable result from the shelf life test outperforming both the conventional low-cure powder coating and the original powder coating. More importantly, the DBC sample could retain the low-cure performance as well as a good shelf life without sacrificing the coating quality. Comparing with the conventional low-cure powder coating, the DBC sample provided much smoother and glossy finish. Visual observations concluded that utilization of DBC would not cause surface defect of the coating.

Reference

[1] Lee S., Koo J.H., Lee S.S., Chai S.G., Lim J.C, 2003, Gloss reduction in low temperature curable hybrid powder coatings, Progress in Organic Coatings, 46, 266-272.

[2] Yang J., Sliva A., Banerjee A., Dave R., Pfeffer R., 2005, Dry particle coating for improving the flowability of cohesive powders, *Powder Technology*, 158(1-3), 21-33.

[3] Molerus O., 1987, Effect of interparticle cohesive force on the flow behaviour of powders, *Powder Technology*, 20, 161-175.

[4] Visser J., 1989, "An invited review-Van der Waals and other cohesive forces affecting powder fluidization", *Powder Technology*, 58, 1-10.

[5] Fu J., Krant M., Zhang H., Zhu J., Kuo H., Wang Y.M., Liz K., 2011, Investigation of the recyclability of powder coatings, *Powder Technology*.

[6] Zhu J., Zhang H., 2004, Fluidization additives to fine powders, *US Patent 6833185*.

[7] *ASTM standard D2794*, Test Method for Resistance of Organic Coatings to the Effects of Rapid Deformation (Impact).

[8] *ASTM standard D4752*, Standard Practice for Measuring MEK Resistance of Ethyl Silicate (Inorganic) Zinc-Rich Primers by Solvent Rub.

[9] *ASTM standard D523*, Standard Test Method for Specular Gloss.

[10] Gedan-Smolka M., Lehmann D., Cetin S., 1998, Basic investigations for development of new curing mechanisms for powder coatings, *Progress in Organic Coatings*, 33, 177-185.

[11] Mafi R., Mirabedini S.M., Attar M.M., Moradian S., 2005, Cure characterization of epoxy and polyester clear powder coatings using Differential Scanning Calorimetry (DSC) and Dynamic Mechanical Thermal Analysis (DMTA), *Process in Organic Coatings*, 54, 164-169.

CHAPTER 9：DEVELOPMENT OF THE COLD BONDING TECHNIQUE FOR PROCESSING METALIC COLOR POWDER COATINGS

9.1 Introduction

Powder coating is popular for many applications due to its unique advantages of zero VOC (Volatile Organic Compound) emission and its recyclability over-sprayed materials. In general, powder coatings provide less decorative coatings with plain colors and they have been mainly used on lower-end products with marginal market prices.

Nowadays, powder manufacturers start to offer powder coatings that can provide much better aesthetic appearances for applications on premium products. The metallic color powder coating is a typical example. The metallic color powder coating can create a metallic effect on its final coating so as to provide extra shine and deepness to the color. The metallic color powder coatings are much more expensive than the regular powder coatings. It is not just because of its unique aesthetic appearance but also the high production cost due its complicated manufacturing process. The processing of the metallic color powder coating is accomplished by a heat blending of the metallic pigment and the powder coating. During the process, powder particles have to be softened by the heat generated from the blender for a better adhesion with the metallic pigment. However, the heat can also cause curing of the powder coating. Therefore, the temperature of the blending process of the two materials is critical. Expansive measures are always necessary for ensuring the productions of metallic color powder coatings.

The bonding between the metallic pigment and the powder coating particles provided from the conventional blending technique is weak and the two materials can easily separate from each other. For that reason, the metallic color powder coating always encounters problems during spraying. Corona charge spraying is usually used for applying powder coatings. During application, powder particles collide with the free electrons generated by the corona spray gun and particles gained charges by the attached the free electrons from the collision [1-3]. Due to the distinctions in shape and surface conductivity, the separated metallic pigment has a different charging performance from the powder particles. As a result, the transfer efficiency of the two materials will vary. Therefore, the recycled metallic color powder coatings are less likely to be reused since they always have different contents of the metallic pigment.

The objective of this study was to improve the processing technique for the metallic color powder coating so to resolve the problem associated with the current metallic color powder coatings. The root cause of the problem is the insufficient bonding between the metallic pigment and the powder coating particles. Unlike the conventional blending process, the proposed new technique was to utilize a liquid bonder to glue the metallic pigment on the powder particles. Because of that, heating of the particles was no longer required so that the process was much easier to operate. The resin based liquid bonder was able to provide excellent bonding between the powder particles and the metallic pigment so to reduce the separations of the two materials during spraying. Therefore, the recyclability problem was expected to be resolved. Series of experiments were conducted to evaluate the new technique in the study.

9.2 Materials and Methods

Fabrication method

The new technique for processing the metallic color powder coating started with the mixing of the metallic pigment and the liquid bonder. In the study, the liquid bonder was diluted by its solvent before adding into the metallic pigment. In doing so, the liquid bonder can be better dispersed since it allows a longer drying time for the mixing. A liquid bonder with high solvent content may not need to be further diluted. The mixture was then blended into the powder coating by a high shear blender before it was completely dried. Finally, the product of the metallic powder coating was obtained by completely drying the blended material. In the experiment, water soluble PA (poly acrylic) resin was used as the liquid bonder and aluminum flakes (manufactured by Silberline Manufacturing Co., Inc., USA) was used as the metallic pigment.

Evaluation method

The metallic powder coating made from the new technique was evaluated by the comparisons with the sample made from the conventional technique. Results from the following respects were obtained:

1. The content of the metallic pigment in the powder coating after spraying;
2. Observations of the bonding between the powder coating particles and the metallic pigment;
3. The actual metallic effect shown by the final coating.

First of all, the content of the metallic pigment was investigated by the spraying test. An epoxy clear coat powder with no other additives was used for preparing the metallic color powder coating samples. Sample made from the new technique was named new sample

whereas the sample made from the conventional technique was named control sample. Spraying of the powder samples was done by a corona spray gun manufactured by GEMA. Ash tests, which followed the ASTM D5630-06 [4], were conducted to measure the content of the metallic pigment in the virgin samples (sample prior to the spraying) and the sprayed samples (sample collected from the coating surface). In the ash test, powder samples were burned in a furnace with a temperature of 530 ^{o}C which was lower than the burning point of the metallic pigment but higher than the clear coat. Therefore, powder coating could be burned off from the process and the metallic pigments remained. The content of the metallic pigment could be determined by:

$$\%\,\text{Pigment} = \frac{W_{\text{Residual}}}{W_{Powder}} \qquad \text{Eq.9-2}$$

On the other hand, the actual bonding between the powder coating particles and the metallic pigment was examined by the SEM (scanning electron microscope). Furthermore, tests panels were sprayed for the observations of metallic effect on the final coatings. The observations relied on the inspections from the naked eyes, since measurements by the instruments were not accurate due to the metallic effect on the coating. A black color high gloss polyester powder coating (supplied by Prism, Model PB-0191-H) was selected to use for better observing the coating quality and the metallic effect.

Process optimization

The influence from the blending was first explored because the blending intensity in the new technique could affect the metallic effect on the final coatings. A lab-scale blender was used for the blending of the powder coating and the liquid bonder coated metallic pigment and three blending duration, 5 s, 10 s and 20 s, were selected. The content of the metallic

pigment was 3 wt% of the powder coating. Images shown in Figure 9-1 are the coatings obtained from the powders with the different blending durations. It was observed that a longer blending duration led to more metallic effect, which was indicated by a better dispersion of the metallic pigment in the coating. Although the content of the metallic pigment was the same, the sample with the shortest duration provided very limited metallic effect in the coating.

Left: 5s blending; Middle: 10s of blending; Right 20s of blending

Figure 9-1: The influence of the blending time on the metallic effect of the coating

Based on the observations under SEM, the 5 s sample had severe stacking problem of the metallic pigment as shown in Figure 9-2a. Due to the thin and flat profile of the metallic pieces, the staking metallic pigment could easily occur during the mixing with the liquid bonder. With insufficient blending, they could hardly be separated causing poor dispersion in the powder coating. It explained the much less significant metallic effect observed from the coating. Moreover, the stacking metallic pigment was not desired for spraying. The much

heavier weight causes separation of the stacking metallic pigment from the much lighter powder particles while flying towards the coating surface.

On the other hand, the stacking problem could be solved by an extended blending duration of 20 seconds. Yet, bending and cracking started to appear on the metallic pieces as disclosed by Figure 9-2b. Thus, a longer blending duration than 20 seconds could probably cause more serious damages to the metallic pieces. Furthermore, excessive blending could also cause de-bonding of the materials due to the extensive collisions among the powder particles. Based on the obtained results, 20 seconds seemed to be a reasonable blending duration. Therefore, it was selected for the fabrication of the samples in the remaining experiments.

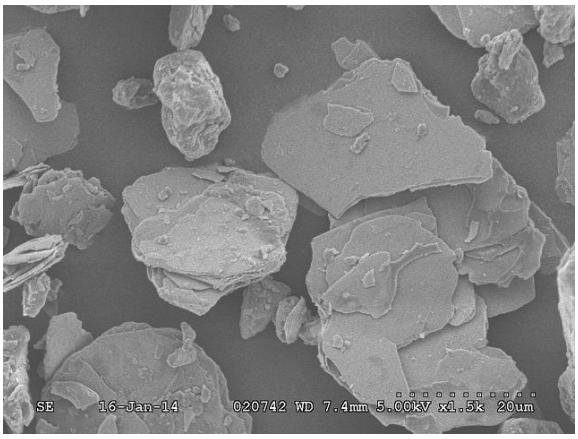

a. Stacking of the metallic pigment due to insufficient blending (5 s sample)

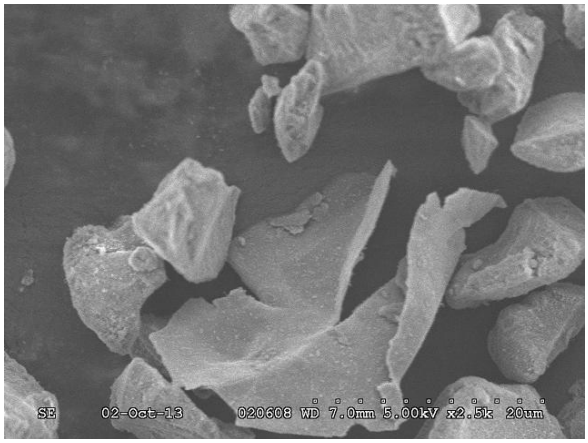

b. Damaged metallic pigment due to over blending (20 s sample)

Figure 9-2: SEM image of the metallic pigment during blending

9.3 Results and Discussion

9.3.1 Spraying test

The mixing of the liquid bonder and the metallic pigment was the most vital process for fabricating the metallic powder coating in the new technique. The changes in the solvent content and the concentration of the liquid bonder were likely to cause different bonding results due to the variations of the dispersion and the bonding strength. In this study, PA was used as the liquid bonder and water was used as the bonder solvent. With different combination of the PA and water, 12 samples listed in Table 9-1 were prepared for the spraying test. This experiment was also an optimization work for the formulation of the PA solution. All of the 12 samples had 2 wt% the metallic pigment loaded into the epoxy clear coat. A control sample made from the conventional blending technique was prepared for comparison.

Table 9-1: Samples of the metallic powder coating prepared by the new technique for the spraying test

2 wt% Metallic pigment loading	**PA resin (g)**			
		0.01	**0.03**	**0.06**
H_2O(g)	**0.1**	Sample 1	Sample 5	Sample 9
	0.2	Sample 2	Sample 6	Sample 10
	0.3	Sample 3	Sample 7	Sample 11
	0.5	Sample 4	Sample 8	Sample 12

The results from the spraying test are reviewed in Table 9-2. The coated control sample had an increased content of metallic pigment from 2.14% to 6.35%. It indicated that more metallic pigment was sprayed onto the coating surface. In other words, the content of the metallic pigment in the recycled control powder was less than desired. The content of metallic pigment in the coated sample 5, 9, 10 and 11 were quite comparable to their

corresponding virgin powders. It implied that the recycled powders of these samples had similar content of metallic pigment to their corresponding virgin powders. The spraying test indicated that the new technique was able to solve the recyclability problem of the metallic powder coatings.

Table 9-2: The measured content of the samples from spraying tests

Sample	Virgin powder (%Al)	Coated powder (%Al)	Sample	Virgin powder (%Al)	Coated powder (%Al)
Control	2.14	6.35	Sample 7	1.98	3.84
Sample 1	2.19	7.6	Sample 8	2.19	6.14
Sample 2	2.1	7.2	Sample 9	2.23	2.25
Sample 3	1.99	6.96	Sample 10	2.04	2.1
Sample 4	2.06	8.09	Sample 11	2.22	2.6
Sample 5	2.19	2.96	Sample 12	2.14	3.38
Sample 6	2.18	3.23			

The results were further analyzed to characterize the influence from the formulation of PA on the change in the content of the metallic pigment, Δ%Pigment. Δ%Pigment was determined by:

$$\Delta\%\,\text{Pigment} = \frac{\%Pigment_{coated} - \%Pigment_{virgin}}{\%Pigment_{virgin}} \qquad \text{Eq. 9-2}$$

Figure 9-3 demonstrates the three series of results obtained from the samples prepared by the new technique distinguished by the amount of added PA. Δ%Pigment is plotted with respect to the water content. The samples with 0.01 g PA had the highest Δ%Pigment in their sprayed powders indicating the worst bonding performances overall. As the amount of PA increased, the Δ%Pigment for the sprayed powder was drastically reduced. The samples with

0.06 g PA had the least Δ%Pigment for their coated powders. It indicates that increased amount of added PA can enhance the bonding performance. On the other hand, Δ%Pigment for the coated powder can also be reduced by the less water content. In conclusion, increased amount of PA or decreased amount of water is preferable for obtaining a low Δ%Pigment. In addition, the amount of PA has more significant influence on the Δ%Pigment. However, the water content should not be kept too low; otherwise, it can cause poor dispersion of the metallic pigment in the powder coating. Therefore, the combination of 0.06 g PA with 0.2 g H_2O is selected as the optimum formulation of the PA solution from the experiment.

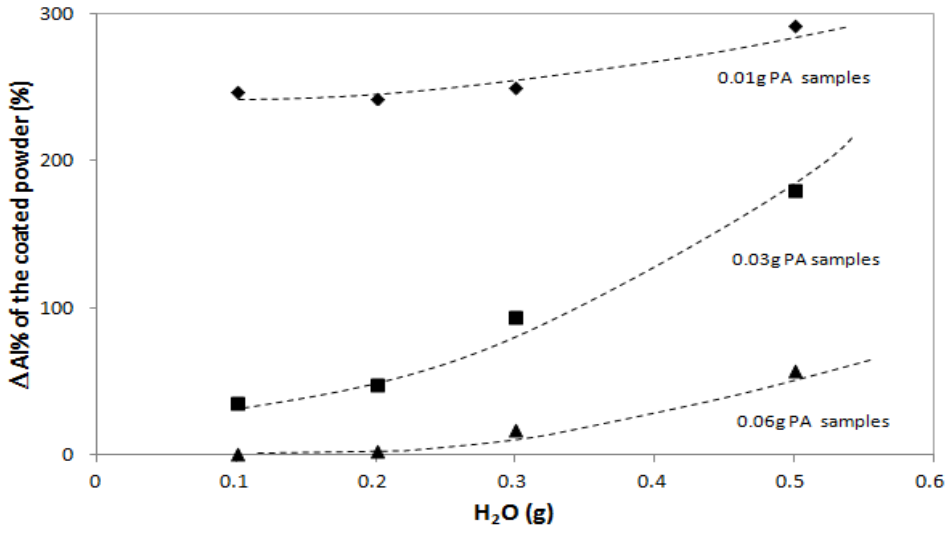

Figure 9-3: Change in the content of the aluminum measured from the coated powder comparing with the according virgin powder

9.3.2 Observations of the Bonding of Powder Particles and Metallic Pigment

Figure 9-4 shows the images taken from the observations on the metallic color powder coatings under SEM. The fabrication of the metallic powder coating made from the new technique, named new sample, utilized the optimized formulation of PA solution. The sample made from conventional blending technique was named control sample.

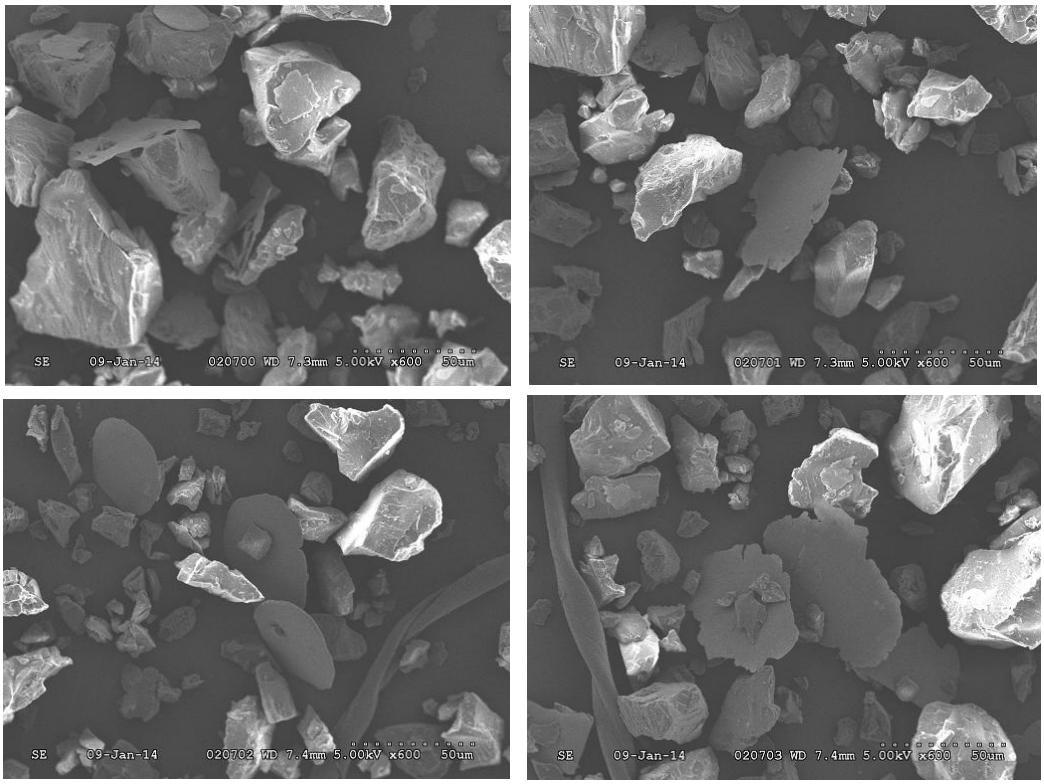

a. Control sample

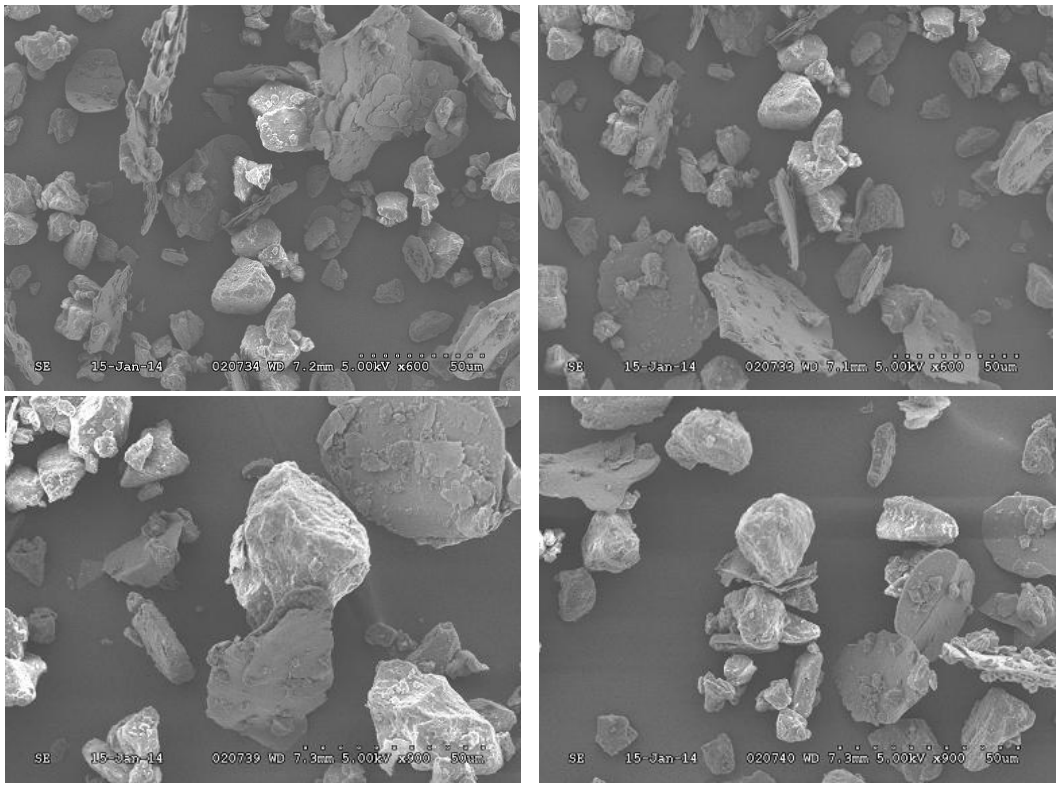

b. New sample

Figure 9-4: Images of the metallic powder coatings taken from SEM observations

The images show that the control sample had numbers of metallic pigment with no particles attached and the remaining metallic pigment had only several small particles on its surface. In comparison, the new sample had much better bonding between the metallic pigment and the powder particles. Image indicated that the metallic pigment which was coated by PA was able to attract much larger particles. In addition, the numbers of particles on metallic pigment were increased in general. Furthermore, some of the metallic pigment even had particles attached on both of sides. Nevertheless, the stacking of the metallic pigment was found from the new sample, where the smaller pieces of the metallic pigment were attached to the larger pieces of the metallic pigment. Although the stacking problem found in the new sample was not severe, an improvement on the new technique is required to resolve this issue.

9.3.3 Observations of Metallic Effect

The two panels shown in Figure 9-5 were coated with the control sample and the new sample. By observations, the two coatings had similar metallic effects under direct sunlight. Moreover, there was no surface defect observed from the new sample. Furthermore, the orange peel effect and gloss of the two coatings were comparable. Nevertheless, the coating obtained from the new sample showed slightly less even metallic effect than the original sample. It can be caused by the stacking problem of the metallic pigment as found in the SEM observations.

Figure 9-5: The coatings obtained from the new sample (left) and the control sample (right)

9.4 Future Work

It is recognized that the new technique the metallic color powder coating is able to provide stronger bonding between the metallic pigment and the powder particles than the conventional blending technique. However, it is also found that stacking problem of the metallic pigment can be caused by the new processing technique. For the future works, additional experiments will have to conduct to overcome this problem. One approach is to pre-disperse sub-micron size particles into the metallic pigment. These small particles among the metallic pieces can act as “spacers” to increase the distance the pieces of the metallic pigment. Therefore, it will have less chance of having stacking problem while mixing the metallic pigment with the PA solution. Another approach is to optimize the blending process by testing with different blending methods. Although more systematic experiments on blending are pending, the results from the preliminary test as in Figure 9-1 implied the significance of the blending manner to the dispersion of the metallic pigment.

On the other hand, current new technique required to fabricate the metallic color powder coating right after preparing the metallic pigment since the blending process has to proceed before the PA dried up. It is not economical and efficiency for mass productions due to the difficulties in time management and material inventory. Therefore, a “master batch” technique will have to be adopted. The “master batch” powder is the “pre-made” metallic color powder coating which has high content of the metallic pigment. It can be added with various amounts of powder coatings to obtain a desired concentration of the metallic pigment according to requirements. Since the “master batch” can be made and stored in advance, the process becomes much more flexibility for the mass production. The difference between the “master patch” and regular sample is in the content of the metallic pigment. Since loaded of the metallic pigment increases, the formulation of the liquid bonder has to be changed accordingly. Therefore, another part of the future work can focus on the optimization of the new technique for “master batch” preparations.

9.5 Conclusion

This study evaluated a new processing technique for the metallic color powder coatings. The new technique utilized a liquid bonder to bond the metallic pigment and powder particles to replace the conventional blending method. It was easier and less expensive to operate.

Experiments from the study examined the bonding performance of the metallic powder coating made from the new technique. The results from the spraying test indicate the new technique is able to create stronger bonding between the powder particle and the metallic pigment so as to resolve the recyclability problem associated with conventional method. It is also disclosed that a higher amount of liquid bonder and less content of the liquid bonder solvent are more preferable for obtaining stronger bonding performance. More importantly,

the expansive and complicated blending process from the conventional method can be avoided.

On the other hand, low content of the liquid bonder solvent may not be always better. SEM observations of the samples made from the new technique indicated that the low content of the liquid bonder could cause stacking of the metallic pigment, which could cause reduction in the metallic effect in the final coating. Therefore, a balance between these factors has to be considered while determining the amount of liquid bonder solvent. Finally, inspection on the final coatings confirms that the new technique does not cause surface defects on the final coating.

Reference

[1] Meng X., Zhu J., Zhang H., 2007, The characteristics of current density distribution during corona charging process of different particulates, *J. Phys. D: Appl. Phys.*, 41(17).

[2] Meng X, Zhang H., Zhu J., 2008, The characteristics of particle charging and deposition during powder coating process with coarse powder, *J. Phys. D: Appl. Phys.*, 41(19).

[3] Meng X, Zhu J, Zhang H., 2009, The characteristics of particles charging and deposition during powder coating processes with ultrafine powder, *J.Phys. D: Appl. Phys.*, 42(6).

[4] *ASTM Standard D5630-06*, Standard Test Method for Ash Content in Plastics.

CHAPTER 10: GENERAL DISSCUSSION

Powder coating is a dry coating technology which can eliminate the usage of the harmful VOCs (Volatile Organic Compounds). It is favorable for various applications not just because it is environmentally friendly but it also provides the excellent coating properties and high efficiency of material utilizations. Comparing with liquid coating, powder coating has not gained a high market share even with developments of nearly half century. The reason for that was mainly due to the relatively poorer appearance and excessive thickness of its coating finish. Powder coatings usually provide thicker and rougher coatings than the liquid coatings.

The problem of the coating finish seems to be the only challenge to overcome but it really turns out to be a complicated issue in the real application. People discovered that the poor coating finish was caused by the large particle size of the powder coating and reduced sizes of the powder particles could essentially improve the coating finish. However, various problems are encounter during the applications of fine powder coatings. First of all, fine powder coatings were experienced to have more flowability issues than regular powder coatings. Moreover, the produced fine powder coatings always have wider particle size distributions. Furthermore, lower coating efficiency and stronger Faraday Cage effect of the fine powder coatings cause difficulties in spraying operations.

This thesis work resolved some of the problems associated with fine powder coatings in a comprehensive way. It started with the study on the flowability characterizations of the fine powder coatings. Then, manufacturing processes of the fine powders were revised for obtaining narrower particle size distribution. On the other hand, new application methods were developed to improve the spraying performances of the fine powder coatings. Finally, novel techniques for processing the featured powder coatings were also explored in the study.

Fine powder coatings are usually group C powders according to the Geldart's chart. Therefore, they are more cohesive than the regular powder coatings which are group A powders. Due to the increased powder cohesion, the flowabilities of the produced fine powder coatings need to be carefully measured. During industrial applications, the medium particle size and D_{10} are the two common parameters used for ensuring the flowabilities of the produced fine powder coatings. However, this study found that neither of these two parameters was able to accurately characterize the flowabilities of the produced fine powder coatings. The main reason was because the produced fine powder coatings always have diverse medium particle sizes and the particle size distributions due to the variations in the manufacturing processes. Experiments indicated that utilizing each of the parameters individually was not able to obtain a linear relationship with the flowabilities of the produced fine powder coatings. This study suggested that the effects from the two parameters should be combined while characterizing the flowability of the produced fine powder coatings. A parameter, span, which represented the profile of the particle size distribution of the powder, was proposed to be used for the flowability characterization. Experiments indicated that the span was in a linear relationship with the flowabilities of produced fine powder coatings with medium particle sizes from 23 to 30 μm. It implied that the span or a similar parameter, which combined the effects from the medium particle size and D_{10}, was recommended for obtaining a more accurate characterization of the flowabilities of fine powder coatings.

Narrow particle size distribution is desirable for fine powder coatings since fewer amounts of large particles can improve coating finishes and fewer amounts of small particles can enhance powder flowability. However, narrowing the particle size distribution is never an easy task for the current manufacturing processing of fine powder coatings. Mass production of fine powder coatings mainly relies on the grindings of bulk materials. While producing

powder coatings, especially fine powder coatings, larger amount of small particles are generated.

Several manufacturing processes were revised in this study for reducing the particle size distributions of the produced powder coatings. One of the encouraging discoveries was that classifying cyclone proposed by this study could utilized the reverse air flow remove small particles from powder coatings during collecting process so as to reduce the particle size distributions. Similar ideas were found in previous designs of cyclone classifiers; nevertheless, the drastically reduced collection efficiency of the cyclone due to the reverse air flow was stated as a major drawback of the designs. Comparing with the designs from other researchers, the classifying cyclone proposed by this study modified the intake of the reverse air flow. Based on the computer simulation, the modification could enhance the air spin in the bottom of the cyclone cone. As a result of that, most of the particles are expected to be retained due to the centrifugal forces. The experimental results are in agreement with the theory and it disclosed that the collection efficiency of the classifying cyclone was comparable to an ordinary cyclone. On the other hand, the classifying cyclone was able to provide noticeable reductions in the particle size distributions of the collected fine powder coatings. In addition, the classifying cyclone does not require external power supply for inducing the reverse air flow. Therefore, it can be easily implemented in real productions.

Moreover, this study also discovered that the particle size distributions of fine powder coatings were possible to be reduced by a revised grinder. Generally, the grindings of the fine powder coatings were accomplished by a hammer mill that had rotating grinding elements to crash the powders during high speed rotation. The conventional design has the grinding elements impact on all powder particles regardless the particle sizes. It can maximize the grinding efficiency, yet it can also increase the particle size distribution of the powder. This

study proposed a design revision for the grinding element. The revised grinding element would have a concave impact surface instead of the conventional flat or convex impact surface. The purpose of the modified design was to build up an air pressure on the impact surface so that the small particles that had low momentum were not expected to receive full impact from the element. In this study, the modification was made to the grinding blade of a high speed grinder. Test results indicated that the modified grinder was able to reduce the particle size distribution of the produced fine powder coatings; in the mean time, the grinding efficiency was not significantly reduced. Scale-up experiment on an industrial grinder has not yet been completed due to the limitations on resources and the fabrication capability at this stage. However, it is anticipated that a similar improvement should be expected in the larger scale grinder.

The corona spraying method was also revised by this study for improving the coating performances of fine powder coatings. Experiment result indicated that that the transfer efficiency of fine powder coatings could be improved by adding moisture on the surfaces of the powder particles and the mechanisms behind this finding were investigated. The investigation disclosed that the increased moisture content on the particle surfaces reduced the resistivity of the fine powder coatings. As a result, the fine powder coatings were able to dissipate the charge much quicker in the particle layer on the coating surface. Because of that, the back ionization which mainly caused by the over-accumulated charge from the particles could be largely reduced so to allow more charged particles to deposit on the coating surface. Therefore, the transfer efficiency was improved. Regular size powder coatings could also take the same advantage from the added moisture. Yet, the effect was found much less significant than the fine powder coatings and the transfer efficiency was not significantly improved. Flowability measurements with respect to the moisture gained by the particles implied that the proposed humidification method would not cause flowability issue of the

powder coatings. Furthermore, the observations of the coatings under SEM confirmed that the added moisture on the powder particles would not cause coating defects.

In this study, the resistance of the Faraday Cage effect in a corona spray process was improved by utilizing a novel spray gun design. The new spray gun utilized alternative charging pattern with a 4-electrode configuration instead of the constant charging pattern with a single-electrode configuration in an ordinary spray gun design. The new spray gun could provide empty period of charging so to partially eliminate the Faraday Cage effect during corona spraying. In addition, the multi-electrode charging was able to create a repellence of the generated electrostatic fields so as to reduce the Faraday Cage intensity within the space of the sprayed powder cloud. Results obtained from the evaluation of the new spray gun were promising. The Faraday Cage resistance could be improved for corona spraying of both fine and regular size powder coatings.

Besides that, experimental results indicated the transfer efficiency of the regular size powder coatings could be improved by the new spray gun due to the reduction of the secondary charging. On the other hand, the transfer efficiency of the fine powder coatings obtained from the new spray gun was comparable to which obtained from an ordinary spray gun. Since the fine powder coatings were much less influenced by the secondary charging, the differential of the transfer efficiency between the two powders was understood.

In the end, this study developed new processing techniques for several featured powder coatings. The featured powder coatings were usually more costly than the regular powder coatings. It was not only because of distinct features they provided but also the more challenging manufacturing processes. The new techniques were developed to overcome the drawbacks and problems associated with the conventional techniques.

One of the most popular featured powder coatings was the low-cure powder coatings. Low-cure powder coatings are favourable to be applied on temperature sensitive coating parts since they had low curing temperature. They are also favourable for applications on large size parts due to their shorter curing time. Nevertheless, the pre-curing problem often occurs during the mixing of the raw materials in a hot extruder. It was due to the lower curing point of the low-cure powder coatings. The new technique proposed by this study was to resolve this problem by utilizing DBC (dry blended catalyst) into powder coatings. Since the ingredient of the curing promoter was added after extrusion, the pre-curing problem could be eliminated.

Experiment indicated that the sample made by the new technique had comparable low-cure performances to which made by the conventional technique. Furthermore, the sample made from the new technique could provide coatings with much better finishes. It was because that the dispersed DBC was not in effect until the curing process occurred. As another advantage from that, the shelf life of the low-cure powder coatings could be extended. The formulation of DBC was optimized in the study.

Another development was made to the processing technique for the metallic color powder coatings. The metallic powder coatings provide decorative features to the coating due to the blended metallic pigment. The conventional processing technique was to heat-blend the metallic pigment with powder coatings. The heat generated from the blender softens the surfaces of powder particles; at the same time, the metallic pigment is attached to the particle surface under high speed impacts. This process is difficult to operate since heat generated from the blender could also melt and cure the powder coatings. Therefore, intensive effort for temperature control is always required. More importantly, the conventional blending technique is not able to create strong bonding between the powder particles and the metallic

pigment. It causes separations of the two materials during spraying. Consequently, the contents of the metallic pigment in the recycled powder coatings always vary so that the recycled powder coatings are usually not reusable.

The new technique proposed by the study utilized liquid resin as a bonding agent to create better adherences between the powder particles and the metallic pigment. Based on the results from the spraying tests, the sample made from the new technique was able to retain its content of the metallic pigment during spraying. It implies that the new technique could provide outstanding bonding between the powder particles and the metallic pigment. Therefore, the recyclability problem could be solved. The improved bonding performance of the materials was also confirmed by the observations from SEM. Further analysis of the results disclosed that the increased amount of the added bonding agent and the increased concentration of the bonding agent were both desirable for obtaining better bonding between the powder particles and the metallic pigment. Yet, over bonding could occur when the concentration of the bonding agent was high causing stacking of the metallic pigments. The stacking of the metallic pigment could deteriorate the metallic effect in the final coating. Future work would have to be conducted to resolve the stacking problem of the metallic pigment. In addition, optimization of the new technique for “master batch” operation would also be included in the future work.

Overall, this thesis study revealed most of the challenges currently encountered during productions and applications of powder coatings. On the other hand, it proposed various new methods to overcome these challenges. Furthermore, series of experiments confirmed and explained the improvements provided by the new methods. It was believed that this work would be of great help for the development of new powder coating technologies.

CHAPTER 11: GENERAL CONCLUSIONS

This thesis study investigate powder coating flowability and developed several new methods for improving the manufacturing and application processes of powder coatings. General conclusions of the research works were stated in the following.

- Investigation on the fine powder coatings disclosed that the medium size and the D_{10} were not suitable for the flowability characterization of fine powder coatings. Instead, the span of the particle size distribution, or a similar parameter that combined the significances from both the medium particle size and the D_{10} should be considered for the flowability characterization. The investigation also concluded that the medium particle size was not a dominant factor for the flowability of a fine powder coating in range of 23 to 29 μm.

- New designs of the classifying cyclone and the grinder for narrowing the particle size distributions of the produced fine powder coatings were developed. Experiments found that a reverse flow in the classifying cyclone could reduce the particle size distributions of the collected fine powder coatings. Furthermore, the proposed classifying cyclone design was able to provide comparable collection efficiency to an ordinary cyclone. On the other hand, the new design of the grinder, which had the grinding elements with concave impact surfaces, could also produce fine powder coatings with narrower particle size distributions. The grinding efficiency of the new grinder was slightly lower than an ordinary grinder.

- The study on powder coating application method concluded that the moisture gained by the powder coating particles reduced the resistivity of the powder. As a result, the reduced resistivity could cause less severe back ionization of the sprayed powder so as

to improve the transfer efficiency of the powder coating. The influence of the gained moisture was found to be more significant to the fine powder coatings rather than the regular size powder coatings. The study also concluded that the powder flowabilities of the powder coatings would not affected by the gained moisture if the proper procedures were followed. In addition, the coating qualities of the powder coatings were not deteriorated by the gained moisture in the powder coatings.

- The study also concluded that the developed alternatively charging spray gun with multiple electrodes was able to reduce the Faraday Cage effect during corona spraying of powder coatings. Furthermore, the new spray gun showed a large potential of improving the transfer efficiency of the regular size powder coatings. The transfer efficiency of the fine powder coatings with the new spray gun was similar to which with an ordinary spray gun. Moreover, the location of the electrodes of the new spray gun could influence its Faraday Cage resistance while spraying fine powder coatings.

- Furthermore, the study developed new processing techniques for several feature powder coatings. Concluded from the experimental results, the DBC technique could eliminate the pre-curing problem encountered during the processing of the low-cure powder coatings in a conventional technique. More importantly, the DBC technique could also provide much extended shelf life for the low-cure powder coatings. In the end, the DBC technique could produce low-cure powder coatings with excellent low-curing performances and outstanding coating qualities.

- In addition, the liquid bonder technique for the metallic color powder coatings could eliminate the expansive and complicated heat-blending process utilized in the conventional method. The new technique was also found to improve the bonding

between the metallic pigment and the powder coating particles so that the content of the metallic pigment in the recycled powder coatings was retained. The bonding performance provided by the new technique could be enhanced by neither utilizing a reduced content of the liquid bonder solvent or an increased amount of the added liquid bonder during in the new technique. Yet, over bonding could occur as the bonding performance improved. It could cause stacking of the metallic pigment which could reduce the metallic effect in the final coatings.

It is believed that the discoveries from this study provide valuable suggestions to the development of new powder coating technologies. However, some of remaining issues from the study have to be investigated before the implementations in applications. Recommendations in below are recommended for the further research:

- The powder flowability of the fine powders was shown to have linear relationship with the span of the particle size distribution in this study. However, the influences from the flow additives have to be further investigated.

- The new design of the cyclone was tested in small scale in this study. A full scale testing will have to be conducted with extended operating durations. Problems such as powder accumulations and impact fusion can occur in a large scale testing. The design of the new cyclone may have to be further revised.

- The new design of the grinding blades has to be transplanted to the ACM (air classifying mill) which is a common miller for powder coating production. Since the ACM grinding involved air classification, the new design will need to be examined in a much more complicated air field.

- A more reliable mechanism will have to be developed for the alternative charging gun. The current alternation mechanism relies on a mechanical charge distributor which is not suitable for continuous operations required by industrial applications. Furthermore, most of the automatic spraying system utilized several spray guns in a ray for large coverage and even distribution of the powder coatings. Therefore, testing of the new gun design on a multi-gun setup is also needed for examining the interference of the electrostatic fields generated from the adjacent guns.

- Master batch technique will have to be optimized for processing of the metallic color powder coatings. The stacking problem of the metallic pigment will have to be resolved.

APPENDICS

Appendix I Modeling Setup and Boundary Conditions for the Cyclone Simulation

DEFINE				SETTING
Model		Solver		3D; Steady; Formulation-Implicit.
		Energy Eqn.		Un-selected.
		Viscous Model		K-epsilon model with "Swirl Dominated Flow' selected; Standard wall.
		DPM	Tracking	Max. number of parameters: 10000; Step length scale: 0.001m; Drag law-spherical; Interaction with continuous phase-selected.
			Physical Models	Erosion/Accretion-selected
Injections			Point Properties	Injection type-surface injection from Inlet; inlet velocity: 30m/s; Particle diameter: 25μm; Total flow rate: 0.001kg/s; Material: anthracite.
			Turbulent Dispersion	Discrete random wall model: selected; Number of tries: 5; Time scale constant: 0.15.
Material				Fluid-air; Solid-aluminum; Interparticle: -anthractie.
Operating condition				Operation pressure: 101325 Pa; Gravity: -9.81m/s^2.
Boundary Condition	Cyclone walls		Momentum	Stationary wall; Roughness constant: 0.5
			DPM boundary cond. type	Reflect
	Collecting box wall		Momentum	Stationary wall, Roughness constant: 0.5.
			DPM boundary cond. type	Trap
	Cyclone inlet		Momentum	Pressure = 0 pa
			DPM boundary cond. type	Pressure inlet
	Vortex finder		Momentum	Pressure = -1000 pa
			DPM boundary cond. type	Pressure outlet-
	Solids outlet		Momentum	N/A
			DPM boundary cond. type	Interio
	Secondary air inlet		Momentum	Pressure = 0pa
			DPM boundary cond. type	Pressure inlet
			UDS	Specified value: 0
Convergence criteria				10e-6

Appendix II Experimental data

Table A-1: Measured particle sizes and flowabilities of fine powder coating samples (Group 1 samples)

Sample	D_{10} (μm)	D_{50} (μm)	D_{90} (μm)	Span	AVA (deg.)	RBER
1	6.53	18.32	35.73	1.593	59.0	1.065
2	6.82	18.96	36.92	1.588	57.6	1.067
3	6.50	18.55	36.33	1.624	62.8	1.102
4	6.84	19.11	37.33	1.595	59.1	1.056
5	6.82	18.96	36.93	1.588	59.8	1.060
6	7.04	19.34	37.32	1.566	58.9	1.049
7	7.32	19.66	37.48	1.534	59.0	1.053
8	6.95	19.6	38.55	1.612	61.4	1.119
9	6.91	19.48	38.29	1.611	59.7	1.059
10	7.51	19.96	37.73	1.514	58.2	1.068
11	7.72	20.86	39.76	1.536	61.2	1.536
12	7.49	20.47	39.36	1.557	63.2	1.100
13	8.07	21.44	40.46	1.511	55.6	1.067
14	8.04	21.33	40.15	1.505	59.5	1.097
15	7.53	20.74	40.02	1.567	59.2	1.070
16	8.13	21.78	41.41	1.528	63.4	1.043

Table A-2: Measured particle sizes and flowabilities of fine powder coating samples (Group 2 samples)

Sample	D_{10} (μm)	D_{50} (μm)	D_{90} (μm)	Span	AVA (deg.)	RBER
17	9.37	23.49	42.84	1.425	56.6	1.080
18	8.77	23.70	45.15	1.535	57.7	1.077
19	8.51	23.57	45.78	1.581	61.3	1.111
20	9.78	24.33	44.08	1.410	55.1	1.085
21	8.24	23.50	46.73	1.638	59.6	1.068
22	8.90	25.03	49.13	1.607	59.4	1.052
23	9.46	25.92	49.79	1.556	59.9	1.118
24	10.60	26.25	48.08	1.428	56.9	1.073
25	9.93	26.59	50.56	1.528	58.2	1.091
26	9.1	25.49	49.62	1.590	59.8	1.106
27	11.32	27.62	49.32	1.376	52.5	1.086
28	11.89	29.15	52.54	1.395	53.3	1.084
29	9.10	24.48	46.70	1.536	57.7	1.075
30	6.15	23.35	46.47	1.727	61.8	1.088
31	9.28	26.5	62.68	1.638	58.9	1.079

Table A-3: The performances of various cyclones with straight-vanes classifier installed

Cyclone	D_{10} (μm)	D_{50} (μm)	D_{90} (μm)	Span	Fed powder weight	Collected powder weight	Collection efficiency
Control	12.72	31.08	55.44	1.375	95.51	89.16	0.93
	8.75	23.41	44.35	1.521	92.42	75.51	0.82
	9.99	26.30	49.34	1.496	94.57	82.53	0.87
	10.96	28.57	53.42	1.486	95.32	84.12	0.88
SA1	12.93	30.16	52.57	1.314	95.41	83.86	0.88
	9.92	24.24	43.50	1.385	91.10	57.37	0.63
	11.36	27.65	49.28	1.371	94.08	77.87	0.83
	12.45	29.96	53.21	1.360	95.07	80.09	0.85
SA2	15.50	33.63	55.73	1.196	95.28	69.06	0.72
	14.65	31.71	52.71	1.200	94.60	60.96	0.64
	13.02	28.85	48.65	1.235	92.58	50.41	0.54
	11.93	26.05	43.50	1.212	91.10	41.75	0.46
SAG1	9.22	23.64	43.73	1.460	90.78	80.94	0.89
	9.75	25.75	48.56	1.507	93.89	84.15	0.90
	10.78	27.85	51.77	1.472	94.99	86.72	0.91
	11.75	30.28	56.05	1.463	95.52	92.8	0.97
SAG2	9.32	22.85	41.01	1.387	90.86	72.19	0.79
	10.37	25.39	45.48	1.383	93.39	78.98	0.85
	11.43	28.00	51.65	1.436	94.91	81.78	0.86
	12.42	30.49	54.73	1.388	95.41	86.06	0.90
SAG3	9.23	22.03	38.97	1.350	88.50	66.58	0.75
	10.67	25.21	44.14	1.328	90.67	73.50	0.81
	13.00	30.28	52.70	1.311	94.97	79.13	0.83
	13.87	32.28	56.11	1.309	95.50	81.34	0.85

Table A-4: The performances of various cyclones with angled-vanes classifier installed

Cyclone	D_{10} (μm)	D_{50} (μm)	D_{90} (μm)	Span	Fed powder weight	Collected powder weight	Collection efficiency
Control	8.92	23.20	43.29	1.481	93.50	88.84	0.95
	6.35	19.48	40.41	1.748	89.84	74.11	0.82
	6.93	19.95	39.69	1.642	93.38	79.13	0.85
	7.70	21.09	40.57	1.559	93.89	85.10	0.91
SA1	9.62	22.64	39.56	1.322	91.16	63.75	0.70
	9.30	22.14	39.09	1.346	93.51	74.03	0.79
	9.80	23.30	41.03	1.340	93.94	75.29	0.80
	10.26	24.04	42.02	1.321	93.58	77.81	0.83
SA2	12.28	27.42	46.48	1.247	87.30	26.14	0.30
	11.86	26.84	45.71	1.261	90.74	35.48	0.39
	11.87	26.79	45.52	1.256	93.72	40.99	0.44
	12.28	27.26	46.01	1.237	93.90	45.72	0.49
SAG1	8.70	22.15	40.64	1.442	93.83	83.43	0.89
	7.92	20.87	39.28	1.503	90.20	74.87	0.83
	8.18	21.36	39.84	1.482	92.46	80.71	0.87
	8.52	22.18	41.43	1.484	93.63	87.85	0.94
SAG2	7.50	19.98	37.82	1.518	86.35	74.20	0.86
	8.25	20.81	38.41	1.449	91.90	73.60	0.80
	8.34	21.03	38.52	1.435	93.70	78.91	0.84
	9.03	22.16	39.75	1.386	93.73	86.65	0.92
SAG3	9.24	21.99	38.84	1.346	90.89	67.99	0.75
	9.43	22.13	38.70	1.323	93.21	69.37	0.74
	9.67	22.55	39.17	1.308	93.94	72.03	0.77
	10.15	24.00	42.21	1.336	93.67	80.99	0.86

Table A-5: Measured particle sizes of the powder samples ground from different grinders

Grinder	Grinding time (s)	D_{10} (μm)	D_{50} (μm)	D_{90} (μm)	Span
Control	10	6.53	32.15	9.78	2.621
	20	3.81	21.73	67.36	2.925
	30	2.85	15.59	47.27	2.849
	40	2.55	13.73	41.06	2.805
	50	2.05	11.62	35.90	2.913
	60	2.01	11.10	33.84	2.868
Modified	10	6.54	29.36	77.95	2.432
	20	4.58	22.82	65.09	2.652
	30	3.71	18.08	50.55	2.591
	40	3.19	16.30	47.38	2.711
	50	2.65	13.63	39.65	2.715
	60	2.84	14.12	40.00	2.632

Table A-6: The measured moisture contents on the powder coating particles during fluidization with humidified air

Fluidization time (min.)	Moisture content of the powder coating (%)		
	Powder A	Powder C_1	Powder C_2
0	0.229	0.213	0.251
2	0.266	0.354	0.296
3	0.254	0.382	0.310
6	0.287	0.414	0.343
20	0.382	0.563	0.508
60	0.398	0.671	0.683
80	N/A	0.720	0.738
100	N/A	0.781	0.741

Table A-7: The measured resistivity of the powder samples with respect to the fluidization time (humidification in a fluidized bed)

Sample	Fluidization time (min.)	Resistance (10^{-13}ohm)	Powder depth (mm)	Resistivity (10^{16}ohm/mm)
Powder A	0	2.88	0.413	28.20
	1	0.58	0.358	7.93
	2	0.52	0.410	6.20
	5	0.38	0.318	5.85
	20	0.42	0.303	45.05
Powder C_1	0	2.88	0.313	15.36
	1	0.55	0.175	8.18
	2	0.41	0.245	6.92
	5	0.51	0.360	5.11
	20	0.52	0.498	9.88
Powder C_2	0	0.97	0.128	29.78
	1	0.79	0.148	26.18
	2	0.83	0.188	21.64
	5	0.75	0.153	24.04
	20	0.77	0.203	18.59

Table A-8: The FPTE of powder A with 30%RH of the fluidization air

Fluidization time (min.)	Loaded powder (g)	Coated powder (g)	FPTE	Average FPTE	Deviation (%)
0	-	-	-	0.420	-
0.5	7.82	3.39	0.434	0.434	0
	7.70	3.42	0.444		2.3
	7.76	3.28	0.423		2.5
3.25	7.87	3.43	0.436	0.444	1.8
	7.80	3.48	0.446		0.5
	7.76	3.54	0.451		1.6
6.27	7.86	3.42	0.435	0.444	2.0
	7.78	3.46	0.445		0.2
	7.93	3.58	0.451		1.6
9.5	7.68	3.41	0.444	0.445	0.2
	7.83	3.47	0.443		0.4
	7.91	3.55	0.449		0.9

Table A-9: The FPTE of powder A with 50%RH of the fluidization air

Fluidization time (min.)	Loaded powder (g)	Coated powder (g)	FPTE	Average FPTE	Deviation (%)
0	-	-	-	0.420	-
0.5	7.88	3.40	0.431	0.436	1.1
	7.70	3.30	0.428		1.8
	7.78	3.49	0.449		3.0
3.25	7.58	3.57	0.471	0.453	7.9
	7.85	3.51	0.447		1.3
	7.72	3.54	0.458		1.1
5.5	7.84	3.51	0.448	0.451	0.7
	7.73	3.47	0.449		0.4
	7.65	3.50	0.457		1.3
8.75	7.73	3.60	0.466	0.453	2.9
	7.95	3.57	0.449		0.9
	7.89	3.61	0.457		0.9

Table A-10: The FPTE of powder A with 70%RH of the fluidization air

Fluidization time (min.)	Loaded powder (g)	Coated powder (g)	FPTE	Average FPTE	Deviation (%)
0	-	-	-	0.420	-
0.5	7.84	3.47	0.443	0.442	2.0
	7.89	3.63	0.460		4.0
	7.93	3.36	0.424		4.0
3.25	7.93	3.56	0.449	0.459	2.2
	7.81	3.65	0.467		1.7
	7.88	3.63	0.460		0.2
6	7.91	3.66	0.462	0.459	0.7
	7.93	3.57	0.450		2.0
	7.73	3.52	0.455		0.9
8.67	7.86	3.63	0.462	0.459	0.7
	7.80	3.51	0.450		2.0
	7.73	3.53	0.456		0.7

Table A-11: The FPTE of powder A with 90%RH of the fluidization air

Fluidization time (min.)	Loaded powder (g)	Coated powder (g)	FPTE	Average FPTE	Deviation (%)
0	-	-	-	0.378	-
0.5	7.44	2.99	0.402	0.396	1.5
	7.51	3.02	0.402		1.5
	7.59	2.91	0.383		3.3
2	7.60	3.14	0.413	0.418	1.2
	7.61	3.23	0.424		1.4
	7.56	3.14	0.415		0.7
5	7.48	3.27	0.437	0.421	3.8
	7.47	3.15	0.422		0.2
	7.68	3.10	0.404		4.0
10	7.58	3.20	0.422	0.417	1.2
	7.52	3.19	0.424		1.7
	7.56	3.07	0.406		2.6

Table A-12: The measured performances of an ordinary powder spray gun (with fine powder coating)

Spraying duration (s)	Gun voltage (-kV)	Powder on Panel A (g)	Powder on Panel B (g)	Powder on Panel C (g)	Faraday Cage resistance	Sprayed powder (g)	Coated powder (g)	FPTE
4	30	0.12	0.10	0.05	0.45	2.07	0.64	0.311
	60	0.19	0.09	0.18	0.49		1.17	0.566
	90	0.20	0.09	0.22	0.43		1.25	0.604
8	30	0.20	0.07	0.20	0.35	4.14	1.41	0.341
	60	0.32	0.10	0.26	0.34		2.21	0.534
	90	0.29	0.10	0.28	0.35		2.05	0.496
12	30	0.29	0.08	0.25	0.30	6.20	2.03	0.328
	60	0.46	0.17	0.40	0.40		3.11	0.502
	90	0.44	0.19	0.34	0.49		3.31	0.533

Table A-13: The measured performances of a modified powder spray gun (with fine powder coating and spraying duration of 4s)

Gun voltage (-kV)	Distributor voltage (V)	Powder on Panel A (g)	Powder on Panel B (g)	Powder on Panel C (g)	Faraday Cage resistance	Sprayed powder (g)	Coated powder (g)	FPTE
30	4	0.12	0.06	0.12	0.500	2.07	0.70	0.337
	8	0.12	0.06	0.13	0.480		0.71	0.345
	12	0.13	0.06	0.12	0.480		0.72	0.347
60	4	0.13	0.08	0.19	0.500		1.19	0.575
	8	0.14	0.08	0.20	0.471		1.12	0.540
	12	0.20	0.10	0.21	0.488		1.11	0.538
90	4	0.19	0.11	0.22	0.537		1.24	0.599
	8	0.19	0.08	0.22	0.390		1.17	0.568
	12	0.20	0.09	0.22	0.429		1.12	0.542

Table A-14: The measured performances of a modified powder spray gun (with fine powder coating and spraying duration of 8s)

Gun voltage (-kV)	Distributor voltage (V)	Powder on Panel A (g)	Powder on Panel B (g)	Powder on Panel C (g)	Faraday Cage resistance	Sprayed powder (g)	Coated powder (g)	FPTE
30	4	0.19	0.08	0.20	0.410	4.14	1.26	0.304
	8	0.22	0.07	0.21	0.326		1.43	0.346
	12	0.23	0.08	0.21	0.364		1.38	0.333
60	4	0.27	0.14	0.36	0.444		2.08	0.504
	8	0.24	0.12	0.33	0.421		2.05	0.495
	12	0.29	0.14	0.33	0.452		2.12	0.512
90	4	0.24	0.15	0.41	0.462		2.38	0.577
	8	0.38	0.15	0.37	0.400		2.36	0.570
	12	0.45	0.18	0.31	0.474		2.49	0.601

Table A-15: The measured performances of a modified powder spray gun (with fine powder coating and spraying duration of 12s)

Gun voltage (-kV)	Distributor voltage (V)	Powder on Panel A (g)	Powder on Panel B (g)	Powder on Panel C (g)	Faraday Cage resistance	Sprayed powder (g)	Coated powder (g)	FPTE
30	4	0.28	0.10	0.30	0.345	6.20	2.07	0.334
	8	0.33	0.11	0.30	0.349		2.08	0.335
	12	0.29	0.10	0.28	0.351		2.08	0.335
60	4	0.36	0.19	0.46	0.463		2.97	0.479
	8	0.46	0.20	0.47	0.430		3.03	0.489
	12	0.31	0.14	0.45	0.368		3.09	0.498
90	4	0.47	0.22	0.39	0.512		3.12	0.503
	8	0.48	0.22	0.41	0.494		3.06	0.494
	12	0.43	0.21	0.45	0.477		2.97	0.479

Table A-16: The measured performances of an ordinary powder spray gun (with coarse powder coating)

Spraying duration (s)	Gun voltage (-kV)	Powder on Panel A (g)	Powder on Panel B (g)	Powder on Panel C (g)	Faraday Cage resistance	Sprayed powder (g)	Coated powder (g)	FPTE
4	30	0.12	0.05	0.09	0.476	2.07	0.78	0.378
	60	0.16	0.06	0.11	0.444		0.92	0.443
	90	0.10	0.05	0.23	0.303		1.22	0.592
8	30	0.21	0.06	0.15	0.333	4.14	1.48	0.359
	60	0.27	0.08	0.17	0.364		1.53	0.369
	90	0.17	0.07	0.34	0.275		2.07	0.500
12	30	0.31	0.08	0.20	0.314	6.20	2.10	0.338
	60	0.24	0.09	0.40	0.281		2.50	0.403
	90	0.25	0.11	0.50	0.293		3.05	0.492

Table A-17: The measured performances of a modified powder spray gun (with coarse powder coating and spraying duration of 4s)

Gun voltage (-kV)	Distributor voltage (V)	Powder on Panel A (g)	Powder on Panel B (g)	Powder on Panel C (g)	Faraday Cage resistance	Sprayed powder (g)	Coated powder (g)	FPTE
30	4	0.12	0.04	0.10	0.364	2.07	0.59	0.285
	8	0.15	0.05	0.11	0.385		0.67	0.322
	12	0.13	0.06	0.12	0.480		0.65	0.345
60	4	0.24	0.07	0.15	0.359		1.21	0.585
	8	0.29	0.07	0.15	0.333		1.15	0.556
	12	0.22	0.06	0.15	0.324		1.17	0.565
90	4	0.28	0.09	0.22	0.360		1.29	0.623
	8	0.22	0.07	0.15	0.378		1.23	0.596
	12	0.22	0.08	0.17	0.410		1.21	0.585

Table A-18: The measured performances of a modified powder spray gun (with coarse powder coating and spraying duration of 8s)

Gun voltage (-kV)	Distributor voltage (V)	Powder on Panel A (g)	Powder on Panel B (g)	Powder on Panel C (g)	Faraday Cage resistance	Sprayed powder (g)	Coated powder (g)	FPTE
30	4	0.17	0.06	0.14	0.387	4.14	1.25	0.301
	8	0.17	0.05	0.12	0.345		1.30	0.313
	12	0.16	0.06	0.12	0.429		1.26	0.304
60	4	0.42	0.11	0.28	0.314		2.23	0.540
	8	0.42	0.10	0.26	0.294		2.27	0.548
	12	0.36	0.09	0.24	0.300		2.11	0.509
90	4	0.37	0.11	0.27	0.344		2.43	0.588
	8	0.38	0.12	0.26	0.375		2.61	0.631
	12	0.31	0.09	0.26	0.316		2.16	0.522

Table A-19: The measured performances of a modified powder spray gun (with coarse powder coating and spraying duration of 12s)

Gun voltage (-kV)	Distributor voltage (V)	Powder on Panel A (g)	Powder on Panel B (g)	Powder on Panel C (g)	Faraday Cage resistance	Sprayed powder (g)	Coated powder (g)	FPTE
30	4	0.24	0.07	0.18	0.333	6.20	1.85	0.297
	8	0.26	0.07	0.21	0.298		1.99	0.321
	12	0.27	0.08	0.20	0.340		1.77	0.285
60	4	0.55	0.16	0.36	0.352		3.33	0.536
	8	0.59	0.15	0.34	0.323		3.18	0.512
	12	0.48	0.11	0.31	0.278		3.17	0.510
90	4	0.49	0.16	0.33	0.390		3.37	0.542
	8	0.45	0.14	0.35	0.350		3.36	0.541
	12	0.39	0.13	0.32	0.366		3.12	0.504

Table A-20: The measured performances of a modified powder spray gun with different electrode locations at gun voltage of -30kV (with fine powder coating; spraying duration of 8s; distributor voltage of 4V)

Distances from gun center to electrode (cm)	Powder on Panel A (g)	Powder on Panel B (g)	Powder on Panel C (g)	Faraday Cage resistance	Sprayed powder (g)	Coated powder (g)	FPTE
1.25	0.23	0.07	0.19	0.333	4.14	1.28	0.310
1.5	0.22	0.07	0.21	0.326		1.32	0.318
1.75	0.18	0.06	0.17	0.343		1.26	0.304
2.25	0.19	0.07	0.20	0.359		1.34	0.323
2.75	0.20	0.06	0.17	0.324		1.15	0.279

Table A-21: The measured performances of a modified powder spray gun with different electrode locations at gun voltage of -60kV (with fine powder coating; spraying duration of 8s; distributor voltage of 4V)

Distances from gun center to electrode (cm)	Powder on Panel A (g)	Powder on Panel B (g)	Powder on Panel C (g)	Faraday Cage resistance	Sprayed powder (g)	Coated powder (g)	FPTE
1.25	0.34	0.14	0.34	0.412	4.14	1.93	0.466
1.5	0.31	0.13	0.31	0.430		2.00	0.482
1.75	0.45	0.16	0.27	0.444		2.09	0.504
2.25	0.29	0.14	0.33	0.452		1.85	0.448
2.75	0.24	0.10	0.29	0.377		1.81	0.438

Table A-22: The measured performances of a modified powder spray gun with different electrode locations at gun voltage of -90kV (with fine powder coating; spraying duration of 8s; distributor voltage of 4V)

Distances from gun center to electrode (cm)	Powder on Panel A (g)	Powder on Panel B (g)	Powder on Panel C (g)	Faraday Cage resistance	Sprayed powder (g)	Coated powder (g)	FPTE
1.25	0.36	0.15	0.37	0.411	4.14	2.30	0.557
1.5	0.33	0.16	0.40	0.438		2.22	0.536
1.75	0.27	0.15	0.38	0.462		2.39	0.577
2.25	0.32	0.16	0.35	0.478		2.29	0.554
2.75	0.31	0.1	0.34	0.308		0.209	0.505

Table A-23: The measured performances of a modified powder spray gun with different electrode locations at gun voltage of -30kV (with coarse powder coating; spraying duration of 8s; distributor voltage of 4V)

Distances from gun center to electrode (cm)	Powder on Panel A (g)	Powder on Panel B (g)	Powder on Panel C (g)	Faraday Cage resistance	Sprayed powder (g)	Coated powder (g)	FPTE
1.25	0.20	0.07	0.16	0.389	4.14	1.16	0.280
1.5	0.29	0.13	0.21	0.520		1.42	0.343
1.75	0.25	0.10	0.16	0.488		1.25	0.301
2.25	0.26	0.11	0.18	0.500		1.33	0.322
2.75	0.25	0.11	0.15	0.550		1.39	0.335

Table A-24: The measured performances of a modified powder spray gun with different electrode locations at gun voltage of -60kV (with coarse powder coating; spraying duration of 8s; distributor voltage of 4V)

Distances from gun center to electrode (cm)	Powder on Panel A (g)	Powder on Panel B (g)	Powder on Panel C (g)	Faraday Cage resistance	Sprayed powder (g)	Coated powder (g)	FPTE
1.25	0.4	0.12	0.26	0.364	4.14	2.19	0.526
1.5	0.41	0.12	0.27	0.353		2.35	0.568
1.75	0.38	0.11	0.29	0.328		2.23	0.539
2.25	0.41	0.12	0.28	0.348		2.17	0.526
2.75	0.39	0.13	0.31	0.371		2.47	0.597

Table A-25: The measured performances of a modified powder spray gun with different electrode locations at gun voltage of -90kV (with coarse powder coating; spraying duration of 8s; distributor voltage of 4V)

Distances from gun center to electrode (cm)	Powder on Panel A (g)	Powder on Panel B (g)	Powder on Panel C (g)	Faraday Cage resistance	Sprayed powder (g)	Coated powder (g)	FPTE
1.25	0.35	0.11	0.27	0.355	4.14	2.11	0.509
1.5	0.36	0.12	0.28	0.375		0.18	0.527
1.75	0.36	0.12	0.28	0.375		2.43	0.587
2.25	0.37	0.12	0.31	0.353		2.47	0.598
2.75	0.39	0.13	0.31	0.371		2.64	0.628

Table A-26: Ash test results for metallic color powder coating samples

Add PA resin (g)	Added H_2O (g)	Virgin powder sample (%Al)	Coated powder sample (%Al)	Change in %Al (%)
0	0	2.14	6.35	196.73
0.01	0.1	2.19	7.60	247
	0.2	2.10	7.20	242.86
	0.3	1.99	6.96	249.75
	0.5	2.06	8.09	292.72
0.03	0.1	2.19	2.96	35.16
	0.2	2.18	3.23	48.17
	0.3	1.98	3.84	93.94
	0.5	2.19	6.14	180.37
0.06	0.1	2.23	2.25	0.90
	0.2	2.04	2.10	2.94
	0.3	2.22	2.60	17.12
	0.5	2.14	3.38	57.94

Appendix III Related Publications

III-1 Fu J., Zhang H., Zhu J., 2011, The Effect of Different Factors on Material Utilization Efficiency of Powder Coatings, *61th CSChE conference*.

III-2 Fu J., Zhang H., Zhu J., 2013, Improvement on the first pass transfer efficiency of fine polymer coating powders for corona spraying process, *Advanced Powder Technology*.

III-1

The Effects of Different Factors on Material Utilization Efficiency of Powder Coating

Jing Fu, Hui Zhang, Jesse Zhu

Department of Chemical and Biochemical Engineering, The University of Western Ontario

London, Ontario

Abstract

Powder coating, which can avoid toxic VOCs (Volatile Organic Compound), is a fast growing and "green" coating technology applied in many industrial fields. One of the key advantages to keep this technology outstanding in the market is its ability to reclaim the over-sprayed materials. However, real applications showed the material utilization efficiency of powder coating was limited, mainly due to the decreased powder flow performance. Therefore, this study was to find out the cause of this issue by investigating the three different factors, which could usually be encountered during the powder coating processes. These three factors are the change in humidity, the change in flow additive concentration and the change in particle sizes. The research discovered that the changes in humidity and flow additive concentration had no significant effect on reducing the flow performance of reclaimed powders under normal powder coating procedures. On the other hand, the particle size of the powder was found decreased after electrostatic spraying. After comparing the flow characteristics with simulated reclaimed powders, it was discovered that this decreased particle size was the most significant factor causing the reduction in flow performance of the reclaimed powder.

III-2

IMPROVEMENT ON THE FIRST PASS TRANSFER EFFICIENCY OF FINE POLYMER COATING POWDERS FOR CORONA SPRAYING PROCESS

Jing Fu, Hui Zhang, Jesse Zhu

Department of Mechanical and Material Engineering, University of Western Ontario

London, Ontario, Canada, N6A 5B9

Abstract

Corona charge spraying has been widely used in the powder coating application since it provides outstanding charging performance which leads to high coating efficiency. Yet, this spraying technology has not been working very well with fine powders that started to be used by powder industry in recent years. Fine powders are known as the powders that have median sizes smaller than 30μm. Utilizing fine powders can improve coating quality and reduce film thickness. However, it has been experienced that the fine powders have much lower first pass transfer efficiency (FPTE). This study provided a solution for the problem by humidifying the powder coating particles. The gained moisture on the particle surfaces can reduce the powder resistivity. As a result, the electric field strength inside the deposited particle layer on the target is reduced, allowing more charged particles to be deposited. Therefore the FPTE of the fine powder is increased. Discovered by the experiments, a maximum of 17% increase in the FPTE was achieved with the humidified fine powder. The improved FPTE of the fine powder was comparable to the regular powder. The study also evaluated the influence of the increased humidity on the fine powder flowability. Based on

the results obtained from the powder characterization tests, the suggested humidification process would not significantly deteriorate the fine powder flowability.

1 Introduction

In corona charge spraying, powder materials are charged by ions generated from a corona discharge during pneumatic spraying. It is one of the most popular spraying methods for dry powder coatings due to its flexibility, reliability and excellent coating efficiency. Comparing to tribo charge spraying, it is much more stable and reliable. During the process, there are three different charging phenomena depending on the size of the material being charged: field charging for particles larger than 0.5 μm [2-3], diffusion charging for particles smaller than 0.2 μm [4-5] and combination of field and diffusion charging for particle in between 0.2 μm and 0.5 μm. Since the materials for corona spraying are generally in the size between 10μm and 100 μm, the field charging dominates. In the field charging process, powder particles collide with the ions in adjacent to the corona discharging electrode. The particles catch the ions during the collision to gain charges.

The corona charge spraying is a typical negative corona point-to-plane discharge process. Based on the previous studies [6-7], there are two regions between the corona electrode (the tip of the corona spraying gun) and the plane electrode (the target workpiece being coated). The first region is the space around the corona electrode known as the ionization region, where ions are generated from the ionization process. The powder particles charged by these ions while flying out from the spray gun are mainly under the aerodynamic force [8]. The second region is called the drift region, which is in between the ionization region and the target that has a weaker electric field. When the powder enters the drift region via the air stream, the motions of the powder particles are affected not only by the aerodynamic force but also the electrostatic force and gravity [8]. As the powder moves closer to the target

(about 10 mm), the electrostatic force starts to dominate the motions of the particles [6]. The deposited particles are finally held on the grounded target by electrostatic forces.

During corona charge spraying, the electrical field strength E_p [V/m] across the deposited powder on the target can be calculated by [9]:

$$E_p = \rho_p J \tag{1}$$

where ρ_p is the resistivity of the powder material and J is the corona current density. For polymer powders, E_p usually reaches or surpasses the breakdown field strength easily under high voltage charging. Consequently, random powder breakdowns or more severely, an onset of a spark can occur. This phenomenon is known as back ionization [9].

The first pass transfer efficiency (FPTE) is an important parameter indicating the spraying efficiency. It is the mass ratio of powder deposited on the target to the total mass of the powder sprayed. For most applications, a high FPTE is desired. A typical example is the fine powder coating (median particle size < 30 μm). In recent years, fine powder coating attracts much attention from the coating industry. Comparing with regular powder coating (median particle size of the powder between 30-60 μm), it can provide benefits such as better coating quality and thinner coating film. However, such benefits are accompanied by the drawback of the reduction in FPTE [10]. A higher corona voltage is always used to compensate this problem. The increased voltage can improve the charging efficiency so to direct more particles onto the target. On the other hand, the deposited powder reaches its breakdown field strength much quicker under higher voltage so that the back ionization can occur much sooner, limiting the improvement of the FPTE. More importantly, the risk of receiving

surface defects such as craters and pin holes will be higher. Therefore, simply increasing the corona voltage cannot effectively improve the FPTE of fine powders.

Studies by Sharma et al. [11] and Messaoudi et al. [12] disclosed that back ionization could be reduced by increasing the humidity level inside a spray booth. The increased humidity could accelerate the charge decay across the deposited powder so to reduce the electrical field strength in the powder layer. It delayed the back ionization and it improved the FPTE. However, the humidity level inside the spray booth is usually kept below 60% RH in commercial applications. Higher humidity levels could cause a decrease in the retention of the electrostatic charges [13]. The reason is the ion cluster formations [12]. Berger stated that clustering was attributed to the salvations of the negative or positive ions by water; in other words, the ions were surrounded by water molecules [14]. Therefore, these ion clusters which were heavier and bigger due to the increased amount of the moisture in the spray booth reduce the charge mobility in the space so to extend the charging time [15]. It was also discovered by Meng that the extra moisture inside the spray booth could reduce the corona current measured on the target implying that the improvement on the FPTE is limited [16]. Moreover, humidifying an industrial spray booth requires much more energy and it is not economical.

This study suggested a novel method to improve the FPTE of fine powders for corona charge spraying process by utilizing humidity. The moisture content on the particle surface was intended to be increased before spraying. The added moisture could reduce the resistivity of the particles. According to Eq. (1), the electric field strength of the accumulated particles on the target could be reduced. Hence, more charged particles could be deposited before reaching the limit of the breakdown field strength. Furthermore, the additional moisture could also improve particle charging. Indicated by Pauthenier limit [2, 4 and 5]:

$$Q_{max} = 4\pi\varepsilon_0 r^2 pE \quad (2)$$

where $p = 3\varepsilon_r / (\varepsilon_r + 2)$, r is the particle radius, ε_0 is the permittivity of free space and E is the electric field of charging. The increased moisture content of the particle increased the dielectric constant ε_r of the particles, leading to a higher value of p. Therefore, the charge capacity of a particle was increased and a higher particle charge was in favour of a higher FPTE of the powder. In addition, humidification method would not affect the humidity level inside the spray booth. Therefore, the formation of charge clusters could be avoided.

2 Materials and Methods

Five powder materials were used for the study named as powder A, B, C_1, C_2 and C_3. These powders were commercial coating powders provided by the manufacturers. Powder A and B were polyester-epoxy (hybrid) powders and powder C_1, C_2 and C_3 were polyurethane powders. Powder A, B, C_1 and C_2 had median particle size around 25 μm listed in Table 1. Powder A and B were very similar materials with only difference in the contents of filler, pigment and additives. Powder C_1 and C_2 were from different batches of the same product. Powder C_3 was the same powder as powder C_1 and C_2 but with a regular median size of 37 μm. It was prepared for the comparisons with the fine powders. The compressed air used for spraying and fluidization had controlled humidity level of 12-14% RH. The spray booth was always air conditioned with ambient temperature of 23-25 ^oC and 35-40% RH.

Table 1: Particle sizes of the test powders

Powder	Particle size distribution		
	D10 (μm)	D50 (μm)	D90 (μm)
A	12.6	24.7	45.5
B	12.3	24.3	44.8
C	11.2	24.0	47.0
D	11.1	25.8	52.4
E	13.1	37.8	75.6

The effect of moisture on electrical properties of the fine powders was the first to investigate. The resistivity of the humidified powder was measured according to ASTM standard D257. Keithley 610C electrometer was used with a 7 cm X 7 cm square testing cell. Polyester-epoxy (hybrid) fine powder A, polyurethane fine powder C_1 and polyurethane regular powder C_3 were used in the experiment. The powders were humidified in a fluidized bed by humidified air with 90% RH. Both of the moisture content and resistivity changes of the humidified samples taken at different humidification time were measured. In order to increase the accuracy of the readings, Mettler Toledo scale (model XS205) with readability of 0.01 mg was used. In addition, the testing cell for the resistivity measurements was shielded within a Faraday Cage to reduce the electrical noises.

The experiments of corona charge spraying were then conducted to evaluate the actual performance of the humidified powders. The FPTE was calculated as the mass of the powder sprayed on the substrate ($m_{substrate}$) divided by the total mass of the powder sprayed (m_{total}):

$$FPTE = \frac{m_{substrate}}{m_{total}} \tag{3}$$

The FPTE obtained from the experiments was compared for discovering improvements. The improvement of the FPTE was obtained by:

$$Improvement = \frac{|(FPTE_{improved} - FPTE_{original})|}{FPTE_{original}} \quad (4)$$

Preliminary experiments

Due to the limitation on materials inventory, preliminary experiments were firstly conducted to testify the proposed idea. A low powder feeding rate and low gun voltage were used to extend the spraying duration to delay the occurring of the back ionization. As a result, powder accumulation on the target became slower and the effects of the variations such as the air turbulence and corona quenching [16] could be reduced. The changes of the FPTE between the sprays could be better observed. Powders A, B and C_1 were used in the experiment. Demonstrated in Figure 1, the humidifier A that in series to the fluidized bed was switch on and the moisture content of the powders was expected to be increased during fluidization. The processed powders taken from the fluidized bed were then fed into the venture pump by a vibrating feeder (FMC Syntron vibrating feeder).

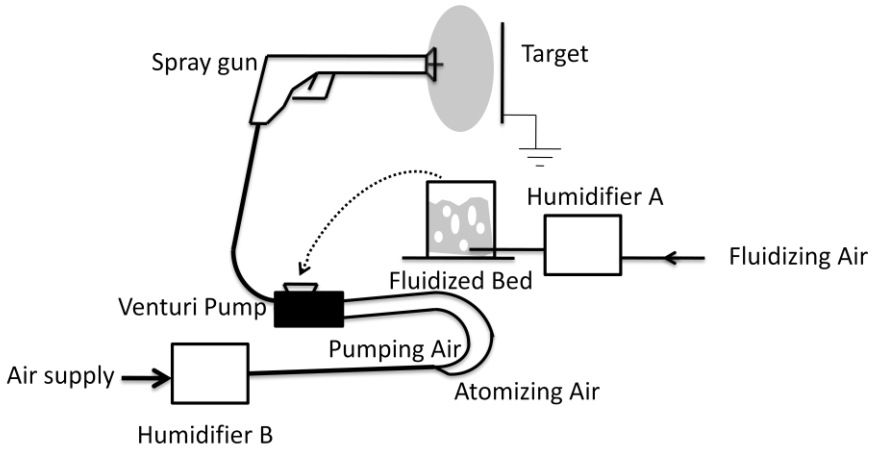

Figure 1: Schematic diagram of the apparatus setup for powder humidification

Full scale experiments

Full scale experiments were then conducted to further investigate the method in a more realistic spraying condition. The spraying settings were adjusted to parameters that commonly used by the powder coating industry. The gun voltage and the feeding rate were higher and the spraying duration was much shorter. On the other hand, the loading mechanism was increased. A belt feeder was used instead of the vibrating feeder because the feeding rate of the vibrating feeder could hardly be maintained for short spraying durations.

Furthermore, the effect of using humidified pneumatic transportation air was also investigated. As shown in Figure 1, the humidifier B that in series to the pneumatic transportation line (atomizing and pumping air supplies) was switched on. At the same time, the humidifier A was turned off, keeping the fluidized air in normal operating condition. Powder particles were expected to start obtaining moisture while encountering the humidified air streams. The feeding task was accomplished by a screw feeder (SHENCK AccuRate).

Observations on powder flowability and coating quality

On the other hand, the powder flowability that represents the ability of free-flowing in normal handling processes such as fluidization, pneumatic transportation and spraying is crucial in industrial application. Poor flowability could cause application issues and coating defects. Thus, the flowability of the humidified fine powder had to be examined. The powder samples were placed in a highly humidified environment (99% RH) to simulate the stagnate condition in a fluidized bed. The humidification was more severe since the air humidity level was much higher. It disclosed how the powders would behave in an extreme case of the humidification.

The flowability was evaluated by two characterization methods: the avalanche angle (AVA) and the rotational bed expansion ratio (RBER). The AVA was measured by a rotational powder analyzer (Revolution Powder Analyzer, Mercury Scientific Inc., Sandy Hook, CT, USA). The test requires 120 ml of powder (tapped volume) in a drum container (diameter of 10.9 cm and width of 3.5 cm) with transparent side walls made of glass. The drum is powered by an electric motor and it runs at the speed of 0.6 rpm. In the measurements, the powder rotates with the drum under friction force. And then, the powder collapses at an angle, which the inter-particle forces cannot sustain the mass of the powder. The angle is the AVA. The powder motion is recorded by the computer controlled camera and the final result is averaged from 200 readings. Previous study found that the AVA was proportional to the angle of repose representing the same aspect of powder flowability [17]. However, the measurement of AVA is more stable and accurate since more readings are taken and the data-acquisition is fully automatic.

The RBER was also measured by the rotational powder analyzer. The same procedure was followed to load the drum. Unlike the AVA, the drum runs much faster in this test. When the drum speeds up, the air enters the powder and the volume of the powder expands. In order to measure how well the powder fluidized, the volumetric expansion ratio (expanded powder volume divided by the initial powder volume) is obtained. The measurement is taken at the drum speed of 70 rpm which is the maximum speed for most of the powder coating material. A higher rotational speed can throw the powder on the wall of the drum due to the centrifugal effect. Comparing with the conventional bed expansion, the RBER is obtained from the sealed container. It reduces the error of the readings and it can also ensure that there is no loss of particles during the whole measurement. The RBER can represent similar aspect of the flowability as the conventional bed expansion [17].

Between the two characterizations, the RBER is a more dynamic powder flowability which indicates how well the powder flows during fluidization or pneumatic transportation. On the other hand, the AVA is a more static powder flowability that indicates how easy the powder will get agglomerated or accumulated. These characterization tests are necessary to fully predict the powder flowability [17-18]. A smaller AVA and a larger RBER implies better flowability of the powder.

3 Results and Discussion

3.1 Effect of humidity on the electrical property of the powders

The fine powder A, C_1 and regular size powder C_3 were used in this part of the study. The powder samples were humidified in the fluidized bed air with 90% RH. Figure 2 indicates the changes in the moisture content of the samples with respect to humidification time. All of the three powders picked up moisture rapidly in the first few minutes. However, they started to slow down at about 20 minutes and became stable in the end. Powder C_1 and E were the same powder with different particle sizes. They showed very similar trend of the moisture gain overall, although it was noticeable that the finer particles gained moisture quicker than the coarser particles. On the other hand, powder A obtained much less moisture than powder C_1 and C_3 showing that the variations in moisture gain between types of materials or other ingredients such as fillers.

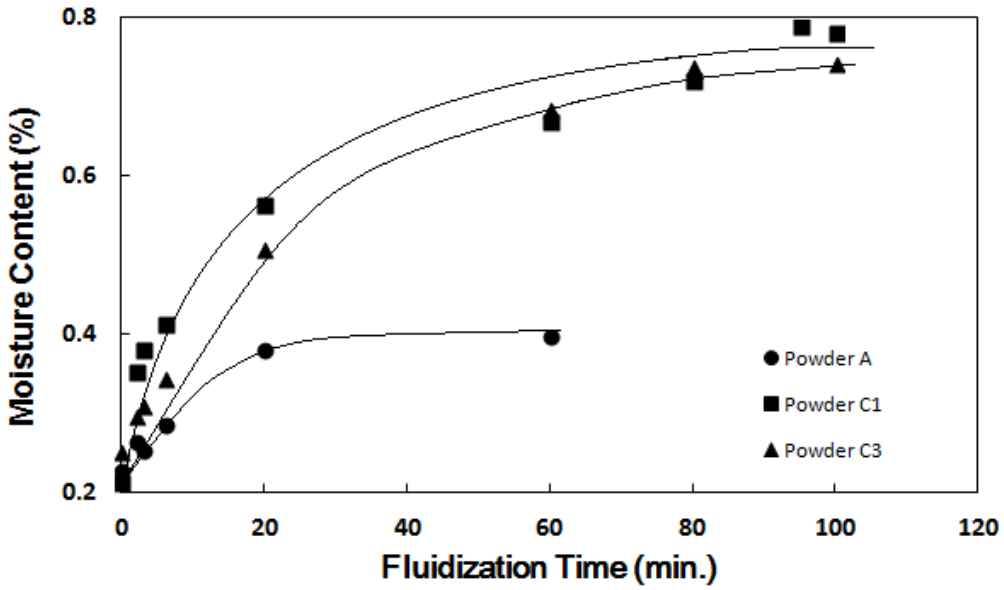

Figure 2: The changes in moisture content of the humidified powders

Figure 3 demonstrates the influence of the humidification on powder resistivity. It was found that the resistivity of the fine powders decreased drastically in the first 3 minutes. However, it stopped decreasing in the rest of the humidification process. Therefore, the moisture gained on the powder particle surface in the first few minutes had the largest effect on the powder resistivity reduction. Comparing with powder C_1, the regular size powder C_3 had smaller initial resistivity and the magnitude of decrease was smaller than that of the fine powders.

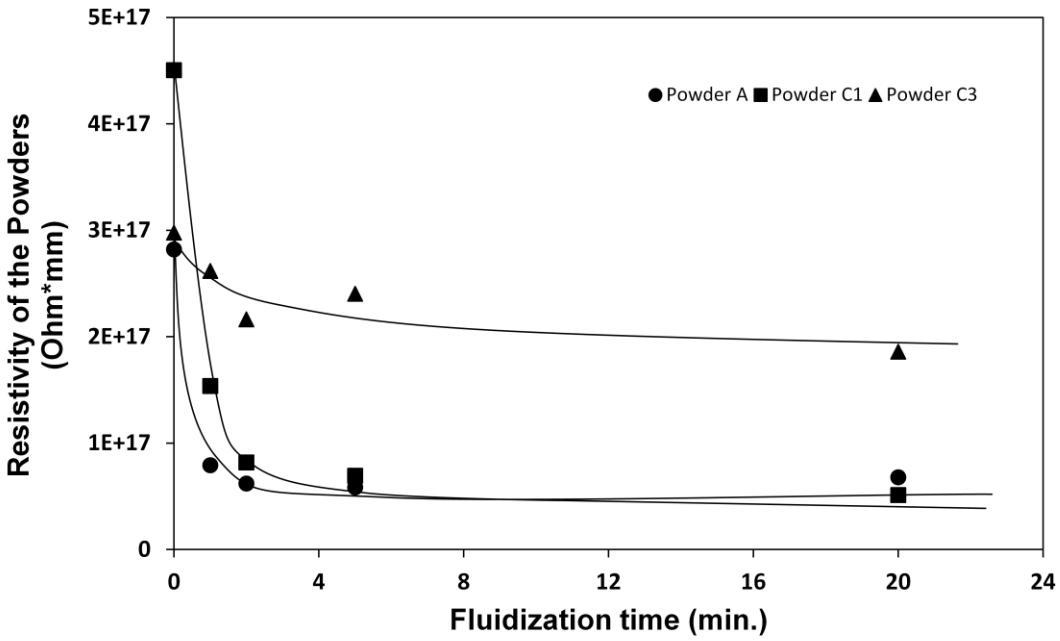

Figure 3: Changes in resistivity of the humidified powders

3.2 Preliminary spraying test

In the preliminary spraying test, powders A, B and C_1 were fluidized by a regulated humidified fluidizing air at the velocity of 0.5 cm/s. The humidity of the fluidizing air was 89%. The voltage of the corona spray gun (ITW Gema) was set at – 35 kV and the spraying duration was 60 seconds. Powders were transported to a vibrating feeder which had a feeding rate of 0.1 g/s. The spraying target was a circular copper plate with 30cm diameter and the spraying distance was 20 cm.

The results shown in Figure 4 demonstrate that the FPTE of the fine powders was improved by the humidification in the first 3 minutes. Referring back to Figure 2 and 3, the gained moisture in the first few minutes largely reduced the resistivity of the particles. According to Eq. (1), lower resistivity could weaken the electrical field strength of the accumulated particles on the target [11]. Therefore, the back ionization could have been delayed or avoided and more charged particles were deposited during spraying. As a result, the FPTE

was improved. The FPTE of the powders became stable afterward and this indicated that the rest of the humidification did not further improve the FPTE. It agreed with the findings in Figure 3 that the resistivity of the powder stayed unchanged after the first few minutes of the humidification.

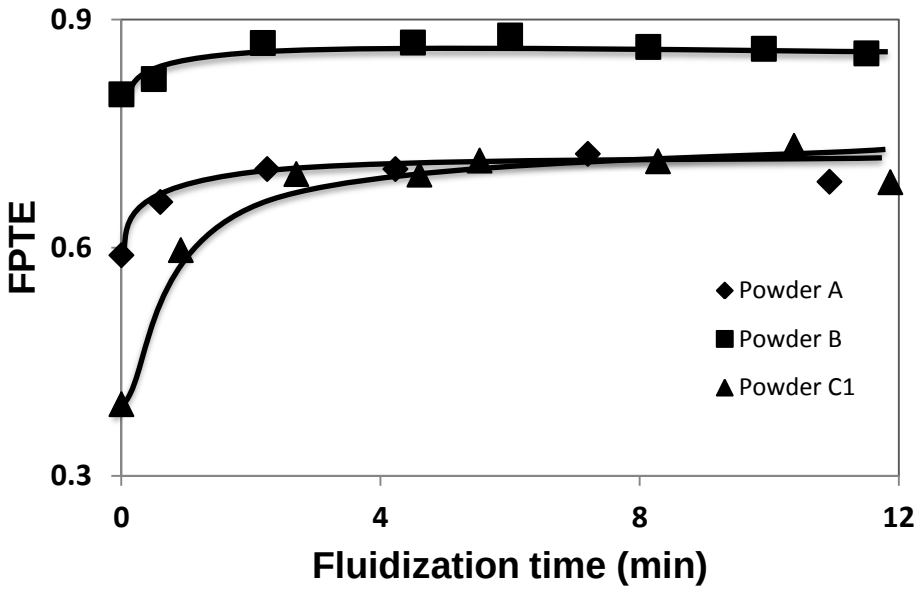

Figure 4: FPTE from the preliminary experiment
(Method of using humidified fluidizing air)

Powder C_1 was more sensitive to the additional moisture. The improvement of the FPTEs was up to 74%. Powder A and B had relatively less improvement of 9% and 24% respectively. The various responses to the humidification among powder A, B and C_1 could be attributed to the differences of the materials. On the other hand, surface properties could be another possible reason as well. Rajesh et al. [19] discovered that the surface resistivity of the particles with different surface roughness could vary in different relative humidity levels. Furthermore, the powders could have different hydrophobicity on the particle surfaces. Rajesh et al. [19] also discussed that particles with more hydrophilic surface tended to absorb more moisture affecting particle charging. In addition, a more hydrophilic surface of

a particle could better retain the moisture during the spraying process. It could also provide better effects on improving the FPTE.

3.3 Full scale spraying test

The polyurethane based powder C_2 was used to evaluate the improvement of the FPTE in the full scale experiment. The scheme of the experiment was similar to the preliminary experiments as shown in Figure 1. However, the feeding rate of the powder was increased to 2.16 g/s and the gun voltage was increased to –60 kV. The feeding task was handed over to a belt feeder because the feeding rate of the vibrating feeder was not consistent as the spraying duration decreased from 60 to 3.5 seconds. The powder loaded in the feeder filled up a portion of a conveyor belt. By calibrating the conveying speed according to the length of the belt, the powder feeding rate could be controlled during spraying. The target, the spraying distance, the fluidizing air velocity and the humidity level of the fluidizing air were remained unchanged as those in the preliminary experiment.

The results in Figure 5 show similar trend of improvement in FPTE to that in Figure 4. The FPTE increased from about 0.36 to about 0.42 in the first 2 to 3 minutes. After that, the FPTE of the powder stayed unchanged for further fluidizations. The improvement of the FPTE was up to 17%.

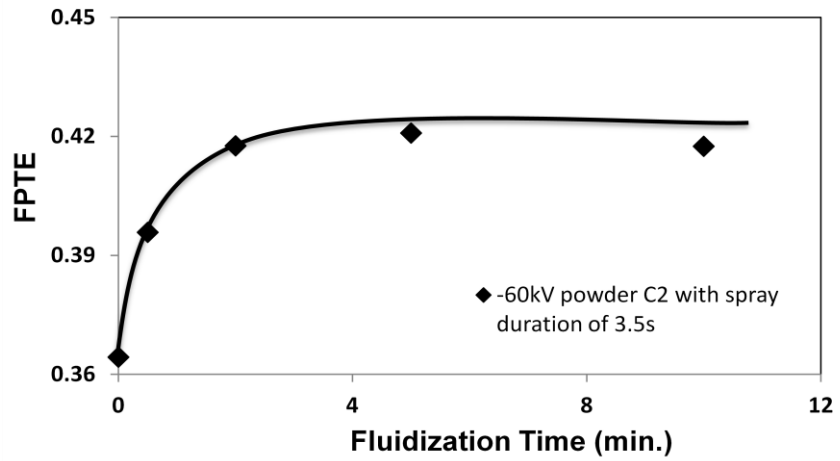

Figure 5: FPTE of powder C_2 in the full scale experiment (Method of using humidified fluidizing air)

On the other hand, another approach to humidify the powder by using the pneumatic transportation air instead of the fluidizing air was also tested. The polyurethane based powder C_1 was used. It was difficult to increase the humidity level of the pneumatic transportation air, since the air velocity was much higher than the fluidizing air. A maximum of 60% RH was finally achieved in the experiment. The feeding rate was 2.16 g/s and the spraying durations were set as 2, 3 and 5 seconds.

As shown in Figure 6, the FPTE of the dry powder indicated by the dotted lines decreased as the spraying duration increased for both dry and humidified powders. It was because of the back ionization caused by the accumulations of the charged particles on the target over time. When the back ionization occurs, the maximum electric field strength was reached and it became much more difficult to deposit the new arriving particles on the target [10]. In addition, the effect of secondary charge, which was the additional charging on the deposited powder layer from the point electrode overtime, was more severe in a longer spraying duration. It could accelerate the back ionization to reduce the FPTE [20]. The higher gun voltage could create higher particle charges and stronger electric field directing more

particles towards the target. Comparing with the results obtained from –30kV, the FPTE from –60 kV was increased. However, an even higher FPTE could not be acquired when the voltage was increased to –90 kV; instead, the FPTE decreased comparing with – 60 kV. It was because the charges of the particles were too high so that the electric field across the particle layer on the target surface increased much more quickly. As a result, back ionization occurred much sooner rejecting more charged particles to deposit. Moreover, the higher corona voltage could also cause more significant effects from the secondary charge accelerating back ionizations. Thus, simply increasing the corona voltage could not affectively improve the FPTE of the fine powders.

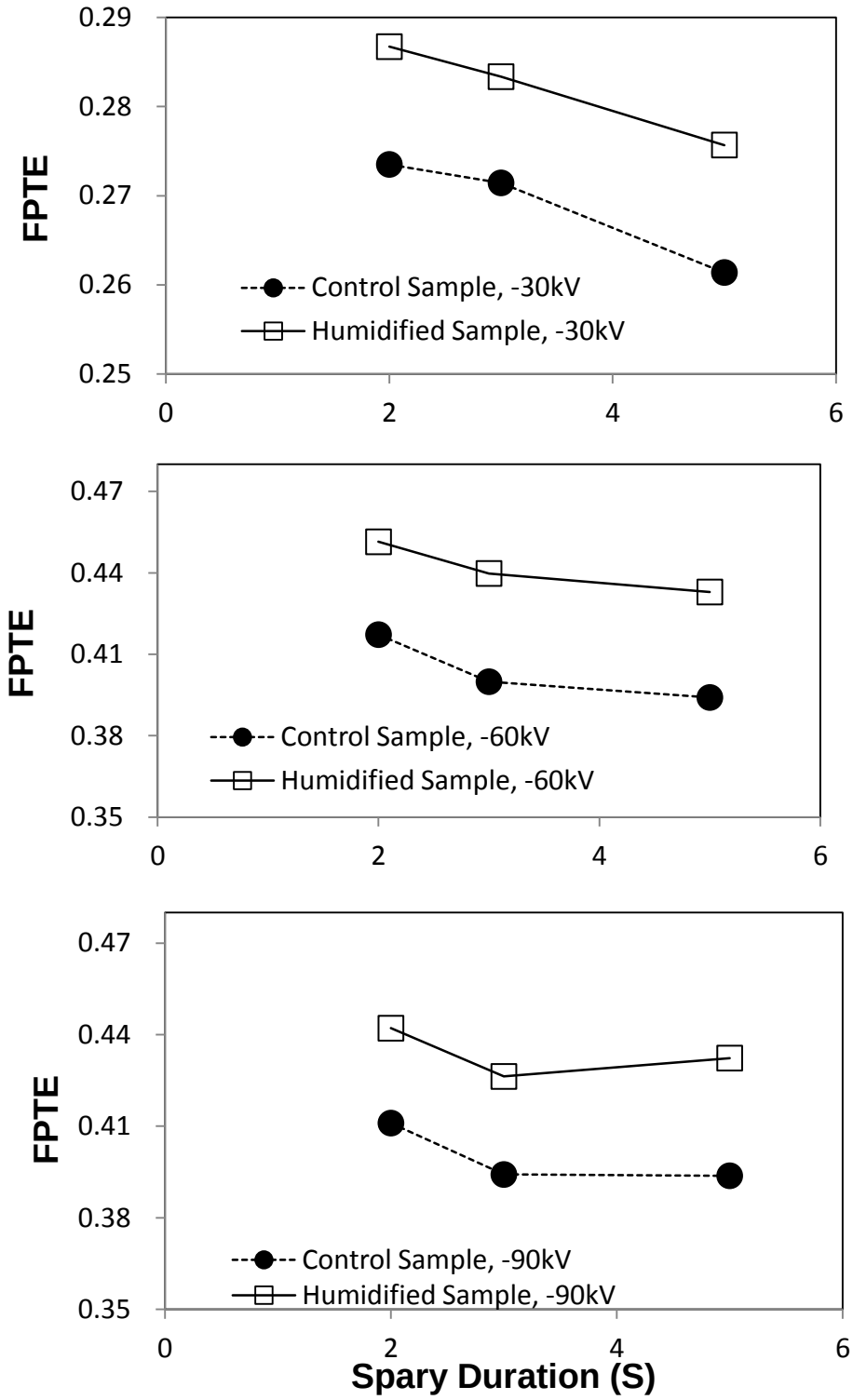

Figure 6: FPTE of powder C_1 in the full scale experiment (Method of using humidified pneumatic transportation air)

Figure 6 also indicated that the FPTE of the humidified powders shown by the solid lines were better. The improvement of the FPTE was from to 5.5% to 9.8%. In comparison, the humidified pneumatic transportation air could have less effect on improving the transfer efficiency. It may cause by the poorer interactions between the particles and air. The pneumatic transportation air traveled with the particles from the venture pump to the gun tip in roughly 2 seconds, while the humidified fluidizing air was agitating the particles in minutes. The better and longer interactions between particles and air could ensure sufficient moisture gain to influence the resistivity of the powders. Furthermore, the lower humidity level of the pneumatic transportation air could be another factor. The powder samples which were sprayed with both dry and humidified pneumatic transportation air were collected and their moisture contents were measured. As shown in Table 2, the moisture content of the powder sprayed by the humidified air was only 0.3%, which was much less than those humidified by the fluidization air. According to the data from Figure 2, it was equivalent to about 2 minutes of humidification in the fluidized bed. Based on the results in Figure 5, the 2 minutes humidification in the fluidized bed could only provide less than 4% increase in FPTE. Therefore, the increased moisture content in the particles and the humidified air sprayed out from the gun were both responsible for the improvement of the FPTE found in this part of the study.

Table 2: The moisture content of the powder C_1 sprayed by dry and humidified pneumatic transportation air

Pneumatic transportation air	Moisture Content of the powder sample	Standard deviation of the results
Dry	0.19%	0.023%
Humidified	0.30%	0.027%

Sims [9] disclosed that FPTE was highly sensitive to the particle size of the powder. This study found that the FPTE of the fine powders could be improved. However, one question still remained: if the same improvement would apply to the regular powder (median particle size above 30 μm)? To answer this question, polyurethane powder C_3 was tested. The same spraying process and parameters as the experiment for powder C_2 were followed.

The results shown in Figure 7 indicate no significant improvement of the FPTE. Unlike the fine powders, the FPTE of powder C_3 did not increase drastically during the test. As demonstrated by Figure 3, the resistivity of the powder C_3 reduced much less comparing with fine powders. Although the gained moisture by powder C_3 might more or less accelerate the charge decay, it could hardly provide significant improvement on FPTE.

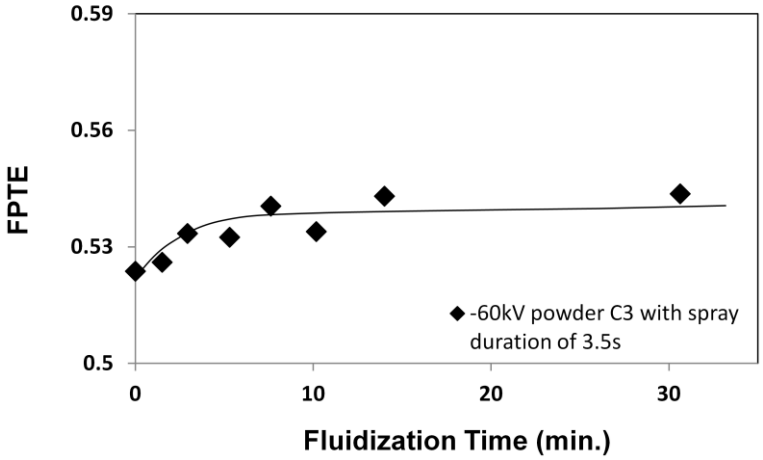

Figure 7: FPTE of powder C_3 in the full scale experiment
(Method of humidified fluidizing air)

3.4 The effects of the humidity on fine powder flowability and coating quality

The powder flowability could be deteriorated by the additional moisture. It increased the risk of causing unfavorable issues during the application such as powder agglomeration and

powder de-fluidization. Therefore, the effect of the increased humidity on fine powder flowability was also investigated.

In this part of the study, powder A and powder C_1 were both exposed in an environment with the humidity of 95-98%. Along with the humidity exposure time, the powders were observed and the flowability of the powder was measured. Based on visual inspections, both powders did not show obvious changes within the first 192 hours. However, small powder agglomerations could be found in powder C_1 after gentle agitations by a stir bar after 192 hours, showed in Figure 8 (a). In addition, the powder started to accumulate on the side wall of the container. Powder A behaved much better than powder C_1. Although less accumulation of the powder on the side wall was also seen, powder agglomerations were not found. The observation was stopped at about 366 hours, because of the poor flowability of powder C_1. After agitations, large powder agglomerations were observed from powder C_1 shown in Figure 8 (b). On the other hand, powder A had no obvious difference from 192 hours.

(a) After 192 hours (left: powder C; right: powder A)

(b) After 366 hours (left: powder C; right: powder A)

Figure 8: Visual inspection after Humidity exposure

The above visual observations were similar to the flowability test results listed in Table 2. Both powder A and C_1 could almost maintain their original flowability within the first 96 hours. By 580 hours, powder A had slightly worse AVA and RBER. However, powder C_1 was much more sensitive to the increased humidity. The AVA of powder C_1 increased about 1.5 degrees and the RBER was unable to be measured after 120 hours due to strong powder cohesion. Therefore, additional moisture was possible to deteriorate the fine powder flowability in this situation. The moisture content of the powder humidified by the fluidizing

air was up to about 0.8% as shown by Figure 3. Discovering from Figure 9, that was equivalent to about 100 hours of stagnation in this experiment. According to the characterization results, 100 hour exposure would not largely affect the fine powder flowability.

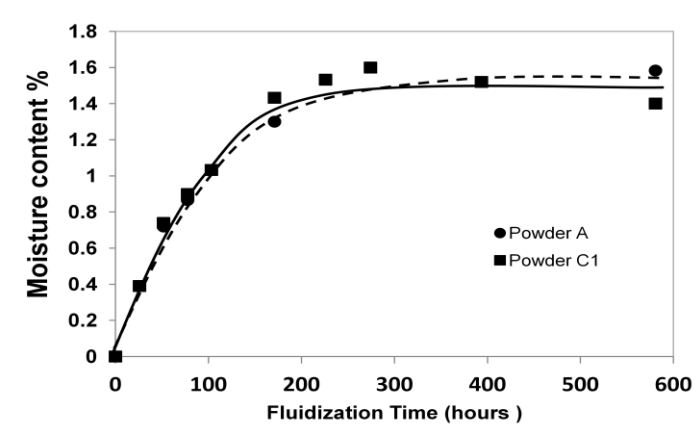

Figure 9: The moisture content of the powders after stagnated in an extreme humid environment

Table 3: Flowability of the powders during humidity exposure

Samples	AVA (°)			RBER		
Exposure time (hr)	0	96	580	0	96	580
Powder A	42.4	42.5	43.5	1.43	1.42	1.41
Powder C_1	44.7	44.6	46.2	1.26	1.22	n/a

A humidified fine powder might also cause formation of micro-agglomerations that aggregated by fine particles acting like larger particles. In addition, micro-agglomerations could also cause coating defects. Therefore, further observation in a micro scale was necessary on the pre- and post-humidified fine powders.

The SEM images in Figure 10 indicate that the particles of both powders were not aggregated after fluidization with humidified air and micro-agglomerations were not found. The pre- and post-humidified powders were then sprayed on the sample panels and the coating qualities were examined. By comparing the cured panels between pre- and post-humidified powders, there were no powder balls, seeds or pin hole observed by the necked eyes. The sample panel were also inspected under SEM. The coating surfaces in high magnification were showed in Figure 11 (cutting line were included in the image for better focus). As observed, all the coating surfaces had small bits with size under 10μm which were normally fillers or additives but not micro-agglomerations. There was no large bump on the coating surfaces of the post-humidified powders.

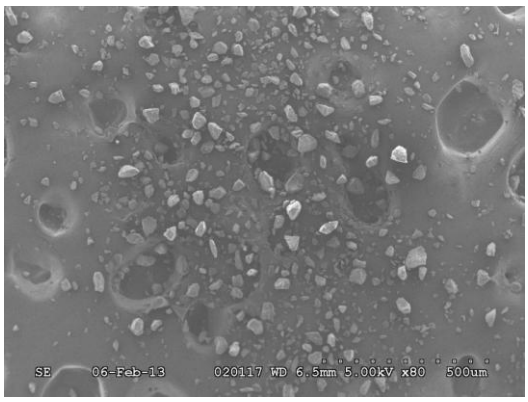

a) Pre-humidified Powder C particles

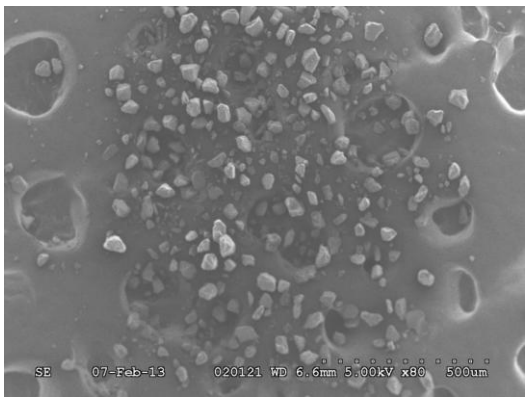

b) Post-humidified Powder C particles

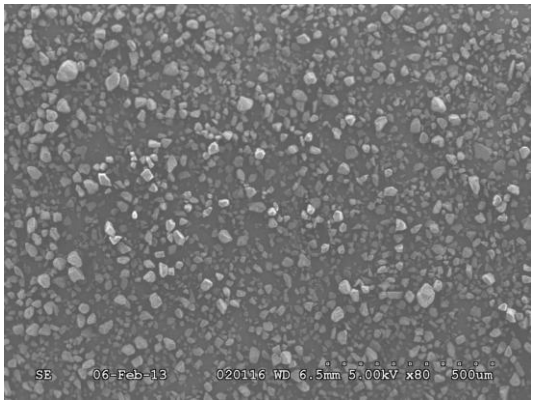

c) Pre-humidified Powder A particles

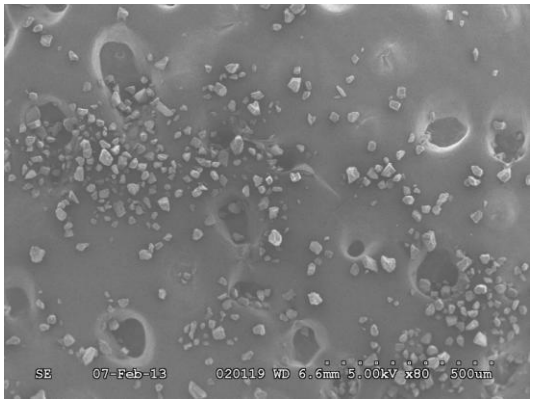

d) Post-humidified Powder A particles

Figure 10: SEM images of the pre- and post-humidified powders (humidification of 60 minutes)

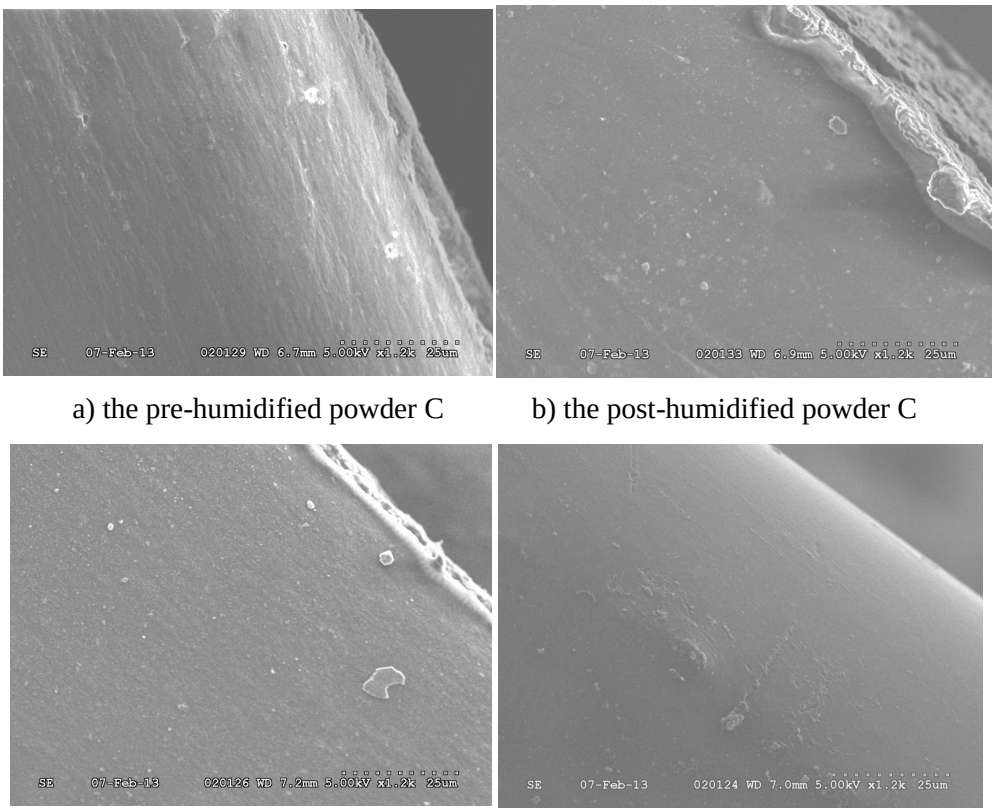

a) the pre-humidified powder C b) the post-humidified powder C

c) pre-humidified powder A d) post-humidified powder A

Figure 11: SEM images of the coating surfaces (humidification of 60 minutes)

Based on the results, it can be concluded that humidification of fine powders with tested conditions would not cause micro-agglomerations and the coating quality of the humidified powders would not be affected. On the other hand, the suggested method of humidification by the study would have low risk of deterioration in fine powder flowability. As an advice for real application, the humidified powders could be fluidized by dry air for a few minutes before shutting down. This would remove the additional moisture on the particle surface to further reduce the risk of causing flowability issues.

4 Conclusions

This study revealed that the increased moisture content on the particle surfaces had significant and positive impact on the FPTE of fine powders in corona charge spraying. The resistivity of the particle was found to be reduced by moisture, therefore the back ionization was delayed and more charged particles could be deposited. The study also disclosed that particles had better humidification in the fluidized bed rather than in the pneumatic transportation process. It suggested that the humidified fluidizing air is more favourable to be used. On the other hand, excessive moisture in particles was found to deteriorate the fine powder flowability. However, the moisture gained by the powder during fluidization humidification under the test condition was not over loaded and it had no unfavourable effect on the flowability. Finally, there was no micro-agglomeration observed in the humidified powders and the coating quality was not affected.

References

[1] Utech B., A Guide to High Performance Powder Coating. *Society of Manufacturing Engineers*, 2001.

[2] White H.J., Industrial Electrostatic Precipitation (Addison-Wesley Publishing Company, INC.), 1963.

[3] Wu S., Electrostatic charging and deposition of powder coatings, *Polym.-Plast. Tec.;. Eng.*, 7, (1976) 119-220.

[4] Cross J.A., *Electrostatics: Principles*, Problems and Applications, (Bristol: Hiler), 1987.

[5] Mazumder M.K., Sims R.A., Biris A.S., Srirama P.K., Saini D., Yurteri C.U., Trigwell S., De S., and Sharma R., Twenty-first century research needs in electrostatic processes applied to industry and medicine, *Chem. Eng. Sci.*, 61 (2006), 2192-2211.

[6] Chang J.S., Lawless P.A., Yamamoto T., Corona discharge processes, *IEEE Trans. Plasma Sci.*, 19 (1991), 1152-1166.

[7] Meek J.M., Craggs J.D., *Electrical Breakdown of Gases*, (*New York: Wiley*), 1978.

[8] Bailey A.G., The science and technology of electrostatic powder spraying, transport and coating, *J. Electrostat*., 45 (1998), 85-120.

[9] Masuda S., Washes M., Mizuno A., Abuts K., Boxer Charger Proceedings of the 13th IEEE-IAS Annual Meeting (Toronto, Canada), 1B (1978), 16-22.

[10] Sims R.A., Mazumder M.K., Liu Xiaohong, Chok W., Mountain J.R., Wankum D.L., Pettit P., Chasser T., Electrostatic Effects on First Pass Transfer Efficiency in the Application of Powder Coatings, *IEEE Transactions on industry applications*, 37(6) (1997), 1610-1617.

[11] Sharma R., Trigwell S., Biris A.S., Sims R.A., Mazumder M.K., Effect of Ambient Relative Humidity and Surface Modification on the Charge Decay, *Properties of Polymer Powders in Powder Coating*, 39(1) (2003), 87-95.

[12] Messaoudi R., Younsi A., Massines F., Despax B., Mayoux C., Influence of Humidity on Current Waveform and Light Emission of a Low-frequency Discharge Controlled by a Dielectric Barrier 3(4) (1996), 537-543.

[13] Powers H., Dec. Improving First-Pass Transfer Efficiency, *Product Finishing Magazine*, Gardner Publications Inc. 2005.

[14] Berger G., Marode E., Belabed O., Senouci B., Gallimbert I., Osgualdo A., Effect of Water Vapor on the Discharge Regimes and the Deviation from Similarity Law in Compressed SF for Positive Polarity, *J. Phys. D: Appl. Phys.*, 24 (1991). 1551-1556.

[15] Mohnen V.A., Discussion of the Formation of Major Positive and Negative Ions up to the 50 km Level, *Pure and Applied Geophysics*, 84 (1971), 141-153.

[16] Meng X.B., Hui Z., Jesse Z., Edge effects and effects of relative humidty on current and current density distribution during negative point-to-plane corona discharges, *PhD Thesis of UWO*, 2008, 65-80.

[17] Krantz M., Zhang H., Zhu J., Characterization of powder flow: static and dynamic testing. *Powder Technology*, 194(3) (2009), 239-245.

[18] Hang Q., Zhang H., Zhu J., Flow properties of fine powders in powder coating, *Particuology*, 8(1) (2010), 19-27.

[19] Sharma R., Trigwell S., Biris A.S., Sims R.A., Mazumder M.K., Effect of Ambient Relative Humidity and Surface Modification on the Charge Decay Properties of Polymer Powders in Powder Coating, *IEEE Transactions of Industry Applications*, 39(1) (2003), 87-95.

[20] Wu S., Electrostatic charging and deposition of powder coatings, *Polym.-Plast. Technol. Eng.*, 7, 1976, 119-220.

CURRICULUM VITA

Name: Jing Fu

Education: BASc Mechanical Engineering;
University of Ottawa, 2004-2008

MESc Mechanical and Material Engineering
Western University, 2008-2010

PhD, Chemical and Biochemical Engineering
Western University, 2010-2014

Working Experiences: Engineering Intern,
TOYTOA Motor Co., 2006

Research Assistant,
Western University, 2008-2004

Publication: **Fu J.**, Zhang H., Zhu J., 2011, The Effect of Different Factors on Material Utilization Efficiency of Powder Coatings, *61th CSChE conference*.

Fu J., Zhang H., Zhu J., 2013, Improvement on the first pass transfer efficiency of fine polymer coating powders for corona spraying process, *Advanced Powder Technology*.

Fu J., Krantz M., Zhang H., Zhu J., Kuo H., Wang Y.M., Lis K., 2011, Investigation of the recyclability of powder coatings, *Powder Technology*.